Experimental Investigations of The Influence of Reynolds Number and Boundary Conditions on a Plane Air Jet

by

Ravinesh C. DEO

MSc Hons (*Canterbury*): BSc (*USP*)

a thesis submitted in fulfillment of the

requirements for the degree of

doctor of philosophy

In

ENGINEERING

At

Turbulence, Energy and Combustion Group

School of Mechanical Engineering

The University of Adelaide

South Australia SA 5005

SEPTEMBER 30, 2005

Experimental Investigations of the Influence of Reynolds Number and Boundary Conditions on a Plane Air Jet

RAVINESH C DEO

JUNE 07, 2005 THESIS SUBMITTED

OCTOBER 07, 2005 DEGREE AWARDED

Thesis for Doctor of Philosophy in Engineering

Supervisors: Assoc. Professor G J Nathan

Senior Research Fellow Dr. J Mi

Originality Statement

I, Ravinesh C. DEO, hereby declare that this thesis, titled "Experimental Investigations of the Influence of Reynolds Number and Boundary Conditions on a Plane Air Jet", submitted for the award of a Doctor of Philosophy in Engineering at The University of Adelaide, is original in every respect. It contains no material which has been accepted for the award of any other degree or diploma in any university. Further to the best of my knowledge and belief, this Ph.D. thesis contains no material previously published or written by another person, except where due reference is made in the thesis.

Ravinesh C. DEO date

Copying Permission

In presenting the fulfillment of the requirements for the degree of Doctor of Philosophy in Engineering at The University of Adelaide, I agree that the Library shall make it freely available for inspection and copying under the Copyright Law of Australia. It is understood that any copying or publication of this Ph.D. research for financial gain shall not be allowed without my written permission. I hereby grant permission to the library at The University of Adelaide to photocopy my work for scholarly purposes only.

Ravinesh C. DEO date

Contents

List of Tables

List of Figures

Abstract

A plane jet is a statistically two-dimensional flow, with the dominant flow in the streamwise (x) direction, spread in the lateral (y) direction and zero entrainment in the spanwise (z) direction respectively (see Figure 1). A plane jet has several industrial applications, mostly in engineering environments, although seldom is a jet issuing through a smooth contoured nozzle encountered in real life. Notably, the Reynolds number and boundary conditions between industrial and laboratory environments are different. In view of these, it is important to establish effects of nozzle boundary conditions as well as the influence of Reynolds number, on jet development. Such establishments are essential to gain an insight into their mixing field, particularly relevant to engineering applications. To satisfy this need, this thesis examines the influence of boundary conditions, especially those associated with the formation of the jet and jet exit Reynolds number, on the flow field of a turbulent plane air jet by measuring velocity with a hot wire anemometer. A systematic variation is performed, of the Reynolds number Re over the range $1{,}500 \leq Re \leq 16{,}500$, the inner-wall nozzle contraction profile r^* over the range $0 \leq r^* \leq 3.60$ and nozzle aspect ratio AR over the range $15 \leq AR \leq 72$ (see notation for symbols). An independent assessment of the effect of sidewalls on a plane jet is also performed. Key outcomes are as follows:

(1) *Effects of Reynolds number Re*

Both the mean and turbulence fields show significant dependence on Re. The normalized initial mean velocity and turbulence intensity profiles are Re-dependent. An increase in the thickness of boundary layer at the nozzle lip with a decrease in Re is evident. This dependence appears to become negligible for $Re \geq 10{,}000$. The centerline mean velocity decay and jet spreading rates are found to decrease as Re is increased. Furthermore, the mean velocity field appears to remain sensitive to Reynolds number at $Re = 16{,}500$. Unlike the mean velocity field, the turbulent velocity field has a negligible Re-dependence for $Re \geq 10{,}000$. An increase in Reynolds number leads to an increase in the entrainment rate in the near field but a reduced rate in the far field. The centerline skewness and the flatness factors show a systematic dependence on Reynolds number too.

(2) *Effects of the inner-wall nozzle exit contraction profile r^**

The inner-wall nozzle exit contraction profile r^* influences the initial velocity and turbulence intensity profiles. Saddle-backed mean velocity profiles are evident for the sharp-edged orifice configuration ($r^* \simeq 0$) and top hat profiles emerge when $r^* \geq 1.80$. As r^* is increased from 0 to 3.60, both the near and the far field decay and the spreading rates of the plane jet are found to decrease. Hence, the sharp-edged orifice-jet ($r^* \simeq 0$) decays and spreads more rapidly than the jet through a radially contoured configuration ($r^* \simeq 3.60$). The asymptotic values of the centerline turbulence intensity, skewness and flatness factors of the velocity fluctuations increase as r^* tends toward zero. The non-dimensional vortex shedding frequency of $St_H \simeq 0.39$, is higher for the sharp-edged orifice nozzle ($r^* \simeq 0$), than for the radially contoured ($r^* \simeq 3.60$) nozzle whose $St_H \simeq 0.24$. Thus, the vortex shedding should be strongly dependent on flow geometry and on nozzle boundary conditions.

(3) *Effects of nozzle aspect ratio AR*

The initial velocity and turbulence intensity profiles are slightly dependent on nozzle aspect ratio of the plane air jet. It is believed that a coupled influence of the nozzle aspect ratio and sidewalls produce changes in the initial flow field. The axial extent over which a statistically 'two-dimensional' flow is achieved, is found to depend upon nozzle aspect ratio. This could be possibly due to the influence of the evolving boundary layer on the sidewalls or due to increased three-dimensionality, whose influence becomes significantly larger as nozzle aspect ratio is reduced. A statistically two dimensional flow is only achieved over a very limited extent for $AR = 15$. In the self-similar region, the rates of centreline velocity decay, spreading of the mean velocity field and jet entrainment increase with an increase in nozzle aspect ratio. An estimate of the 'critical' jet aspect ratio, where three-dimensional effects first emerge and its axial location is made. Results show that the critical aspect ratio increases with nozzle aspect ratio up to $AR < 30$. For $AR \geq 30$, the critical aspect ratio based on jet half width, attains a constant value of about 0.15. Thus, it appears that when the width of the flow approximately equals the spacing between the sidewalls, the plane air jet undergoes a transition from 2-D to 3-D. A distinct hump of the locally normalized turbulence intensity at an axial distance between 10 to 12 nozzle widths downstream, characterizes the centerline turbulence intensity for all nozzle aspect ratios. This hump is smaller when nozzle aspect ratio is larger.

(4) *Effects of the sidewalls*

A jet issuing from a nozzle of $AR = 60$ and measured at $Re = 7{,}000$ is tested with sidewalls, i.e. plane-jet and without sidewalls, i.e. free-rectangular-jet. It is found that the entire flow field behaves differently for the two cases. The initial velocity profiles are top hat for both jets. The free rectangular jet decays and spreads more rapidly in both the near and far field. It is found that the free rectangular jet behaves statistically two-dimensional up to a shorter axial distance ($x/H = 70$) as opposed to the plane jet whose two-dimensional region extends up to $x/H = 160$. Also noted are that the axial extent of the two-dimensional region depends strongly on nozzle aspect ratio. Beyond the 2-D region, the free rectangular jet tends to behave, statistically, like a round jet. The locally normalized centerline turbulence intensity also depend on sidewalls. Turbulence intensity for the plane jet asymptotes closer to the nozzle (around $x/H = 30$) whereas for the free rectangular jet, turbulence intensity varies as far downstream as $x/H = 100$, and then asymptotes. A constant St_H of 0.36 is found for the free rectangular jet whereas an St_H of 0.22 is obtained for the plane jet.

It is noted that the effects of jet exit Reynolds number, inner-wall nozzle exit contraction profile, nozzle aspect ratio and sidewalls on the plane air jet are all non-negligible. The effect of viscosity is expected to weaken with increased Reynolds number and this may contribute to the downstream effects on the velocity field. Both the nozzle contraction profile and nozzle aspect ratio provide different exit boundaries for the jet. Such boundary conditions not only govern the formation of the initial jet but also its downstream flow properties. Hence, the initial growth of the shear layers and the structures within these layers are likely to evolve differently with different boundary conditions. Thus, the interaction of the large-scale structures with the surroundings seems to depend on nozzle boundary conditions and consequently, influences the downstream flow. In summary, the present study supports the notion that the near and far fields of the plane jet are strongly dependent on Reynolds number and boundary conditions. Therefore, the present thesis contains immensely useful information that will be helpful for laboratory-based engineers in selection of appropriate nozzle configurations for industrial applications.

…Thankyou My Lord…

To

My Loving Parents

Amma & Daddy

For Their Blessings & Inheritance

For The Achievement of my PhD

And

My Dear Wife

Aruna

For Her Love, Sacrifice & Encouragement

Towards my PhD

Acknowledgements

Most sincere gratitude goes to my supervisors, Associate Professor Graham (Gus) Nathan and Dr. J Mi for their tremendous efforts in making this research a great success. Their contributions to my research degree, over the past $3\frac{1}{2}$ years is immeasurable. I clearly understand that it is not possible for me to thank them by these few words. Evidence of their continued professional support, encouragement, guidance and friendship is revealed though the quality of my work, and every bit of it goes to them.

Since August 2001, Gus has been providing me tremendous support, not only in his capacity as my supervisor, but also as a close colleague and friend in working together towards the completion of this project. I also acknowledge him for providing me with the ARC Supplementary Scholarship and FCT short-term scholarship. My experimental skills are entirely dedicated to Dr. J Mi who not only taught me the techniques of hot-wire anemometry but also worked with me side-by-side everyday to assist me in solving problems that I encountered during my research. In the midst of 2003 when a significant event occurred that changed my wife and my life, Gus and Jamie were over-supportive and extremely cooperative with us. During this period, they provided me emotional support and guidance, so I thank them from my inner conscience. I must admit that Gus and J Mi are the best supervisors any postgraduate student can possibly have!

I acknowledge Dr. Peter Venon Lanspeary for acting as my co-supervisor in the initial stages of my Ph.D. His assistance in producing technical drawings of the nozzle designs are greatly appreciated. I would also like to thank Dr. Richard Kelso for few thoughtful discussions and George Osborne for designing hot-wire probes, Derek Franklin for setting up the traverse and Bill Finch / Bob Dyer for building my nozzles. Other workshop staff, in particular, Ron Jager and Malcom Bethune assisted me in setting up the plane jet facility. I acknowledge School of Mechanical Engineering for allowing me to pursue a Ph.D. in Engineering without having any prior engineering background. Acknowledgement is made to the school for funding my 15^{th} AFMC conference. Thanks to the computer officer, Billy for his efforts in solving my PC problems!

My Ph.D. was supported by an International Postgraduate Research Scholarship (IPRS) and the Adelaide University Scholarship (AUS). Hence, I extend very special thanks to the Australian Government and Adelaide University for providing me funding. Acknowledgement is made to Australian Research Council (ARC) Discovery Grant for providing extra living allowances and incidental expenses towards the project. I thank the University of Adelaide for organizing the Intergrated Bridging Programme (IBP) for enhancing our skills in research and to Ms Karen Adams for her advice, guidance and interesting classes organized through the IBP.

On this landmark day, I acknowledge and remember three most important people in my life. Their contributions towards my Ph.D. are worthy of very special and humble thanks and remembrance. They are my loving **mum** and **dad** and my dear wife **Aruna**. My **parents**, **Mr and Mrs Bisun Deo**, deserve the highest level of respect for their benediction towards my achievement, endurance in educating me and for providing me the inheritance to be the first professional doctorate in our family. Indeed this Ph.D. is a dream they have visualized through me and I thank them for their sacrifice, prayers and blessings.

It is impossible for me to quantify the amount of support provided by my **wife**, **Aruna** on every stage of my career. Her words of encouragement, enthusiasm and advice still beeps in my ears, especially those which convinced me not to quit! The strength of her determination that I will be able to complete this huge task was a driving force behind my success. She sacrificed a large portion of her own career, luxury and indeed her invaluable time towards my doctorate. *It is to my parents and my wife that I dedicate my entire thesis.*

I would like to acknowledge my other parents (Mr and Mrs Chandar Deo) for providing heaps of blessings. In fact, mum deserves a lot of thanks for doing the cooking and housework when we were in desperate need! I wish to thank my brotherly friend Nilesh, for his inspirational discussions, his wife Neeliya for coming over to Adelaide to share my family load when we were in desperate need, and my close friend and colleague, Shakeel for being with us in this anonymous land, assisting me with some of my experimental setup and discussing with me my problems and progress regularly. I acknowledge my brothers (Rakesh, Pritam), sister (Madhu) + family members, relatives and friends whom I have not been able to include. Very special acknowledgment goes to well-known academics, Professor W K George (Chalmers University of Technology, Sweden) and Dr S Rajgopalan

(University of Newcastle, Australia) for providing a thoughtful and an excellent thesis review and commendations for this work.

Above all, thankyou my Lord for giving me the potentials for an extraordinary opportunity in my life. Your guidance has always been there, and without your will, nothing would have been possible!

© R C Deo
BSc (The University of the South Pacific Fiji)
MSc Hon (The University of Canterbury New Zealand)
SEPTEMBER 30, 2005 Email physcd@yahoo.com

Vita

Born in a remote village of Naleba in the township of Labasa, Fiji Islands, Ravinesh gained his primary education at Naleba Bhartiya School from Classes 1-6 and junior secondary education at Naleba College from Forms 1-4. He undertook high school education from Forms 5-7 at Labasa College. He was the High School 'Dux' (Best High School academic student) in 1995, for achieving the highest standards in Mathematics, Biology, Chemistry and Physics. During this year, he broke the *Year 13 National Examination* (Fiji Seventh Form Examination) **ALL-TIME** record, by scoring the highest mark of 360/400 for the *first* time in the Fiji. His exam results created a new record of 97 % in Physics and 96 % in Chemistry.

Ravinesh completed his BSc in 1998, with subject majors, Physics and Mathematics from University of the South Pacific in Fiji. He was awarded the University Gold Medal and Motibhai Prize for being the outstanding Physics student. Overall, his GPA was at the High Distinction level (4.4/4.5). He continued for further education, to pursue an MSc in Meteorological Physics at University of Canterbury, New Zealand. He completed his masters successfully in May 2001, with degree awarded (with Honors) in July 2001. From August 2001 - April 2005, Ravinesh worked on his PhD project, within the Turbulence, Energy and Combustion [TEC] Group, School of Mechanical Engineering, University of Adelaide.

This doctoral dissertation was officially submitted on 07 June 2005. The Adelaide Graduate Center officially confirmed the award of a PhD (subject to minor amendations satisfactory to the supervisors) on 22 August 2005. Ravinesh now works as an Associate

Lecturer in Physics at University of the South Pacific in Fiji. His interest in fluid mechanics continues, and he hopes to pursue a post-doctoral, subject to career opportunity.

Nomenclature

0.1 Acronyms

H	length of the short side of nozzle
w	length of the long side of the nozzle
r	contraction radius of the nozzle profile
AR	nozzle aspect ratio, where $AR = w/H$
r^*	contraction ratio of the nozzle profile, where $r^* = r/H$
l_w	length of the hot-wire sensor
d_w	diameter of the hot-wire sensor
$U_{o,b}$	bulk mean velocity
$U_{o,c}$	exit centerline mean velocity
U_c	local centerline mean velocity
$U_{m,c}$	centerline mean velocity maximum
$U_{ic,m}$	centerline instantaneous velocity maximum
U	mean velocity along lateral (y) direction
U_i	instantaneous velocity
U_n	normalized mean velocity, where $U_n = U/U_c$
$U_{n,c}$	normalized centerline mean velocity, where $U_{n,c} = U_c/U_{o,c}$
U_{co}	co-flow mean velocity
Re	Reynolds number defined by $Re = U_{o,c}\, H \;/\; \nu$
u	fluctuating component in the streamwise (x) direction, $u = U_i$ - U_c
$u^{'}$	root-mean-square (rms) of u, such that $u^{'} = (< u^2 >)^{1/2}$
$u_c^{'}$	centerline rms, such that $u_c^{'} = (< u_c^2 >)^{1/2}$
$u_n^{'}$	normalized rms (turbulence intensity), where $u_n^{'} = u^{'}/U_c$
$u_{n,c}^{'}$	normalized centerline rms, (centerline turbulence intensity), where $u_{n,c}^{'} = u_c^{'}/U_c$
$u_{c,\infty}^{'}$	asymptotic value of centerline turbulence intensity
$u_{c,max}^{'}$	magnitude of the local maximum of turbulence intensity
S_u	centerline skewness factor, where $S_u = < u^3 > /(< u^2 >)^{3/2}$
F_u	centerline flatness factor, where $F_u = < u^4 > /(< u^2 >)^2$

$S_u^{c,\infty}$ asymptotic value of centerline skewness factor

S_u^{min} minimum value of centerline skewness factor

S_u^{max} maximum value of centerline skewness factor

$F_u^{c,\infty}$ asymptotic value of centerline flatness factor

F_u^{min} minimum value of centerline flatness factor

F_u^{max} maximum value of centerline flatness factor

x_p jet potential core length

$y_{0.5}$ velocity half-width of the jet, i.e. the y-location from the centerline, where $U = \frac{1}{2}U_c$

K_u decay rate of normalized centerline mean velocity

K_y jet spreading rate

d internal diameter of a round nozzle

x_{01} virtual origin from the normalized mean centerline velocity

x_{02} virtual origin from the normalized velocity half-widths

x_m downstream distance at which a hump in turbulence intensity occurs

$x_{m,\infty}$ downstream distance at which the asymptotic value of turbulence intensity occurs

$x_{p,\,\max}$ maximum downstream distance up to which the flow is planar

$y_{05}^{'}/w$ characteristic jet aspect ratio, where $y_{0.5}^{'}$ is the velocity-half widths at $x_{p,\,\max}$.

R_o adjustable overheat resistance of the CTA

R_T total resistance of the sensor and cables

A_R laboratory room area in the same plane as the nozzle opening width H

A_n nozzle area

H_R height of room

H_j height from the bottom of room up to the nozzle

ΔT time constant of the CTA system

f_c optimum cut-off frequency of the CTA system

v fluctuating component in the spanwise (y) direction, $v = V_i$ - V_c

w fluctuating component in the transverse (z) direction, $w = W_i$ - W_c

q turbulence kinetic energy, defined by $q = \frac{1}{2}(u^2 + v^2 + w^2)$

$q_{c,\infty}$ far-field turbulent kinetic energy

St_H Strouhal number for a plane jet, defined by $St_H = f\,H/U_{o,b}$

St_p Strouhal number for a round jet, defined by $St_p = f_p\,D/U_{o,b}$

m mass flux at any axial distance downstream from the nozzle exit

D geometric diameter of a round nozzle

D_e equivalent diameter of a round nozzle with the same exit area as a rectangular nozzle, where $D_e \simeq 1.13\,AR^{0.5}\,H$

0.2 Greek Symbols

ν kinematic viscosity of air, $\nu \simeq 1.47 \times 10^{-5}\ m^3 s^{-1}$ at 25^o ambient conditions

α overheat ratio of CTA system, usually $\simeq 1.8$

δ thickness of the boundary layer at the nozzle lip, $\delta \simeq \int_{y=0}^{y=\infty} (1 - {}^{U}/_{U_{o,c}})\, dy$

ϕ_u power spectrum of u where $\int \phi_u(f)\ df = \overline{u^2}$

ϵ kinetic energy dissipation term, $\varepsilon \simeq 15\upsilon \left\langle \left({}^{du}/_{dx}\right)^2 \right\rangle$

τ_w viscous stress term, $\left(\tau_w = \rho\nu \frac{\partial U}{\partial y}\right)$

ρ density of test medium, for air $\rho \simeq 1.2\ kg\, m^{-3}$ at 25^o ambient conditions

0.3 Some Special Terms

(1) Nozzle profile factor: denoted as r^* and defined by r/H.

(2) Plane jet: a jet which issues through a rectangular nozzle with sidewalls.

(3) Quasi-plane jet: a jet which issues through a large aspect ratio rectangular nozzle but no sidewalls.

(4) Round jet: a jet that issues through a round nozzle.

(5) Pipe jet: a jet through a long pipe.

0.4 Coordinate System

x axial (streamwise) coordinate

y lateral (transverse) coordinate

z spanwise coordinate

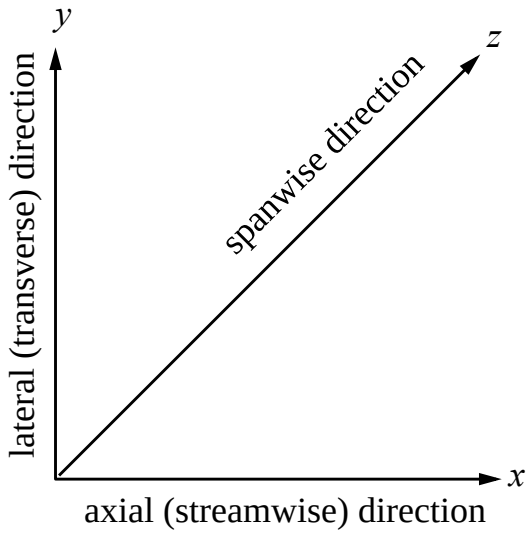

Figure 1: The coordinate system used in the present study.

Chapter 1

INTRODUCTION

1.1 Introductory Note

The plane jet represents one of the two fundamental classes of symmetrical jet flows[1]. The symmetrical nature of the plane jet has broad significance, for example, to reduce computational time in numerical modelling. Plane jets have received significant research attention both in experimental and numerical investigations. Experimental data are not only required to study the fundamental features of the plane jet but also to provide validation in the development of turbulence models (Gouldin et al. 1986).

Even though direct applications of truly plane jets are currently limited, there are nevertheless numerous applications of broadly planar flows. These include aerospace engineering environments e.g. in propulsion units and lift-producing devices (Quinn 1994). Plane jets have also found practical application in air curtain devices (Stephane et al. 2000). Air curtain devices work on the basic principle of blowing a plane air jet between two environments to isolate one volume from the other, thus reducing heat and mass transfer. In their practical application, air curtains are among the popular devices used for energy saving in public buildings, foundry furnaces, refrigeration storages or for air quality control in food, electronic industries and surgical units. In biological applications, these devices assist in the reduction of chemical species, odors, bacteria, dust, insects, moisture and radioactive particle transfer. In fire safety applications for underground tunnels, air curtains reduce the movement of toxic smoke while preserving full access to emergency exits (Stephane et al. 2000).

Plane wall jets are also of considerable research interest for practical applications in the

[1]The two classes of symmetrical jet flows are an axisymmetric (round) jet and a plane (two-dimensional) jet.

field of heating, ventilation and air conditioning. Moshfegh et al. (2004) conducted experimental and numerical investigations of the propagation of warm and cold plane air jets under the influence of a heat sink or a heat source in an insulated room. Such a study is of great significance to prospective improvements in heating, ventilation and air conditioning. Therefore, a study of plane jets has practical implications for fluid engineers and scientists.

1.2 History of Plane Jets

The work of Schlichting (1933) brought plane jets into research attention. In his landmark paper, he examined the propagation of a jet issuing from a small hole into a stationary fluid for two cases. His simplification of axial symmetry allowed integration of the governing equations in a closed form. In his view, a plane jet issues through a long narrow orifice (opening) and its fluid motion is taken to be statistically two-dimensional. Hence, Schlichting (1933) noted that the governing equations can be integrated by an approximate numerical method and the resulting solutions revealed a relatively simple nature of the plane jet. This numerical study marked the beginning of an era for research into plane jets.

Later Bickley (1937) extended the study of Schlichting (1933). He calculated numerically, the mass flow rates of a plane jet using the continuity equation. He noted that the axial progress of the jet is accompanied by an entrainment of ambient fluid which produces a decrease in the axial centerline velocity. Consequently, the momentum remains constant. Such a numerical analysis of the flow field of a plane jet was found to be simple when compared with the relatively complex nature of most turbulent flows. Henceforth, plane jets attracted more research attention and further investigations, mostly experimental in nature were conducted. Forthman (1934) measured the mean velocity of a plane air jet over the axial range 0 to 25 nozzle widths downstream using total head pressure tubes. Although, admittedly, his study appears to be the first experimental work on a plane jet, the axial range of his measurements is quite small and in the region where the jet, most likely, had not reached its asymptotic state.

A more comprehensive study by Miller and Comings (1957) provided the mean, root-mean-square (rms) and static pressure distributions using hot wire anemometry over an axial distance of 40 nozzle widths. Additionally, Van Der Hegge Zijnen (1958) conducted an experimental investigation on the measurements of lateral mean velocity and Reynolds

stresses using both total head tubes and hot wire anemometry over the same axial distance as that of Forthman (1934). He measured a plane jet at two nozzle aspect ratios and found that the spreading and decay rates of the centerline mean velocity are different for the two cases.

Bradbury (1965) then measured a plane jet exhausting into a slowly moving air stream (called a co-flow). Ratios of co-flow to jet velocity $U_{co}/U_{jet} = 7\,\%$ and $16\,\%$ were used. Here, U_{co} and U_{jet} are the co-flow and the jet velocity respectively. It was noted that the turbulence intensity near the edges of the jet for $U_{amb}/U_{jet} \simeq 7\,\%$ were too high to enable accurate measurements. Hence, detailed measurements for the case which had $U_{amb}/U_{jet} \simeq 7\,\%$ were not presented. His analysis showed that the jet compared well with a plane wake and attained self-similarity at approximately 30 nozzle widths downstream. A more thorough investigation of a plane jet issuing through a sharp-edged orifice nozzle was undertaken by Heskestad (1965) using hot wire anemometry. His axial range of measurements covered up to 160 nozzle widths and provided various axial and lateral properties, intermittency, flatness factors and an energy budget. The effects of Reynolds number on axial turbulence intensity were assessed but not in detail. His investigation was followed by others e.g. Jenkins and Goldschmidt (1973), Gutmark and Wygnanski (1976) and Thomas and Goldschmidt (1986). These investigations measured a plane jet at different initial conditions and provide a comprehensive account of the flow properties. For these investigations, the location at which the mean and turbulence statistics assume an asymptotic behaviour were different. These differences are consistent with the findings of George (1989), that is, differences in jet asymptotic behaviour are caused by differences in initial conditions.

1.3 Characteristics of a Plane Jet

A plane jet is a statistically two-dimensional flow[2] with a dominant mean motion in the streamwise (x) direction, jet spread in the lateral (y) direction and zero entrainment in the spanwise (z) direction. Thus, the flow statistics are independent of the spanwise coordinate z. To illustrate this, a schematic view of a plane jet is shown in Figure 1.1. True plane jets efflux from rectangular nozzles. The jet is confined within two parallel sidewalls attached to the short sides of the nozzle and oriented in the x-y plane. Such a configuration allows the jet to spread in the lateral (y) direction only.

[2]In general, turbulent motions are three-dimensional but the time-averaged mean velocity field of the plane jet is two-dimensional.

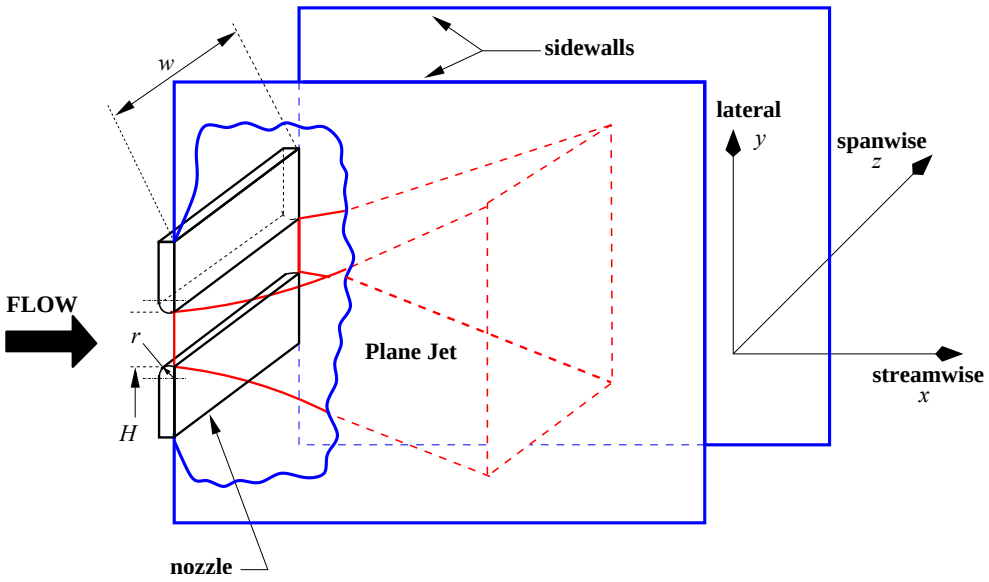

Figure 1.1: A schematic view of a plane jet nozzle.

For a plane jet, its characteristic velocity is the area-averaged exit velocity, also called the 'bulk mean velocity', $U_{o,b}$. The far-field[3] variation of the centerline velocity is found to meet

$$\left(\frac{U_{o,b}}{U_c}\right)^2 = K_u \left[\frac{x - x_{01}}{H}\right], \tag{1.1}$$

where U_c is the local centerline mean velocity, x_{01} is the virtual origin, H is the nozzle opening width and K_u is the slope that describes the velocity decay for a plane jet. To deduce the decay rate of a plane jet, K_u is used. For a complete derivation, refer to George (1995).

Figure 1.2 demonstrates the time-averaged field of a plane jet. Plane jets are usually structured issuing into a quiescent fluid although a co-flow can also be used. An initial region lying between the jet origin and about $4H$ to $6H$ downstream is the potential core where the mean velocity is uniform. Within the potential core, the mean centerline velocity U_c is approximately equal to $U_{o,b}$. Following the potential core is the interaction or transition region, usually found between $6H$ and $20H$ downstream (Browne et al. 1982). In this region, large-scale vortices interact and facilitate momentum transport. Further downstream, the flow becomes self-similar and spreading, decay rates, turbulence intensity, etc, asymptote to a single dimensionless value.

[3]For a plane jet, the 'far-field' typically occurs downstream from $x/H \simeq 15$ to 20. The distance can vary, based on experimental conditions.

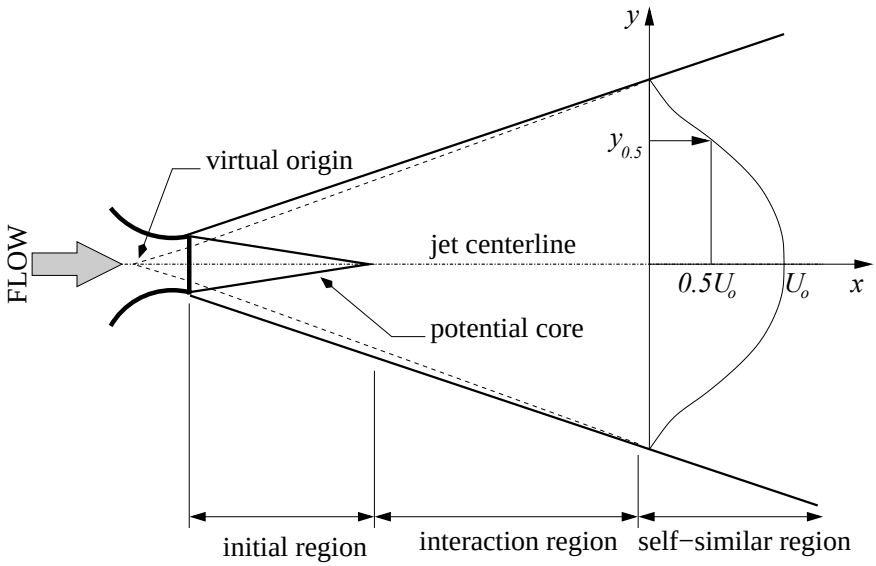

Figure 1.2: A schematic view of the time-averaged flow field of a plane jet. Redrawn after Browne et al. (1984).

The spreading rate of a plane jet is deduced from its lateral velocity measurements conducted across the jet at a number of downstream locations. Figure 1.2 shows a typical lateral profile of the mean velocity. The velocity half-widths $y_{0.5}$ is derived from the lateral profile following the definition: $y_{0.5}$ equals the y-value where the mean velocity U is $0.5\,U_{o,c}$. The velocity half-widths $y_{0.5}$ of a plane jet is known to meet

$$\frac{y_{0.5}}{H} = K_y \left(\frac{x - x_{02}}{H} \right), \tag{1.2}$$

where x_{02} is the virtual origin and K_y is the slope which describes the linear variation of $y_{0.5}$ and x. K_y is taken to be a measure of the jet spreading rate. Previous experimental studies show that a plane jet flow is governed by its initial and boundary conditions. Initial conditions include the jet exit Reynolds number and boundary conditions include the nozzle design parameters. Their concise definitions are presented below.

1.4 Definitions of Initial and Boundary Conditions

1.4.1 Reynolds Number of a Plane Jet

For a plane jet, the jet exit Reynolds number Re is defined using the nozzle opening width H, bulk mean velocity $U_{o,b}$ and kinematic viscosity ν of the test fluid using the expression

$$\mathrm{Re_o} = \frac{U_{o,b}\ H}{\upsilon} \tag{1.3}$$

If the jet issues through a smoothly contoured plane nozzle, its initial velocity profile is top hat. Hence, its bulk mean velocity $U_{o,b}$ is approximately equal to its centerline exit velocity $U_{o,c}$. This leads to an alternate definition of Reynolds number as $\mathrm{Re_{o,c}} = \frac{U_{o,c}H}{\upsilon}$. This definition is used in most terminology for the present investigation. The magnitude of Re is well-known to govern the flow field of a plane jet e.g. Lemieux and Oosthuizen (1984, 1985).

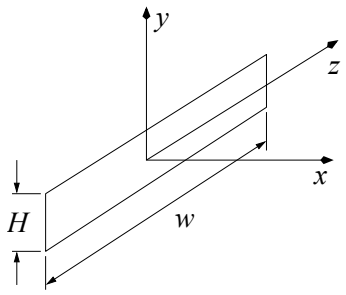

Figure 1.3: The nozzle aspect ratio, defined by $AR = w/H$ for a plane jet of nozzle dimensions $w \times H$.

1.4.2 Nozzle Aspect Ratio of a Plane Jet

The ratio of major axis (z) to minor axis (y) can be used to define the nozzle aspect ratio of a plane jet. This is calculated using the length of the long (w) and short (H) side of the plane nozzle respectively:

$$AR = \frac{w}{H} \tag{1.4}$$

As Pope (2002) pointed out, the nozzle aspect ratio (AR) of a plane nozzle must be large, typically 50 or more. This will ensure that, when measured in the center-plane ($z = 0$) of the plane nozzle, the flow is statistically two-dimensional and free from the effects of sidewalls.

1.4.3 Nozzle Geometry and Inner-Wall Nozzle Exit Contraction Profile

Based on the geometry of a particular nozzle e.g. circular, elliptic or rectangular, the flow field may vary to a significant extent. For example, the far field centerline mean velocity of a round jet issuing through a round nozzle varies as $U_c \sim x^{-1}$ whereas, for a plane jet issuing through a rectangular nozzle, the far field centerline mean velocity varies as $U_c \sim x^{-0.5}$. The transition of a laminar to a turbulent flow may also depend on nozzle geometry (Frank 1999). Therefore, nozzle geometry plays a key role in determining the flow features of turbulent jets.

The inner-wall nozzle contraction profile determines the nature of the downstream flow. The nozzle profile can be sharp-edged, smoothly or radially contoured or may constitute a long channel i.e. a pipe flow. The most commonly used nozzle profiles are a sharp-edged plate and a smooth contraction.

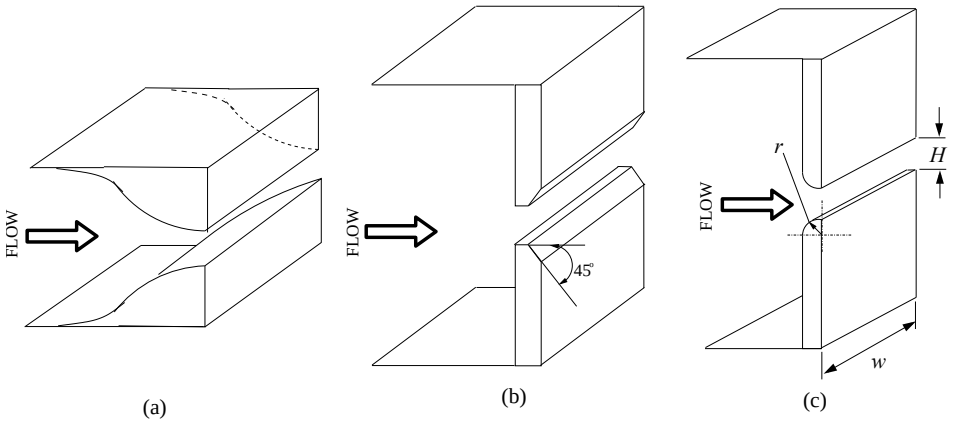

Figure 1.4: A schematic view of (a) a smooth contraction (b) a sharp-edged and (c) a radially contoured rectangular nozzle.

Figure 1.4 displays a typical smoothly contoured, sharp-edged orifice type and radially contoured rectangular nozzle. (Note that placing two sidewalls on either side of the short side of the rectangular nozzle will make the flow planar). There are significant differences between the inner-wall nozzle contraction profile of a smooth contraction and a sharp-edged orifice nozzle. A smoothly contoured nozzle has an inner-wall smooth contraction profile defined by a polynomial or sinusoidal curve. In particular, a smooth contraction nozzle produces a top hat initial velocity profile (Browne et al. 1982) and a sharp-edged orifice nozzle produces a saddle-backed initial velocity profile (Mi, Nathan and Nobes 2001). Correspondingly, the downstream flow properties of the two configurations are different. In principle, a top hat velocity profile achieves a laminar flow state at the nozzle exit. Such a configuration is capable of minimizing pressure drop in supply pipes and is widely accepted in industrial applications e.g. burner nozzles and compact mixing devices (Mi, Nathan and Nobes 2001). The standard sharp-edged orifice nozzle usually has a 45° bevel facing downstream (i.e. at the outer nozzle lip) and provides an 'inner sharp-edge' for the emerging jet. The saddle-backed profile results because the emerging fluid has an initial lateral inward component of velocity. This produces an initial rapid increase in the jet spreading rate. Because they are easier to manufacture, sharp-edged orifice nozzles both, round and rectangular, have found significant application in technical areas such as propulsion units of both conventional and V/STOL aircrafts, in dispersion of pollutant effluent, boiler furnaces and gas turbines (Quinn 1992b).

Another type of smoothly contoured nozzle is a radially contoured nozzle such as that used by Lemieux and Oosthuzin (1984, 1985). There are significant differences between smooth contraction and radial contraction nozzles. In a radially contoured nozzle, the nozzle contraction profile factor r^* is defined by

$$r^* = \frac{r}{H} \tag{1.5}$$

where r and H are inner-wall contraction radius and the nozzle opening widths respectively. The magnitude of r^* may be varied to change the inner-wall nozzle contraction profile. A very small r^*, say $r^* < 0.5$ provides a contraction profile approaching to that of a sharp-edged orifice nozzle. On the other hand, if the contraction profile factor is large, say $r^* > 2.0$, then the nozzle resembles a smooth contraction nozzle. The inner-wall nozzle contraction profile plays a significant role in determining the downstream flow of rectangular (and planar) jets.

1.4.4 Sidewalls in a Plane Jet

As shown in Figure 1.1, the sidewalls placed in the x-y plane are necessary to force the jet to behave in a statistically two-dimensional manner. Despite enhancing two-dimensionality, sidewalls impose a complex boundary condition on a plane jet. It is well known e.g. Frank (1999) that the drag force on a flat plate due to a boundary shear and hence due to the boundary layer development produces a significant effect (see Figure 1.14) on the flow. In general, the boundary layer increases in thickness with axial distance. In their study on vortex shedding from a circular cylinder, Szepessy and Bearman (1992) stated that the use of end plates on either side of the cylinder produces three-dimensional effects by interaction with the end plate boundary layer. End plates in cylinder wakes, which are usually slightly inclined to the flow (to adjust pressure gradient at cylinder ends), induce parallel vortex shedding. Thus, the use of sidewalls in a plane jet also imposes a particular boundary condition to the plane nozzle. In other words, a plane jet tested with and without sidewalls will have different boundary conditions. For the purpose of discussions in this thesis, the jet issuing through a rectangular nozzle with sidewalls will be called a *plane jet* and that without sidewalls will be called a *free rectangular jet*.

1.5 Literature Review

Previous investigations of round, rectangular and plane jets have assessed some dependencies of their properties on nozzle boundary conditions and Reynolds number. Early investigations by Corrsin (1943), Corrsin and Uberoi (1950), Corrsin and Uerio (1951),

Corrsin and Kistler (1955) and Corrsin (1962) on round jets, by Forthman (1934), Miller and Comings (1957) and Van Der Hegge Zijnen (1958) on plane jets and Sforza et al. (1966) and Trendscoste and Sforza (1967) on rectangular jets have demonstrated that each jet develops uniquely, depending on its boundary conditions. A comparison of the results of these investigations shows some dependencies of the flow statistics on boundary conditions and Reynolds number. The next section reviews the effect of these conditions on round, rectangular and plane jets.

1.5.1 Influence of Jet Exit Reynolds Number

Round Jets

Flow visualizations and qualitative analyses of the scalar field images of round jets unveil the dependence of the mixing field on the jet exit Reynolds number. Dimotakis et al. (1983) quantified the scalar-mixing behaviour of two round jets at $Re = 2.5 \times 10^3$ and 10^4 by measuring jet fluid concentrations in the plane of symmetry over the range $0 \leq x/D \leq 35$ and $0 \leq x/D \leq 200$. Here, x and D are the streamwise coordinates and round nozzle diameter respectively. Notably, their analysis identified a qualitative transition in the turbulence and turbulent mixing behaviour for Reynolds number in order of 10^4. Their visualization images showed unmixed reservoir fluid for $Re = 2.5 \times 10^3$ which encompassed the entire turbulent region while for $Re \simeq 10^4$, jet fluid of varying concentrations, and possibly better mixed, were noted throughout the turbulent region.

Miller and Dimotakis (1991) studied the effect of Reynolds number on the scalar field mixing in a high Schmidt number round jet. Their liquid phase data indicated a decrease in the scalar fluctuations with an increase in Re and an asymptotic behaviour of the scalar fluctuations at $Re \simeq 2.0 \times 10^4$. Thus, a more homogeneous, more chaotic and a well mixed state of scalar field was evident at a larger Re. In a somewhat related study on the mixing field of a chemically reacting gas phase turbulent jet, Gilbrech (1991) explored the relationship between Reynolds number and the slope of a flame length versus stoichiometric mixture ratio which was regarded as prime measure of the mixing rate with respect to Reynolds number. The far field mixing of the turbulent jet demonstrated a significant increase in the mixing rate at increased Re. An asymptotic state of jet mixing was noted at $Re = 2.0 \times 10^4$. Thus, their data verified that jet mixing became invariant at a critical Reynolds number of $Re = 2.0 \times 10^4$. Furthermore, Koochesfahani and Dimotakis (1986) produced scalar images of Laser-induced fluorescence streaks in a liquid phase shear layer at $Re = 1.75 \times 10^3$ and $Re = 2.30 \times 10^4$ (Figure 1.5). In their visualization, a more qualitative well mixing state of the scalar field is evident at $Re =$

2.30×10^4 when compared with $Re = 1.75 \times 10^3$. This indicates that mixing transition is more rapid when Reynolds number is larger.

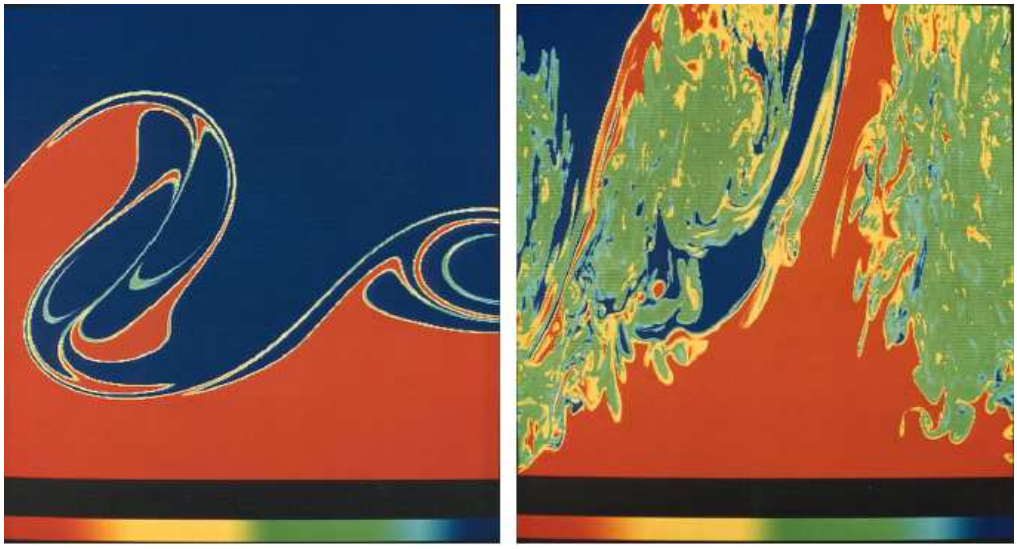

(a) (b)

Figure 1.5: Laser-induced fluorescence streak images of the scalar field in a liquid-phase shear layer for (a) $Re = 1.75 \times 10^3$ and (b) $Re = 2.30 \times 10^4$. Data from Koochesfahani and Dimotakis (1986).

It is quite well established experimentally that, at sufficiently high Reynolds number, the normalized mean velocity profiles and spreading rates of a round jet are almost independent of Reynolds number. This is demonstrated by Panchapakesan and Lumley (1993) (Re = 11,000) and Hussain et al. (1994) (Re = 95,500) who performed experiments using hot wire anemometry and Laser Doppler anemometry. Both investigations indicated that under these conditions, any difference in normalized mean velocity profiles and jet spreading rates are within experimental uncertainty and cannot definitely be attributed to any effect of Reynolds number. Similarly, the visualization of Mungal and Hollingsworth (1989) for their round jet at high Reynolds number ($Re \simeq 2.0 \times 10^8$) showed that its spreading rates and normalized mean velocity profiles are close to those of a laminar jet. In contrast, at low Reynolds numbers typically $<$ 10,000, both the mean and turbulence field depend significantly on Reynolds number. This is evident for example, from the results of Oosthuizen (1983) for a round jet measured at Reynolds numbers between 1,500 and 25,000 and from $x/D = 0$ and $x/D = 60$. He found significant dependence of centerline mean velocity and centerline turbulence intensity on Re. This dependence was even strong for Reynolds numbers below 10,000. Also found for a round jet by Ricou and Spalding (1961) was a decrease in entrainment rate with an increase in Reynolds number.

Their entrainment rates reached an asymptotic value when $Re \geq 25{,}000$. After a careful review of reacting and non reacting flows, a criterion for fully developed turbulence for round jets was developed by Dimotakis (2000). This criterion states that 'In view of the wide variety of different flows, there exist a property of turbulence which induces it to transition to a well mixed state, is associated with Reynolds numbers in access of $\sim 10^4$ regardless of flow geometry'. Such a notion appears to be a more general view of turbulence. However, its validity has yet to be assessed for a plane jet whose nozzle geometry may induce differences in the downstream flow.

Plane Jets

Similar to a round jet, the flow field of a plane jet is also found to be *Re*-dependent. In his doctoral thesis on the mixing field in a two-dimensional turbulent flow, Konrad (1976) noted that the transition of the gas phase shear layer to three-dimensionality and the subsequent ability of the flow to sustain such three-dimensional fluctuations first occur when $Re \simeq 10^4$. Lemieux and Oosthuzin (1984, 1985) studied a plane air jet at *Re* over the range $700 \leq Re \leq 4{,}200$ using plane nozzles with rounded edges (i.e. radially contoured). Lemieux and Oosthuzin noted a strong influence of Reynolds number on the lateral and normal shear stresses, jet decay and spreading rates. Furthermore, a small influence of *Re* was found on the longitudinal normal stresses and the normalized mean velocity profiles. Importantly, Lemieux and Oosthuzin (1984, 1985) concluded that their jet properties become *Re*-independent when $Re > 4{,}200$. However, their conclusion is questionable because they did not assess the effect of Reynolds number greater than 4,200. The certainty of their statement is unveiled by the measurements of Namar and Ötügen (1988). They studied the effect of Reynolds number in a quasi-plane jet[4]. Over the range $Re = 1{,}000$ to 7,000, their studies revealed that Reynolds number has a significant effect on jet development throughout the entire mixing field. A more detailed study by Everitt and Robbins (1973) for plane jets of *Re* over the range 16,000 to 75,000 and of nozzle aspect ratios over the range $21 \leq AR \leq 128$ found a large scatter in the decay of centerline mean velocity. Since their nozzle aspect ratios also vary with Reynolds number, this scatter is probably associated with that variation. That is, at (Re, AR) = (16,000, 128), $K_u \simeq 0.18$-0.21, at (Re, AR) = (30,000, 64), $K_u \simeq 0.17$-0.19 and at (Re, AR) = (75,000, 21), $K_u \simeq 0.19$-0.22. Such an investigation is incapable of determining

[4]'Quasi-plane' jet is a plane jet that is statistically two-dimensional up to a reasonable axial extent because it issues through a very high aspect ratio rectangular nozzle. The rectangular nozzle does not have sidewalls, thus, three-dimensional are likely to take place, even in the near field where the flow is statistically two-dimensional. Hence, the present plane jet is distinct from a quasi-plane jet. This effect is discussed separately in Chapter 6, where a quasi-plane jet is also called a free rectangular jet.

which parameters contribute most to the differences in the flow field.

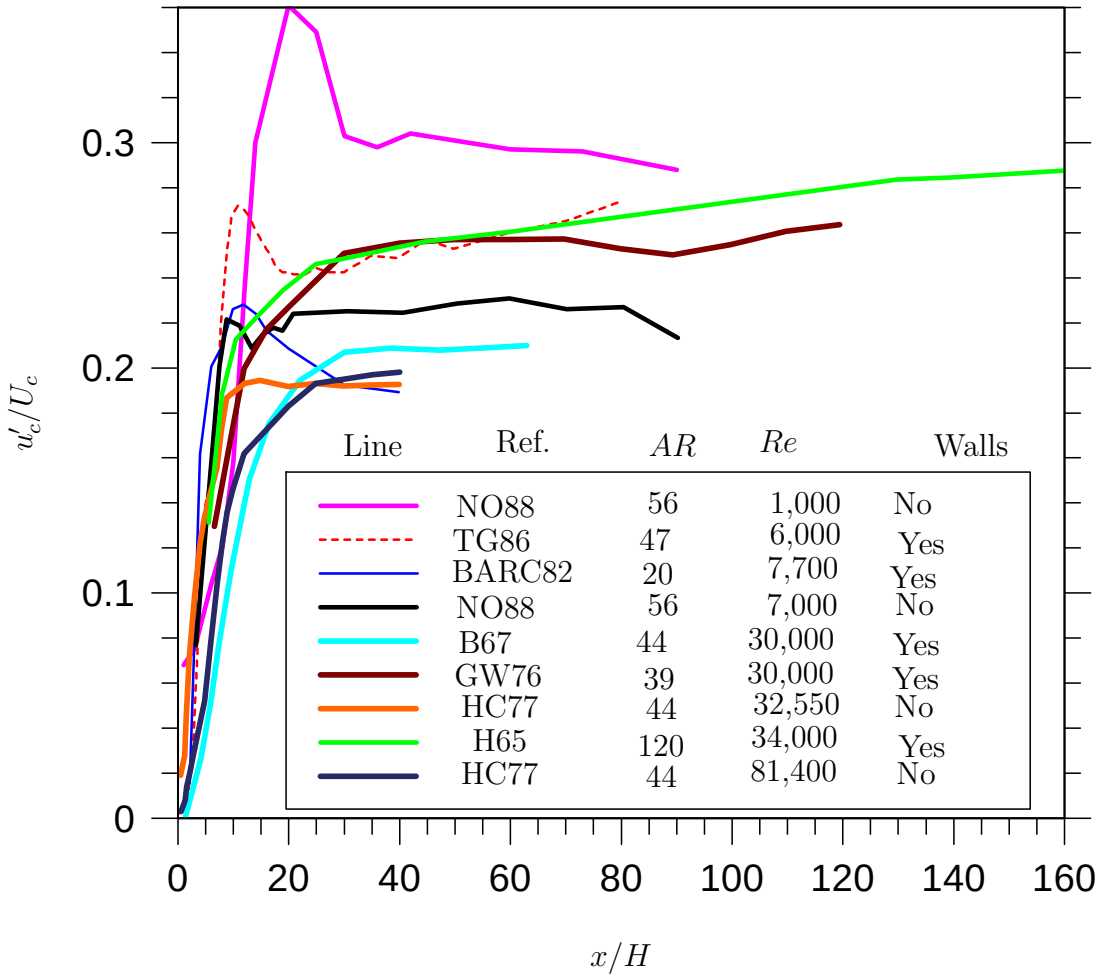

Figure 1.6: Summary of previous measurements of Reynolds number effect on the centerline turbulence intensity of a plane jet. Note: HC77 - Hussain and Clark (1977), GW76 - Gutmark and Wygnanski (1976), B67 - Bradbury (1965), H65 - Heskestad (1965), BARC82 - Browne *et al.* (1982), NO88 - Namar and Ötügen (1988) and TG86 - Thomas and Goldschmidt (1986).

Although the finding that Reynolds number has an influence on a plane (or quasi-plane) jet is widely recognized, there are significant inconsistencies between the data of previous investigations even at comparable Reynolds numbers, nozzle aspect ratios and with similar boundary conditions. Figure 1.6 displays the centerline variations of the turbulence intensity $u_{n,c}^{'} = u_c'/U_c$, where U_c and u_c' are the centerline mean and root-mean-square (rms) of the axial velocity respectively, of plane jets. As is well known (e.g. Boersma et al. (1998)), the presented data of $u_{n,c}^{'}$ shows a hump for $x/H < 3$, which is associated with the passage of coherent Kelvin-Helmholtz vortices in the mixing layers of the jet. The best agreement is between the data of Gutmark and Wygnanski (1976) and those of

Heskestad (1965) with different nozzle aspect ratios, $AR = 39$ and 120 respectively but similar Reynolds numbers. Their results agree closely within the mid field i.e. $x/H \leq 60$ but there is some difference in the very far field i.e. $x/H > 60$. These differences may be due to the nozzle geometry i.e. sharp-edged for Heskestad (1965) and smooth contraction for Gutmark and Wygnanski (1976). However, the results from smoothly contracting nozzles of Gutmark and Wygnanski (1976) and Bradbury (1965) for relatively high aspect ratios ($AR = 39$ and 40) and identical Reynolds numbers ($Re = 30{,}000$ for both) are quite different. These differences might be attributed to the use of a co-flow (co-flow-to-jet velocity ratio $\simeq 16\,\%$) in Bradbury (1965), any associated differences between the nozzle surface finish (for instance, rough or smooth) or to some errors in their measurements. However, it is considered that the above mentioned magnitude of a co-flow may explain the different centerline turbulence intensity.

Further comparison between the results of Browne et al. (1982) and Thomas and Goldschmidt (1986) also reveal significant differences. These flows have similar Reynolds numbers of $Re = 7{,}700$ and 6,000 but different nozzle aspect ratios of 20 and 44. Significant differences are evident in the near field where the effect of nozzle aspect ratio is expected to be weaker than in the far field. The configurations of Thomas and Goldschmidt (1986) and Namar and Ötügen (1988) have similar nozzle aspect ratios and Reynolds numbers but the jet of Namar and Ötügen (1988) is not comparable with a planar jet due to the absence of sidewalls in their facility. This is also the case of Hussain and Clark (1977) who studied at $Re = 32{,}500$ and 61,400, a quasi-plane nozzle of aspect ratio of $AR = 44$, even though they claimed their jet to be planar. Their results have the lowest mid-field turbulence intensity despite this value being similar to that of Browne et al. (1982), who did use sidewalls but a lower Reynolds number of 7,700. Their mid-field turbulence intensity is also significantly lower than that of Namar and Ötügen (1988) who used $Re = 7{,}000$.

It is important to mention that the differences in normalized rms evident in Figure 1.6 are due to a combination of differences in Reynolds number and boundary conditions. The probable cause of the differences in turbulence intensities noted in Figure 1.6 include the different *local* Reynolds numbers for these jets. Here, the local Reynolds number, Re_{local} is calculated by $Re_{local} = 2(y_{0.5})(U_c)/\nu$. Since the spreading rates of all these jets are different, Re_{local} must play some role in determining the region of self-similarity. As deduced analytically by George (2005) that for a plane jet, Re_{local} increase as $x^{1/2}$. Therefore, no matter how low the initial Reynolds number is, all plane jets ultimately approach very high local Reynolds numbers in the far field. Thus, the viscosity term

in the momentum equation, which scales with $1/Re_{local}$, will diminish with downstream distance. In other words, the moments of velocity fluctuations must asymptote in the far field. Nevertheless, if the initial Reynolds number is low, then a larger downstream distance is required for Re_{local} to become appropriately large, for the viscous terms to become negligible. However, nozzle aspect ratio also influences the self-similar state of a plane jet. For a real plane jet with a finite nozzle aspect ratio, it is only possible to have planar flow for a limited distance downstream. Hence, low Reynolds number plane jet can only achieve a high Reynolds state if the nozzle aspect ratio is sufficiently large. Otherwise, the plane jet will cease to be planar before the high Reynolds number state is achieved and will therefore never attain self-similarity. This foresees that the turbulence intensity of a plane jet issuing from a high-aspect-ratio nozzle, but measured at a low Reynolds number will eventually asymptote at a larger downstream distance compared to another nozzle of equivalent aspect ratio measured at a high Reynolds number.

Clearly, the wide range of different conditions makes it impossible to isolate the effect of Reynolds number from that of other variables. The most recent work on plane jets were conducted by Stanley et al. (2002) and Klein et al. (2003) using direct numerical simulations (DNS) at Re = 3,000 and for $Re \leq$ 6,000, respectively. Both investigations only examine the near and transition fields i.e. for $x/H \leq 15$ and $x/H \leq 20$, respectively, even though Klein et al. (2003) claimed that their investigation covered the far field. Although, importantly, Klein et al. (2003) measured the influence of Reynolds number, their work is only limited to $Re \leq$ 6,000. It is clear that the conclusive quantitative data describing the Re dependence of a plane jet is not presently available.

1.5.2 Effect of Inner-Wall Nozzle Exit Contraction Profile

The structural design of a nozzle determines to some extent the downstream flow properties of a round, rectangular or a plane jet. A careful assessment of a variety of previous investigations reveal that the initial velocity profiles of a round jet are dependent on the nozzle geometry (Mi, Nathan and Nobes 2001). This is also true for rectangular jets. For instance, Tsuchiya et al. (1989) studied the effect of nozzle geometry, i.e. nozzle profile and aspect ratio using a rectangular nozzle. The most commonly used configuration is that of a smooth contraction (Figure 1.7). For example, Namar and Ötügen (1988) used a smoothly contoured quasi-plane nozzle to measure the velocity field while Husain and Hussain (1983) measured a round jet. A carefully designed smoothly contoured configuration prevents internal flow separation and produces a 'top hat' velocity profile at the exit plane. A top hat velocity profile has a very thin boundary layer. In this case, a

large velocity difference exist between the jet and its ambient fluid resulting in the shear layer being highly unstable (Alkislar and Lourenco 2004). A schematic view of a smooth contraction plane nozzle is shown in Figure 1.7.

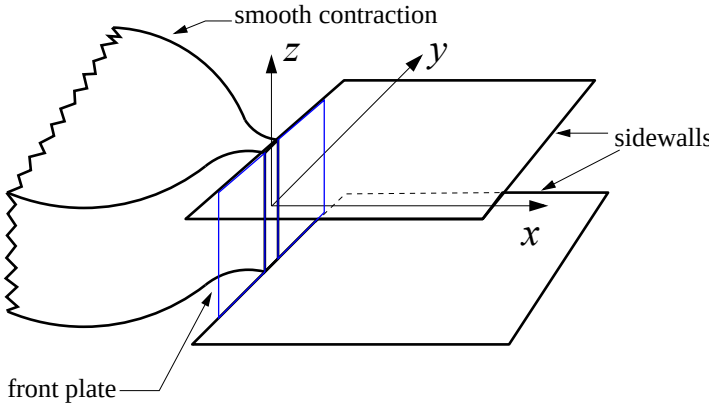

Figure 1.7: A schematic view of a smooth contraction plane nozzle, used by Antonia *et al.* (1982), Thomas and Goldschmidt (1986) and Gutmark and Wygnanski (1976).

For a round jet, a pipe flow has also been investigated. The difference in the initial flow of a pipe and a smoothly contoured nozzle is significant. For a round pipe jet, the profile closely approximates the relation $U/U_c = (1 - 2r/D)^{1/n}$ where r and D represent the radial distance from the center and the nozzle diameter, respectively (Mi, Nathan and Nobes 2001); n = 5-7, Schlichting (1979), pp 596-600. On the other hand, sharp-edged orifice nozzles have also been investigated. A sharp-edged orifice nozzle has an inner-wall sharp-edge with the downstream facing a 45° bevel to force the flow to undergo a sudden expansion upstream from the exit plane. This expansion leads to an initial separation of the flow, a few diameters upstream from the exit and thus produces a saddle-backed initial velocity profile. (Quinn 1992b).

Some studies have been performed on the influence of nozzle contraction profiles i.e. sharp-edged orifice, smoothly contracting or a pipe flow configuration of round jets but no systematic study of these issues are available for plane jets. Hussain and Zedan (1978) showed that, for a round jet the spreading rates and turbulence intensity are dependent on whether the flow is initially laminar or turbulent. Higher spreading rates and increased turbulence intensity were evident for an initially turbulent boundary layer. Other investigations on the effect of nozzle contraction profiles of round jets for the velocity and scalar fields include Mi, Nathan and Nobes (2001), Mi and Nathan (2004), Antonia and Zhao (2001) and Ferdman et al. (2000). These have compared the flow from a smoothly contracting, a sharp-edged orifice nozzle and pipe flow. Mi and Nathan (2004) noted that

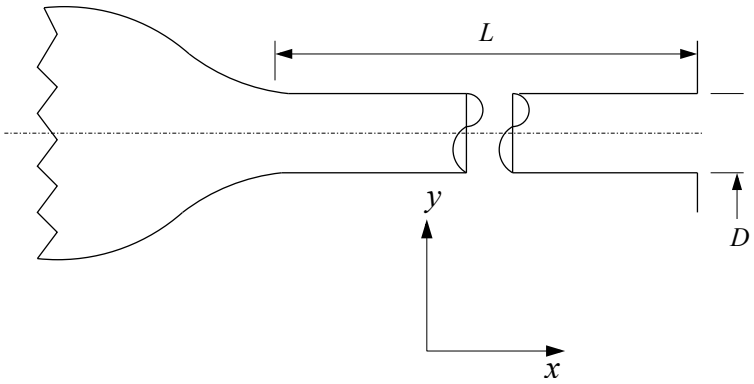

Figure 1.8: A long pipe nozzle $L >> D$ as used by Antonia and Zhao (2001), Mi *et al.* (2001) and Mi and Nathan (2004).

a round orifice nozzle produces the highest centerline mean velocity decay, followed by the smoothly contoured nozzle and then the long pipe. They also noted a higher vortex formation frequency $St_D = f\,D/U_o$ of 0.70 for a sharp-edged nozzle when compared with a reduced St_D of 0.40 for a smoothly contoured nozzle. Here, f was obtained by detecting the dominant peak in the velocity power spectra measured at $x/D = 3$ (within potential core) and in the shear layers of their axisymmetric jet.

Ashforth-Frost and Jambunathan (1997) studied the effect of nozzle geometry in round jets. They compared a fully developed turbulent and a flat plate top hat velocity profile from a round nozzle using LDA measurements. The uniform velocity region was 7 % longer for the jet with fully developed initial velocity profile. A more rapid increase in turbulence intensity for $x/D < 2$ was noted for the jet with a flat initial velocity profile. It was found that the maximum turbulence level in the flat-profile jet was higher, which occurred further upstream than in the fully developed jet. Also, the turbulence intensity was found to decay more rapidly for the jet with a flat initial velocity profile. The axial turbulence intensity showed a distinct peak which occurred in the flat-profile jet at $x/D = 8$ as opposed to a gradual rise to a plateau in the fully-developed-profile jet. Hence, for round jet, these findings show that the nozzle contraction profile not only affects the mean, but also the turbulence field.

In contrast, only a few measurements of the influence of nozzle profiles on a plane jet have been conducted. Hussain and Clark (1977) investigated the influence of the initial boundary layer on the velocity field using a smoothly contoured quasi-plane nozzle. As with the findings of Hussain and Zedan (1978), they noted the downstream mean and turbulent quantity to be highly dependent on the initial boundary layer. A laminar boundary

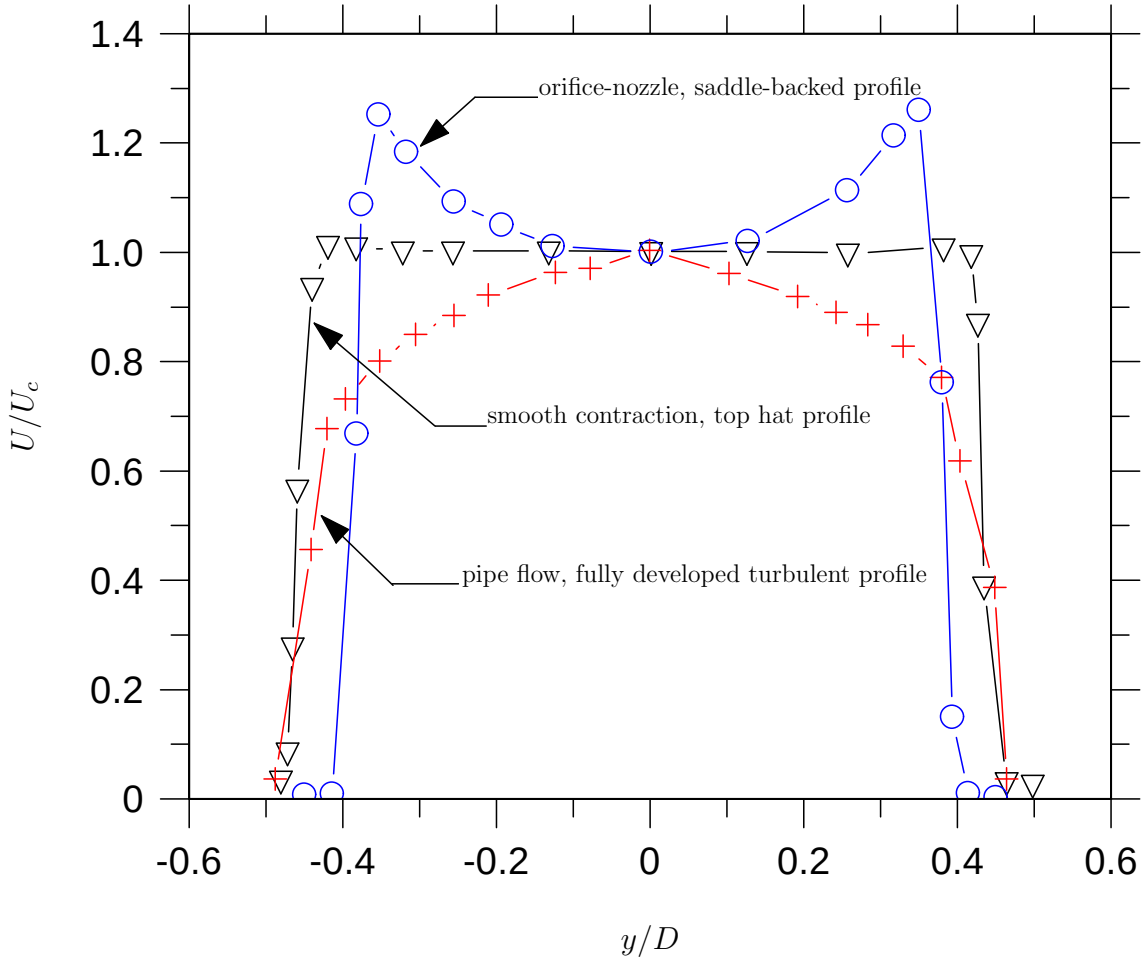

Figure 1.9: Initial velocity profiles from a sharp-edged orifice plate, a smooth contraction nozzle and a long pipe for a round jet. Data extracted from Mi, Nathan and Nobes (2001).

layer resulted in a larger mass flux and an earlier development of turbulence intensity into their self-preserving state for Hussain and Clark's quasi-plane jet. Later, in a study on the spreading rate from a contoured planar nozzle, Goldschmidt and Bradshaw (1981) obtained a larger jet spreading angle for jets with higher exit turbulence intensity at the jet centerline. For their work, the intensity levels were varied using different turbulence generators upstream from the smoothly contoured nozzle. Two cases, one with an initially laminar boundary layer and the other with a turbulent boundary layer were investigated by Chambers et al. (1985). Such a condition was achieved by using a standard smooth contraction nozzle and the other, a smooth contraction nozzle followed by a long channel extending to $40D$ downstream (similar to Figure 1.8). Using Schlieren photography and spectral analysis, they showed highly organized and symmetric large-scale structures in the shear layers for an laminar case. Also speculated from their data are strong mixing rates for the initially laminar case. For their initially turbulent case, the structures were highly three-dimensional and asymmetric about the centerline. Hence, some dependence

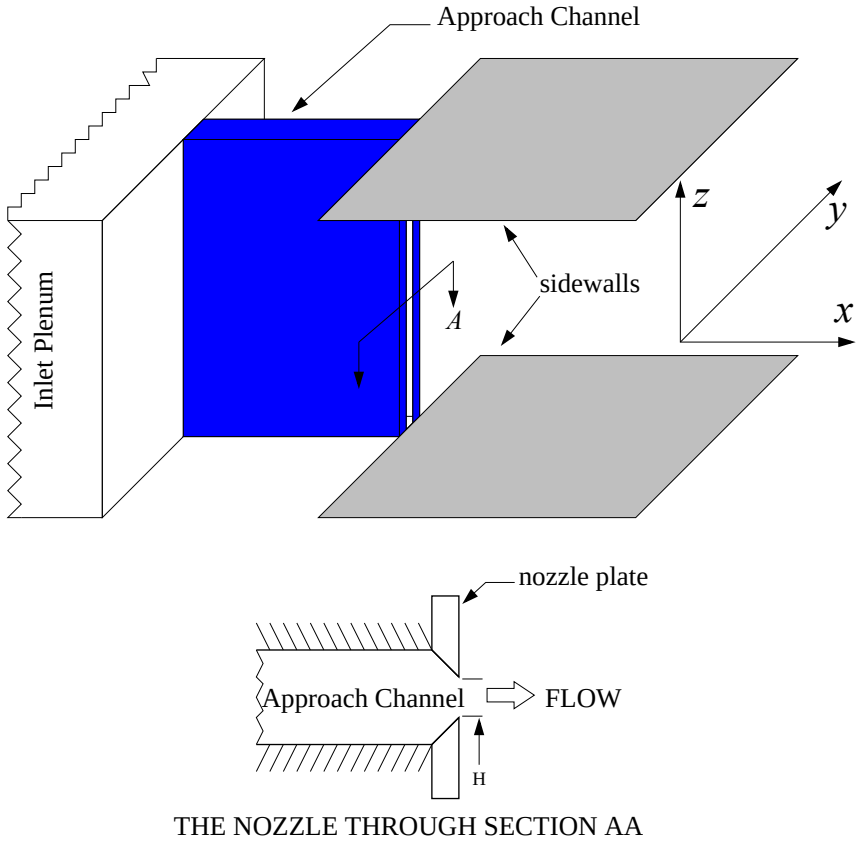

Figure 1.10: A schematic view of the sharp-edged orifice nozzle used by Heskestad (1965).

of flow statistics on nozzle profiles have already been established for a plane jets.

The present survey of published data reveals that there is a limited number of previous investigations of sharp-edged orifice plane nozzles. It appears that Heskestad (1965) is the only previous investigator who has measured the flow through a plane orifice nozzle. Thus, more studies using sharp-edged orifice plane nozzles are warranted. Given the sensitivity of jet flow to initial and boundary conditions, a direct assessment of the effect of nozzle contraction profile (i.e. a sharp-edged or contoured) requires comparisons to be made in the same laboratory using identical facilities and instrumentation.

In addition, a sharp-edged orifice nozzle is typically easier to manufacture than a smooth contraction nozzle (Mi and Nathan 2004) and have significant potential for practical application (Quinn 1992b). For example, rectangular orifice nozzles are used propulsion units in aircraft, in dispersion of the effluent pollutant, in some boilers and furnaces and gas turbine power plants (Quinn 1992b). This has stimulated a number of fundamental investigations on sharp-edged orifice nozzles for round jets (Mi and Nathan 2004, Mi, Nathan and

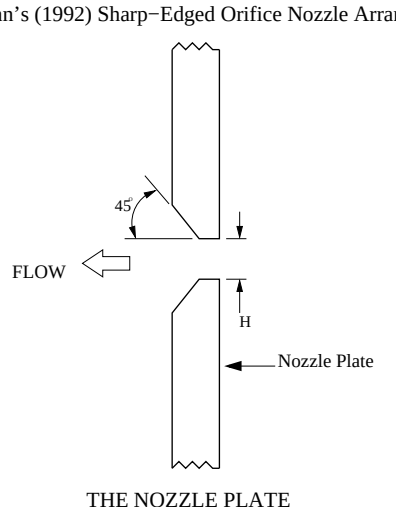

Figure 1.11: The orifice plate used by Quinn (1992b).

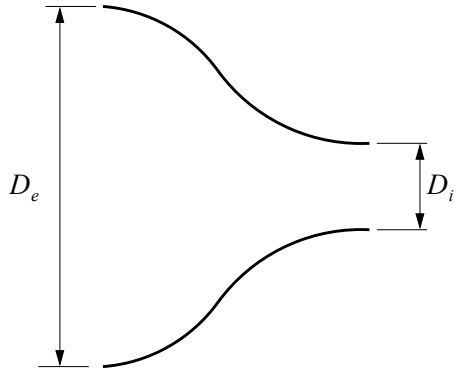

Figure 1.12: The round nozzle used by Klein and Ramjee (1972) and Ramjee and Hussain (1976). Note that the nozzle contraction ratio is the ratio of D_i and D_e.

Nobes 2001, Hussain and Zedan 1978, Antonia and Zhao 2001). Likewise, it has also stimulated fundamental research on sharp-edged orifice rectangular jets (Quinn 1992a, Tsuchiya et al. 1985, Gutmark and Schadow 1987). Hence the present investigation will expand the existing body of literature of plane jets issuing from sharp-edged orifice nozzles.

Additionally, no previous study has performed a systematic investigation of the effect of varying the inner-wall nozzle contraction profile of a plane nozzle and hence of varying the initial velocity profiles from that of a saddle-backed i.e. typical of a sharp-edged orifice nozzle, to a uniform top hat i.e. typical of an ideally contoured nozzle. However, as revealed by literature, some data on the effect of having different contractions i.e. the ratio of the nozzle internal diameter to nozzle exit diameter, is already available for a round nozzle. Klein and Ramjee (1972) explored the effects of contraction geometry on non-isotropic free-stream turbulence using eight circular cross sections of varying contour

shapes and non-dimensional lengths. Their study found an increase in turbulent kinetic energy in both the lateral and longitudinal directions along the contractions. Importantly, they found that neither the contour shapes, nor the ratio of length to diameter of the nozzle, produce any variations in turbulent kinetic energy. These parameters also did not affect the turbulence intensity at the nozzle exit. Nonetheless, the only parameter that produced a significant influence on the turbulent kinetic energy was the contraction ratio CP, where $CP = \left(\frac{D_i}{D_e}\right)^2$. Here, D_i and D_e are the inlet and exit diameters of the round nozzle respectively. See Figure 1.12 for details.

Ramjee and Hussain (1976) measured the effect of the round nozzle contraction profile CP on the initial turbulence intensity using hot wire anemometry. Varying the nozzle contraction profile ratio CP between $11 \leq CP \leq 100$, they noted an increase in total kinetic energy with an increase in CP. Furthermore, their study demonstrated that the magnitude of CP is highly effective in controlling the turbulence intensity in the initial region of the round nozzle. In particular, they noted that as CP was increased, the levels of the turbulence intensity were reduced. Although, they did not measure the downstream flow, their study shows that the initial turbulence intensity depends on nozzle contraction profile. Considering the finding by George (1989), that the nature of the far field flow is sensitive to the initial flow, we can expect the nozzle contraction profile will have a definite influence on the downstream flow. However, no study has been performed on this issue for a plane jet, stimulating the present investigation to address this need.

1.5.3 Effect of Nozzle Aspect Ratio on Rectangular and Plane Jets

Nozzle aspect ratio is a critical boundary condition for any pseudo two-dimensional flow. Determined from the nozzle design parameters, this conditions is known to affect the downstream flow. The assessment by Gouldin et al. (1986) revealed that statistical variations in jet flow properties of plane, rectangular and round jets are manifestations of nozzle boundary conditions. In particular, nozzle aspect ratio was postulated to affect the axial distance at which a rectangular jet attains self-similarity. Their documentation revealed that previous investigations speculated that attainment of a jet flow to self-similarity is dependent on nozzle aspect ratio. With a view to clear such speculations, studies that varied nozzle aspect ratio of rectangular jets have already been performed. However, it is important to note that almost all these investigations have been performed for free rectangular jets, which are distinctly different from plane jets. In particular, Trendscoste and Sforza (1967), Quinn (1992b) and Marsters and Fotheringham (1980) have measured

free rectangular jets of different nozzle aspect ratios.

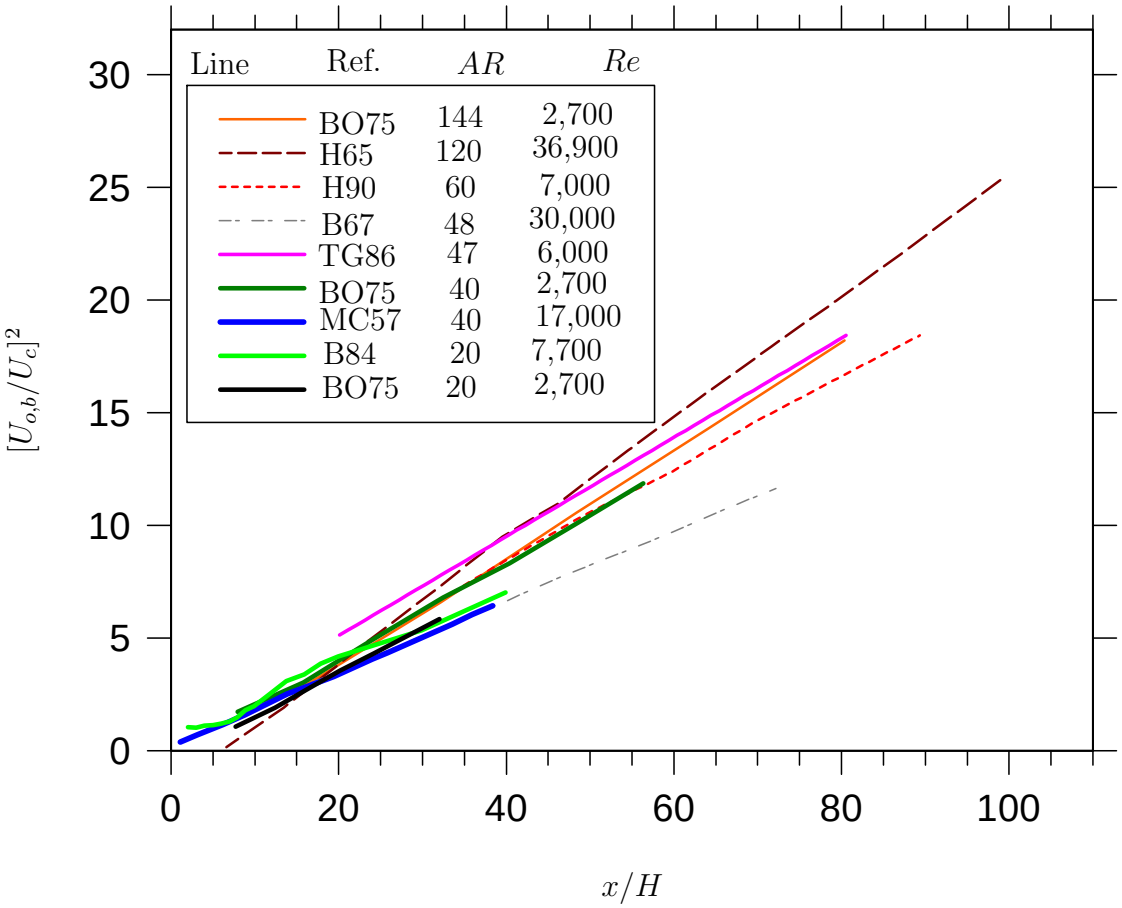

Figure 1.13: The range of data sets of previous measurements of the mean velocity decay of a plane jet at various nozzle aspect ratios. Here, BO75 refers to Bashir and Uberio (1975), H65: Heskestad (1965), H90: Hitchman *et al.* (1965), TG86: Thomas and Goldschmidt (1986), MC57: Miller and Commings (1957) and B84: Browne *et al.* (1984).

Trendscoste and Sforza (1967) undertook a pioneering investigation on the effect of AR on a free rectangular jet. Their nozzle aspect ratios were in the range $2.5 \leq AR \leq 100$. Increasing lengths of the jet potential core, decreasing decay of centerline velocity and a smaller jet spreading rate were noted for increasing nozzle aspect ratios. Just over a decade later, Sfeir (1979) performed another independent study using sharp-edged rectangular nozzles. He examined nozzle aspect ratios in the range $10 \leq AR \leq 60$ and found similar dependencies to those of Sfeir (1979). Given that these previous studies were subjected to a much larger range of aspect ratios, Marsters and Fotheringham (1980) further investigated a lower range of aspect ratios between $3.39 \leq AR \leq 11.88$. Later, many other studies (Krothapalli et al. 1981, Tsuchiya et al. 1985, Quinn 1992a) were performed, all of which focused on the nozzle aspect ratio issues. In particular, Quinn (1992a) investigated

nozzle aspect ratios between $2 \leq AR \leq 20$ found that the rate of near field mixing increases with increasing aspect ratio up to $AR = 20$ and hence increased three-dimensionality. His work found that the shortest jet potential core, highest shear layer turbulent kinetic energy and Reynolds shear stresses and largest turbulent transport of Reynolds stresses occur for $AR = 20$ relative to other nozzle aspect ratios. Furthermore, Tsuchiya et al. (1989) produced flow visualization images of rectangular 'pipe-type' jets[5] of nozzle aspect ratios 2, 5 and 10. Similar to Quinn (1992b), Tsuchiya found a shorter potential core, an increase in spreading rate and an enhanced mixing rate for $AR = 10$ relative to $AR = 2$. Recently, we documented the characterization of rectangular jets from high aspect ratio nozzles (Mi et al. 2005b), between $15 \leq AR \leq 120$ (see appendix for the paper which has been reviewed and accepted for publication). In this study, we noted that a rectangular jet may be characterized by three distinct zones: an initial quasi-plane jet zone, a transition zone and a final quasi-axisymmetric-jet zone. The extent of the quasi-plane zone was found to be dependent on nozzle aspect ratio. Together with published data, the fundamental findings of our experiments indicated a strong influence of nozzle aspect ratio in rectangular jets.

The results of the investigations on free rectangular jets are sufficient to deduce that nozzle aspect ratio is important in determining the downstream flow for a plane jet. This foresees that a plane jet may also show a similar dependence. Van Der Hegge Zijnen (1958) and Bashir and Uberoi (1975) have performed some measurements to address the effect of nozzle aspect ratio on plane jets. In their measurements of velocity decay rates for $AR = 20$ and 25, Van Der Hegge Zijnen (1958) found that, as AR is increased, the jet attains a higher decay and its virtual origin moves upstream. Similarly, Bashir and Uberoi (1975) presented similar findings for $AR = 20$, 40 and 144 for their heated plane jet. However, all of their measurements were performed in the self-similar region. On the other hand, Bashir and Uberoi (1975) and Van Der Hegge Zijnen (1958) did not attempt to actually study the near field flow or the moments of higher order fluctuations. In other words, a complete assessment of the nozzle aspect ratio on a plane jet was not made.

Gouldin et al. (1986) suggested that the transition of a rectangular jet from a two-dimensional to a three-dimensional flow is more rapid when nozzles have a smaller aspect ratio. This is because the axial growth of the sidewall boundary layer and perhaps some secondary influence may induce significant interference to the two-dimensional jet. Thus

[5] 'Their pipe-type jet' had a rectangular parallel part of length $l = 300$ mm, extending from a plenum.

a very low aspect ratio jet may never attain self-similarity. Their perception provides sufficient evidence to conclude that nozzle aspect ratio has an impact on the self-similarity of a true plane jet. In fact, Gouldin et al. (1986) have criticized the measurements of Browne et al. (1982) from their plane nozzle of aspect ratio = 20 to be not free from three-dimensional effects stemming from their low aspect ratio nozzle. This highlights the need for a study of differing aspect ratio of planar nozzles.

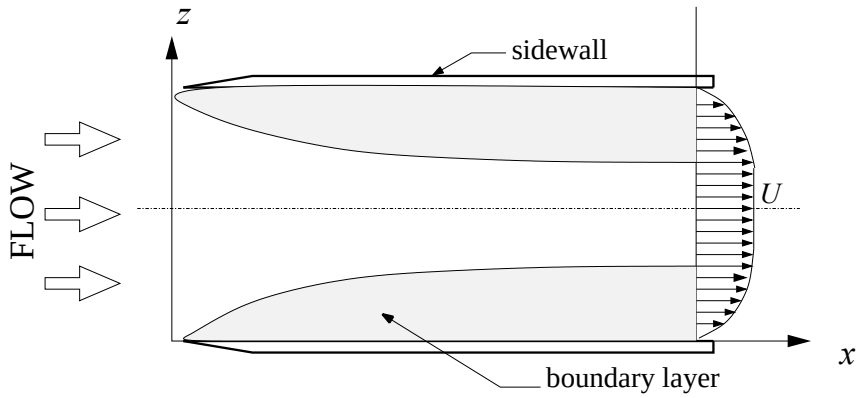

Figure 1.14: The growth of boundary layer due to a flow past a wall. Modified after Frank (1999).

From published data on plane jets, it can be deduced that nozzle aspect ratio influences the maximum range of axial distances (x/H) up to where measurements can be taken without the significant effects of boundary layers induced by the sidewalls. A schematic view of the growth of boundary layer due a a flow past a sidewall is shown in Figure 1.14. This figure has been modified after Figure 3.11 in Frank (1999) which discussed the drag force on a flat plate due to boundary shear. It is notable that, with an increase in x, the boundary layer gets thicker. Thus, when the aspect ratio of the nozzle is too small, the boundary layers from both sides of the wall will merge into the jet. Based on this knowledge, the measured range of x/H can depend on the nozzle aspect ratio. Hence, it is deduced that for realistic investigations of plane jets, the axial extent of measurements will be limited by nozzle aspect ratio.

To verify the limitations in the range of x/H for plane jet measurements, we turn to published data. Figure 1.13 shows the normalized profiles of the mean centerline axial velocity for plane jets. It shows clearly that investigations whose AR are large (typically $>$ 45) are able to provide data of their plane jets up to $x/H = 100$. For example, Heskestad (1965), Hitchman et al. (1990), Bradbury (1965) and Thomas and Goldschmidt (1986) present data beyond $x/H = 40$. However, the lower aspect ratio investigations do not.

This suggests that the authors did not undertake far field measurements in regions where the influence of the sidewalls were significant. The results of Bashir and Uberoi (1975) who investigated three aspect ratios support this deduction since their different range for each nozzle aspect ratio is clearly not limited by the apparatus in their investigation. For instance, when $AR = 20$, their data extends up to $x/H = 40$ whereas for $AR = 144$, their data extends up $x/H = 80$. These trends are clearly evident in Figure 1.15. While some authors acknowledge that aspect ratio may limit their ranges of x/H, none of them produced any direct measure of its extent.

Although plane jet investigations have been conducted at several nozzle aspect ratios, there are significant inconsistencies that prevent a thorough examination of the effect of nozzle aspect ratio. Most significantly, these investigations have been performed with different initial conditions, preventing isolation of the role of aspect ratio alone. For example, Bradbury (1965) and Thomas and Goldschmidt (1986) examined plane jets with similar aspect ratios but their Reynolds numbers, nozzle geometry and co-flow conditions are different i.e. Re = 30,000 for Bradbury (1965) but measured with a co-flow, while Re = 6,000 for Thomas and Goldschmidt (1986) but measured without a co-flow. Such differences could account for the significant differences in the decay of their mean centerline velocity. The best indication of nozzle aspect ratio dependencies are given by Bashir and Uberoi (1975) who investigated smoothly contoured nozzle flow at Re = 2,770 and nozzle aspect ratios between $20 \leq AR \leq 144$. Their data shows that the $AR = 144$ jet decays most rapidly (Figure 1.13) and the asymptotic values of normalized turbulence intensity are lowest (Figure 1.15). However, due to lack of sufficient data in the near field, no conclusions regarding the near field mean velocity and turbulence intensity can be made. The sharp-edged orifice nozzle of Heskestad (1965) with $AR = 120$ showed the highest decay of mean centerline velocity and the biggest turbulence intensity. While it appears that Bashir and Oberoi's findings broadly support Heskestad's results, other contributing factors such as the use of a sharp-edged orifice nozzle by Heskestad prevents a definitive comparison. Although there is reasonably good agreement between the mean centerline velocity data of Bashir and Uberoi (1975) and Browne et al. (1982) for $AR = 20$ (Figure 1.13), their turbulence intensities are quite divergent (Figure 1.15). This could possibly be an effect of Reynolds number difference (Re = 2,770 for Bashir and Oberoi and Re = 7,700 for Browne et al. (1982)) or some other experimental conditions.

Clearly, the wide range of differing conditions and the large scatter in data makes it impossible to determine exactly how nozzle aspect ratio affects the flow in the near and

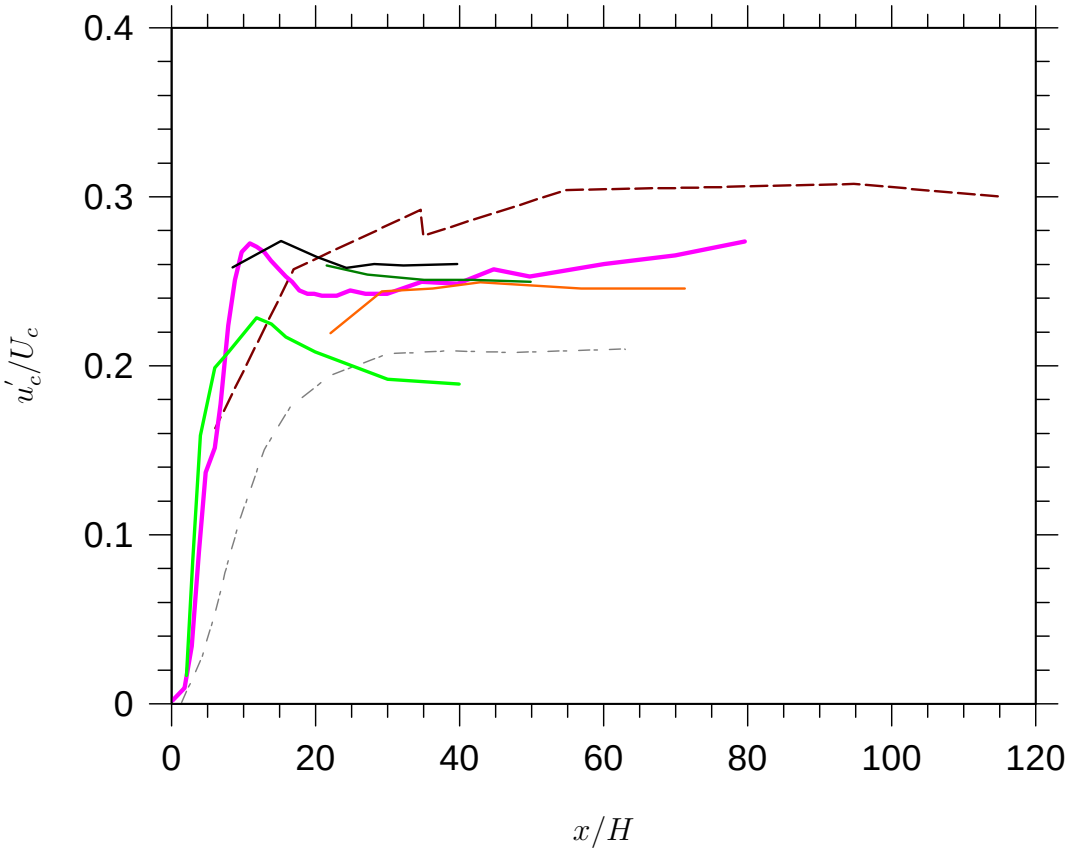

Figure 1.15: A summary of previous measurements of the turbulence intensity of plane jet investigations, at different nozzle aspect ratios. Note: Symbols identical to Figure 1.13.

far field. Thus, a systematic study of the effect of nozzle aspect ratio for both the near and far field is needed. This need is addressed in the present investigation.

1.5.4 Sidewalls in a Plane Jet

Chapter 1.3 has defined a plane jet as a statistically two-dimensional jet which has a dominant mean motion in the streamwise (x) direction, jet spread in the lateral (y) direction and zero entrainment in the spanwise (z) direction (see Figure 1.1 for the coordinates system and schematic view of a plane jet). To comply with the requirement for two-dimensionality, sidewalls attached to the short sides of the nozzle and placed in the x-y plane are necessary. In fact, published data on plane jets emphasize the importance of the sidewalls in achieving and maintaining the two-dimensionality of a plane jet over a reasonably large axial distance. For instance, Lemieux and Oosthuizen (1985), Browne et al. (1982) and Heskestad (1965) have all stressed the importance of having the sidewalls in a plane jet.

An extensive review of literature reveals that previous investigations have documented

measurements from rectangular nozzle facilities without sidewalls. Key previous investigations: include Trendscoste and Sforza (1967), Marsters and Fotheringham (1980), Sfeir (1979), Krothapalli et al. (1981), Tsuchiya et al. (1985) and Quinn (1992a). Using plane jet facilities with sidewalls are Heskestad (1965), Bradbury (1965), Gutmark and Wygnanski (1976), Browne et al. (1982), Antonia et al. (1980) and Jenkins and Goldschmidt (1973). Given the wide differences in boundary conditions amongst rectangular and plane jets, a conclusive comparison to deduce the effect of sidewalls cannot be made.

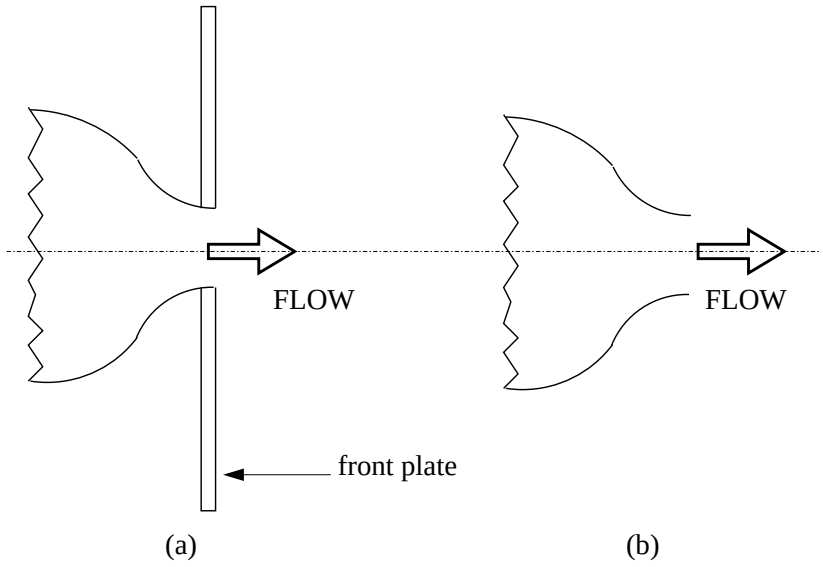

Figure 1.16: A schematic view of the smooth contraction (round) nozzle, (a) with and (b) without, front plates.

Some investigators e.g. Namar and Ötügen (1988) and Hussain and Clark (1977) measured a jet issuing from a very large aspect ratio rectangular nozzle claiming it to be planar even though their experimental facility did not have sidewalls. Such claims have not been justified by an independent experiment. The most direct study on the effect of sidewalls on a plane jet was conducted by Hitchman et al. (1990). Their mean centerline velocity measurements were undertaken from a smoothly contoured nozzle of aspect ratio 60 up to 90 nozzle widths downstream for jet with sidewalls and 70 nozzle widths downstream for the jet without sidewalls. However, their data are questionable. They did not provide any explanation as to why their axial range of measurements were different i.e. up to 70 nozzle widths for the jet without sidewalls and up to 90 nozzle widths for the jet with sidewalls. The difference in the measured axial range could have been different if the nozzle opening widths H - based on their normalization, were different which was not the case for their investigation. One may suspect that the smaller axial range of measurements for the jet without sidewalls could be due to the existence of

possible three-dimensional effects which occur during the transition of their jet (without sidewalls) into a quasi-axisymmetric (round) jet at a certain distance downstream. Such a transition of the free rectangular jet into an axisymmetric (round) jet occurs due to axis switching; see Piffaut (2003) and our paper, Mi et al. (2005b) in Appendix **??**. Once the jet without sidewalls has transformed into a round jet, the decay of the mean centerline velocity is unlikely to follow the inverse square dependence i.e. $U_c \sim x^{-0.5}$ will not be true. It is our deduction from Chapter 6 that Hitchman's jet without sidewalls incorporated three-dimensional effects and the inverse square dependence mentioned above was not met. Hence, they did not present data for $x/H > 70$ for their jet which did not have sidewalls. Moreover, their data are limited to the mean velocity measurements only and did not provide any about the development of axial turbulence intensity or moments of higher order fluctuations. Hence, a more complete investigation of the jet with and without sidewalls is required to fully assess the merits and demerits of the two types of nozzle configurations.

Some other studies which relate broadly, if not directly, to the present discussion on sidewalls effects on jets were conducted on round jets. Abdel-Rahman et al. (1997) conducted some LDA measurements of two types of round jets. They used a round nozzle with a front plate and one without a front plate at their nozzle exit. For clarity, their configurations are re-drawn in Figure 1.16. Their hot wire measurements indicate that the front plate reduced the exchange of their jet with its surrounding. That is, it reduced the decay rate of the mean centerline velocity, jet spreading, kinematic momentum flux and the kinematic mass flux. The jet was seen to behave more intermittently when front plates were used as evidenced by the larger lateral skewness and flatness factors across the jet.

For the jet without sidewalls (free rectangular jet), the following questions therefore arise:

- Over what axial extent is the jet statistically two-dimensional? What happens beyond this location?
- Where is the point of transition from two-dimensionality to three-dimensionality?
- Is the near field two-dimensional region of a free rectangular jet equivalent to the near field region of a true plane jet?

These questions cannot be answered from previous research and will be the addressed by present investigation.

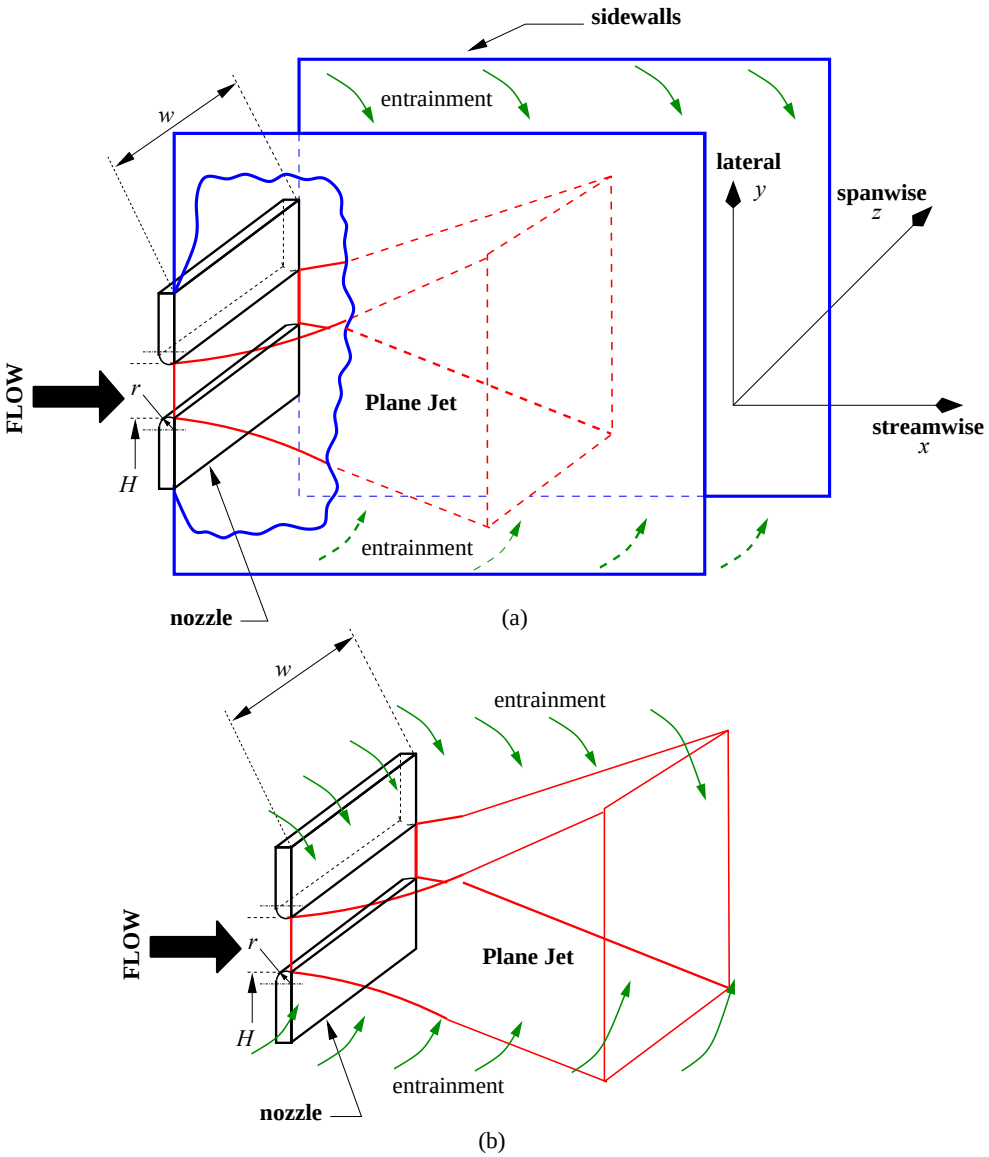

Figure 1.17: A model of the entrainment into a radially contoured plane jet (a) with and (b) without sidewalls.

1.6 Motivation for Present Work

The broad significance of Reynolds number and boundary conditions to plane jets is demonstrated above. Also, the investigations on different types of jet nozzles e.g. round, rectangular or plane, have shown that the entire flow field depends on the nozzle boundary conditions.

Specific boundary conditions of importance include the nozzle aspect ratio, the inner-wall nozzle contraction profile that defines the nature of exit velocity profiles e.g saddle-backed, top hat, fully developed turbulent profile, the particular nozzle geometry e.g. rectangular,

round, triangular, orifice-plate and the use of sidewalls. Other experimental conditions such as a velocity of any co-flow also affect the downstream flow (Bradbury 1965). Together with these, the jet exit Reynolds number is also known to affect the downstream flow which characterizes, in particular, whether the flow is in the laminar or in the turbulent regime (Frank 1999, Dimotakis 2000). For a plane jet, published data show that very few of these experimental conditions have been systematically assessed. Previous investigations have tested to some degree, the effect of nozzle geometry (Hussain and Clark 1977), the influence of nozzle aspect ratio (Bashir and Uberoi 1975, Van Der Hegge Zijnen 1958), the effect of nozzle exit turbulence intensity (Goldschmidt and Bradshaw 1981), the effect of sidewalls (Hitchman et al. 1990) and the effect of jet exit Reynolds number (Namar and Ötügen 1988, Löfdahl et al. 1997, Klein et al. 2003). Assessment of the findings from these investigations have indicated that each of these conditions affect the flow differently. In short, the effects of boundary conditions are inter-dependent (i.e. coupled) and the effect of a particular condition cannot be assessed without isolating the influence of the others.

Therefore, independent studies which vary one parameter independently i.e. while keeping other variables fixed, are warranted. Shortage of published data for a plane jet, especially in areas of the influence of jet exit Reynolds number, the nozzle aspect ratio, the nozzle contraction profile and the use of sidewalls is the motivation for the present experimental investigation. From here onwards, the objectives of the present research will be defined, followed by an account of the thesis outline.

1.7 Thesis Objectives

Based on the above literature review, the objectives of the present investigation are defined. The main aim of this research is to investigate experimentally the effects of Reynolds number and boundary conditions on the flow mechanics of a turbulent plane air jet. It also aims to fill the specific gaps in previous knowledge and to expand the existing body of literature on plane jet flows. Specifically, the thesis aims:

(1) to examine the effect of jet exit Reynolds number over the range $1{,}500 \leq Re \leq 16{,}500$ on its velocity field, where the upper limit is set by the facility.

(2) to study the statistical differences in the velocity field caused by changing the nozzle contraction profile r^* over the range $0 \leq r^* \leq 3.60$.

(3) to assess the effect of nozzle aspect ratio AR over the range $15 \leq AR \leq 72$ on the

downstream flow.

(4) to compare and study the flow field of a free rectangular and a true plane jet.

1.8 Thesis Outline

Chapter 1 introduces the research topic by presenting the significance and a history of plane jets. Following this, the chapter outlines definitions of initial and boundary conditions for a plane jet. A review of published literature on round, rectangular and plane jets is also presented. This review reveals the gaps in previous knowledge on the influence of Reynolds number and boundary conditions of plane jets. Therefore, based on the literature information, the motivation and objectives of the present research are presented.

Chapter 2 describes the experimentation technique. The wind tunnel and plane jet facility are described in detail. Following this, hot wire anemometry is introduced, with a short history of the technique, advantages and disadvantages and the theoretical and practical issues of the hot wire anemometer circuit. The issues of data acquisition are also discussed. The chapter concludes by presenting an analysis of the experimental uncertainties in the present velocity measurements.

Chapter 3 assess the influence of Reynolds number on the velocity field of a plane air jet. In this chapter, Reynolds number is varied between $1{,}500 \leq Re \leq 16{,}500$ while other experimental conditions are kept fixed. Followed by a short introduction and experimental details, the results are presented. Firstly, the lateral profiles of the mean velocity and turbulence intensity, measured $x = 0.5H$, are presented. These profiles show that, as Reynolds number is increased, the nozzle boundary layer thickness increases. After presenting the initial velocity field, the statistical variations in the centerline mean and turbulence field are investigated. The centerline mean velocity, lateral profiles of the mean velocity, jet decay and spreading rates are described. It is revealed that an increase in Reynolds number leads to a lower decay of the centerline mean velocity and decreased spreading rate of the plane jet. The centerline turbulence intensity, skewness and the flatness factors and the lateral distributions of turbulence intensity are all dependent on Re. In particular, an increase in Re leads to a reduction in the magnitude of near field hump and far field asymptotic value of the centerline turbulence intensity. Subsequently a further discussion of the results and a conclusion are presented.

Chapter 4 examines the effect of inner-wall nozzle contraction profile r^* on the plane

air jet. The beginning of this chapter contains a short introduction and a description of the experimental details. For the entire range of measurements, the Reynolds number and nozzle aspect ratio are fixed at 18,000 and 72 respectively. The inner-wall nozzle contraction profile is varied gradually. Five nozzle configurations i.e. $r^* = 0$ (sharp-edged orifice nozzle), 0.45, 0.90, 1.80 and 3.60 (radially contoured) are measured. Firstly, the initial velocity field is characterized by measuring the mean velocity and turbulence intensity profiles at $x = 0.25H$. It is shown that for $r^* = 0$ (sharp-edged orifice nozzle), the initial velocity profile is saddle-backed while for $r^* = 3.60$ (radially contoured nozzle), it approximates to top hat. The results indicate that the initial velocity profile approximates to a top hat when $r^* \geq 1.80$. Increased initial turbulence intensity within the shear layer and decreased initial turbulence intensity within the central region of the sharp-edged orifice nozzle is noted. The near field is characterized by a 'vena contracta' for the plane nozzles whose contraction profile factor r^* ranges between $0 \leq r^* \leq 0.90$. Also, in the near field, increased decay of centerline mean velocity is evident for the sharp-edged orifice nozzle. In the far field, centerline decay of the mean velocity and the jet spreading rate is higher for the sharp-edged orifice nozzle, than for a radially contoured configuration. Furthermore, the centerline turbulence intensity reveals a hump for the sharp-edged orifice nozzle, around $x/H \simeq 10$ to 12 whereas the turbulence intensity hump is absent for the radially contoured configuration. It is also evident that the sharp-edged orifice nozzle encounters a larger magnitude of the asymptotic turbulence intensity. The chapter then presents a detailed discussion of the results and a short account of the main conclusions.

The effect of nozzle aspect ratio, measured over the range $15 \leq AR \leq 72$ for a plane air jet is explored in Chapter 5. The measurements are conducted at a Reynolds number of 18,000 and an inner-wall nozzle contraction profile $r^* = 3.60$. This magnitude of r^* was found to produce an approximate top hat initial velocity profile. After an introduction, the chapter presents a short account of the experimental details specific to this investigation. Then the lateral profiles of the initial velocity and turbulence measured at $x = 0.25H$ are discussed. The near field variation of the centerline mean velocity is also presented. The results show that, as nozzle aspect ratio is increased, the rate of near field entrainment and jet spreading decreases. In the far field, an increase in aspect ratio leads to an increase in the decay of centerline mean velocity and an increase in the jet spreading rate. The relationship between the maximum distance to which the flow field is planar/two-dimensional (and free from sidewall effects) and the nozzle aspect ratio is discussed. The results indicate that the nozzle aspect ratio is a limiting factor for the maximum distance up to which the flow is planar. A critical jet aspect ratio defined

by the aspect ratio of the jet (as opposed to the nozzle) at which the flow ceases to be planar, was found to be approximately 0.15 for $AR \geq 30$. The results also revealed that a plane jet undergoes a transition from planar to three-dimensional when the width of the flow is approximately equal to the spacing between the sidewalls. Then, the turbulence field is presented. In particular, a larger near field hump in turbulence intensity and a larger magnitude of 'far field' asymptotic turbulence intensity is evident for the jet which has a lower nozzle aspect ratio. Then, the centerline skewness and flatness factors are presented, and found to depend on the nozzle aspect ratio too. Towards the end, further discussion of the results are provided and the chapter ends with the conclusions.

Chapter 6 investigates effect of sidewalls. Specifically, the flow field of a free rectangular (without sidewalls) and true plane (with sidewalls) jet are compared. Hot wire measurements of a free rectangular jet and a plane jet are conducted at a Reynolds number of 7,000 from a nozzle of aspect ratio of 60 and an inner-wall nozzle contraction profile r^* of 2.14. The chapter begins by an introduction and a simple description of the experimental facility. Then the results are presented. Using the mean velocity data, increased near field entrainment (and consequently a reduced potential core length) is evident for the free rectangular jet. Then, the far field centerline velocity measurements are presented. It is revealed that the plane jet has a longer region of statistically two-dimensional flow than does the free rectangular jet. It is also shown that this region for a free rectangular jet depends on the nozzle aspect ratio. The mean data reveals that at greater axial distances, the flow field of a free rectangular jet develops statistically, into a round jet. In the self-similar and two-dimensional region, the decay of centerline mean velocity and jet spreading rates are found to be higher for the free rectangular jet. After discussing the mean field, the results of the turbulence field are presented. The present work shows that a distinct hump in turbulence intensity around $x/H \simeq 10$ to 12 is evident for both jets. However, the magnitude of the hump is bigger for the plane jet. Towards the end of the results section, the skewness and flatness factors are described, and found to depend on sidewalls. Finally, the chapter discusses the results and then presents the conclusions.

Chapter 7 presents the overall conclusions of the present thesis.

Chapter 2

EXPERIMENTATION

This chapter describes the general experimental technique used to measure the velocity field of a turbulent plane air jet. Figure 2.1 shows the overall experimental arrangement that includes a plane jet facility, a hot wire anemometer, a PF-30F data acquisition system and a traverse system. Data were collected using a PII personal computer using WaveView2.0 running under Win98. The chapter begins by introducing the wind tunnel and plane jet facility and then introduces the technique of hot wire anemometry, its history and technical details of the method. Further, the chapter describes the acquisition of data and concludes by presenting an account of uncertainties in the present velocity measurements.

2.1 Wind Tunnel Facility

Figure 2.2 shows a schematic view of the present wind tunnel. The open-circuit wind tunnel consists of a 14.5 kW aerofoil-type centrifugal fan driven by a speed controlled a.c. motor. For present investigation, an open circuit wind tunnel was most suitable given that it was already available, does not suffer significantly from temperature variation, provides a steady flow rate and the fan fitted upstream of the flow does not disturb flow from the working section (Mehta and Bradshaw 1979). A wide angle diffuser, installed between the blower and settling chamber is screened to stabilize the emerging flow. Quite a few experimentalists e.g. Kline et al. (1959), Feil (1964) and Carlson et al. (1967), stated that diffusers are essential to achieve a reasonably uniform flow. The settling chamber is installed with a honey-comb and screens. Screens improve flow uniformity by imposing a static pressure drop proportional to the square of the speed (Mehta and Bradshaw 1979). However, screens also reduce the boundary layer thickness and refract the incident flow towards the local normal direction, reducing the intensity of large scale turbulence in the flow field. They also introduce fine scale turbulence but this decays over a short distance.

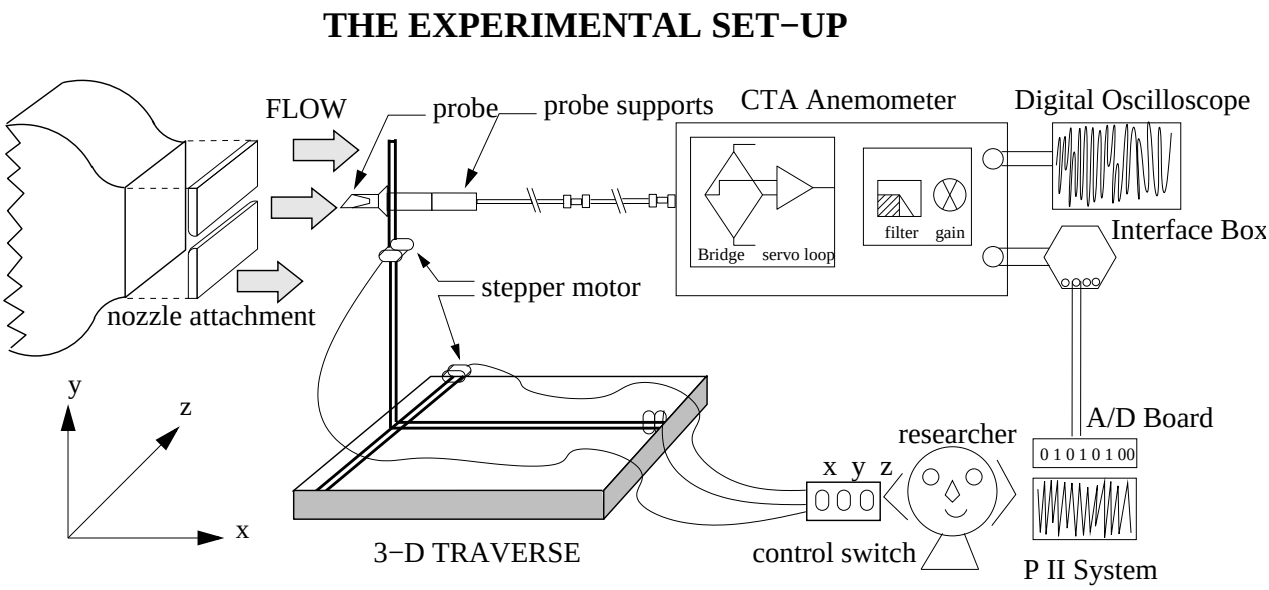

Figure 2.1: The overall experimental arrangement showing the nozzle attachment to the wind tunnel, hot wire probes, connections, anemometer and data acquisition system. Note that sidewalls are omitted for clarity.

The honeycomb will act to reduce any swirl and lateral velocity variations and hence the turbulence level within the emerging flow. The purpose of the settling chamber is to allow the fine vortex motions generated by screens to dissipate. Finally, the tunnel has a smooth contraction of area ratio 6:1. A contraction not only increases the mean velocity but also produces a lower variance of the mean flow to avoid flow separation. The tunnel exit section of dimensions 720 mm $\times$ 340 mm. To this was attached the plane nozzle (Figure 2.2).

2.2 Plane Nozzle Facility

The rectangular nozzle comprises a flat plate with a slot machined into it, mounted to the end of wind tunnel contraction (Figure 2.2). Its exit dimensions are w and H where H is the long side and w is the short side of the nozzle. The specific dimensions of H and w are dependent on the particular investigation and are specified in their respective chapters later. Two sidewalls of nominal dimensions 1800 mm $\times$ 1200 mm are attached to the short ends of the nozzle oriented in the x-y plane. The functional requirement of the sidewalls to enhance two-dimensionality in a plane jet facility has been strongly advised by previous investigators (Gutmark and Wygnanski 1976, Browne et al. 1982, Hitchman et al. 1990). Sidewalls restrict the transverse (z-direction) entrainment of jet at the short sides of the rectangular nozzle which otherwise tend to spread faster than at the middle. Hence, by avoiding non-uniform entrainment at the ends and middle of the jet, sidewalls

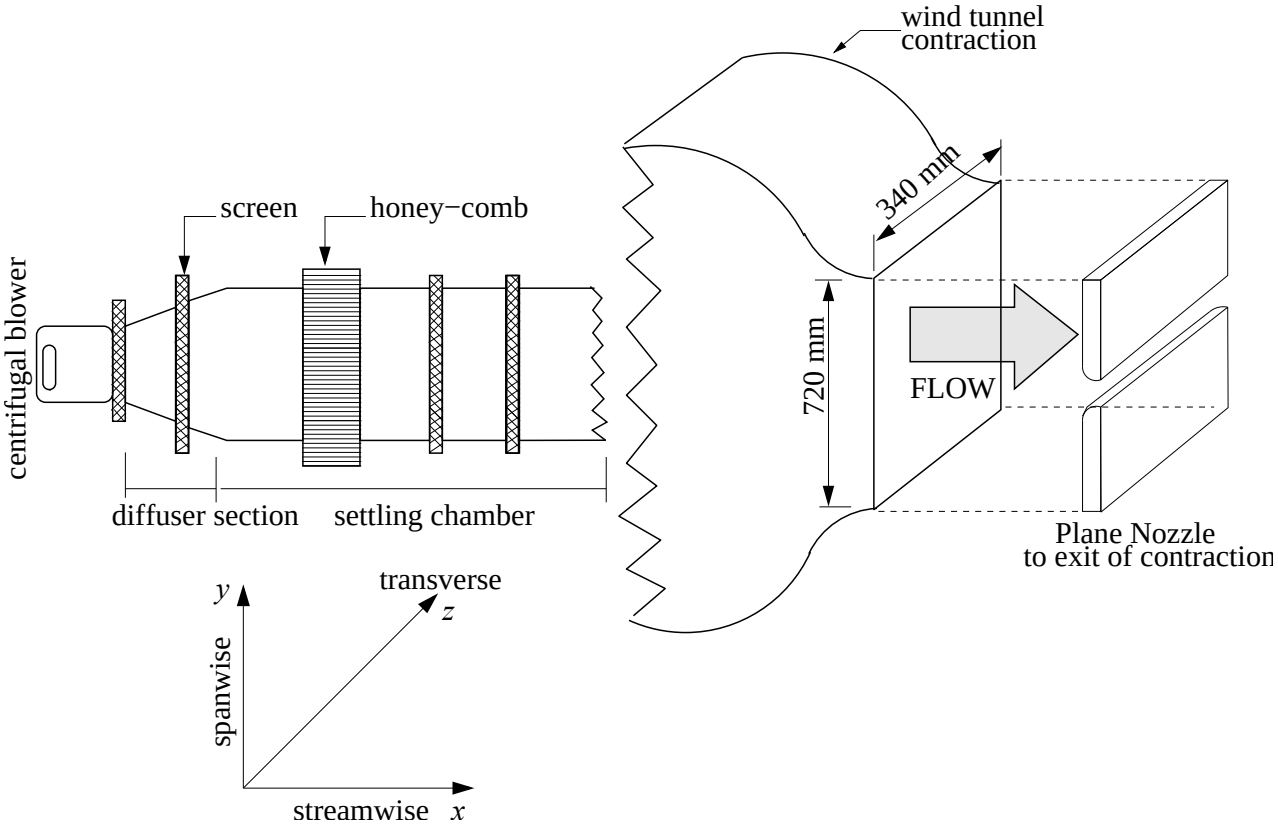

Figure 2.2: A schematic view of the present wind tunnel facility.

also avoid the axis-switching phenomenon. In his masters thesis on axis switching of coaxial square jets, Piffaut (2003) demonstrated that the spreading at short edges of his nozzle was enhanced when sidewalls are not used. Other studies on free rectangular jets (without sidewalls) also demonstrate this phenomenon. To name a few, Sforza et al. (1966), Sfeir (1979), Krothapalli et al. (1981) and more recently Bonnafous (2001) have shown some form of axis switching in non-circular and rectangular jets without sidewalls.

It is important to note that the distinction between the present plane nozzle and those in previous plane jet investigations. In particular, the present nozzle is radially contoured at the exit plane in contrast to a smooth contraction for majority of previous investigations. For example, Browne et al. (1982) and Gutmark and Wygnanski (1976) used a smoothly contoured nozzle such as the one shown in Figure 2.3a. The present radially contoured nozzle (Figure 2.3b) has a plate-length (L) to nozzle slot width (H) ratio of at least $L/H >> 60$ to classify it as having an effectively infinitely long front plate at the exit plane. Such a configuration whose $L/H \simeq 38$ was first used by Oosthuizen (1983). Furthermore, the ratio r/H defines the nozzle profile and nature of its initial flow. The choice of a radially contoured nozzle for the present investigation offered us some advantages. The

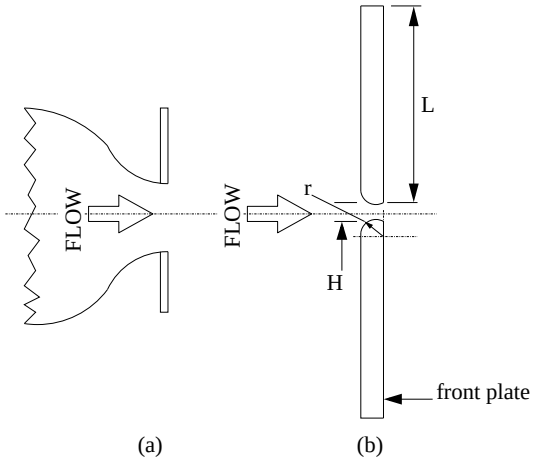

Figure 2.3: A schematic view of (a) a standard smooth contraction and (b) a radial contraction nozzle. Note: $L/H >> 60$.

flexibility of changing the nozzle profile i.e. the r/H factor to investigate the effect of nozzle boundary conditions for the present study is greatly advantageous. In a conventional smooth contraction nozzle, such changes to the nozzle profile require new nozzles to be designed whereas for our case it only requires replacement of the front plate with a different contraction radius without replacing the whole setup. A radially contoured nozzle is easier to design and manufacture than a smoothly contoured nozzle. This is because the inner-wall profile nozzle profile of a smoothly contoured nozzle is defined by a more complex function such as a sinusoidal or polynomial curve. On the other hand, a radially contoured nozzle has a small radius that equals the width of the nozzle plate. Apart from Oosthuizen (1983), no other study actually investigated a radially contoured nozzle. Thus, the present study conducted at a wide range of r/H will expand the existing body of literature on a radially contoured nozzle. Admittedly, the present radially contoured nozzle has a potential disadvantage of a slightly complicating comparisons with previous investigations of smoothly contoured nozzles.

2.3 Assessment of Effects of Room Confinement

It is well established that experiments which are conducted in a confined environment i.e. a small enclosure, will encounter a reduction in the jet momentum (Hussain et al. 1994). Indeed, Hussain et al. (1994) found that Wygnanski and Fiedler's (1969) investigation of a round jet within a wire enclosure obtained $\frac{M}{M_o} \simeq 0.53$ at $x/D > 50$ (here, M and M_o are the axial momentum at any downstream distance and momentum at the nozzle exit, respectively.) Thus, in Wygnanski and Fiedler's investigation, only 53 % of the total initial momentum was sustained at 50 nozzle widths downstream. Likewise, the decay of

centerline mean velocity of a round jet measured by Capp (1983) in an air tight enclosure did not follow the relation $U_c \sim x^{-1}$ for $x/D \geq 100$. The deviation from the linear decay of mean velocity for his round jet provides an evidence that the confined jet did not conserve momentum for axial locations greater than 100. Thus, to avoid significant losses in the plane jet momentum, we conducted the present experiments in a laboratory which was large enough to avoid the effects of room entrainment on the plane jet. This is discussed below.

2.3.1 Experimental Facility Parameters

The entire plane jet facility was located in a large laboratory of floor dimensions 18.0 m $\times$ 7.0 m. (Figure 2.4). The height of the room H_R was 2.50 m and the plane jet was located horizontally at about the mid point between the floor and ceiling. The ratio of the room-height to the nozzle-width, $\frac{H_R}{H}$ was between 250 and 400 for any particular experiment. The ratio of the room-area (in the same plane as the nozzle opening width) to the nozzle-area for the present investigation, $\frac{A_R}{A_n}$ was between 2,500 and 10,000. These numbers are within the range where confinement effects are small for most previous investigations. Those previous investigations are described below.

Hussain et al. (1994) used $\frac{H_R}{D} \simeq 200$ and $\frac{A_R}{A_n} \simeq 50{,}000$ for a round jet. Using these dimensions, they found that their round jet retained 99 % of its initial momentum. On the other hand, Malmstrom et al. (1997) used $\frac{H_R}{D}$ between 40 and 170 and $\frac{A_R}{A_n}$ between 2,000 and 30,000 for their round nozzles. Correspondingly, Malmstrom noted that his flow coefficient α, (where α approaches 1 for the experiment which incorporates negligible momentum losses) was between $0.95 \leq \alpha \leq 1$. The experiment by Nottage (1951) for a round jet is also of relevance to the present discussion. He employed $\frac{H_R}{D}$ of 36 and $\frac{A_R}{A_n}$ of 4,000. When compared with the $\frac{H_R}{D}$ and $\frac{A_R}{A_n}$ of Hussain and Malmstrom, Nottage obtained quite low values. Consequently, his results indicated that the flow rates for his experiment decreased for $x/D > 80$ for his high velocity jet. Therefore, momentum was not conserved in Nottage's jet for $x/D > 80$. In fact, Malmstrom attributed this decrease to the effects of room enclosure for Nottage's confined round jet. In light of these comparisons, one may argue that the relative magnitudes of $\frac{H_R}{D}$ and $\frac{A_R}{A_n}$ must be sufficiently large to eliminate the effects of room enclosure.

Thus, it is expected that the present investigation incorporates very small influences of room entrainment on the plane jet. Specific calculations of the jet axial momentum will follow next.

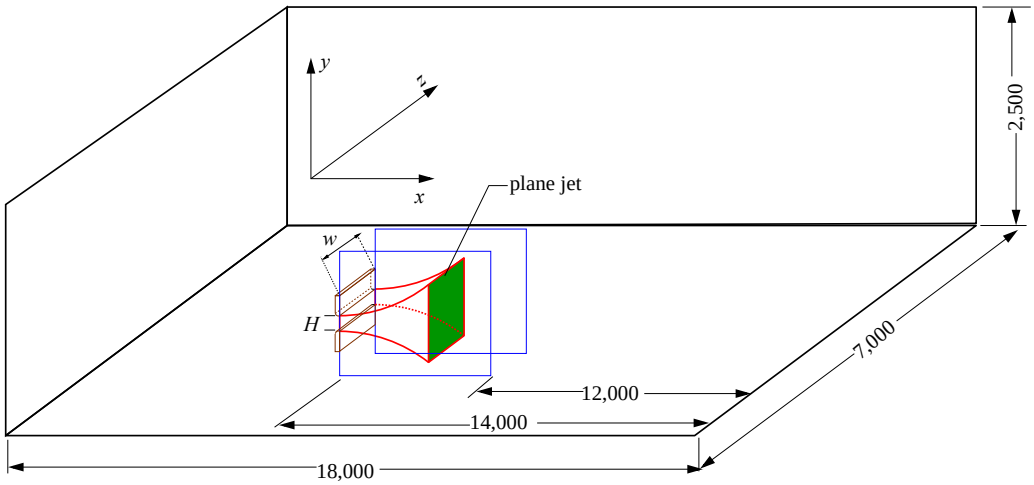

Figure 2.4: A schematic view of the experimental laboratory. All dimensions in mm. Diagram not to scale.

2.3.2 Loss of Axial Momentum

It is of interest to verify the accuracy of the present velocity measurements by assessing the magnitude of the effect of room entrainment on Reynolds number and thus on the velocity measurements, if any. The comparison of confinement in the present experiment with those in other facilities in Section 2.3.1 suggest that confinement effects will be small for the present measurements. Nevertheless, it is important to directly assess the influence. Using the model proposed by Hussain et al. (1994) for a round jet, we derived the loss in the mean axial momentum of the present plane jet. Appendix E.1 provides a complete derivation. It is interesting to note that at $x/H = 100$, $M/M_o \simeq (0.992 \pm 0.005)$ for $Re = 1{,}500$ when compared with $M/M_o \simeq (0.995 \pm 0.005)$ for $Re = 16{,}500$. Note that these calculations have at least 5 % error, due to errors arising from calculations using the lateral profiles of mean velocity, and by using the assumption that the exit velocity profile is top-hat for all Reynolds numbers. In their measurements on a round jet, Hussain et al. (1994) used this criterion to assess their enclosure effects on the loss of axial momentum. According to their assessment at $x/D = 200$, their jet retained 90 % of its exit momentum. The present investigation whose axial momentum is retained by 97.4. % for $Re = 1{,}500$ and by 97.8 % for $Re = 16{,}500$ provides evidence that the loss in axial momentum at $x/H = 160$ is small. The difference between the relative magnitudes of M/M_o for $Re = 1{,}500$ and for $Re = 16{,}500$ is also small and is within experimental uncertainty.

2.3.3 Similarity of the Mean Velocity Field for the Plane Jet

Further support for the accuracy of the present velocity measurements is found in Figure 3.5, which demonstrates that in the self-similar region, $U_c \sim x^{-0.5}$. This dependence is

typical of a plane jet (Pope 2002). If room entrainment were to impose an effect on the momentum of the plane jet, we would expect the centerline decay of mean velocity to depart from the 0.5-decay power law.

A similar view was taken by Hussain et al. (1994); see their paper Figures 7 and 8, who reviewed the round jet data of Wygnaski and Fiedler (1969) and of Capp (1983). They stated that the centerline velocity decay of Wygnaski and Fiedler (1969) and of Capp (1983) failed to stabilize to a constant value. Wygnanski's data departed from the linear dependence for a round jet i.e. their data did not follow $U_c \sim x^{-1.0}$, with a constant slope of -1.0, but had an increasing slope for $x/D > 72$. Likewise, Capp's data also diverted from the linear dependence between U_c and x for $x/D > 100$. For both cases, Hussain et al. (1994) provided a plausible reason for the divergence of Wygnanski's and Capp's data. That is, these experiments were confined by the enclosure. Therefore, for $x/D > 72$ and for $x/D >$100, Wygnanski and Fiedler's and Capp's round jet failed to conserve axial momentum.

The present measurements do not exhibit any divergence from the 0.5-decay power law dependence ie. U_c varies as $x^{-0.5}$ throughout the measured range, as shown later, in Figure 3.5. This provides confidence in the present measurements and confirms that the loss in axial momentum at at least 100 nozzle widths downstream is insignificant. Thus, it is confirmed that none of the plane jets in the present study encounter significant momentum losses and any effects of enclosure are within the present experimental uncertainty. In other words, these plane jets are deduced to be in an approximately infinite environment.

2.4 Hot Wire Anemometry

The technique of Constant Temperature Anemometry (CTA) was used for the present velocity measurements. The CTA anemometer works on the basis of convective heat transfer from a heated sensor to the surrounding fluid, the heat transfer being primarily related to the fluid velocity. By using very fine wire sensors (hot wires) placed in the fluid and electronics with servo-loop technique, it is possible to measure velocity fluctuations of fine scales and of high frequencies.

In hot wire anemometry, single, cross (dual) or tri-axial hot wires can be used. Single-wire probes measure 1-component velocity (U), while cross or triaxial wires are used for 2 or 3-component velocity (V and W) measurements. While each configuration offers offers

merits and demerits over the other, their choice depends on the application. Single wires encounter reduced experimental errors when compared with dual or tri-axial wires, in which the signal may be influenced by the alternate wire sensor. However, they provide a single velocity component only. On the other hand, dual wires can provide a dual component velocity (i.e. U and V), while tri-axial wires can measure U, V and W. Single wires are easier to manufacture and more durable (Jorgensen 2002). In low turbulence intensity measurements, single wires are more viably used.

2.4.1 Historical Aspects

The origin of this well-established technique is difficult to determine precisely (Comte-Bellot 1977). Early studies by Boussinesq (1905) on the thermal transfer characteristics from a heated wire are probably the origin of hot wire measurements. Later, King (1914) verified Boussinesq's (1905) results by an experimental investigation. Further advancements in this technique led Dryden and Kuethe (1929) to undertake the first set of subsonic incompressible flow measurements using CTA. An extension of this technique to compressible flows was made by Kovasznay (1950). He determined that, in subsonic compressible flows, the heat transfer from the wire is a function of velocity, density, total temperature and wire temperature. Such an information led to hot wire corrections to enhance the credibility of their measurements. Since then, the capability of the hot wire technique and their applicability, to a variety of turbulent flows have been vastly expanded. A large number of text books are already available on this subject. Perry (1982) and Brunn (1995) are probably the most comprehensive texts that describe hot wire anemometry.

2.4.2 Advantages and Disadvantages

Advantages of Hot Wire Anemometry

In measuring turbulence, conventional hot wire anemometry is a competitor among other advanced laser-based techniques such as Particle Imaging Velocimetry (PIV) and Laser Doppler Anemometry (LDA). The size of the CTA sensor is very small. The probe is typically 1.0 - 5.0 μm in diameter and 0.25-1.25 mm in length, in comparison to an LDA measuring volume of $\simeq$ 50 μm $\times$ 0.25-1.25 mm. This comparison shows that hot wires are more appropriate to resolve fine-scales in the turbulent flows. PIV or LDA, on the other hand are less able to resolve the smallest scales of velocity fluctuations due to their poor resolutions.

The sensor output is a continuous analogue voltage which provides an instantaneous signal. This allows the manipulation of data in various forms, such as obtaining the mean,

root-mean-square (rms), moments of higher order fluctuations, the probability density functions and frequency spectra. Hence, no information is lost. Consequently, both conventional/conditional time and frequency domain analysis can be carried out. Very high frequency response of the CTA system (in the range 0 to 50 k Hz, makes it possible to measure high-frequency oscillations. In contrast, LDA can measure no more than 30 k Hz (Brunn 1995). Relative to the hot wire technique, LDA are not well suited to spectral analysis because it does not provide a continuous spectra due to the non-uniform distribution of seeder particles. Hence, errors are introduced due to 'gaps' in the signal.

Hot wire anemometry is an intrusive technique that measures at a single point. The use of multiple closely spaced wires allow measurement of one, two or three-components of the velocity. While no seeding is required, they have the disadvantage of probe disturbance, which can be minimized by careful orientation of the probes. On the other hand, LDA and PIV require tracer particles to measure the velocity. Many studies have demonstrated the bias effects due to seeding problems e.g. Ruck (1991).

Hot wires can also be used to undertake simultaneous measurement of velocity and temperature using a multi-sensor probe, where one sensor is operated in the 'cold-wire' mode. The cold-wire mode is called the Constant Current Anemometry (CCA). Probe access is sometimes easier in small enclosures e.g the inside of pipes etc. Thus, the simultaneous measurement of the velocity and scalar is practically easier when using hot wires than PIV.

Hot wire anemometry systems are cheaper than LDA or PIV equipment. Initial costs in designing the system or probes and the on-going costs in maintaining the probes are quite affordable when compared with the high cost installation and/or on-going costs of laser-based systems. If extreme precautions are taken, the hot wire sensor may last up to several months hence no additional costs are incurred. Additionally, the technique, if mastered well, is easier to use than the laser-based techniques.

Problems Associated with Hot Wire Anemometry

The hot wire sensor measures the flow based on the relation between the fluid velocity and heat loss of the cylindrical wire. Hence, a commonly assumed principle is that the fluid is incompressible and it flows around the wire. However, at high velocities, the flow tends to become compressible and effects of compressibility must be taken into account (Jorgensen 2002). On the other hand, the corrections that are required to account for the compressibility effects are very complicated according to many investigators e.g. Norman

(1967), Demin (1973) and Smits et al. (1983). For turbulent flows which have a very high turbulence intensity ($> 30\,\%$), hot wires have problems with flow reversals. Flow reversals are caused by flow over an obstacle, sudden expansion of flow in ducts and pipes or flow separation over strongly curved surface or in swirling flows such as those in combustion chambers (Brunn 1995). Since velocity vector falls outside the opening angle of the sensor, the hot wire sensor cannot detect correct velocities. In such cases, the flying hot wire technique can be used where the probe is moved through the flow, with a speed high enough to move the resulting velocity vector inside the opening (Jorgensen 2002). On the other hand, the LDA and PIV techniques can be used in flows with flow reversals and are simpler than the flying hot wire technique.

Special care must be taken to avoid influence of the probe on the flow which can generate secondary disturbances e.g. vortices. The probe, if not positioned carefully, can modify the local flow and produce errors in the measured velocities. Near-wall velocity measurements also pose potential problem for CTA. Since the hot wire uses heat transfer to measure the velocities, additional heat loss from the fluid probe into the solid wall can cause the measured velocities to be higher (Jorgensen 2002). Wall influences becomes significant at $y^+ \leq yU_\tau/\nu \approx 3.5$, where y is the distance to the wall, U_τ is the friction velocity and ν is the kinematic viscosity. Many investigations e.g. Christman and Podzimek (1981), Khoo et al. (2000) and Hebber (1980) have accounted for the wall influence. The critical distance, depending on the free-stream velocity is roughly between 0.1 - 0.2 mm. This effect is not a problem for other experimental techniques, such as LDA or PIV, although beam reflections also limit the distance at which a probe volume can be placed from a wall.

Probe contamination, due to fouling materials (e.g. dust) are also a significant problem for hot wire measurements. These effects are more pronounced for liquid flows, which potentially cause dust to accumulate faster, than for air flows (Brunn 1995). Such a problem may be rectified by use of a filter to clean the working fluid. Temperature variations may also cause problems in liquid flows. For instance, very small changes in temperature, may produce substantial changes in the calibration function. Hence frequent probe calibrations may be annoying. For these reasons, LDA is more widely used for liquid flow measurements, where naturally occurring particles may assist in seeding.

The tiny hot wire sensor is fragile and slight improper handling can break the probe. On the hand, if handled properly, it may last several months or years. Measurements

very close to the exit plane of a nozzle, chamber or wall are rendered difficult because the probe is likely to be damaged if it touches any solid surface! Nevertheless, this can also be a problem for laser techniques due to intense scattering from surfaces. Hence, to avoid such problems, automatic traverse systems are usually used. Furthermore, use of a high overheat ratio (discussed later) may 'burn' the probe. If a probe has been used for a long time, constant checks on the overheat ratio must be performed to avoid too much probe heating due to the aging process. Hot wire anemometry is not suitable for hostile or non-isothermal environments, such as combustion chambers where the probe is likely to be damaged. In such places, LDA or PIV are more reliable. For flows which have solid particles or fine droplets, hot wire anemometry is never used.

Although single hot wire anemometry has a long history of being used as a measurement technique in fluid mechanics, it has some significant drawbacks. Hussain et al. (1994) quantified the differences between mean flow and turbulence statistics of an axisymmetric jet, acquired from a single hot wire anemometer, a flying hot wire anemometer and a burst mode LDA system. They found that, in flows where the turbulence intensity is very high, may be 30% or more, or in reversing flows, where the velocity vector falls outside the opening angle of the sensor (wire) array, the results have significant errors when measured with a single wire anemometer. Therefore, such flows can be measured more accurately with flying hot-wire systems, where the probe is moved through the flow field with a speed high enough to move the resulting velocity vector inside the opening angle. After linearization, the flying speed is subtracted from the longitudinal velocity component (Kelso et al. 1994, Thompson 1987). Hussain et al. (1994) found that the results obtained from flying hot wires and the burst mode LDA system differ from those obtained using single hot wire anemometer. The most significant differences were found for the moments of higher order velocity fluctuations and for those measurements obtained away from the jet centerline. While these errors from a single wire anemometer are small on the jet centerline, they become increasingly significant when the probe is traversed away from the centerline (for instance, during the measurement of the lateral profiles). Nevertheless, the influence of these errors on the present measurement are not expected to alter the key findings, since the errors are self-preserving (i.e. depend on moments of the turbulence) and relatively equivalent magnitudes of these errors will be present in all experiments conducted in this work. Therefore the present single wire anemometer is useful for comparison of jet properties from one experiment to another. Although these errors will not change the present trends in jet properties, it is important to point out that the measurements conducted away from the jet centerline will have an increasing

error. It is important to mention this, so that if computations are performed using the present findings, modelers will be aware that the absolute magnitudes of the mean and turbulence properties may not truly represent the actual values due to the relative errors accumulated from the single wire measurements.

2.4.3 Hot Wire Probes

CTA probes are selected primarily based on the type of flow and required resolution. Other factors such as the fluid medium, number of velocity components to be measured, the expected velocity range and turbulence levels contributes to the decision-making process.

Anemometer probes are available with four types of sensors, namely miniature wires, gold-plated wires, fibre-film or film-sensors. Most wires are 5 μm in diameter and 1.2 mm long, suspended between two needle-shaped prongs. Gold-plated wires have the same active length but are copper and gold plated at the ends to a total length of 3 mm long in order to minimize prong interference. Fibre-sensors are quartz-fibers, normally 70 μm in diameter with 1.2 mm active length covered by a nickel thin-film, which again is protected by a quartz coating. Fibre-sensors are mounted on prongs in the same arrays as are the wires. Film sensors consist of nickel thin-films deposited on the tip of aerodynamically shaped bodies, wedges or cones.

2.4.4 CTA Circuit

The constant temperature anemometer utilizes a Wheatstone bridge, a feedback amplifier and an electronic-testing subcircuit (Figure 2.5). Attached to these are a signal conditioner, with filter and gains settings. The operating principle of a CTA is now described.

Principle of Operation

The hot wire sensor, exposed to the flow, is placed in one arm of a Wheatstone bridge opposite to a variable resistor which defines the operating resistance. The operating resistance also defines the operating temperature of the sensor. When the bridge is balanced, no voltage (potential) drop exists across its diagonal. With an increase in flow velocity, the wire resistance will tend to decrease, resulting in an error voltage at the input of the regulating amplifier. Consequently, the probe current will inevitably increase. Successive heating of the wire and the corresponding increase in resistance continues until the balance is restored. The current regulating amplifier has a high gain, hence a condition

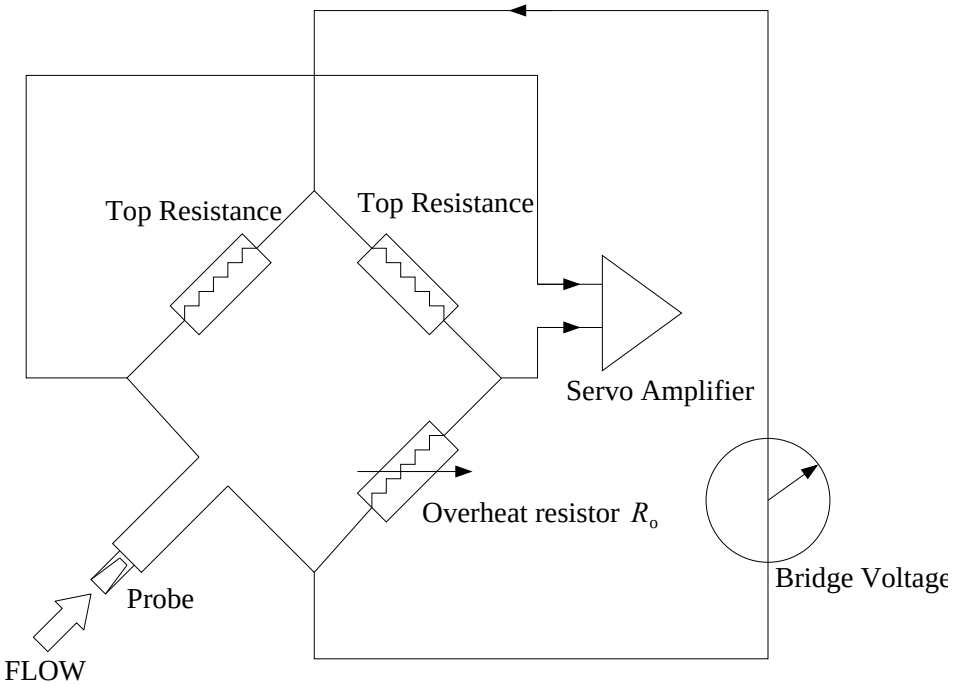

Figure 2.5: The CTA electronic circuit.

of bridge balance exists. This is practically independent of the flow velocity. The time constant of the hot wire is thus reduced by a factor of several hundred from fractions of a millisecond to some few microseconds. Furthermore, the probe current is represented by a voltage drop across the bridge. Since all resistances in the bridge are constant, the squared output voltage directly represents the heat loss from the wire. Thus, by measuring the heat loss, we can deduce the flow velocity. However, approximate adjustments to the CTA must be carried out to optimize the frequency output of the system.

CTA Components

Setting up an anemometer carefully is crucial to the success of an experiment. It consists of setting up a signal conditioner, which involves adjusting the filter, voltage offset and the gain. High pass or low pass filters are required to 'clean' the signal to eliminate excessive noise which could otherwise contaminate the velocity signal. A high pass filter removes any d.c. component of the signal in situations where low frequency fluctuations need to be removed prior to spectral analysis. On the other hand, a low pass filter attenuates electronic and other low frequency noise thus avoiding aliasing. To bring the measurement signal within the expected range (and within the data acquisition system), a voltage offset is usually applied. In situations where the signal is very weak, gain settings are adjusted for amplification application of the raw signal.

Frequency Response

A hot wire anemometer can respond to very high frequencies but appropriate adjustments are required to achieve this. Anemometer setup consists of static balancing i.e. overheat adjustment and dynamic balancing i.e. square wave testing. The overheat adjustment, α, given by

$$\alpha = \frac{R_o}{R_T} \tag{2.1}$$

which determines the working temperature of the hot wire. Here, R_o is the adjustable overheat resistance and R_T is the total resistance of the sensor, probe supports and the cables. The acceptable range of α is between $1.0 \leq \alpha \leq 1.8$. However, a very high overheat ratio could results in sensor damage. Hence, commonly used α are between 1.2 and 1.5. Based on α, the overheat resistor in the right bridge arm is adjusted (Figure 2.5), so that the desired operating temperature of the sensor is established, when the bridge is in operation. Throughout the present experiment, $\alpha \simeq 1.5$ has been used.

Dynamic balancing involves adjusting the frequency output of the CTA system. This serves a dual purpose. Firstly, it is used to optimize the bandwidth of the anemometer and secondly, it checks the stability of the servo-loop. The choice of maximum frequency output of the system depends on the requirements of the experiment. For example, if spectral analysis is used to measure the fine-scale turbulence, a very high filter frequency must be adopted. Square wave testing is carried out by applying a square wave signal to the bridge top. The time it takes for the bridge to get into balance is related to the time constant and hence the bandwidth of the system. This procedure is as follows:

1. Firstly, expose the probe to the expected maximum velocity.
2. Then apply the square wave to the bridge.
3. Adjust amplifier filter and gain until the response curve gets a 15 % undershoot (Figure 2.6). The response should be smooth without ringing either at the top or at the zero line.The response can be optimized by adjusting the amplifier, filter and the gain. Care must be taken while adjusting the gain settings. In case of a very high gain, the servo-loop can become unstable and noise will dominate the signal. Hence the gain should be just enough to observe a reasonably good signal.
4. Determine ΔT, the time it takes the servo-loop to regulate back to $\simeq$ 3 % of its maximum value with an undershoot of $\simeq$ 15 %.

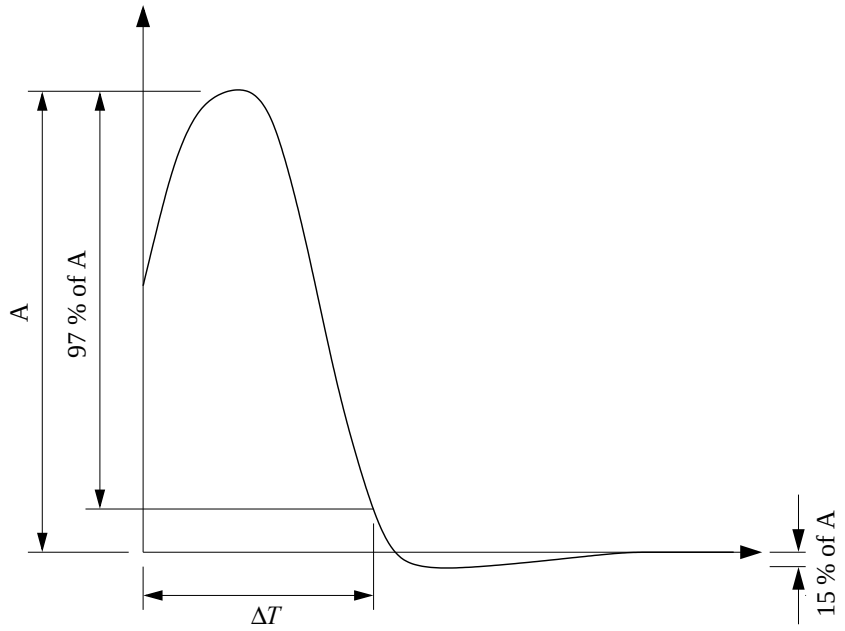

Figure 2.6: The correct square wave test.

5. Calculate the optimum bandwidth of the anemometer system. The optimum cut-off frequency f_c is given by:

$$f_c = \frac{1}{1.3\Delta T} \tag{2.2}$$

Note that for present measurements, the CTA had a built-in square-wave generator, hence an external generater was not required. In some cases, an input for an external square wave generator is needed.

Signal Conditioner Setup

Filtering and amplification are necessary to customize the signal for appropriate manipulation prior to digitizing by an A/D converter. The signal conditioner consists of a filter, voltage offset and an amplifier. To set up the low-pass filter, the highest frequency in the flow must be estimated. This may involve literature investigations on similar flows, to understand the typical frequencies. Hence, the highest frequency f_{max} is estimated from previous investigations of similar flows using the *Nyquist* criterion, $f_{filter} \simeq 2\times f_{max}$ is selected. A serious consequence of not having low pass filter might lead to contamination of the signal energy at frequencies $< f_{filter}$ by higher frequencies if the *Nyquist* sampling criteria is applied. Hence, a false energy peak in the power spectrum will be evident. On the other hand, high pass filtering is used to clean the signal, if Fast Fourier Transform (FFT) spectral calculations are required. When the CTA signal fluctuates on

a timescale longer than the total length of the data record, it may give unwanted high frequency contributions. High pass filtering makes the signal stationary but it eliminates the low-frequency oscillations. Hence, in most cases digital filtering using software such as MATLAB is more appropriate than using a high pass filter.

A D.C. offset to the instantaneous signal and/or an amplification may also be necessary to match the output voltage to the data logger. This reduces the D.C. offset signal, by subtracting the offset voltage E_{offset}. In most CTA measurements, the signal may not be in the range of the A/D board. For example, if the A/D board can measure only $\pm$ 5 V, it is necessary to modify the raw signal to ensure it always remains in this range. In most low to medium velocity applications with a turbulence intensity between 2 % to 3 %, a 12 bit A/D board is sufficient without the need for amplification (Brunn 1995). For example, a 12 bit A/D board has a resolution of 1.2 mV in the 0-5 V range. Suppose we apply a gain of 16 prior to digitization its resolution is then enhanced to 0.075 mV.

2.4.5 The Present Hot-Wire Configurations

Brunn (1995) describes that heat losses along the ends of the hot wire sensor can be minimized by selecting the appropriate wire configurations. In particular, the length l_w and diameter d_w of the wire are crucial parameters which determine the extent of heat losses from the sensor. In their hot wire measurements, Browne et al. (1982) used l_w/d_w = 208 while Champagne (1978) used a hot wire sensor with $l_w/d_w = 160$ to determine the fine scale structure. Bradshaw (1971) commented that the heat losses at the ends of the sensor are approximately 15 % when $l_w/d_w \simeq 200$ with the wire operated at an overheat ratio of 1.0.

In light of these arguments, the present single component velocity measurements were conduced using a copper plated tungsten wires of length $l_w \approx 1$ mm and diameter d_w = 5 μm. Selecting this configuration and operating the hot wire at an overheat of 1.5 (discussed later) provides us with the ratio $l_w/d_w = 200$ which ensures low heat loss from the edges of the sensor. The probes were locally made. The calculated cut-off frequency f_c for the present experiments was $f_c \simeq 15$ k Hz. Data were filtered at 9.2 k Hz and sampled at a Nyquist frequency of 18.4 k Hz for a total duration of 22.4 seconds. The present measurements are performed using a single wire probe, although a cross-wire could have provided significantly larger information, especially about the v-component of the velocity. However, the main objective of the present study is not to quantify each velocity component, but to study the effect of initial conditions on development of the plane jet

by measuring the axial component of the jet velocity. Hence, a single wire probe is used, as opposed to a cross or tri-axial probe.

2.4.6 Hot Wire Calibration

A hot wire is a relative technique so it must be calibrated against a known flow velocity to establish a relationship between the raw signal output and the flow velocity. Hot wire calibration must be performed as accurately as possible because small errors in calibration could results in large uncertainties in measurements (Brunn 1995, Perry 1982). Ideally, calibration must be performed in a flow with very low turbulence intensity. The present calibration was performed by exposing the probe to a set of known (pitot static tube) velocities U while recording the corresponding voltages E. Then, a curve fit through the points (E,U) represents the transfer function to be used when converting data records from voltages into velocities. In fluid mechanics experiments, calibration is either carried out in a dedicated probe calibrator which normally is a free jet or in a wind-tunnel with a pitot-static tube as the velocity reference. Temperature must either be invariant during the process or the final calibration must be corrected for temperature variations.

Once the output voltage E and the corresponding velocity U have been collected, the transfer function (relationship between U and E) is determined. Perry (1982) discusses two types of transfer functions used for wire calibrations. The famous Kings' Power Law, given by the relation

$$E^2 = A + BU^n \tag{2.3}$$

and the polynomial curve fitting, given by

$$U = C_o + C_1E + C_2E^2 + C_3E^3 + C_4E^4 \tag{2.4}$$

are used. Here, A, B, $C_o..C_4$ are experimental constants and n is a numerical constant usually taken as 0.45 for most hot wires. However, power law fits are less accurate than polynomial fits, particularly when the velocities vary a lot. This is because the factor n is slightly velocity dependent (Brunn 1995). On the other hand, polynomial fits may be incorrect if velocity is outside the calibrated range. Therefore, before using a polynomially fitted transfer function, the range of velocities must be checked to ensure that it lies within the calibrated range.

For the present experiments, a fourth-order polynomial fit was used. The hot wire calibration was performed in the jet potential core where turbulence intensity $\leq 0.5\,\%$, against a pitot static tube velocity. To attain a high level of accuracy, two sets of calibrations were performed, one before and the other after each experiment. This also enabled us to determine drifts in velocity due to changes in ambient conditions. Given the isothermal conditions in the laboratory, very small occasional drifts in velocity were noted. These were compensated for by two ways: either by repeating the particular experiment or by using an 'average' transfer function of the two sets of calibrations, depending upon the extent of the drift. In most circumstances, the experiment was repeated to attain a higher level of accuracy.

2.5 Data Acquisition

Hot wire anemometry requires a data acquisition system. Since the raw signal is a continuous analogue signal, an analogue to digital converter (A/D board) is required together with a suitable data logging software. For the present experiments, a PC-30F data acquisition board attached to a personal computer was utilized. This PC-30F card is a 200 k Hz multi-channel A/D converter with a 12-bit (2.4 mV) resolution. After monitoring the signal on a Tektronix oscilloscope, real-time data were visualized in Waveview2.0. Waveview2.0 is a DOS based data acquisition software which enables collection and preliminary analysis of data. It was developed by Eagle Technology, is extensively configurable and easy to use.

The input range of the A/D board was $\pm$ 5 V. To ensure that the measurement signal remained within this range, an offset was applied to the hot-wire voltage. This offset forced the output signal to vary within $\pm$ 3 V, confirming that the finite range of the A/B board did not clip off the higher order moments of velocity fluctuations. In real-time data acquisition, this is a known problem, for instance see Tan-Atichat et al. (1996).

2.6 Experimental Uncertainties

In hot wire measurements, uncertainties are dependent on wire calibrations, data reduction (conversion of voltages to velocities) and standard errors associated with the measuring instrument. The most significant contributions arise from hot wire calibrations.

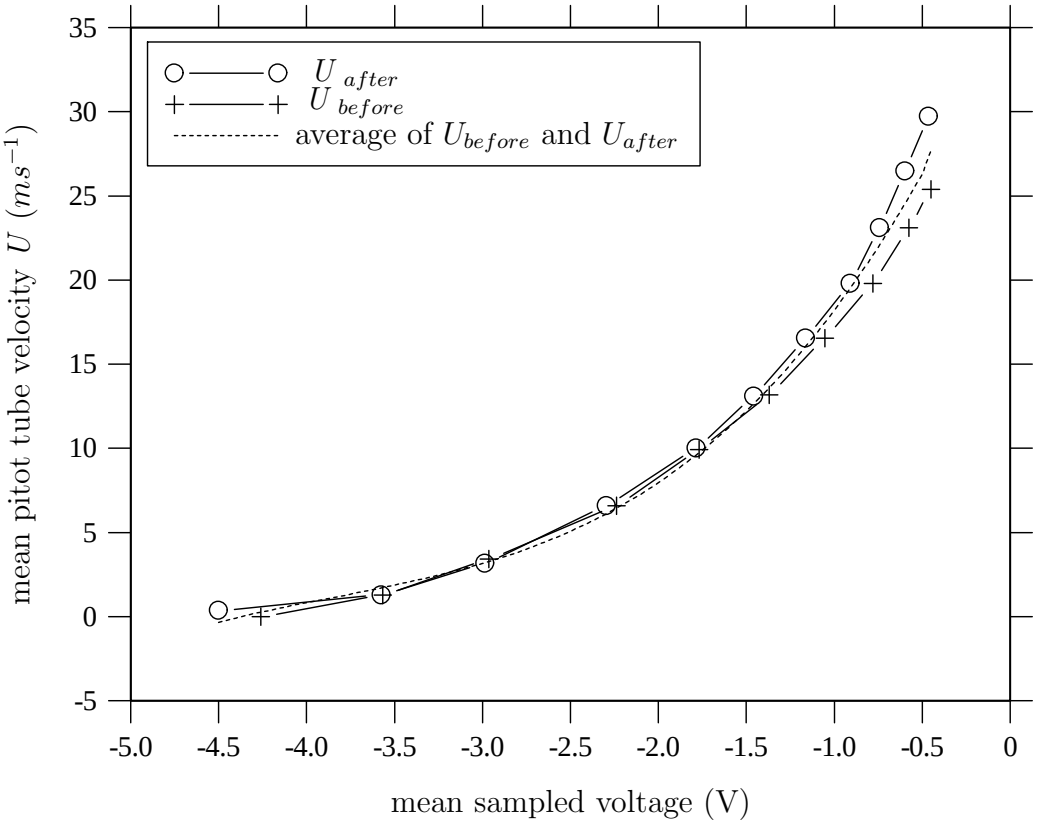

Figure 2.7: A typical fourth-order polynomial curve for the calibration, before and after experiment.

2.6.1 Calibration Error

For each experiment, the hot wire was calibrated against a pitot-static tube velocity using on average, a 10 point calibration. A digital manometer (with an accuracy of $\pm$ 10 Pa) was used to record the dynamic pressure at various wind speeds. Correspondingly, the mean voltage was sampled using an A/D converter, and a transfer function deduced (Equation 2.4.6). Figure 2.7 displays a typical calibration transfer function obtained in the velocity range $0 \leq U \leq 30$ m s^{-1}, before and after the experiment. An average function based on U_{before} and U_{after} is also included.

The experimental uncertainties were computed from the transfer functions as follows: Suppose the functions are given by

$$U_{before} = B_o V^4 + B_1 V^3 + B_2 V^2 + B_3 V + B_4 \tag{2.5}$$

$$U_{after} = C_o V^4 + C_1 V^3 + C_2 V^2 + C_3 V + C_4 \tag{2.6}$$

$$U_{av} = \frac{1}{2}\left[K_{o,av} V^4 + K_{1,av} V^3 + K_{2,av} V^2 + K_{3,av} V + K_{4,av}\right] \tag{2.7}$$

where U_{before}, U_{after} are the calibrated velocities before and after experiment, U_{av} is mean of U_{before} and U_{after}, $B_o...B_4$, $C_o...C_4$ are polynomial constants and $K_{o,av}...K_{4,av}$ is calculated so that $K_{o,av} = 1/2\,(C_o + B_o)$, $K_{1,av} = 1/2\,(C_1 + B_1)$ and so on. Clearly, the errors in the average transfer function will accumulate due to the contributions from $B_o...B_4$, $C_o...C_4$. These errors, if denoted as ΔK, will contribute to ΔU and are thus given by

$$\Delta U = \Delta K_{o,av} + \Delta K_{1,av} + \Delta K_{2,av} + \Delta K_{3,av} + \Delta K_{4,av} \tag{2.8}$$

where $\Delta K_{o,av}$, $\Delta K_{1,av}...\Delta K_{4,av}$ are sum of absolute errors. That is

$$\Delta K_{0,av} = \left| B_o - \frac{1}{2}\,(B_o + C_o) \right| \; or \; \left| \frac{1}{2}\,(B_o + C_o) - C_o \right|$$

$$\Delta K_{1,av} = \left| B_1 - \frac{1}{2}\,(B_1 + C_1) \right| \; or \; \left| \frac{1}{2}\,(B_1 + C_1) - C_1 \right|$$

In present experiment, the errors are effectively minimized by repeating the experiment several times and obtaining an average transfer function with $\Delta U \pm 1.5\%$. Where an uncertainty in U exceeded $\pm 1\%$, data were discarded and the experiment was carefully re-performed.

2.6.2 Data Acquisition System Error

Uncertainties associated with the data acquisition system are very small. Jorgensen (2002) presents a method to calculate the uncertainties contributed by the A/D system. The relative uncertainty is given by

$$\Delta U_{AD} = \frac{1}{\sqrt{3}} \frac{E_{AD}}{2^n} \frac{\partial U}{\partial E} \frac{1}{U} \tag{2.9}$$

where E_{AD} is the input range of the board, n is its resolution in bits, U is the velocity to be measured and $\partial U/\partial E$ is the tangential slope (sensitivity factor) of the calibration curve at the particular velocity at which the measurement is performed. Hence, this error somewhat depends on the calibration curve, its accuracy and the velocity range up to which the wire is calibrated.

For the present A/D board with a 12-bit resolution, $E_{AD} = 10\,V$ and recorded velocities up to 50 $\mathrm{m\,s^{-1}}$, the maximum uncertainty $\Delta U_{AD} \simeq \pm 0.05\,\%$. Typically, in most present-day hot wire experiments, A/D board errors are between 0.05 to 0.08 % (Jorgensen 2002).

2.6.3 Other Uncertainties

Like any other experiment, hot wire anemometry is subject to many other systematic and random errors. The influence of these errors can be severe if an experiment is performed in an uncontrolled environment or without extreme care. The probe positioning which involves aligning the sensor to the flow should be done carefully. For present single-wire measurements, the probe is aligned normal to the flow and its stability is checked to avoid vibrations that could create secondary disturbances. To check the probe alignment with the jet axis, a Tektronix digital oscilloscope was used to monitor the hot wire signal output, while moving the probe across the flow (along the y-direction). The maximum value of the mean centerline velocity was thus noted at that location. This y-position was deduced to be the jet centerline. Such a procedure was performed at all downstream locations where centerline velocity measurements were required. Experiments where temperature variations may occur, corrections must be made to the acquired voltages if ambient conditions vary. Any variations in ambient pressure will influence the density of the surrounding air and hence the velocity. However, since the experiment was performed under isothermal conditions, the combined effect of these minor errors are not significant in the present experiment.

2.6.4 Summary of Errors

The maximum cumulative errors in the present velocity measurements, due to the contributions from various factors discussed so far, are now summarized. The mean and turbulence properties suffer from standard errors due to the probe calibration, its orientation, data reduction and A/D sampling board. Most significant contributions are from the probe calibration. Thus, to reduce the magnitude of errors due to probe calibration, the hot wire probe was calibrated twice during each experiment and data were discarded if errors accumulated to over 2 %.

Table 2.1 summarizes the standard uncertainties due to major contributions such as calibration, data reduction and A/B sampling board. Actual uncertainties in the mean and turbulent statistics are derived from the sources listed the table. We have also estimated the experimental errors in the various primary quantities (mean, rms, skewness and flatness) from estimated inaccuracies due to the sources listed in Table 2.1 and from the observed scatter in the data reported hereafter. Hence, Table 2.2 presents a summary of these errors.

Source of Error	**Typical Value** (%)
Calibration	1.5
Data Reduction	0.5
A/D Board Resolution	0.05
Others	0.01

Table 2.1: Contributions of errors to the mean and turbulent statistics from different sources.

mean ($\pm\ \Delta U$)	**rms** ($\pm\ \Delta\ u^{'}$)	**skewness** ($\pm\ \Delta\ S_u$)	**flatness** ($\pm\ \Delta\ F_u$)
2 %	2.5 %	3.5 %	3 %

Table 2.2: Errors in the mean and turbulent quantities.

Error	**Estimation Strategy**	**Magnitude** %
lateral profiles of initial mean velocity	2 ($\%\,\Delta\,U\ +\ \%\,\Delta\,U_{o,c}$)	8
lateral profiles of initial turbulence intensity	$\%\,\Delta\,u^{'}\ +\ \%\,\Delta\,U$	5
normalized centerline mean $[U_{o,c}/U_c]^2$	2 ($\%\,\Delta\,U_{o,c}\ +\ \%\,\Delta\,U_c$)	8
centerline turbulence intensity $u_c^{'}/U_c$	$\%\,\Delta\,u_c^{'}\ +\ \%\,\Delta\,U_c$	5
decay, spreading rate K_u, K_y	best/'worst-fit' curves	3
velocity half-width $y_{0.5}$	lateral velocity profiles	2
virtual origins x_{01}, x_{02}	best/'worst-fit' curves	10

Table 2.3: Actual errors in jet properties.

The uncertainties in the present measurements are consistent with the standard uncertainties found in literature for hot wire measurements. For example, Zhou et al. (1998) found an error of $\pm 5\%$ in the mean and $\pm 6\%$ in the rms, while Hussain and Clark (1977) found errors up to $\pm 5\%$ for their measurements. Also, Mi, Nathan and Nobes (2001) encountered an error of $\pm 1.5\%$ in their mean and $\pm 2\%$ in their rms. Thus, the uncertainties in our measurements are entirely consistent with those in published literature.

The uncertainties in the derived quantities e.g the turbulence intensity (normalized rms $u'_{n,c}$), normalized mean velocity ($[U_{o,c}/U_c]^2$), decay rates of centerline mean velocity (K_u) are listed in Table 2.3. For most of these quantities, errors are derived from the graphical analysis of the observed scatter or using the best-fit curves. The exact approach used to estimate the errors are enlisted in the table.

2.7 Summary of Experimental Conditions

Chapters 3-6 contain the results of the present investigation. Each chapter has its own set of initial conditions. Table 2.4 summarizes the nozzle type, exit velocity, Reynolds number, nozzle aspect ratio and the nozzle boundary layer state for each investigation.

Chapter	**Investigation**	$U_{o,c}$ (m/s)	Re	**Nozzle Type**	AR	**Boundary Layers**
3	Reynolds Number	3.98-44.19	1,500-16,500	radially contoured, r/H = 2.14	60	laminar
4	Nozzle Contraction Profile	27.0	18,000	r/H = 0 (orifice) to 3.60 (contoured)	72	laminar
5	Nozzle Aspect Ratio	27.0	18,000	radially contoured, r/H = 3.60	15-72	laminar
6	Effect of Sidewalls	18.40	7,000	radially contoured, r/H = 2.14	60	laminar

Table 2.4: A summary of the initial conditions of each experiment, from Chapters 3-6.

Chapter 3

INFLUENCE OF REYNOLDS NUMBER

3.1 Introduction

Several inconsistencies between previous investigations on the Re-dependence of plane jets were identified in Chapter 1.5.1. It was revealed that majority of the previous investigations on plane jet e.g. Bradbury (1965), Heskestad (1965), Gutmark and Wygnanski (1976), Browne et al. (1982) and Thomas and Goldschmidt (1986) used a single Reynolds number. The Reynolds numbers for these previous investigations span a wide range, approximately between 7,000 and 36,900. However, since each individual investigation was conducted at a single Reynolds number, these studies do not provide any information as to how the flow evolves with changes in Reynolds number. It is also not possible to deduce the effect of Reynolds number by comparing these individual experiments because their experimental conditions are different. George (1989) argued theoretically, that, differences in exit conditions could lead to differences in the downstream development of jet flows. Further, experimental work by Hussain and Clark (1977) and Antonia and Zhao (2001) showed that differences in experimental conditions lead to significantly different jet flows. Accordingly, the data of separate investigations at a single Re cannot be used to assess the Re-dependence issue for plane jets specifically.

While Namar and Ötügen (1988) and Löfdahl et al. (1997) measured their jet at $1{,}000 \leq Re \leq 7{,}000$ and $10{,}000 \leq Re \leq 20{,}000$ respectively, their investigations are for either a quasi-planar or a wall jet (see their respective papers). Also, Hussain and Clark (1977) measured a quasi-plane jet at Reynolds numbers of 32,500 and 61,400. At such Reynolds numbers, we do not expect to see significant changes in the flow properties mainly because they have already converged close to their respective asymptotic values (Dimotakis 2000). While Heskestad (1965) presented the centerline turbulence intensity

at Re over the range $4{,}700 \leq Re \leq 36{,}900$, his measurements are sparse, lacking data points, especially, for $x/H < 20$. Although he provided information on the far field flow evolution, his investigation cannot be used to determine the near-region flow evolution of a plane jet. Lemieux and Oosthuizen (1984, 1985) investigated a radially contoured plane nozzle of aspect ratio 58, and for Reynolds numbers over the range $700 \leq Re \leq 4{,}200$. While a substantive dependence of the jet properties on Re were demonstrated, their range of Reynolds numbers were too small. Recently, a study using direct numerical simulation (DNS) by Klein et al. (2003) up to an axial distance of $x/H \leq 20$ and for $Re \leq 6{,}000$ indicated some dependence of the mean flow and turbulence properties on Re. Unfortunately, their Reynolds number range spans across a small range and the data are only in the near field.

Hence, to the best of our knowledge, no specific study of plane jets on Re-dependence that covers a large range from low to moderately high Reynolds numbers is currently available. To broaden our understanding of Re-dependence on plane jets, the present research is conducted to cover Reynolds numbers over the range $1{,}500 \leq Re \leq 16{,}500$. This study also extends the study by Lemieux and Oosthuizen (1984, 1985) to provide data for a wider range of Re using a nozzle of an exit contraction profile similar to theirs. What follows from here onwards is a concise account of the experimental details, results, discussions and conclusions of the present research.

3.2 Experiment Details

Figure 3.1 shows a schematic arrangement of the plane nozzle setup. Two perspex plates of dimensions 720 mm vertical × 340 mm horizontal were aligned at the wind tunnel exit with a gap width $H = 5.6$ mm. G-Clamps were used to attach it firmly to the wind tunnel. The connecting edges were sealed to avoid leakage. The nozzle had an aspect ratio $AR = 60$. Its lip was contoured with an inner-wall contraction profile defined by $r/H = 2.14$. The nozzle was tested and found to produce an approximate top hat initial velocity profile. Thus the findings of this investigation are applicable to conventional smoothly contracting nozzles, whose initial velocity profiles are top hat as well.

Control of the jet Reynolds number Re was achieved by varying the speed of the wind tunnel fan. The maximum achievable Reynolds number was 16,500 without reducing the nozzle aspect ratio. A higher Reynolds number was obtainable, but at the cost of a lower nozzle aspect ratio. The range of Reynolds numbers was thus selected to be

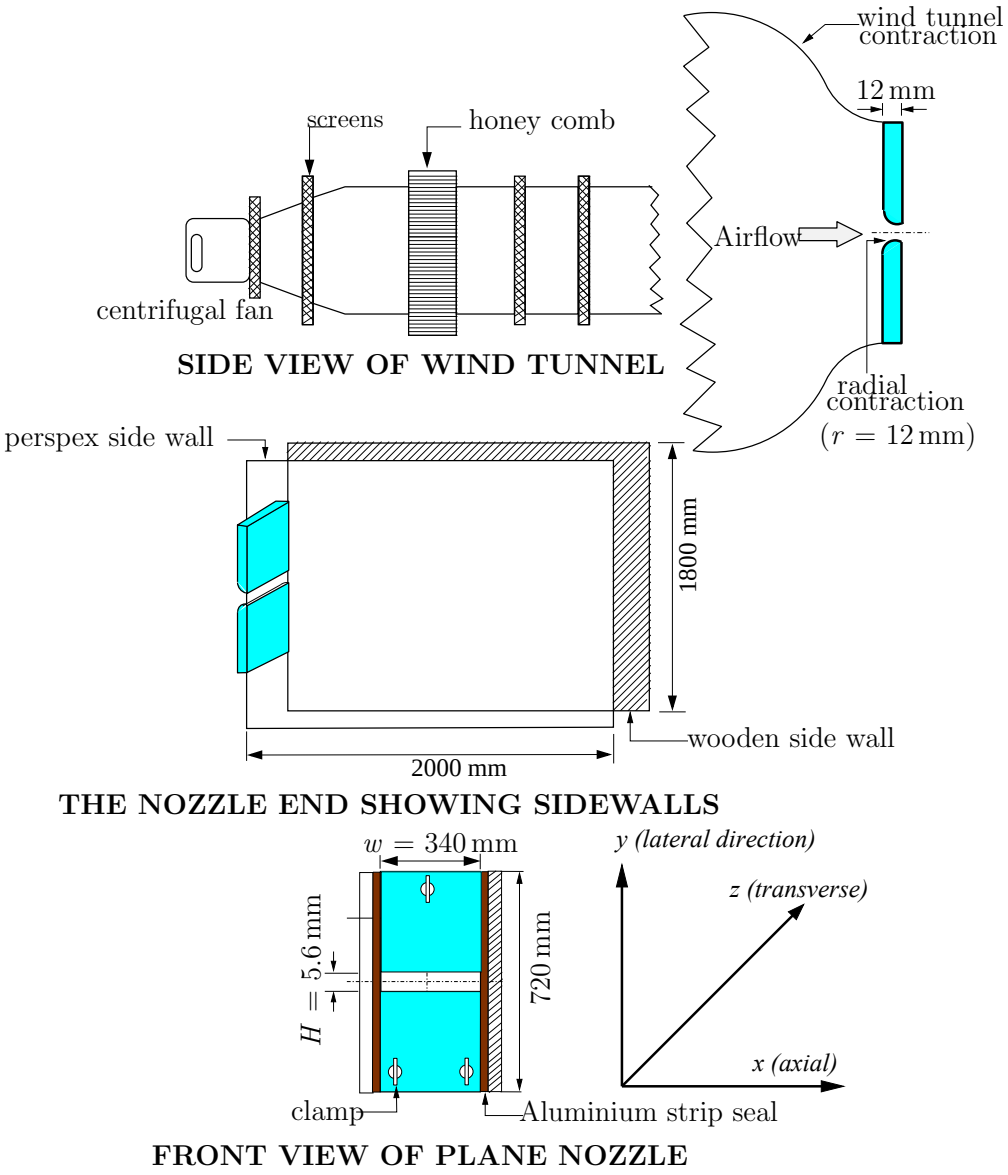

Figure 3.1: A schematic diagram of the plane jet facility, showing the wind tunnel, plane nozzle and sidewalls.

$1{,}500 \leq Re \leq 16{,}500$ with an accuracy of $\pm$ 3 %. To undertake measurements, a three-dimensional traverse system was employed. The hot-wire probe was carefully mounted on a traverse. The alignment of the jet with the nozzle axis and the traverse with the nozzle axis was checked. The initial velocity was measured at 0.5 nozzle widths downstream. Then, the centerline streamwise velocity was measured at various selected Reynolds numbers from $x/H = 0$ to $x/H = 160$. The lateral (y) distribution of the streamwise velocity was also measured.

3.3 Results and Discussion

3.3.1 The Initial Velocity Field

Figure 3.2 shows the lateral profiles of the normalized mean velocity and turbulence intensity obtained at $x \simeq 0.5\,H$ for $1{,}500 \leq Re \leq 16{,}500$. A slight dependence of the normalized mean velocity on Re is noticeable. This dependence is more evident for $Re < 7{,}000$. However, the mean velocity profiles become nearly identical when $Re \geq 7{,}000$. Dependence of mean velocity profiles on Re measured at $x/H = 1$, was noted by Namar and Ötügen (1988) for their quasi-plane jet. In their measurements, the normalized mean velocity profiles did not become identical even at $Re = 7{,}000$.

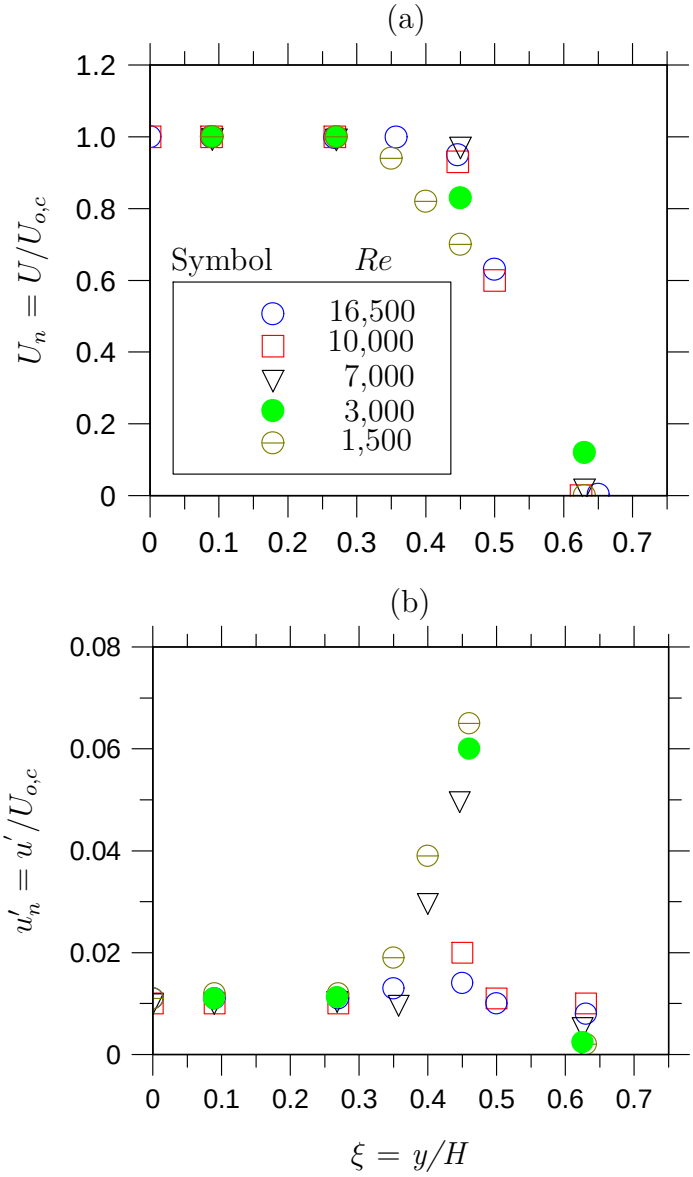

Figure 3.2: Lateral profiles of (a) the normalized mean velocity U_n and (b) the turbulence intensity $u_n^{'}$ obtained at $x/H \simeq 0.5$ for $1{,}500 \leq Re \leq 16{,}500$.

Re	**Displacement Thickness**, δ^*	**Momentum Thickness**, θ	**Shape Factor**, H
1,500	0.746	0.383	1.95
3,000	0.615	0.311	1.98
7,000	0.516	0.253	2.04
10,000	0.550	0.224	2.46
16,500	0.652	0.262	2.49

Table 3.1: Summary of the pseudo-boundary-layer characteristics (mm) of the plane jet at different Reynolds numbers of investigation.

The entire range of Reynolds numbers exhibit a laminar boundary layer at $x = 0.5H$. This is easily verified by estimating of displacement thickness δ^*, the momentum thickness θ and the shape factor $H = \delta^*/\theta$ using the following integrations.

$$\delta^* \equiv \int_{y=0}^{y=\infty} \left(1 - \frac{U}{U_{o,c}}\right) dy \tag{3.1}$$

and

$$\theta \equiv \int_{y=0}^{y=\infty} \frac{U}{U_{o,c}} \left(1 - \frac{U}{U_{o,c}}\right) dy \tag{3.2}$$

While it is obvious that the estimates of δ^*, θ and H will not be very accurate due to the coarse measurement grid, their relative magnitudes will indicate whether the initial boundary layers are laminar, turbulent or transitional. The calculated magnitudes of these parameters are summarized in Table 3.1. From the table, it is evident that the shape factor H increases slightly, from 1.95 to 2.49 as Re is increased from 1,500 to 16,500. Pope (2002) attributes that the flatness of the mean exit velocity profiles to the shape factor, which is the ratio of the displacement to the momentum thickness. Theoretically, for a true laminar boundary layer, the shape factor $H \rightarrow 2.60$. Thus, the present nozzle exhibits a laminar boundary layer at its exit plane. The discrepancies between the theoretical value and calculated value of H is possibly due to a slightly downstream location where the present measurements were performed.

For the present profiles, it is evident that the development of the pseudo-boundary layer[1] is

[1]The term 'pseudo-boundary layer' is used because of the measurement location of 0.5 nozzle widths downstream. Strictly, boundary-layer thickness only refers to measurements at nozzle exit only.

somewhat dependent on Re. In other words, increased thickness of the pseudo-boundary layer is noted with decreased Re. This is consistent with Namar and Ötügen (1988) for their quasi-plane jet, who also found an increase in the thickness of boundary layer. Likewise, when Crow and Champagne (1971) varied Reynolds number for a round jet, over the range $10{,}500 \leq Re \leq 51{,}400$, they found a decrease in δ/D from 0.041 to 0.020. Thus, the dependence of the pseudo-boundary layer thickness on Reynolds number for the present investigation is well supported by published literature of the round and quasi-plane jet.

A dependence of boundary layer thickness on Reynolds number indicates that viscosity effects are dominant in the low Re regime. If so, this should inevitably produce low shear-stress, within the boundary layer at the nozzle lip. However, this is not demonstrated from the present measurements. On the contrary, we observe increased thickness of the boundary layer with a decrease in reduced Reynolds number. While a probably cause of this could be a larger drag, the exact mechanism for this discrepancy is not known. Furthermore, over the range $|\xi| \leq 0.30$ - 0.40 where $\zeta = y/H$, the mean velocity is uniform i.e. $U/U_{o,c} \simeq 1$ and approximates to a top hat profile.

The present turbulence intensity in the central region $|\xi| \leq 0.3$ - 0.4 are below 1.0 % for all Re (Figure 3.2). Namar (1986) emphasized that the initial turbulence level plays a key role in development of the flow structure. In fact, Kulman (1985) showed that, for both round and plane jets, the initial turbulence intensity is indeed a significant contributor to variations on their jet flow properties. For the present data, independence from the low pass filter frequency was confirmed by comparing the raw data measured at frequencies of $f_c = 1.5$ k Hz, 3 k Hz and 9.2 k Hz. The peak values of turbulence intensity occur in the shear layer and their magnitudes decrease as Reynolds number is increased. Again, the differences in the shear layer turbulence intensity for different Reynolds numbers are due to the nature of the laminar and turbulent jet. Due to the unsteady and irregular motions of the high-Reynolds number jet as opposed to the smooth, laminar and fast center motions of the low-Reynolds number jet, the high-Reynolds number jet is expected to have reduced instability in its shear layers. Consequently, we see a lower turbulence intensity at $Re = 16{,}500$ than at $Re = 1{,}500$.

The apparent failure to keep the initial flow constant for all Reynolds numbers is owed an explanation. The present measurements have shown that the initial flow is significantly dependent on jet exit Reynolds number. One may argue that this dependence may be induced by the type of nozzle that was used in the present experiment i.e. a radially

contoured nozzle. However, previous investigations e.g. Namar (1986), who used a conventional smooth contraction nozzle, also noted a significant dependence of the initial flow on Reynolds number. Hence, the present dependence is a genuine effect of all smoothly contoured nozzles. Nevertheless, it is deduced that the extent of the variations in initial flow will be less for a smoothly contoured nozzle as opposed to a larger variation for a radially contoured nozzle. This is because the boundary layer thickness of a smoothly contoured nozzle is less sensitive to changes in Reynolds number. Indeed, pipe-jets which have fully developed initial flows, will encounter even lesser variations in boundary layer thickness. Therefore, the dependence of its initial flow on Re will be even less than those noted for a smoothly contoured nozzle.

3.3.2 The Mean Velocity Field

The evolutions of the near field mean velocity are now presented. (The normalized mean velocity graphs for other Reynolds numbers are not shown here for clarity.) Figure 3.3 presents the near field mean velocity along the centerline, for $Re = 3{,}000$, 7,000 and 16,500. Here, the vertical axis is presented in the logarithmic scale, that represents $U_c/U_{o,c}$. This highlights the length of the jet potential core, x_p as the region where the mean velocity is approximately constant and equal to $U_{o,c}$. It is clear that x_p is a function of Re. For example, $x_p/H \simeq 5$ for $Re = 3{,}000$ and $x_p/H \simeq 3$ for $Re = 16{,}500$. That is, x_p decreases with Re. Correspondingly, the jet is expected to spread more widely for higher Re. This deduction is verified by lateral profiles of the normalized mean velocity U/U_c obtained at $x/H = 5$ (Figure 3.4).

Figure 3.4 clearly demonstrates that an increase in Re results in a higher near field spreading of the mean flow field. Hence, we can conclude that, as the Reynolds number is increased, the jet entrains and then, possibly, mixes the surroundings more rapidly in the near field. For their quasi-plane jet, Namar and Ötügen (1988) found a decrease in x_p from $4H$ to $2H$ with an increase in Re from 1,000 to 7,000. Recall that, due to the absence of sidewalls in their facility, Namar and Ötügen's quasi-plane jet may have three-dimensional effects in the near field (see Chapter 6). For the present results, it is likely that the nozzle boundary layer thickness, which scales with Re, and the turbulence Reynolds number, strongly influences the length of the jet potential core. Hence, it is evident that the difference in x_p noted herein is a manifestation of the influence of jet exit Reynolds number on the initial flow (Figure 3.2). Although the similarity distributions of u and U in the mixing layers for $x/H < 4$ would have provided some insight into the evolutions of Kelvin-Helmholtz vortices, these have not been investigated in this thesis.

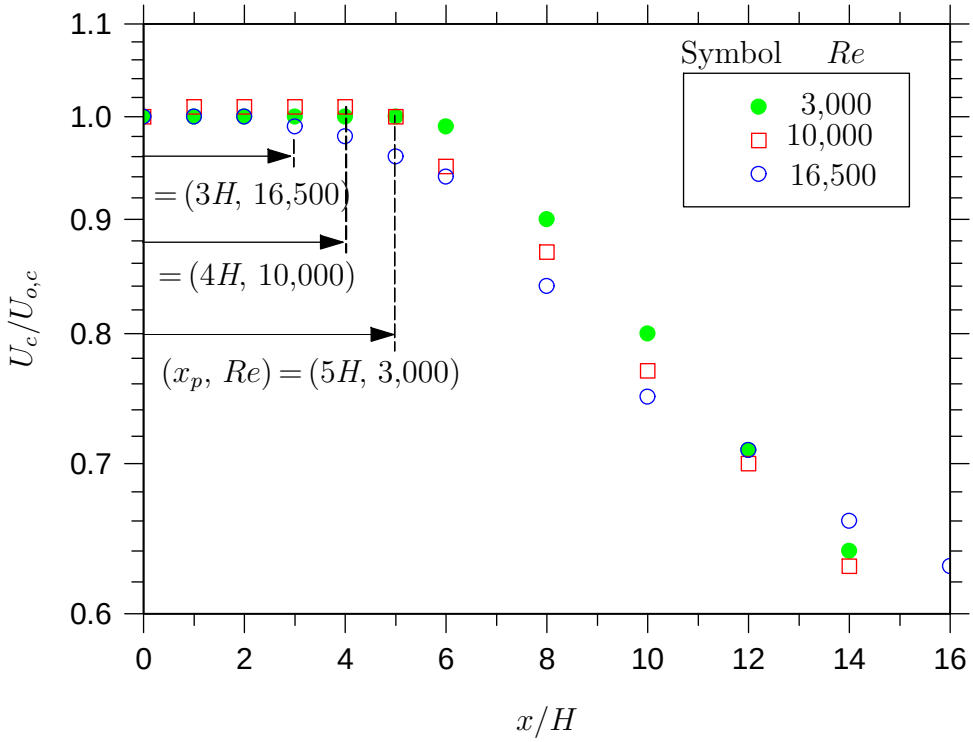

Figure 3.3: The centerline variation of the near field mean velocity $U_c/U_{o,c}$ and the potential core length x_p at different Reynolds number Re.

The normalized mean centerline velocity (representing the velocity decay) over the full measured range is shown in Figure 3.5. For reference, the data from a smooth contraction nozzle of Jenkins and Goldschmidt (1973) for (Re, AR) = (14,000, 24) and Hitchman et al. (1990) for (Re, AR) = (7,000, 60) are included. The present data conform to the well-known relationship expressed by

$$\left(\frac{U_{o,c}}{U_c}\right)^2 = K_u\left[\frac{x}{H} + \frac{x_{01}}{H}\right] \tag{3.3}$$

where K_u is the slope calculated using data over the range $20 \leq x/H \leq 160$, and x_{o1} is the x-location of the virtual origin of the profiles. The normalized mean velocity become self-similar at $x/H > 20$ and closely follow the inverse square relationship.

The present centerline velocity decay rate can be measured by the magnitude of K_u calculated from the linear fit of data between from $20 \leq x/H \leq 160$ with a regression coefficient of $r^2 = 0.99$. Figure 3.6 shows the dependence of K_u on Re. As clearly demonstrated, K_u decreases with increasing Re throughout the measured range. That is, K_u does not

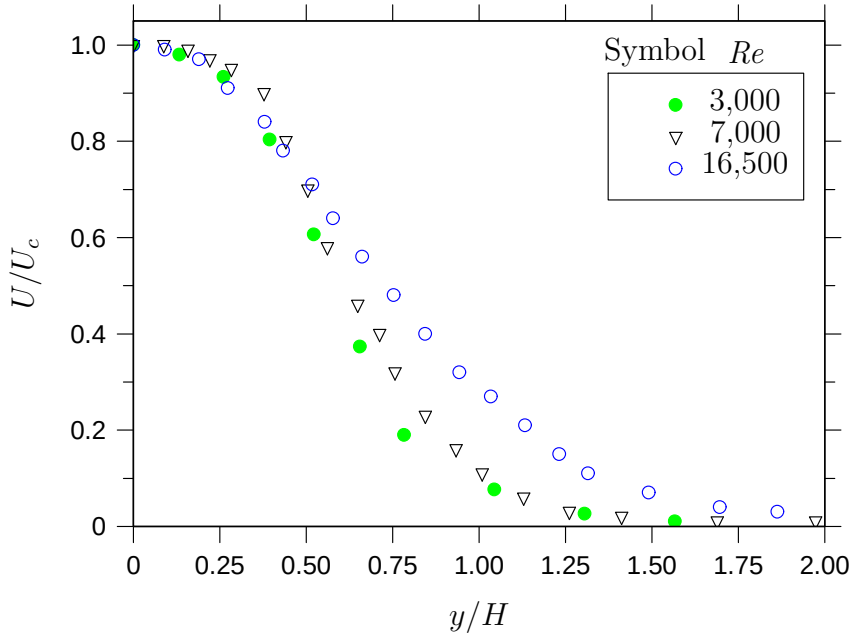

Figure 3.4: Lateral profiles of the mean velocity U/U_c at $x/H = 5$.

approach to an asymptotic value up to $Re = 16{,}500$. This shows that the Reynolds number continues to affect the mean velocity field even at $Re = 16{,}500$. In addition, there is some evidence from Figure 3.6 that the virtual origin x_{o1} is smaller at higher Reynolds number.

The lateral distribution of the mean velocity was measured for a selected set of Reynolds numbers. The normalized profiles of the mean velocity for $1{,}500 \leq Re \leq 16{,}500$ at the selected downstream locations are now presented. Here, the x-coordinate is normalized using the velocity half-widths $y_{0.5}$. Note that $y_{0.5}$ is the lateral distance from the centerline at which the local mean velocity is half of the centerline value. Figures 3.7-3.11 show these normalized mean velocity profiles and their respective comparisons with the Gaussian distribution $U_n = e^{-ln2(y_n)^2}$.

The lateral profiles appears to become congruent at $x/H \simeq 50$ for $Re = 1{,}500$ whereas for $Re = 16{,}500$, the profiles become congruent at $x/H \simeq 3$. This indicates that the distance from the nozzle where the lateral profiles of the normalized mean velocity become self-similar depends upon Reynolds number. As Reynolds number is increased, the mean flow attains self-similarity at an earlier downstream distance. For their LDA measurements from a quasi-plane jet, Namar and Ötügen (1988) found that the mean profiles became self-similar at $x/H = 10$ for $Re = 7{,}000$. This compares reasonably well with the present profiles at $Re = 10{,}000$. Also, for their measurement at $Re = 2{,}000$, the mean profiles

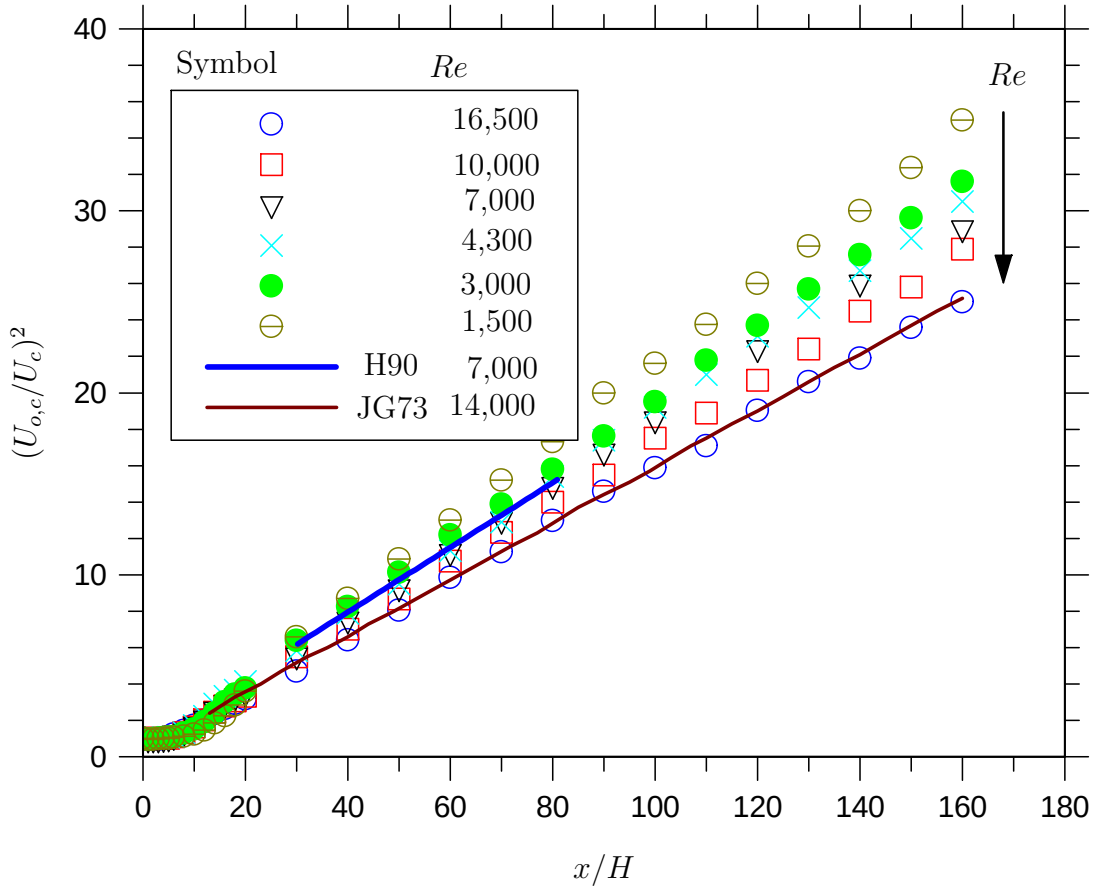

Figure 3.5: The centerline variation of the normalized mean velocity $(U_{o,c}/U_c)^2$ for different Reynolds number Re. Note: H90 - Hitchman (1990), JG73 - Jenkins and Goldschmidth (1973).

became self-similar at $x/H = 25$ when compared with our self-similar location of $x/H = 20$ at $Re = 3{,}000$. Furthermore, Browne et al. (1984) found that for their smooth contraction nozzle measured at $Re = 30{,}000$, the lateral profiles of the mean velocity became self-similar at $x/H \simeq 5$. Subtle difference in the x/H location between our measurements at $Re = 16{,}500$ and theirs are probably attributable to the nozzle geometry (i.e. they used a conventional smoothly contoured nozzle or due to Reynolds number or other initial conditions.

Although the lateral profiles of the normalized mean velocity (Figures 3.7-3.11) exhibit self-similarity for all Reynolds numbers, the axial location of self-similarity region differs. Even for $Re = 10{,}000$ and 16,500, the x-locations are different. (i.e. self-similarity occurs at $\simeq 10$ for the former and 5 for the latter). Such a large difference is surely not subject to errors. Thus, we can further conclude that Reynolds number continues to affect the mean velocity field at $Re = 16{,}500$, at least for the present measurements.

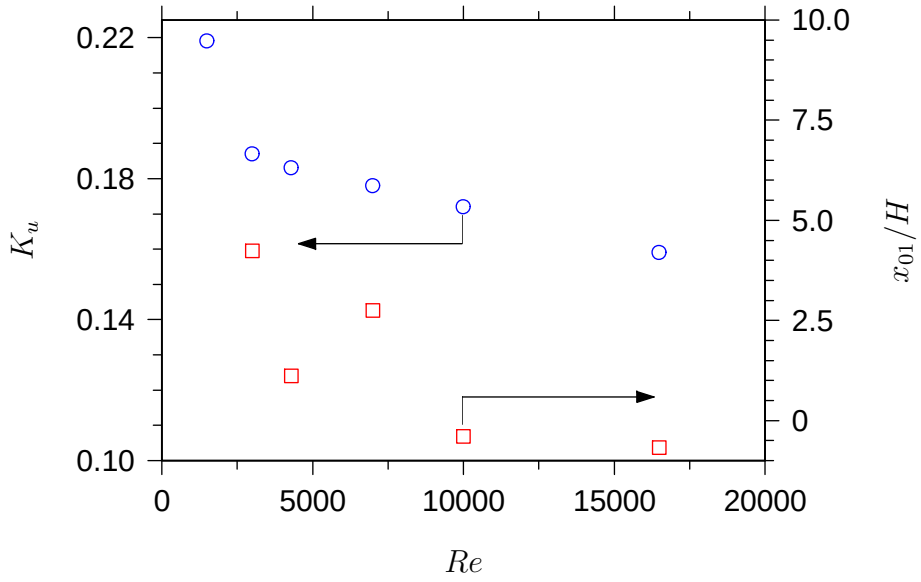

Figure 3.6: Dependence of the centerline decay rate of mean velocity K_u and the virtual origin x_{01} on the Reynolds number Re.

Using the normalized profiles of the mean velocity, the velocity half-widths $y_{0.5}$ were derived. Figure 3.12 shows the streamwise variations of the velocity half-width $y_{0.5}$ at different Reynolds numbers. As expected, the data conform to the following far-field relation

$$\frac{y_{0.5}}{H} = K_y \left[\frac{x}{H} + \frac{x_{02}}{H} \right] \tag{3.4}$$

Here, the constants K_y and x_{02} are the spreading rates and virtual origins respectively, determined by experiment. When Re is increased from 1,500 to 16,500, the half-width decreases consistently. This is better illustrated in Figure 3.13 by the Re-dependence on K_y, where K_y is a measure of the jet spreading rate. A smooth decrease in the spreading rate with an increase in Re is evident, which is consistent with the trend in the decay of U_c (Figure 3.5). Taking together Figures 3.6 and 3.13 prove that, in contrast to the near field case, the far field entrainment rate is reduced by increasing Reynolds number throughout the measured ranges of Re.

For reference, the $y_{0.5}$ of Jenkins and Goldschmidt (1973), Hitchman et al. (1990), Browne et al. (1982) and Lemieux and Oosthuizen (1985) are reproduced in Figure 3.12. Also shown in Figure 3.13 are the spreading rates of Lemieux and Oosthuizen (1985) who measured Reynolds numbers over the range $700 \leq Re \leq 4{,}200$. There is a very close match of the nozzle geometry between our configurations and theirs (i.e. radially contoured nozzle

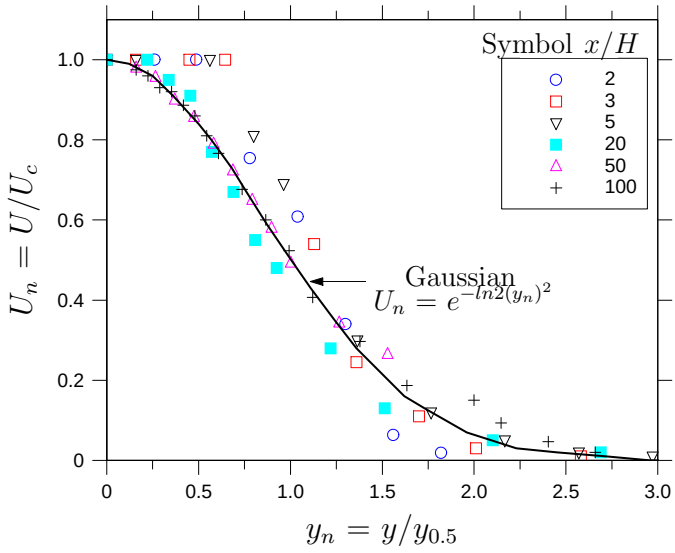

Figure 3.7: Lateral profiles of the normalized mean velocity U_n for Re = 1,500.

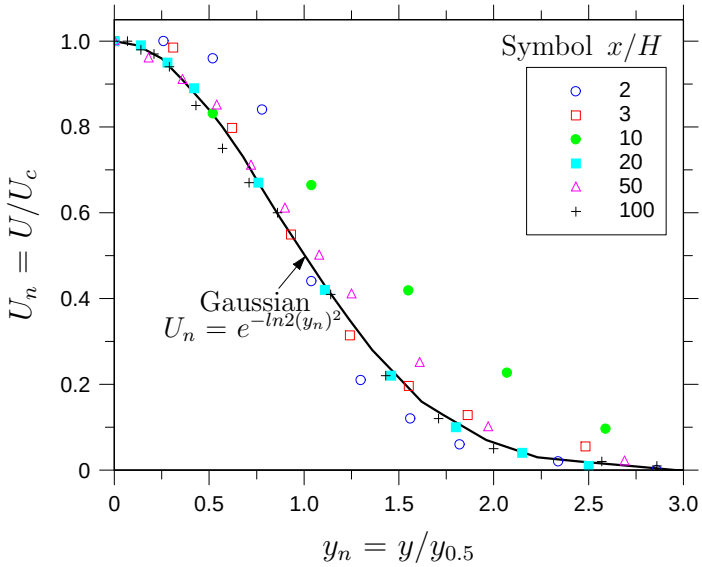

Figure 3.8: Lateral profiles of the normalized mean velocity U_n for Re = 3,000.

for both, $r/H \simeq 1.50$ for theirs versus 2.14 ours) and aspect ratio (58 for theirs and 60 ours). However, the nozzle contraction profile $r/H \simeq 1.50$ for their investigation versus our r/H of 2.14 is also not insignificant. Chapter 4 demonstrates that differing r/H has an impact on the downstream flow properties. Specifically, from Chapter 4, we see that an increase in r/H is found to reduce the velocity half widths. Thus, if we compare the spreading rates of Lemieux and Oosthuizen (1985) at Re = 1,900 and the present spreading rate at Re = 1,500, we observe a smaller magnitude of K_y for Lemieux and Oosthuizen (1985) (i.e. 0.137 ours versus 0.130 theirs). Furthermore, at Re = 4,200, they found K_y = 0.110 in contrast to our K_y of 0.127 at Re = 3,000. While it is likely that the slight difference in Re may also contribute to the discrepancy in K_y, the finding in Chapter 4

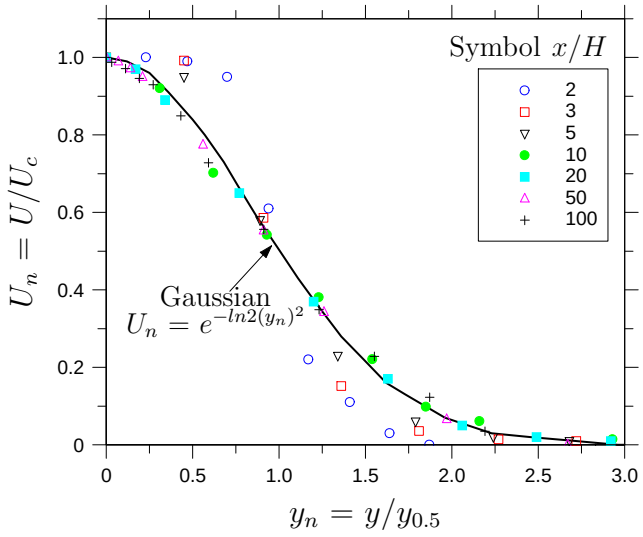

Figure 3.9: Lateral profiles of the normalized mean velocity U_n for Re = 7,000.

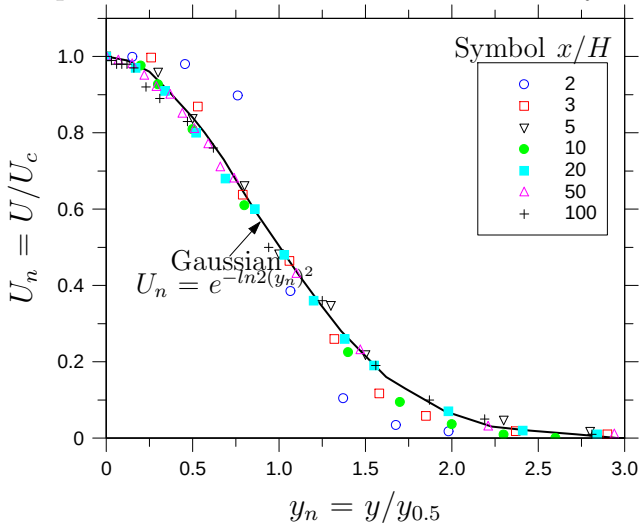

Figure 3.10: Lateral profiles of the normalized mean velocity U_n for Re = 10,000.

of the nozzle profile effect is also consistent. Nevertheless, the present reduction in the jet spreading rates with increased Re is strongly supported by Lemieux and Oosthuizen (1985).

The present measurements cannot be compared directly with other previous investigations. As discussed in the literature review, slight differences in initial conditions can produce significant differences in the flow statistics. For instance, Jenkins and Goldschmidt (1973) measured $K_y = 0.093$ at Re = 14,000 (AR = 24) and the present investigation obtained $K_y = 0.090$ for Re = 16,500. Similarly, the values of $K_y = 0.108$ at Re = 7,000 (AR = 60) by Hitchman et al. (1990) differs from the present $K_y = 0.112$ for Re = 7,000. Both measured a conventional smooth contraction plane nozzle as opposed to a radially contoured plane nozzle for the present investigation. Only the work of Browne

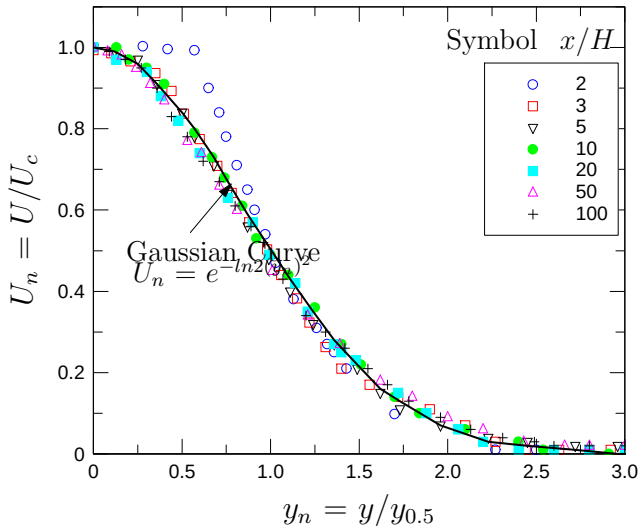

Figure 3.11: Lateral profiles of the normalized mean velocity U_n for Re = 16,500.

et al. (1982) using their conventional smoothly contoured nozzle obtained $K_y = 0.111$ at Re = 7,700 (AR = 20) and this compares well the present $K_y = 0.112$ for Re = 7,000. The small difference between these investigations are likely to be due to the difference in nozzle aspect ratio or for other reasons.

3.3.3 The Fluctuating Velocity Field

Figure 3.14 shows the centerline distributions of the streamwise turbulence intensity $u'_{n,c}$ for the different Reynolds numbers. The shape of the development of $u'_{n,c}$ is similar to that of Browne et al. (1982) for a plane jet (AR = 20 and Re = 7,700) and Thomas and Goldschmidt (1986) for a plane jet (AR = 47 and Re = 6,000). However, the near field local maximum in the intensity $u'_{c,max}$ is different. Browne's local maximum occurs at x/H = 12 and has a magnitude of 0.23 while ours for Re = 7,000, occurs at x/H = 11 and has a magnitude of 0.24. This difference could be due to the large difference in the aspect ratio (our AR = 60 versus AR = 20 in Browne et al. (1982)). Thomas and Goldschmidt (1986) found yet another value of the maximum for Re = 6,000, which occurs at x/H = 11, with a magnitude of 0.27 (Figure 3.14). The discrepancies observed are most likely due to differences in other jet initial conditions such as AR and nozzle profile. Such a notion is consistent with the finding of Mi, Nathan and Nobes (2001) that the occurrence of the pronounced local maximum in the near-field scalar intensity of a round jet depends upon initial conditions.

As noted above, the near field streamwise turbulence intensity grows with axial distance

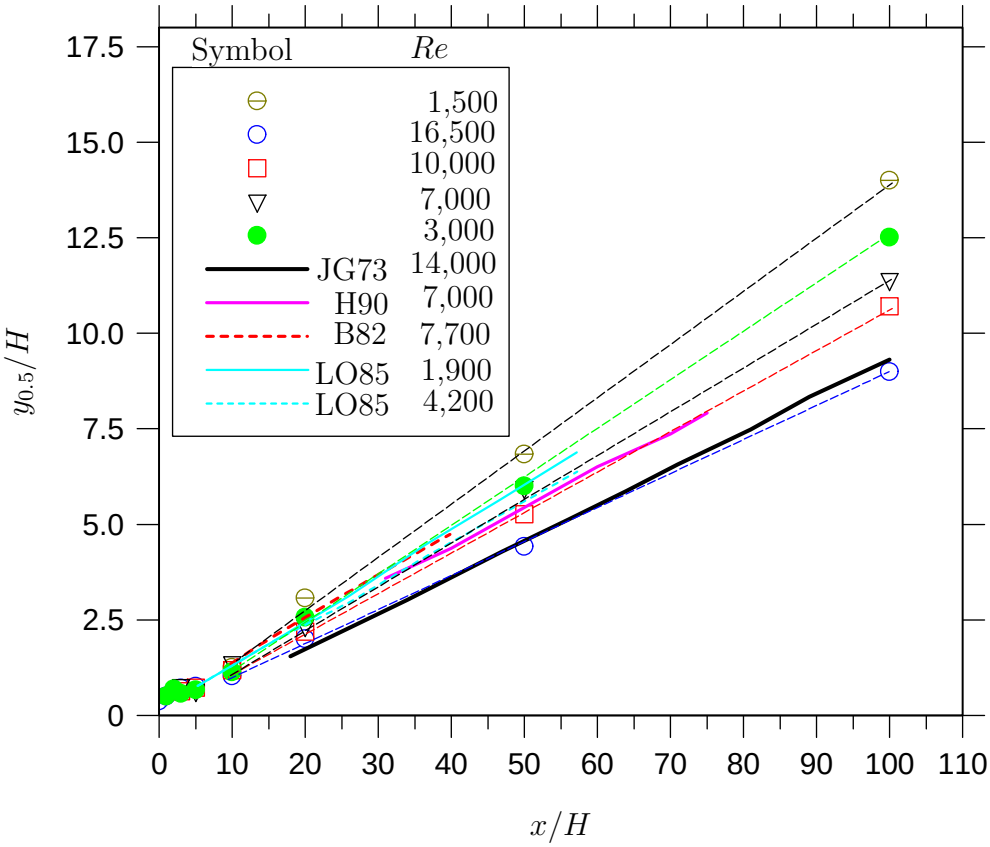

Figure 3.12: The streamwise variation of the velocity half-width $y_{0.5}$ at different Reynolds number Re. Note: H90 - Hitchman et al. (1990), B82 - Browne et al. (1982), JG73 - Jenkins and Goldschmidt (1973) and LO85 - Lemieux and Oosthuizen (1985)

for all Reynolds numbers. In the near field, a local maximum in $u'_{n,c}$ occurs from $x_m = 12$ to $x_m = 18$. As Re is increased from 1,500 to 16,500, the magnitudes of both $u'_{c,max}$ and x_m decrease from 0.31 to 0.22 and from 18 to 12 respectively (see Figure 3.16). The values of $u'_{c,max}$ and x_m are nearly identical for $Re \geq 10{,}000$. Such a significant change in x_m is surely not subject to experimental error. In other words, $u'_{c,max}$ is deduced to be associated with the primary vortex formation. Such vortices have been identified by Browne et al. (1984) for a plane jet, Namar and Ötügen (1988) for a quasi-plane jet and by Hsiao and Sheu (1996) for a plane wall jet at similar axial locations. For a plane wall jet, Hsiao and Sheu (1996) noted that, over the range $3 \leq x/H \leq 8$, the source of high turbulence intensity is mainly from the outer shear layer layer region, where Kelvin-Helmholtz instability mechanisms exist. Kelvin-Helmholtz instability creates small disturbances that roll-up into K-H vortices and lead to the observed $u'_{c,max}$. However, since the present $u'_{c,max}$ occurs further downstream (i.e. at x/H = 12-18), it is likely that these high velocity fluctuations are directly attributable to the occurrences of large scale structures, rather than Kelvin-Helmholtz vortices, which are only present in the near field. This view is

Investigation Reference	Re	AR	Decay K_u	Decay x_{01}/H	Spread K_y	Spread x_{02}/H
Jenkins and Goldschmidt (1973)	14,000	24	0.160	4.00	0.093	-8.20
Hitchman et al. (1990)	7,000	60	0.200	8.05	0.108	-1.94
Browne et al. (1982)	7,700	20	0.147	8.05	0.112	-1.94
Gutmark and Wygnanski (1976)	30,000	39	0.174	-0.72	0.099	-3.21
Lemieux and Oosthuizen (1985)	700	58	-	-	0.160	5.24
Lemieux and Oosthuizen (1985)	1,900	58	-	-	0.130	-1.20
Lemieux and Oosthuizen (1985)	4,200	58	-	-	0.110	-2.06
present investigation	1,500	60	0.219	-	0.137	-2.78
present investigation	3,000	60	0.187	4.24	0.125	-2.89
present investigation	4,300	60	0.183	1.12	-	-
present investigation	7,000	60	0.178	2.75	0.105	-1.48
present investigation	10,000	60	0.172	-0.40	0.098	-0.34
present investigation	16,500	60	0.159	-0.67	0.088	-0.44

Table 3.2: A literature summary of the centerline mean velocity decay and spreading rates of a plane jet. Only data from jets with sidewalls have been summarized.

supported by Mumford (1982), who applied pattern recognition analysis (PRA) to study the fully-developed far field of a plane jet and extracted several types of roller-like eddies experimental data. In addition, Lo (1994) performed large-eddy simulation of a turbulent plane jet and applied pattern recognition analysis to the simulation database. Their work confirmed the existence of double roller structures in the turbulent region of the jet as proposed by Mumford (1982). Therefore, the occurrence of the present $u'_{c,max}$ from 12-18 nozzle widths downstream, can be attributed to such roller (large-scale)structures.

The decrease in both $u'_{c,max}$ and x_m with increased Re is owed an explanation. As mentioned before, such trends were also noted by Hsiao and Sheu (1996) for a plane wall jet and Namar and Ötügen (1988) for a quasi-plane jet. If we assume, based on published literature, that $u'_{c,max}$ is produced by the large-scale vortices, then, as evident from a reduction in x_m in Figure 3.14, we expect a delay in primary vortex formation when Reynolds number is reduced. In fact, Dimotakis et al. (1983) stated that the rapidity at which Kelvin-Helmholtz instability (those primarily responsible for the generation of large-scale structures) develops at some distance downstream, would scale with the nozzle's boundary layer thickness. For the present measurements, we noted a larger thickness of the nozzle boundary layer for Re = 1,500. Correspondingly, the magnitude of x_m is

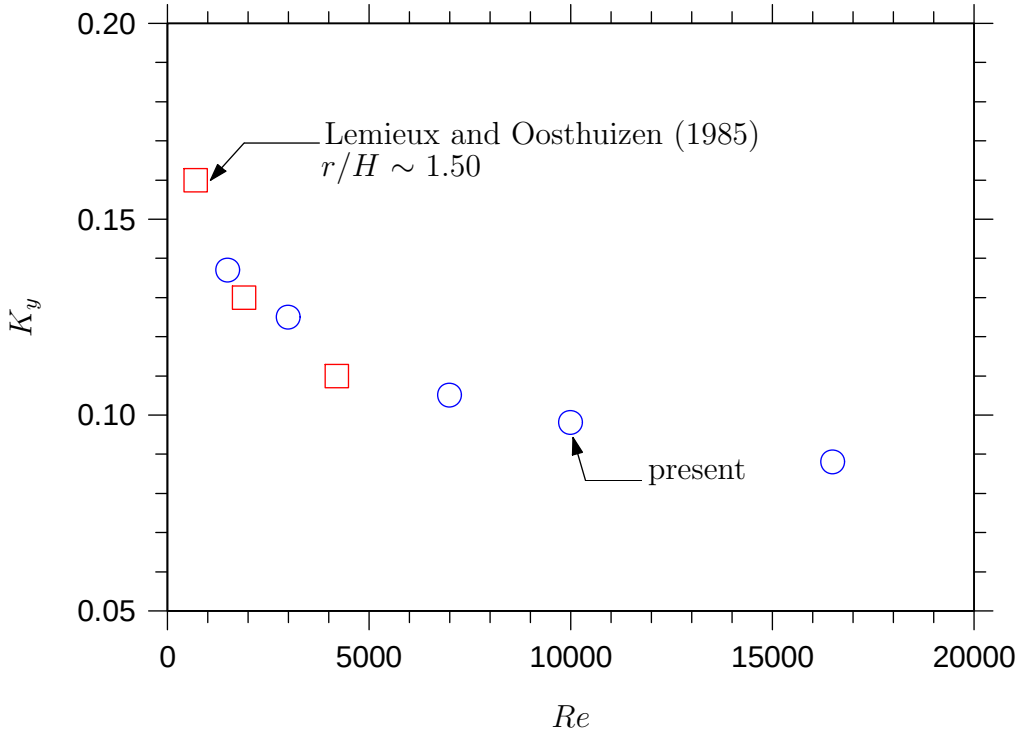

Figure 3.13: Dependence of the jet spreading rate K_y on the Reynolds number Re.

larger for Re = 1,500. Thus, a smaller magnitude of $u'_{c,max}$ and x_m with a decrease in Re indicates that the Kelvin-Helmholtz instability becomes stronger and develops further downstream for the lower Reynolds number jets. It is also true that the occurrence of higher $u'_{c,max}$ for lower Re suggests that the underlying large-scale structures (sometimes referred to as 'coherent structures') are initially more coherent and organized. In such cases, the intermittent incursion of the induced low velocity ambient fluid (as shown by larger fluctuations in u, Fig. 3.15) across the jet produces higher fluctuation amplitudes and lower mean values of the local velocity and thus higher relative turbulence intensity. When Re is increased, the underlying vortices become more three-dimensional, less coherent and consequently the magnitude of $u'_{c,max}$ is reduced. This is confirmed by the trace signal in Fig. 3.15 for Re = 16,500.

Figure 3.16 also shows that $u'_{n,c}$ ultimately converges towards an asymptotic value. However, whether the asymptotic value has been reached by Re = 16,500 is difficult to tell. It appears that for Re = 10,000 and 16,500, $u'_{n,c}$ approaches an asymptotic value of $u'_{c,\infty} \simeq 0.22 \pm 0.01$ for $x/H \geq 60$. For Re < 10,000, both the magnitude and the evolution of turbulence intensity are strongly dependent on the Reynolds number. Over the range $100 \leq x/H \leq 160$, $u'_{n,c}$ asymptotes to different values of $u'_{c,\infty}$ for different Reynolds numbers for Re < 10,000 (Figure 3.16). Clearly from Figure 3.16, $u'_{c,\infty}$ increases with

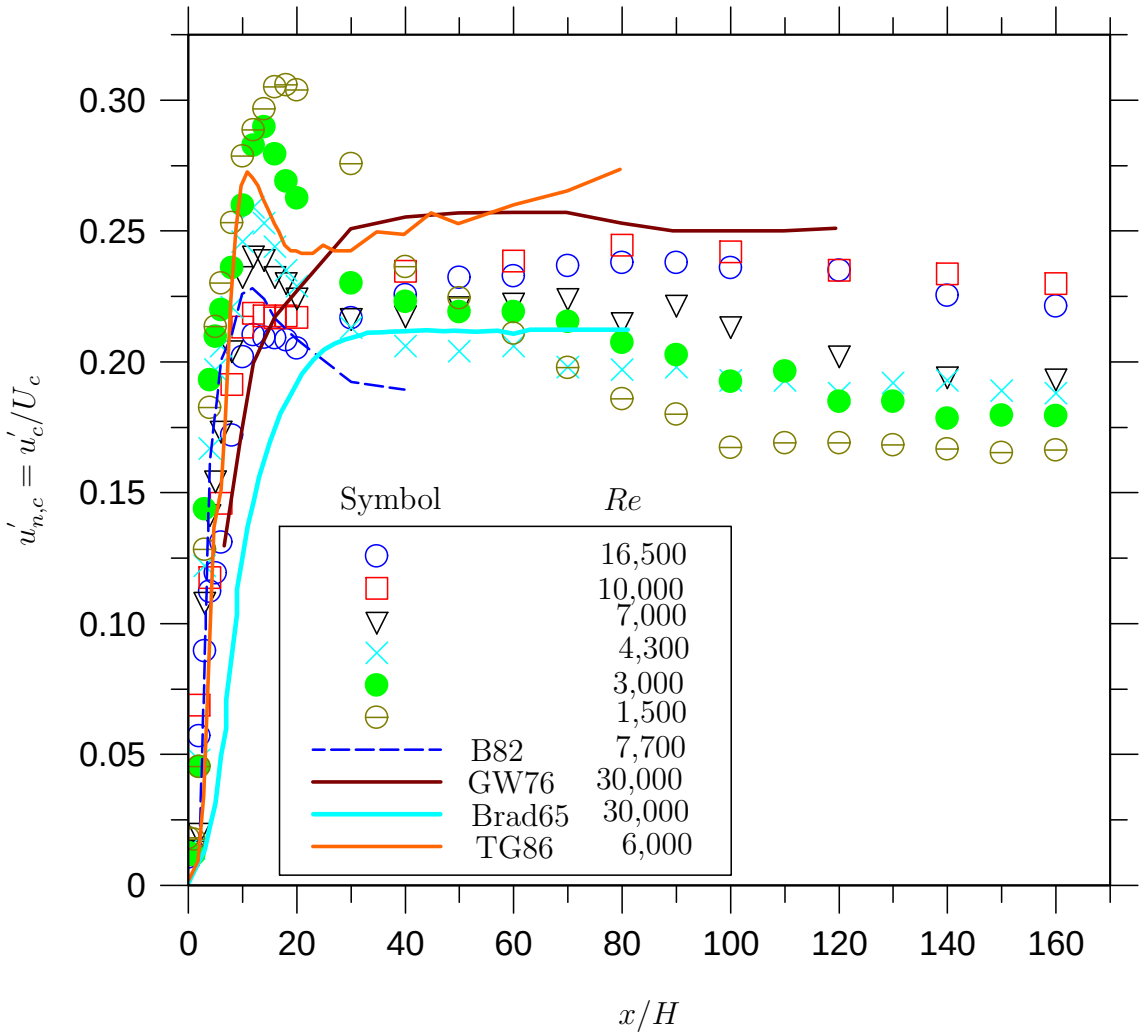

Figure 3.14: Evolutions of the centerline turbulence intensity $u'_{n,c}$ for different Reynolds numbers Re. Note: B82 - Browne et al. (1982), GW76 - Gutmark and Wygnanski (1976), BRAD65 - Bradbury (1965) and TG86 - Thomas and Goldschmidt (1986).

increasing Re.

There is overwhelming support from existing literature for the present trends in $u'_{c,\infty}$, by a very recent work of George (2005). His analytical analysis using equilibrium theory on plane jets show that the local Reynolds number, Re_{local} increases with downstream distance, following the relation $Re_{local} \sim x^{1/2}$. Here, $\mathrm{Re}_{local} = 2y_{0.5}\,U_c/\upsilon$. This is different to that of a round jet, whose Re_{local} remains fairly constant with downstream distance, since the centerline velocity and jet half-width changes in proportion to each other. Figure 3.17 shows the variation of local Reynolds number with downstream distance, for different jet exit Reynolds numbers of investigation. Interestingly, we observe that Re_{local} increases as $x^{1/2}$. For the low Reynolds numbers (Re = 1,500 and 3,000), this increase is slower than the high Re-jets, i.e. for 10,000 and 16,500. Ultimately in the far field, the Re = 1500

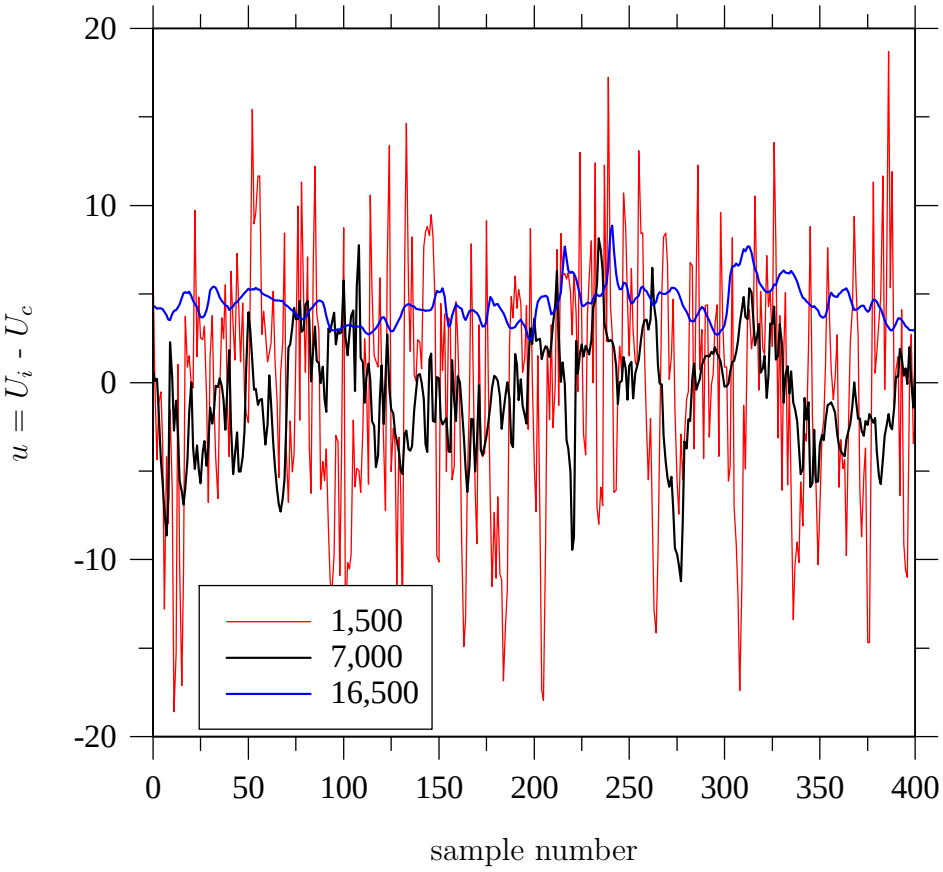

Figure 3.15: Trace signal of the velocity fluctuations, u at an axial location where turbulence intensity, $u'_{n,c} = u'_{c,max}$ for Re = 1,500, 7,000 and 16,500.

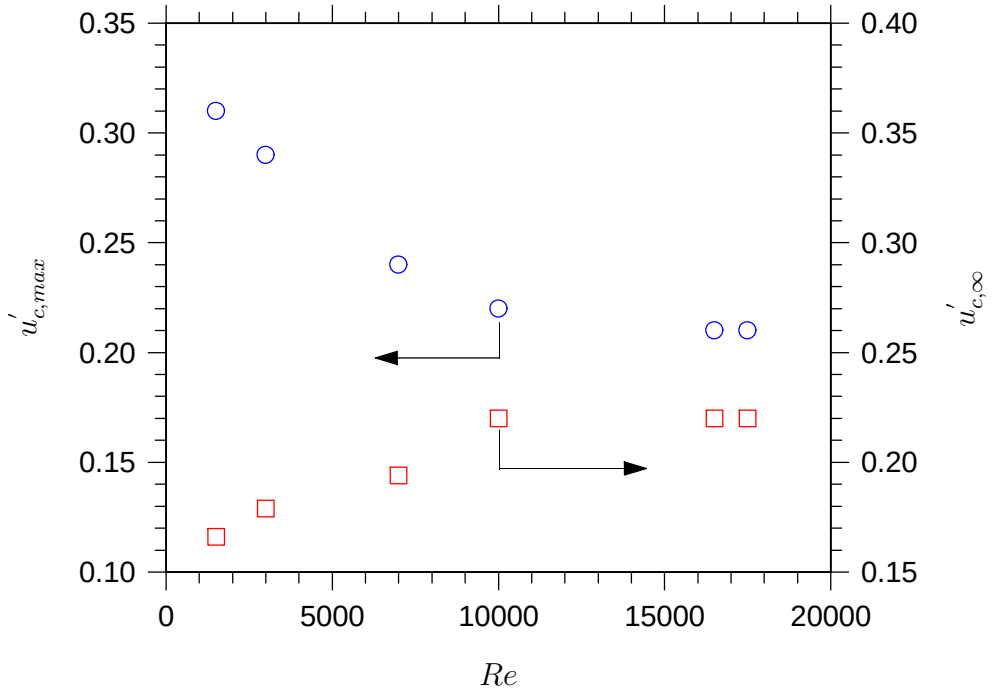

Figure 3.16: Reynolds number Re effect on the near field hump in turbulence intensity $u'_{c,max}$ and on the far field asymptotic turbulence intensity $u'_{c,\infty}$.

jet takes a value of Re_{local} = 10,000 at $x/H \simeq 100$, while the Re = 16,500 jet achieves Re_{local} well above 40,000 for $x/H > 40$. This explains that the viscous terms in the Re = 16,500 jet become negligible at a shorter axial distance, as opposed to a larger axial distance for Re = 1,500. This negligibility proves why our turbulence intensity for Re = 1,500 asymptotes at around $x/H = 100$ and that for Re = 10,000 and 16,500 asymptotes at around $x/H = 40$ only! Exactly the same prediction is provided in George (2005), whose analsyis shows that the higher the source Reynolds number, the closer to the exit plane the similarity of the velocity moments will be realized.

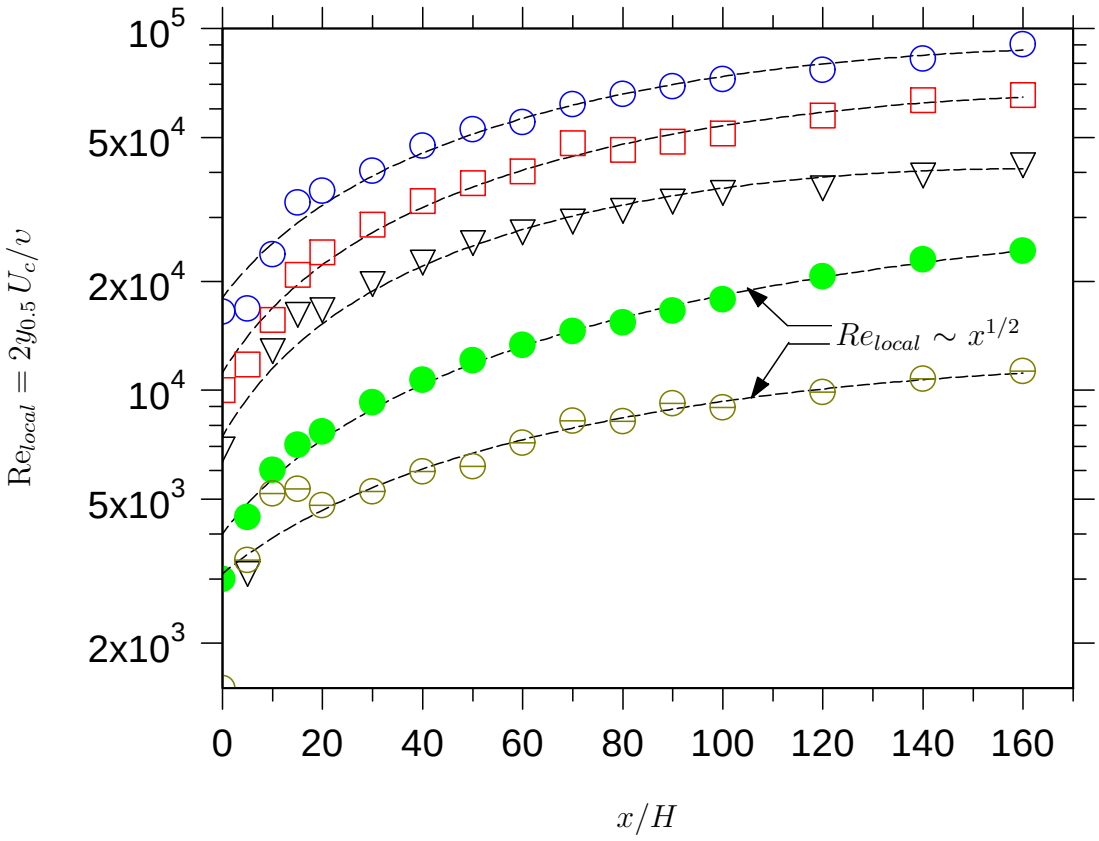

Figure 3.17: The variation of local Reynolds number, Re_{local} with downstream distance, for different jet exit Reynolds numbers. Symbols identical to Figure 3.14.

An interesting insight may be obtained by plotting the dependence of $u'_{c,\infty}$ on Re_{local} for different jet exit Reynolds numbers. Figure 3.18 shows clearly, that for Re $\geq$ 3,000, at least Re_{local} = 20,000 is required for the centerline turbulence intensity to asymptote. However, for Re = 1,500, the turbulence intensity asymptotes when Re_{local} = 10,000 only. Nevertheless, in general, the turbulence intensities for the present plane jets whose $Re \geq$ 3,000 asymptote at almost equal values of Re_{local}. In general, the present findings show

that a relatively high value of Re_{local} is required for the viscous effects to become negligible, and therefore, for the turbulence intensity to take an asymptotic value.

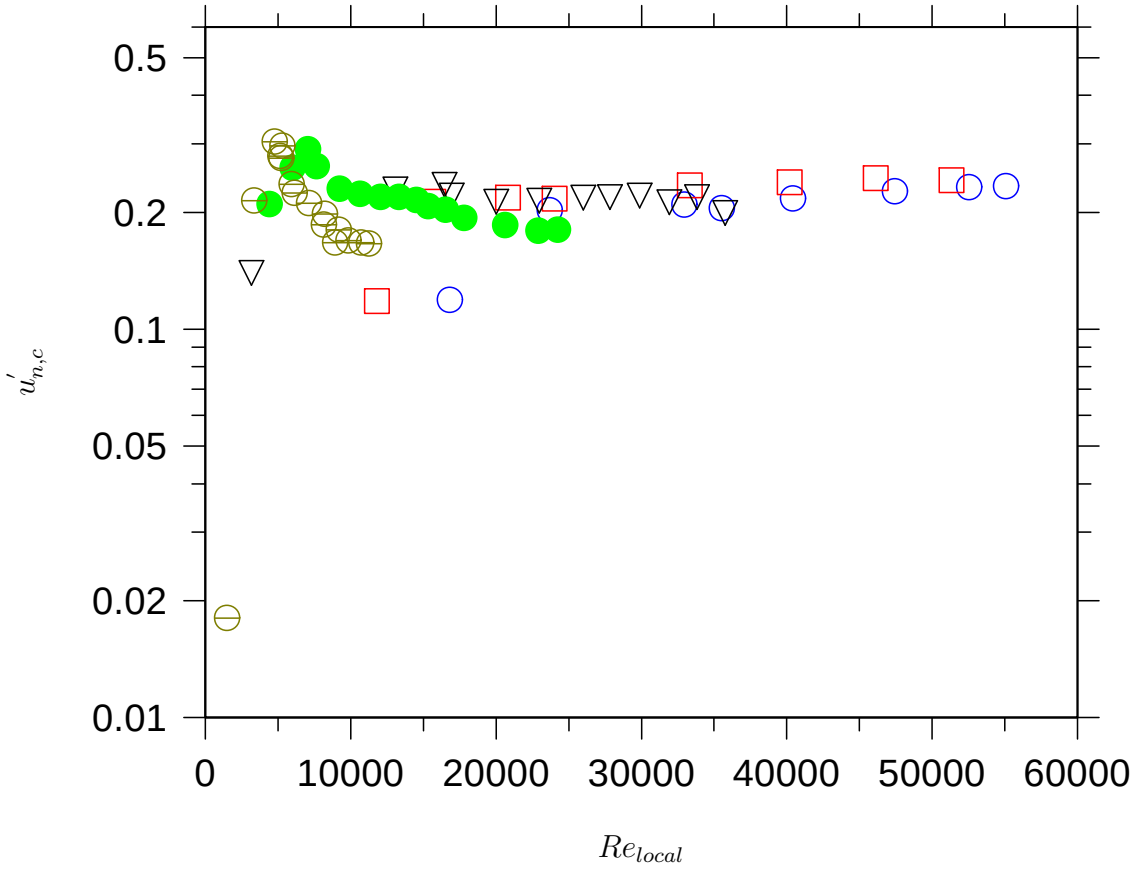

Figure 3.18: The dependence of centerline turbulence intensity, $u'_{n,c}$ on local Reynolds Number, Re_{local} for different jet exit Reynolds numbers. Symbols identical to Figure 3.14.

Following the discussions in the previous paragraph, an increase in Re is expected to reduce the relative significance of viscosity. Hence, a reduction in the dissipation ϵ of the turbulence kinetic energy $q = 0.5\,(u^2 + v^2 + w^2)$ in the self-similar, far field region is expected. Figure 3.19 presents dissipation measurements which reveal a reduction of $\epsilon H/U_{o,c}^3$ with increased Re. This significant finding is also reported in Deo et al. (2005). Our newly developed iterative scheme to calculate the small-scale statistics was used. An account of our scheme was reported in Mi et al. (2005a). Our deduction that $\epsilon H/U_{o,c}^3$ decreases with increased Re is supported by the wake flow data of Sreenivasan (1995). Some interesting observations can be made from Figure 3.19. It appears that $\epsilon \sim x^{-3/2}$ beyond the axial locations at which u_c'/U_c asymptotes. For instance, when Re = 1,500, $\epsilon \sim x^{-3/2}$ for $x/H > 100$, while for Re = 7,000, $\epsilon \sim x^{-3/2}$ for $x/H > 50$. From Fig. 3.14, it is immediately evident that u_c'/U_c asymptotes at $x/H \approx 100$ for Re = 1,500 and at $x/H \approx 50$ for Re = 7,000. Therefore, the present data confirms that $\epsilon \sim x^{-3/2}$ over

the axial range at which $u_c^{'}/U_c$ asymptotes. However, since the magnitudes of ϵ for Re = 10,000 and 16,500 could not be determined due to over-filtering of the raw signal, this deduction cannot be verified for all the Reynolds numbers of investigation. From the present magnitudes of $\epsilon H/U_{o,c}^3$, it is thus expected that $q_\infty/U_{o,c}^2$ and hence $u_{c,\infty}^{'}$ increase as Re is increased.

This trend, however, differs from that observed in the quasi-plane jet of Namar and Ötügen (1988) where $u_{c,\infty}^{'}$ was found to decrease rapidly with Re from Re = 1,000 to Re = 2,000 and then reaches an identical value of 0.22 for $Re \geq 2000$. The cause of this apparent discrepancy is unclear. We have noticed that the jet of Namar and Ötügen (1988) without sidewalls is not a truly plane jet, particularly, in the far field; yet, this is unlikely to account for by itself. Namar and Otugen (1988) did not use sidewalls, whereas the present plane jets did. The use of sidewalls restricts entrainment from the short sides of the nozzle. Chapter 6 shows that otherwise-identical, jets with and without sidewalls have different asymptotic values of centerline turbulence intensities. The jet with sidewalls has a higher asymptotic turbulence intensity than that without sidewalls. It maybe for this reason that $u_{c,\infty}^{'}$ of Namar and Otugen (1988) decreases with an increase in Re. The local Reynolds number, Re_{local} also has a definite influence on $u_{c,\infty}^{'}$ (George 2005). For a plane jet, Re_{local} increases as $x^{1/2}$ with downstream distance, whereas for an axisymmetric jet, it stays approximately constant. Since Namar and Otugen (1988) measured a rectangular axisymmetric jet (no sidewalls), its local-Re may not follow similar trends to those of the present plane jet. Therefore, the viscous terms in the governing equation, which scale with $1/Re_{local}$ may diminish closer to the nozzle exit for the present high-Re plane jet, leading to a closer downstream distance at which the turbulence intensity could asymptote. For Namar's jet, this could show an altogether different trend. However, these arguments can only be used to deduce possibilities as to why we observe differences in asymptotic turbulence intensity. Further studies are required to justify it explicitly. Hence, Namar and Ötügen's data is not included in Figure 3.14. Moreover, it is worth mentioning that Browne et al. (1982) measured at $x/H \leq 40$, Bradbury (1965) at $x/H \leq 80$ and Gutmark and Wygnanski (1976) up to $x/H = 100$. Their data are thus not used to assess this issue. In addition, although the measurements of Heskestad (1965) (not shown in Figure 3.14) extends up to $x = 160\,H$, his $u_{n,c}^{'}$ does not approach any asymptotic value, perhaps due to the use of a sharp-edged-orifice nozzle or other reasons, and so is not comparable with ours. The difference in initial conditions is also expected to influence the flow significantly e.g. Mi, Nathan and Nobes (2001). Further studies are required to assess this issue more fully.

It is important to mention that, to estimate the dissipation we employed the common assumptions associated with the use of Taylor hypothesis ("frozen turbulence" approximation) and a time-series obtained from the measurement of only the axial component of centerline velocity. Due to the limitations of the Taylor's hypothesis itself, and the general problems associated with fine-scale measurements, it is crucial to acknowledge the validity of the present dissipation measurements. Using Taylor's hypothesis, the spatial and temporal derivatives, related by the centerline mean velocity are calculated as $(du/dx)^2 = U_c^{-2}\,(du/dt)^2$. Pope (2000) states that the accuracy of Taylor's hypothesis depends on both the properties of the flow and on the statistics being measured. Due to the inadequacy of local isotropy assumption (Zhou et al. 1998) which is presumably worse at a smaller Reynolds number, the present dissipation cannot be correct in terms of absolute magnitude, although the trends are meaningful. For instance, as required by equilibrium similarity analysis, $\epsilon \sim x^{-3/2}$ (Figure 3.19) for a plane jet, which clearly agrees with the dissipation trends of Antonia et al. (1980). A more complete description of the applicability of Taylor's hypothesis to turbulent flows is found in Dahm and Southerland (1997). Apart from the problems with Taylor's approximation, the spatial resolution of the hot wire sensors, poor signal-noise ratio and inadequate choice of the cut-off low pass filter frequency sometimes cast a limitation on the small-scale statistics. In addition, errors associated with the use of parallel hot wires is also expected to influence the fine-scale measurements (Antonia et al. 1986). George and Taulbee (1992) also provides a good summary of the difficulties faced using hot wires, when estimating the dissipation of jet flows. To reduce such difficulties, we used an appropriate hot-wire sensor configuration, as discussed in section 2.4.5 to reduce errors associated with the spatial resolution of the wire. The signal-to-noise ratio was kept low and the raw signal was filtered at a high cut-off frequency to ensure no loss of information. To filter the signal appropriately, the newly developed iterative scheme (Mi et al. 2005a) was employed. However, for Re = 10,000 and 16,500, the Kolmogorov frequency was too high, which led to over-filtering of the signal. For this reason, dissipation data for these Reynolds numbers are not provided.

The lateral profiles of the turbulence intensity are shown in Figures 3.20-3.24. The profiles of $u_n^{'}$ exhibit a self-similar character at some axial distance downstream for the entire range of Reynolds numbers. This distance depends on Re. For Re = 1,500, it appears that the present lateral profiles do not achieve self-similarity. However, for Re = 3,000, the profiles collapse onto a single curve at $x/H \simeq 50$. Interestingly, the turbulence intensify profiles become congruent at $x/H \simeq 20$ for Re = 7,000 and 10,000 while for Re = 16,500,

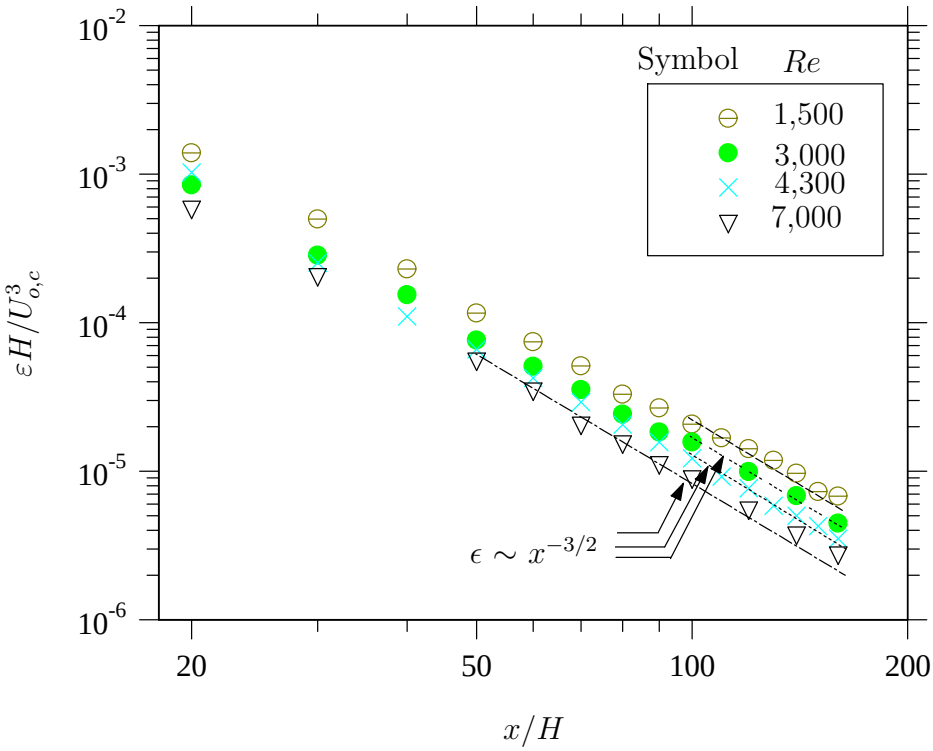

Figure 3.19: Reynolds number Re effect on the turbulent kinetic energy dissipation ϵ.

it becomes congruent at $x/H \simeq 10$. Apparently, the higher the Reynolds number, the closer to the nozzle exit the turbulence intensity profiles become self-similar. The exact reason for this trend is quite clear from the previous work of George (1995) for a plane jet and from Johansson et al. (2003) for a plane wake. They found that, unlike the axisymmetric jet and plane wake, whose *local* Reynolds number remains constant as the flow evolves downstream, the local Reynolds number for a plane jet increases as $x^{1/2}$. Thus, the initially high Reynolds number plane-jet will eventually become very high Reynolds number jet, at a shorter axial distance than does an initially low-Re jet, but only when the nozzle aspect ratio is sufficiently large for this self-similar state to develop. On the other hand, an initially low Reynolds number plane-jet issuing from a large aspect ratio nozzle will take a longer downstream distance to become a high-Re jet. From the analysis of the governing equations by George (1995), we see that, for asymptotic similarity state to evolve, the viscous terms in the similarity equations, which scale with $1/Re_{local}$, must be small. This does not happen for an initially low Re-jet, until the jet has evolved far downstream. Nevertheless, for an initially high Re-jet, the viscous terms disappear at a shorter downstream distance than it does for a low Re-jet. Therefore, the higher the source Reynolds number, the closer to the exit plane the similarity moments are realized. This is exactly true for the present turbulence intensity profiles, which become self-similar closer to the exit plane when the exit Reynolds number is higher. It is also evident that

the lateral distribution of the mean velocity becomes self-similar faster than the lateral distribution of the turbulence intensity. This is consistent with Namar and Ötügen (1988), who also noted that their mean velocity profiles attained a self-similar state closer to the nozzle than did the turbulence intensity profiles.

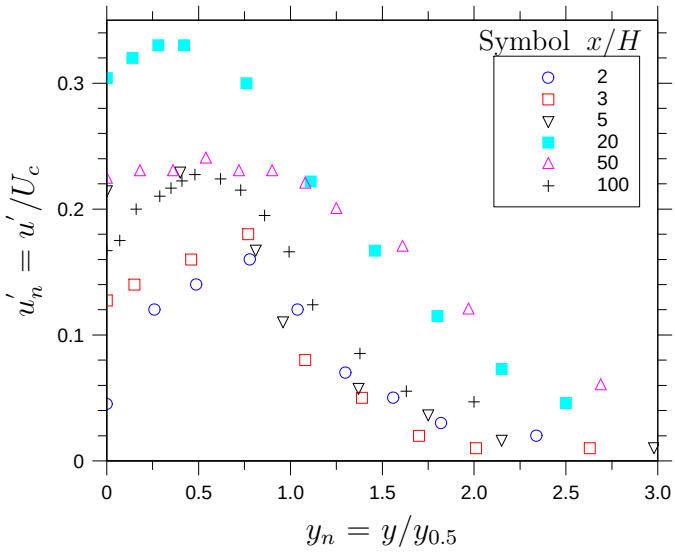

Figure 3.20: Lateral profiles of the turbulence intensity $u_n^{'}$ for Re = 1,500.

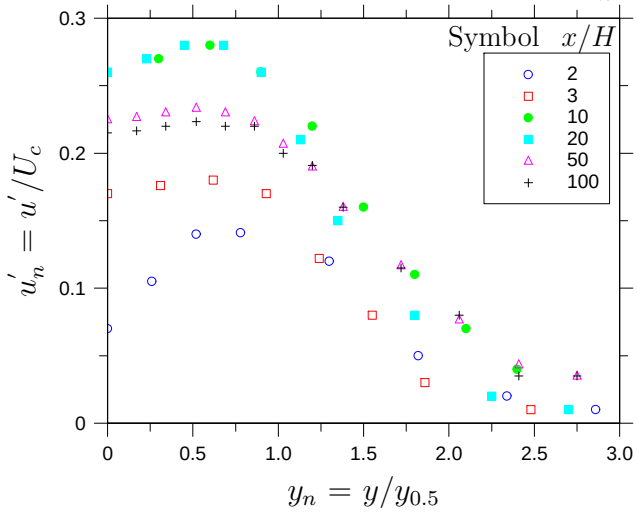

Figure 3.21: Lateral profiles of the turbulence intensity $u_n^{'}$ for Re = 3,000.

Further insight into the flow field may be obtained from the skewness S_u and flatness F_u (kurtosis) factors of the fluctuating velocity u. S_u provides a measure of the statistical symmetry of u while F_u provides a measure of the spikes in the amplitude of u. Figures 3.25 and 3.26 respectively present the centerline evolutions of S_u and F_u up to x/H = 160. It is demonstrated that both factors vary dramatically in the near field for $x/H \leq$ 30, presumably owing to the presence of coherent large-scale mixing. Moving downstream

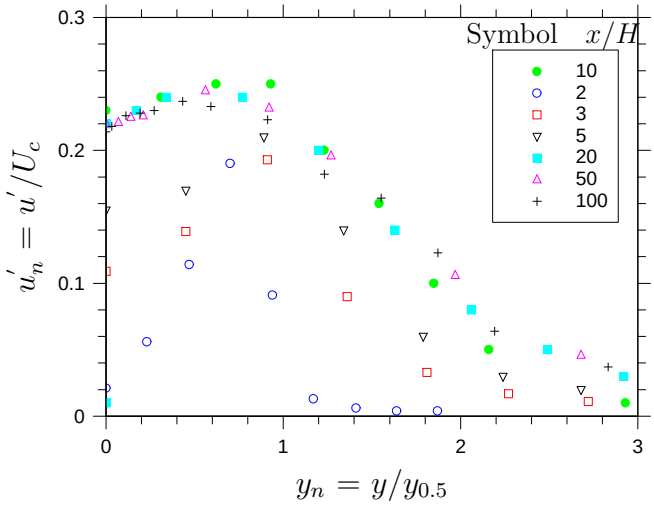

Figure 3.22: Lateral profiles of the the turbulence intensity $u_n^{'}$ for Re = 7,000.

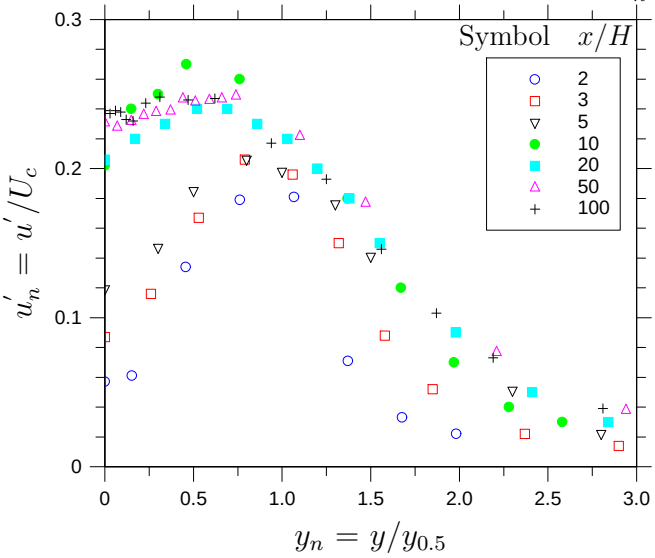

Figure 3.23: Lateral profiles of the the turbulence intensity $u_n^{'}$ for Re = 10,000.

from the origin, both S_u and F_u increase from the nearly Gaussian values (0, 3) and then decrease, resulting in a local maximum in each factor. Further downstream, both factors continue to vary, generating a local minimum and then another local maximum.

The positive peak coincides with the average location of the end of the jet's potential core (Figure 3.3). The initial increase in S_u can therefore be deduced to correspond to the growth in the mixing layer structures (i.e. the Kelvin Helmholtz vortices), till the edge of the potential core. The maxima in S_u is therefore deduced to be associated with the collision and/or merging of the vortices. The minima in the skewness factors are probably associated with the induction of low velocity ambient fluid, due to lateral (y-direction) oscillation of the jets' potential core. In fact, lateral oscillations of the potential core

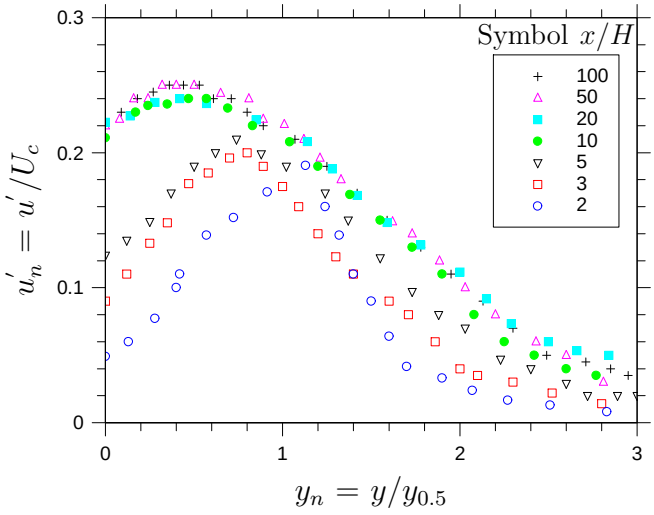

Figure 3.24: Lateral profiles of the the turbulence intensity $u_n^{'}$ for Re = 16,500.

is expected to affect both, S_u^{max} and S_u^{min}. Such an effect has been mentioned briefly elsewhere, e.g. Namar and Otugen (1988). Clearly, the large-scale coherent motions in the near field continue to be Re-dependent till Re = 16,500.

For $x/H \geq 40$, they gradually approach their respective asymptotic values. The present data reveal that the first local maximum of S_u occurs around $x/H = 4$ and 6, while that for F_u occurs around $x/H = 5$ and 10 for the different Reynolds numbers. The difference in the specific x-location results from different Re. Overall, the x-location shifts upstream as Re is increased. This may be explained as follows. It is well known e.g. Antonia, Browne, Rajagopalan and Chambers (1983), that, large-scale vortical rollers occur in the initial region of a plane jet. Increasing the Re will lead these rolls to be more three-dimensional. As a consequence, for higher Re, initially symmetric fluctuations of the centerline velocity ($S_u \simeq 0$) develops to the highest degree of asymmetry ($|S_u| >> 0$) over a shorter distance. It is also interesting to note that, for all the tested values of Re, the second maximum in S_u and F_u occur at approximately identically around x/H of 16 and 20 respectively.

The factors S_u and F_u reach their respective asymptotic values, $S_u^{c,\infty}$, $F_u^{c,\infty}$, beyond x/H = 40 for all Reynolds numbers. However, both $S_u^{c,\infty}$ and $F_u^{c,\infty}$ exhibit a consistent albeit weak, dependence on Re (Figure 3.27). A careful check of the data found that overall, as Re increases, $S_u^{c,\infty}$ increases whereas $F_u^{c,\infty}$ decreases. Note that a higher scattering of the S_u data for Re = 1,500 is due to relatively low velocity (< 1 ms^{-1} for $x/H > 70$), and thus high uncertainties for this case.

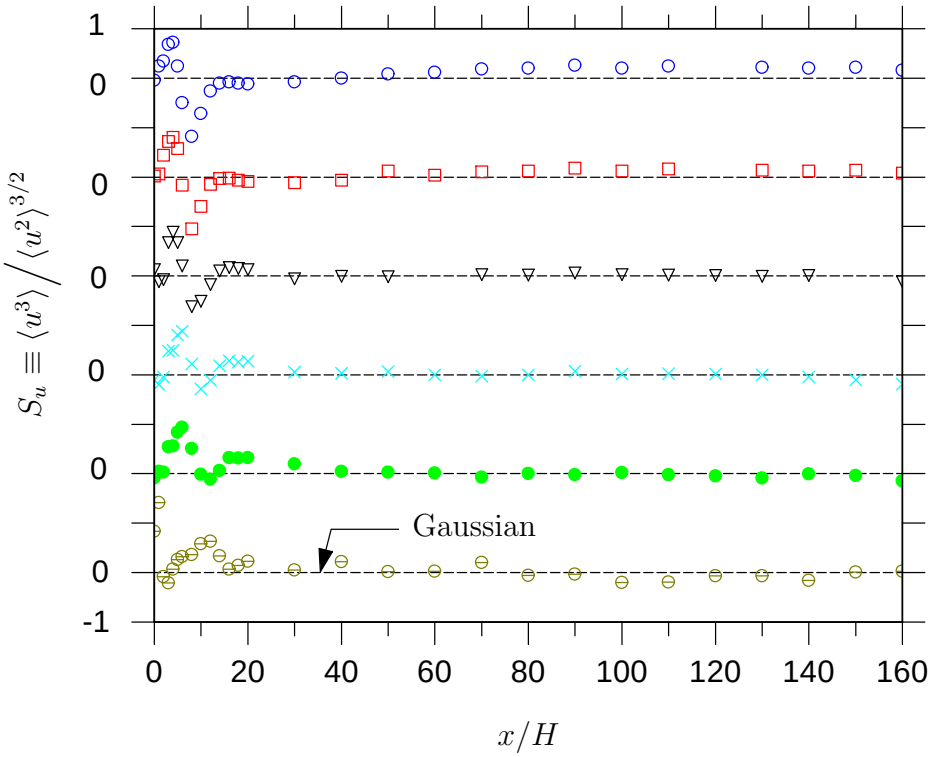

Figure 3.25: The Reynolds number Re dependence of the centerline skewness factors S_u up to $x/H = 160$. Note that the profiles have been shifted by 1. Symbols identical to Figure 3.14.

3.4 Further Discussion

Reynolds number is a significant flow parameter that is well known to affect a wide range of turbulent shear flows. Such flows include jets and wake flows. Most previous studies of plane jets by experiments have been confined to the high Reynolds number regime ($Re >$ 10,000) and performed under a range of different inlet (initial) and boundary conditions, mostly with single Reynolds numbers.

Only the work of Namar and Ötügen (1986, 1988) and Lemieux and Oosthuzin (1984, 1985) offered a systematic investigation of the Reynolds number effect over the range $1{,}000 \leq Re \leq 7{,}000$ and $700 \leq Re \leq 4{,}200$. However, Namar's jet was not constrained by sidewalls so does not provide a truly planar flow. Nevertheless, a plane jet (with sidewall) investigation by Lemieux and Oosthuzin (1984, 1985) on the Reynolds number effect using a nozzle profile similar to ours (i.e. a nozzle with inner rounded edges) over the range $700 \leq Re \leq 4{,}200$ revealed a significant dependence of centerline mean velocity and spreading rates on Re. They noted that generally, an increase in Re from 1,500 to 4,200 led to a decreased decay of the centerline mean velocity. However, their results indicate inconsistencies among their own data, particularly for $Re =$ 1,900 and 700. We

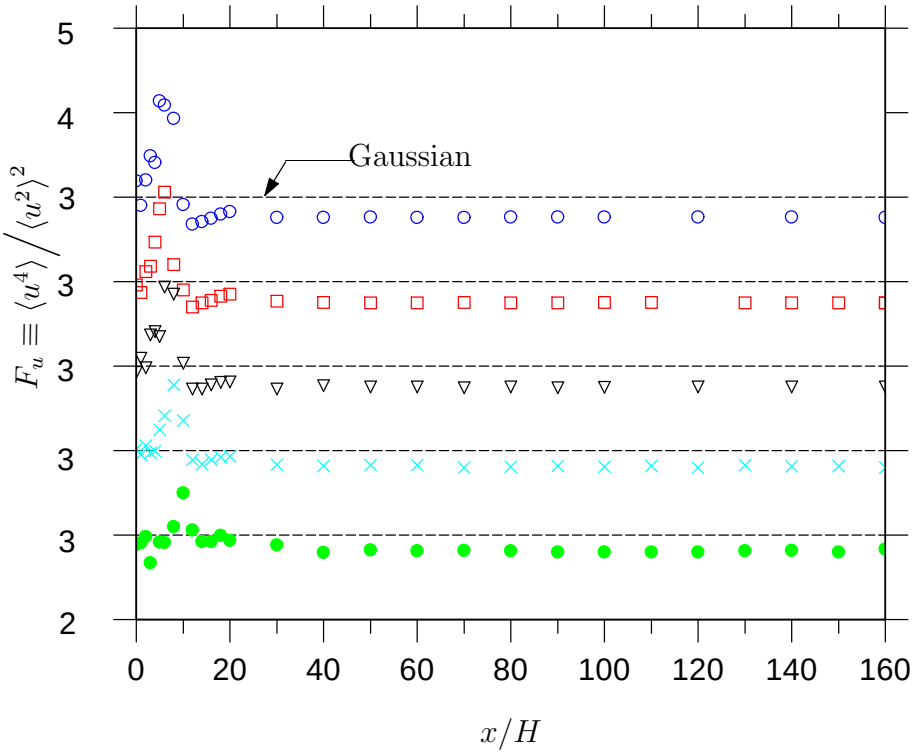

Figure 3.26: The Reynolds number Re dependence of the centerline flatness factor F_u. Note that the profiles have been shifted by 1. Symbols identical to Figure 3.14.

compare the decay rates of their jets in Figure 3.28. Note that that while K_u for Re = 1,500, 2,700 and 4,200 consistently decrease with increased Re, K_u for other Reynolds number do not fall within their respective expected values. It is appreciated that, for Re = 700, experimental errors could account for the observed discrepancies due to a very low velocity i.e. $U_{o,b} \simeq 1\ \mathrm{m\,s^{-1}}$. Hence, their data cannot be used to precisely quantify the Re-dependencies. The recent direct numerical simulation (DNS) of a plane jet has been conducted by Klein et al. (2003), only for $Re \leq 6{,}000$ and $x/H \leq 20$. Accordingly, the effect of Reynolds number variations on a plane jet cannot be adequately deduced from this investigation either.

Other types of flows which have investigated Re effect are round and quasi-plane jets. To examine the dependence of vortex formation on Reynolds number, Figure 3.29 plots the power spectra of the centerline velocity fluctuation at $x/H = 4$ for Reynolds numbers over the range $1{,}500 \leq Re \leq 16{,}500$. To normalize the vortex shedding frequency, a Strouhal number St_H is calculated using the dominant frequency of oscillation f, nozzle opening width H and bulk mean velocity $U_{o,b}$ as follows

$$St_H = \frac{f\ H}{U_{o,b}} \tag{3.5}$$

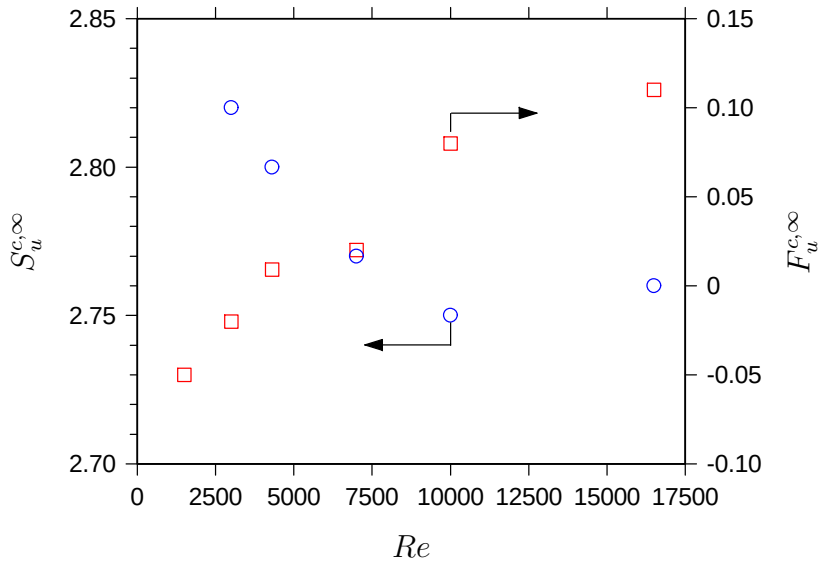

Figure 3.27: Dependence of the far field asymptotic skewness $S_u^{c,\infty}$ and the far field asymptotic flatness $F_u^{c,\infty}$, on Reynolds number, Re.

A weak dependence of the vortex shedding on Re is clearly demonstrated by Figure 3.29. This is at odds with the observations of Namar and Ötügen (1986, 1988), Browand and Laufer (1975) and Crow and Champagne (1971). For previous investigations, an influence of Reynolds number on the vortex passage frequency (Strouhul number, St_D) in round jets was studied by Browand and Laufer (1975) over the range $5{,}000 \leq Re \leq 15{,}000$. They noted that the interaction of large-scale vortices was insensitive to changes in Reynolds number. In order words, Reynolds number played no significant role in determining the vortex passage frequency induced by the large-scale motions in their round jet. Even for their round jet, Crow and Champagne (1971) found that a constant St_D of approximately 0.30 that existed for all Reynolds numbers over the range $10{,}500 \leq Re \leq 30{,}900$. Similar were the findings of Namar and Ötügen (1986, 1988) for their quasi-plane jet. They noted a constant $St_H = 0.27$ for all Re over the range $1{,}000 \leq Re \leq 7{,}000$. Many investigations of plane, round and circular jets have reported vortex shedding frequencies that lie over the range 0.20-0.60. These are summarized in Table 4.2. Later discussions presented in Chapter 4 show that vortex shedding frequencies depend significantly initial conditions, thus any comparisons with the present St_H must be made with caution.

Although an average St_H of approximately 0.210 exist for the present entire ranges of Re, the present trend shows that its absolute value increases slightly with an increase in Re. In fact, the round jet study by Sato (1960) found a constant Strouhal number of 0.23 over the range 1,500 to 8,000 but at higher Reynolds numbers, the rate of vortex formation increased slightly. In contrast, Namar and Ötügen (1986, 1988) found $St_H \simeq 0.27$ for

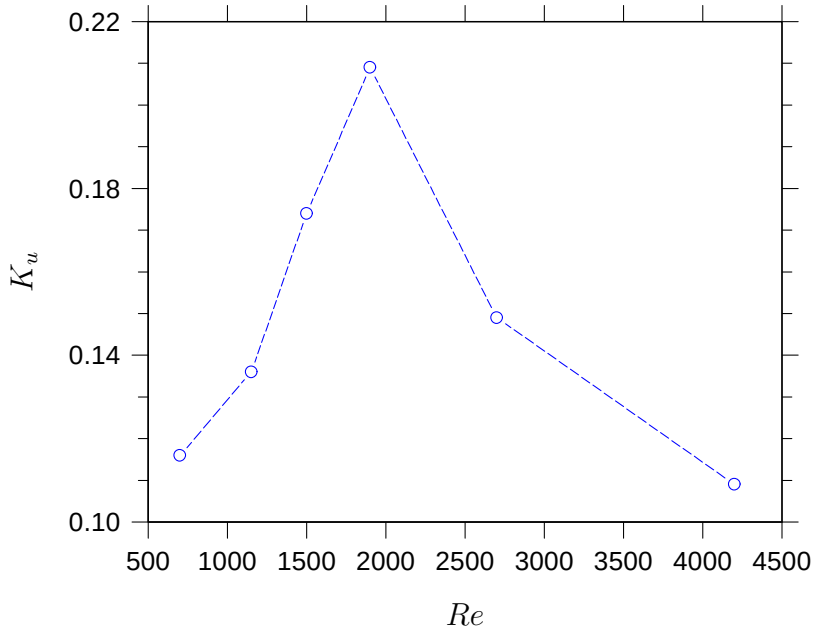

Figure 3.28: The dependence of the centerline decay rate K_u of the mean velocity on Reynolds number Re in the jet of Lemieux and Oosthuizen (1985).

their quasi-plane jet over their entire ranges of Re. Our analysis of a plane jet without sidewalls (Chapter 6) will show that with no sidewalls, the quasi-plane jet has a larger St_H when compared with the plane jet. It may for this reason or others, that Namar and Ötügen (1986, 1988) noted a higher St_H than ours. Hence, based on previous literature and the present results, one may conclude that the rate of vortex formation increases by increasing the Reynolds number. In fact, the present trends in St_H are consistent with changes in boundary layer thickness. Indeed, the rate of vortex formation is a function of the nozzle type (see Chapter 4). Hence, it may be that the radial contraction is more sensitive to Re than a conventional smooth contraction nozzle, and the change in vortex shedding frequency is a cause of the nozzle type itself, i.e. due to a radial contraction.

The influence of Reynolds number on the velocity and scalar fields of cylindrical wake flows were studied by Zhou et al. (1999) and Mi et al. (2004). In their study on the Reynolds stresses and vorticity of a cylindrical wake, Zhou et al. (1999) investigated Re over the range 1,350 to 4,600. Their observations indicate that, as Re is increased, the magnitude of their Reynolds stresses ($\overline{uv}$) and lateral and spanwise vorticity ($\omega_y \approx \frac{\Delta U}{\Delta z} - \frac{\Delta W}{\Delta x}$ and $\omega_z \approx \frac{\Delta V}{\Delta x} - \frac{\Delta U}{\Delta y}$) increases. Hence, it was noted that the size of the large-scale structures increased with an increase in Re. More interesting was their concluding remark that at $Re \geq$ 5,000, the centerline turbulence intensity attained an asymptotic value, hence the effect of Re becomes negligible. Cold-wire measurements by Mi et al. (2004) reported the

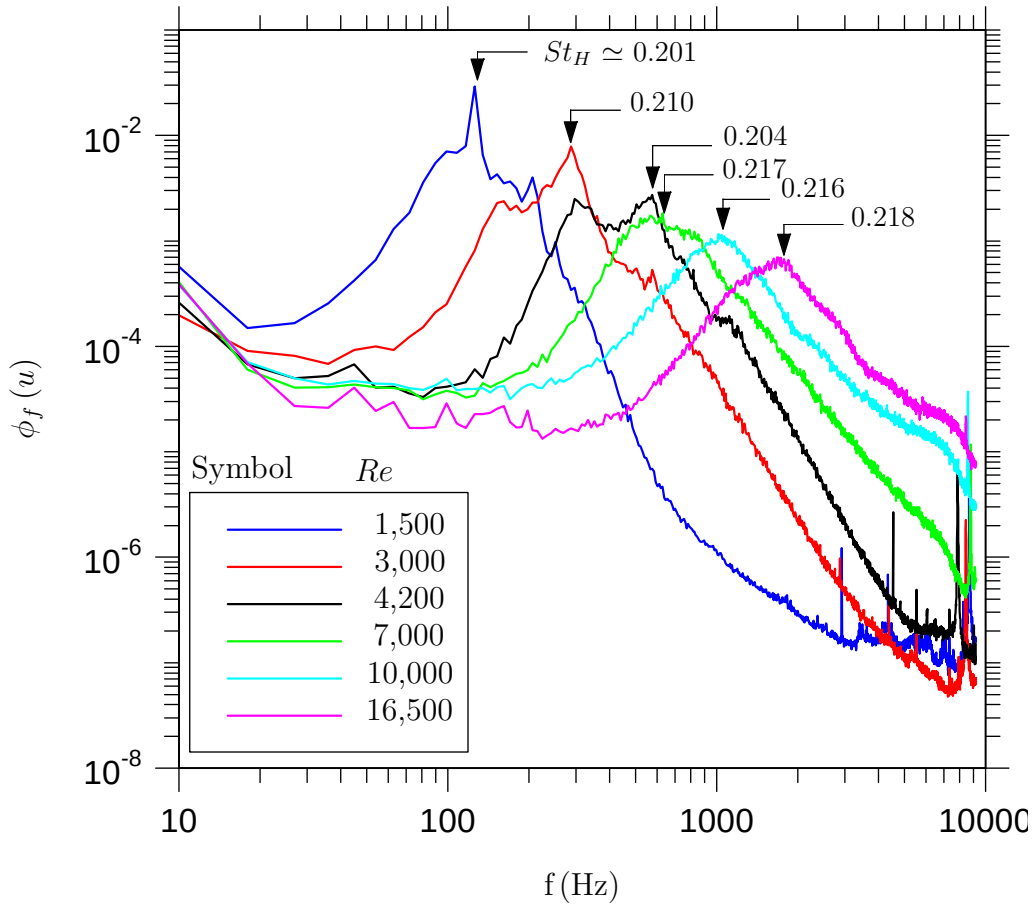

Figure 3.29: Power spectra ϕ_u of the centerline velocity fluctuations u at $x/H = 4$.

effect of Reynolds number on the passive scalar field of a turbulent cylinder wake flow, over the range $1{,}200 \leq Re \leq 8{,}600$. Central to their findings were increased spreading of the scalar field and higher scalar fluctuation intensity at increased Reynolds number. Using their polynomially fitted data to extend it to $Re = 10{,}000$, they found that the effect of Reynolds number on the scalar skewness and flatness factors became negligible when $Re \geq 8{,}000$. In another study by Tong and Warhaft (1995) on round jets, we note the effect of Re in the self-similar region at $x/D = 30$ and 40 (here D is the round jet nozzle diameter) of a slightly heated turbulent round jet (at $2800 \leq Re \leq 18{,}000$). The correlation between the square of temperature fluctuation and square of temperature difference becomes negligible only for $Re > 10{,}000$. In the present work, we have found that for a plane jet, the centerline turbulence intensity approaches an asymptotic value, for $Re \geq 10{,}000$. (The exact status of the asymptotic value could not be determined, but the difference between $Re = 10{,}000$ and 16,500 is small.) Hence, the findings in literature on jets and wakes broadly support ours, on the negligibility of Reynolds number effect on turbulence field beyond $Re = 10{,}000$. Thus, it appears that for both the jet and wake flows, the claim of Dimotakis (2000) that the fully-developed turbulent flow requires a

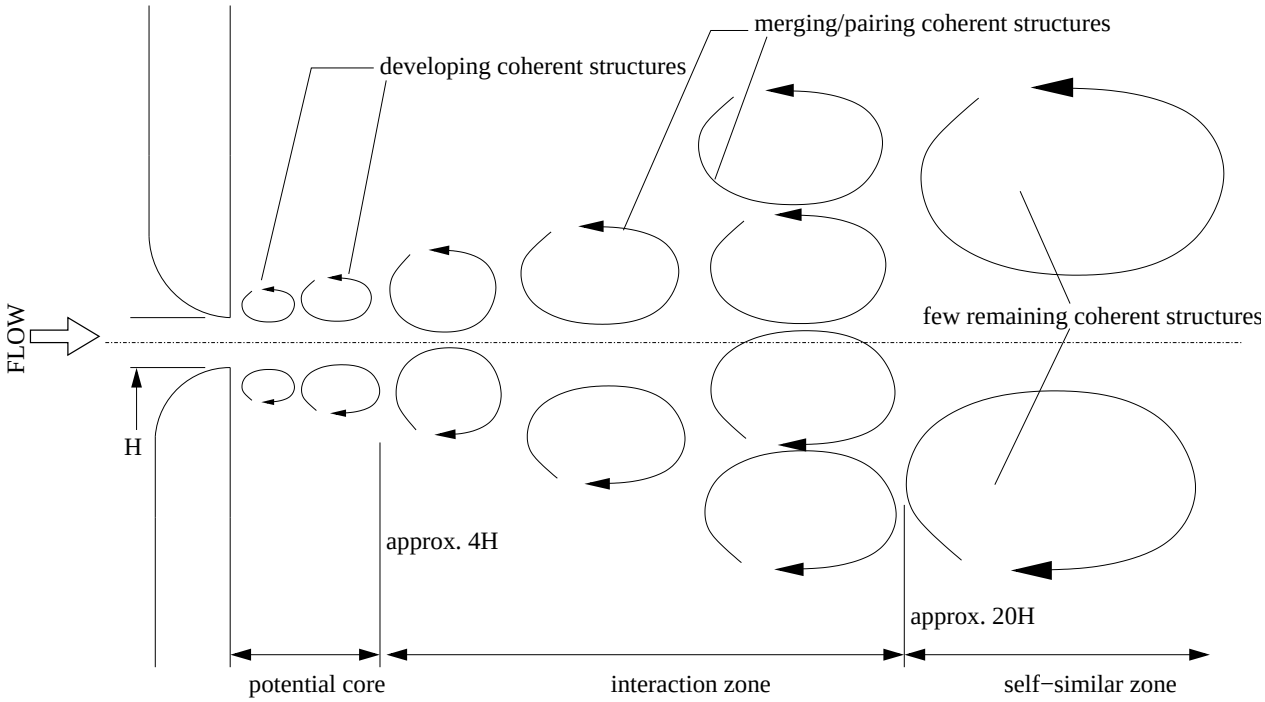

Figure 3.30: A simplified view of the coherent structures in a turbulent plane jet. Redrawn from Browne et al. (1984).

minimum Reynolds number of $Re = 10{,}000$ to be sustained, regardless of flow geometries appears to have some support from the present data.

The appearance of a local maximum in the centerline turbulence intensity for all Reynolds numbers is attributable to the occurrence of counter rotating large-scale coherent structures (see Figure 3.30), within the opposite sides of the shear layers of the plane jet. Browne et al. (1984) defined these coherent structures to be symmetrical about the jet centerline and those which counter-rotate along the spanwise directions. Thus, the rearrangement of the coherent structures within the interaction zone ($6 \leq x/H \leq 20$) is likely to produce a local maximum in the centerline turbulence intensity. On the other hand, Hussian (1983) deduced the coherent structures to be responsible for the large-scale transport of significant mass and momentum. According to their notion, the engulfment of the irrotational (ambient) fluid via the Biot-Savart effect of the vortical structures, are likely to produce intermittent incursions of low velocity ambient fluid thus producing a local maximum in the centerline turbulence intensity. On the other hand, such an engulfment process will inevitably increase the entrainment rate of the jet.

The present investigation has found that, with an increase in Re, there is a reduction in the magnitude of the local maximum in the centerline turbulence intensity. Likewise,

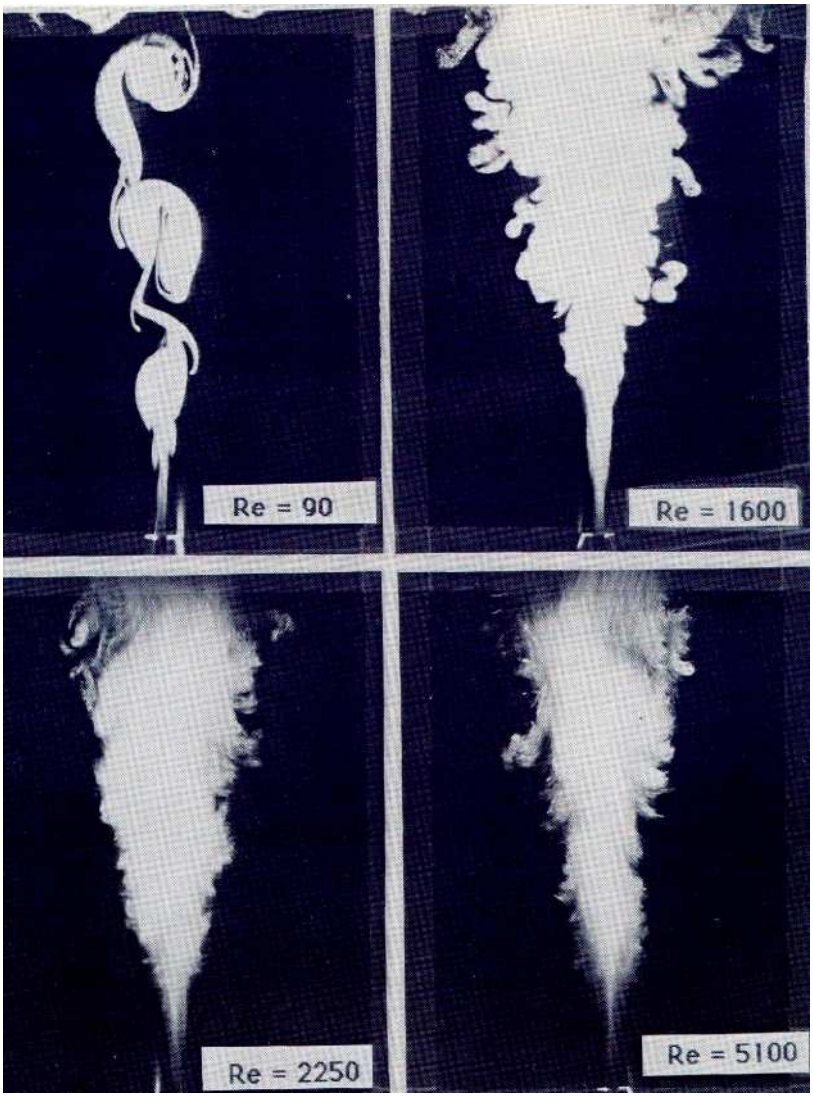

Figure 3.31: Laser Tomographic photographs of a quasi-plane jet measured over the axial range $0 \leq x/H \leq 60$ and Reynolds numbers over the range $90 \leq Re \leq 5{,}100$. After Namar (1986).

the investigation also shows that the spreading rates and the decay of centerline mean velocity are reduced when Re is increased. This can be further explained by observing the flow visualizations of Namar and Ötügen (1986, 1988) for their quasi-plane jet. Figure 3.31 shows the laser tomographic photographs of Namar and Ötügen's data, measured over the axial range $0 \leq x/H \leq 60$ and for Reynolds numbers over the range $90 \leq Re \leq 5{,}100$. The figure reveals that the jet becomes narrower as Reynolds number is increased. For instance, at $Re = 1{,}600$, the jet spreads most rapidly while for $Re = 5{,}100$, the spreads the least. Thus their visualizations support a reduction in the present jet spreading rate at higher Reynolds numbers.

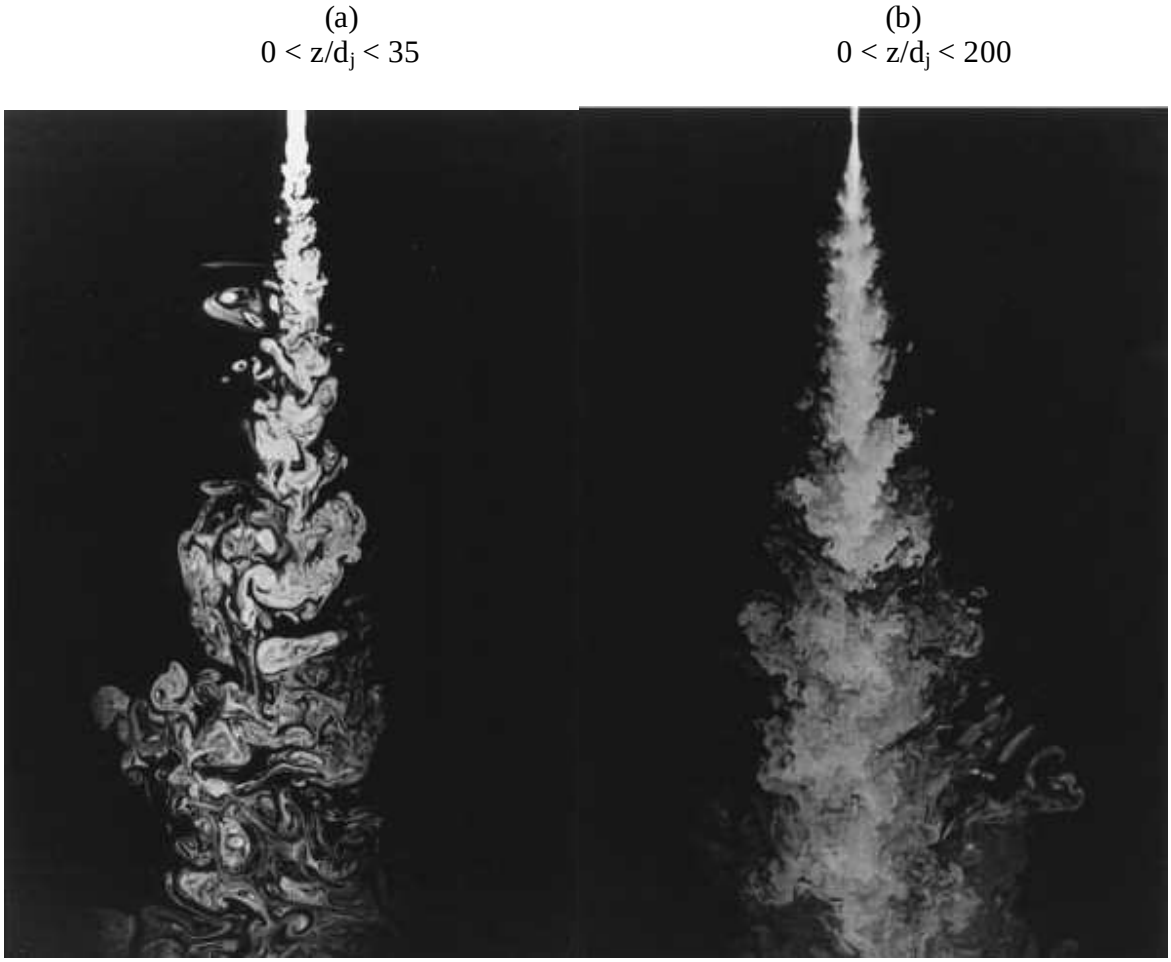

Figure 3.32: Flow visualization images of jet fluid concentration in the plane of symmetry of a turbulent round jet at: (a) $Re \simeq 2.5 \times 10^3$ and (b) $Re \simeq 10^4$. Data from Dimotakis et al. (1983)

With a reduction in the jet spread, a reduction in the decay rate of centerline mean velocity and a lower magnitude of local maximum in turbulence intensity, one expects the coherent structures to become less organized and more three-dimensional. In fact, based on the round jet visualizations of Dimotakis et al. (1983) (Figure 3.32), it can also be deduced that, with an increase in Re, either the number of coherent structures would be less or their structure will change. Importantly, Namar (1986) used Schlieren photograph to verify that in the far field, with an increase in Re, more small scale structures are superimposed on the large-scale structures. That is, smaller structures become increasingly significant and dominate the flow. (This visualization is shown in Figure 3.33). It is also well known, e.g. Frank (1999), that an increase in Reynolds number, will weaken the effect of viscosity. Hence, the large-scale structures become less effective in entraining the ambient fluid thus reducing the spreading and decay rates of the plane jet.

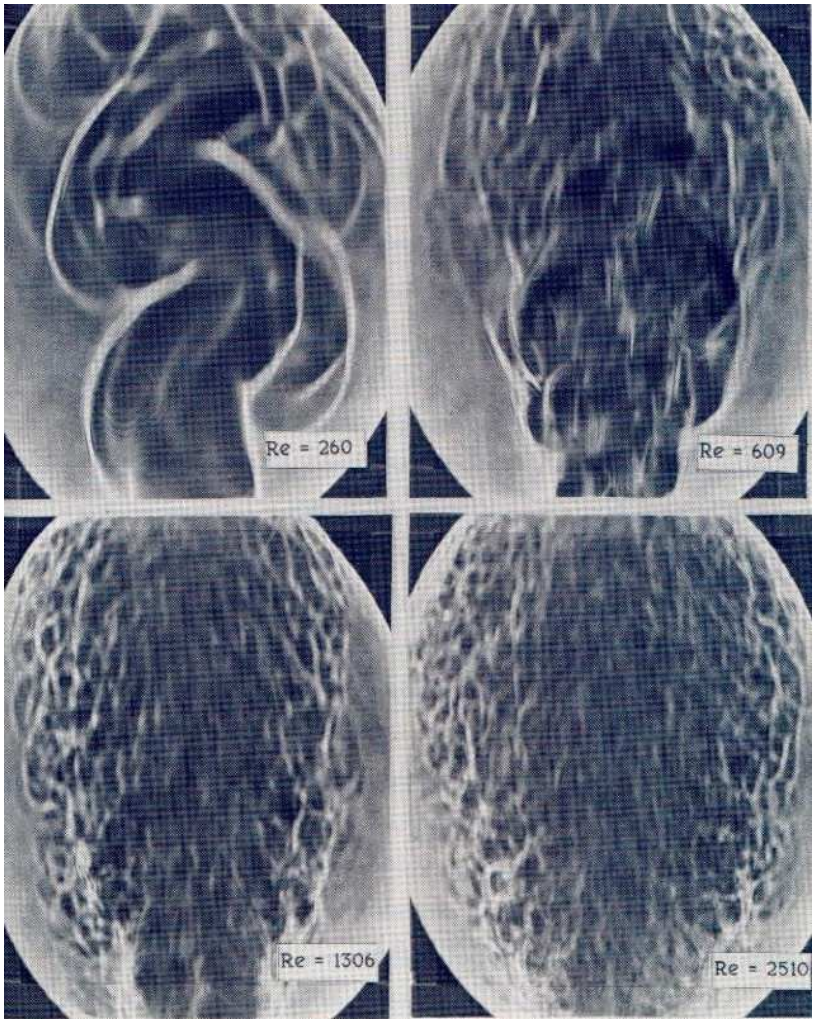

Figure 3.33: Schlieren photograph of a quasi-plane jet measured over the axial range $25 \leq x/H \leq 45$ and Reynolds numbers over the range $260 \leq Re \leq 2{,}510$. After Namar (1986).

Our self-similar region turbulence intensity at different Re have demonstrated that with an increase in Re, the far-field asymptotic turbulence intensity ($u'_{c,\infty}$) decreases. This contradicts the findings by Namar and Ötügen (1988) and Heskestad (1965) both of whom noted an increase in $u'_{c,\infty}$ with increased Re. We have noted that neither Namar and Ötügen (1988) nor Heskestad (1965) have provided any evidence to support their arguments. Nor do they offer any valid explanations for their observed trends in $u'_{c,\infty}$. On the other hand, our findings are supported by our calculations which show a reduction in the dissipation (ϵ) of turbulent kinetic energy (q) at increased Re. If this is true, then we expect an increase in the magnitude of $u'_{c,\infty}$ at an increased Reynolds number. In the general sense, a higher Reynolds number will reduce the damping effects of viscosity (Frank 1999). Thus, we expect a reduction in the dissipation of the turbulent kinetic energy. The arguments by Zhou et al. (1999) for their wake flow support our explanations.

They also found an increase in $u'_{c,\infty}$ for larger Reynolds numbers and validated their claim by calculating the dissipation term (ϵ). An increase in dissipation (ϵ) by almost five times at Re = 2,800 when compared with Re = 9,750 was noted. Correspondingly, their $u'_{c,\infty}$ was also higher for the latter case.

The present measurements demonstrate that the lower Re-jet takes a larger axial distance to develop into a self-similar state. This is shown, for example, by the lateral profiles of the mean velocity, which becomes self similar at x/H = 50 and 3 for Re = 1,500 and 16,500 respectively (Figs. 3.7-3.11) and centerline evolutions of turbulence intensity (Fig. 3.14), which become self-similar at x/H = 100 for Re = 1,500 and at x/H = 40 for Re = 16,500. Clearly, the differences in the self-similar locations depend on Reynolds number. A useful study by Johansson et al. (2003) explains that, unlike the axisymmetric jet whose local Reynolds number remains constant as the flow evolves downstream, the plane wake local Reynolds number drops off with downstream distance. For a plane jet, George (2005) concludes that the local Reynolds number increases with a square-root dependence on axial distance, i.e. $Re_{local} \sim x^{1/2}$. This dependence for the present plane jet is shown in Figure 3.17. Hence, no matter how low the source Reynolds number is, all plane jets will eventually attain very high-Re state as long as the nozzle aspect ratio is sufficiently large. Consequently, the effect of viscosity becomes smaller. Figure 3.17 reveal that, for the initially low Reynolds number jet, the local Reynolds number at an equivalent far field downstream distance becomes bigger but not larger than the initially high-Re jet. Thus, a more dominant viscosity effect for the initially low-Re jet clearly explains why this jet (e.g. Re = 1,500 and 3,000) take longer to evolve into a self-similarity state.

3.5 Conclusions

The main findings from the present work are summarized below.

(1) The present nozzle of a radial contraction with $r^* \simeq 2.14$ closely approximates a top hat profile of the mean velocity at x/H = 0.5. The central uniform part of the profile widens as the Reynolds number increases. The grid resolution is too poor to allow a definitive resolution of the effect of Re on the mean velocity profile. Nevertheless, it is clear that the initial profiles are Re-dependent and it appears that the initial velocity profiles (mean and rms) become almost independent of Re when $Re \geq$ 10,000.

(2) The thickness of the nozzle boundary layer from the present nozzle is a function of Re, although our measurement grid is to coarse to resolve the thickness accurately.

The present trends in the mean velocity profiles at $x/H = 0.25$ indicate that the effect of Re on nozzle boundary thickness become negligible when $Re \geq 10{,}000$.

(3) The length of the potential core x_p, decreases asymptotically with increasing Re. While it is not clear whether the asymptotic state is reached, it is approached closely at $Re = 10{,}000$.

(4) Both the decay and spread rates of the mean velocity in the flow downstream from the potential core decrease with Reynolds number. This trend appears to persist even at $Re = 16{,}500$. Thus, the influence of Reynolds number on the mean velocity field continues to be significant even at $Re = 16{,}500$. The decay rates of the mean velocity do not reach their asymptotic state at $Re = 16{,}500$.

(5) The centerline turbulence intensity $u'_{n,c}$ shows a local maximum $u'_{c,max}$ in the near-field. Below $Re = 10{,}000$, both the magnitude of $u'_{c,max}$ and its location x_m decrease as Reynolds number increases. Identical values of $x_m \simeq 12$ and $u'_{c,max} \simeq 0.22$ are found for $Re \geq 10{,}000$.

(6) In the self-similar region, an increase in Re leads to a reduction in the dissipation of turbulent kinetic energy.

(7) In the far field at $x/H \geq 100$, $u'_{n,c}$ reaches its asymptotic value $u'_{c,\infty}$ for all the tested Reynolds numbers. Increasing Re results in an increase in $u'_{n,c}$. However, $u'_{c,\infty}$ asymptotes when $Re \geq 10{,}000$.

(8) Both the skewness S_u and flatness F_u vary dramatically in the near field at $x/H \leq 30$. Also, their near field evolutions are strongly Re-dependent. These factors become asymptotic over a much shorter distance (approximately $40H$) while $u'_{c,\infty}$ requires at least $80H$ to asymptote, for $Re \leq 10{,}000$. Nevertheless, their asymptotic values continue to be Re-dependent, i.e., increasing Re results in an increase in $S_u^{c,\infty}$ and a slight decrease in $F_u^{c,\infty}$.

The present Re-dependence of a plane air jet using a nozzle of radial contraction does not only apply to radially contoured nozzles, but has broad significance to all smoothly contoured nozzles. Since the present nozzle produces a top hat initial velocity profile similar to a conventional smoothly contoured nozzle, these findings are applicable to all smoothly contoured nozzles.

The dependence of the initial flow on Reynolds number is a feature of, not only the

present radially contoured nozzle, but, is also for all smoothly contoured nozzles. However, it is deduced that this dependence will be less for a conventional smoothly contoured nozzle. For instance, the present increase in vortex shedding frequency St_H with an increase in Reynolds number, was not found by Namar (1986), who used a conventional smooth contraction nozzle. Therefore, an evidence of the dependence of vortex shedding on Re, for a radially contoured nozzle has been established.

It is also imperative to note that the systematic dependence of all flow properties e.g. mean velocity decay and spreading rates, near field hump in turbulence intensity and far field asymptotic values etc on Re, is a feature of all smoothly contoured nozzles. What may vary from one experiment to the other, are their relative magnitudes. Thus, the generic findings of the present research are not only limited to radially contoured nozzles, but can be generally applied to all smoothly contoured nozzles.

Chapter 4

EFFECT OF INNER-WALL NOZZLE EXIT CONTRACTION PROFILE

4.1 Introduction

Chapter 1.5.2 has shown that no systematic study of the variation of the inner-wall nozzle contraction profile on plane jets exists. An early analytical study by Batchelor and Proudman (1954) provided a linear theory of a rapid distortion of a fluid in turbulent motion issuing into a contraction. Uberoi (1956) investigated, experimentally, square cross-sections of various contraction types. A more generalized study was also conducted by Klein and Ramjee (1972) who investigated the effect of contraction geometry on non-isotropic free-stream turbulence using eight nozzles of circular cross-sections, different contour shapes and various non-dimensional lengths. The influence of the axisymmetric contraction ratio on free-stream turbulence was studied more thoroughly by Ramjee and Hussain (1976), with particular applications to wind tunnel designs. Importantly, these studies were conducted to understand the turbulence development within the initial (and upstream) region of the axisymmetric flow but not on the influence of further downstream flow.

For round jets, the effect of the nozzle profiles has been well studied. The initial and downstream flow from a round smoothly contoured nozzle, a round sharp-edged orifice nozzle and a long pipe jet was explored by Mi, Nathan and Nobes (2001). Antonia and Zhao (2001) and Hussain and Zedan (1978) have also studied a smoothly contracting round nozzle and a long pipe jet. On the other hand, Hussain and Clark (1977) quantified to some extent, the downstream effect of having a laminar or turbulent boundary layer at nozzle lip of a quasi-plane jet. Others e.g. Goldschmidt and Bradshaw (1981) studied the

effect of initial turbulence intensity on the flow field of a plane jet. Additionally, Hussian (1983) conducted a flow visualization of an initially laminar plane jet issuing from two nozzles at Re = 2,000: (1) with an exit of a 96:1 contraction and (2) from the end of a channel attached to the downstream end of a contoured nozzle. He noted a dependence of the vortex formation on the nozzle contraction profile. In this context, it is expected that the nozzle profile will affect the downstream flow of a plane jet. However, the effect of varying the nozzle profiles has not been studied systematically.

The present investigation is undertaken to examine the velocity field of a plane jet from nozzles of different inner-wall nozzle contraction profiles. The next section describes the experimental details and thereafter provides the results, a discussions and conclusions.

4.2 Experiment Details

The same wind-tunnel in Figure 3.1 was used in this study. To quantify the effect of variations in nozzle contraction profile, five different sets of nozzle plates were designed and tested. Figure 4.1 shows the nozzle plates for this investigation. To vary the nozzle contraction profile, five values were taken between $r/H \simeq 0$ and r/H = 3.60, given H = 10 mm and w = 720 mm, so that the nozzle aspect ratio AR = 72. Note that the inner-wall contraction profile factor is denoted as $r^* = r/H$ from here onwards.

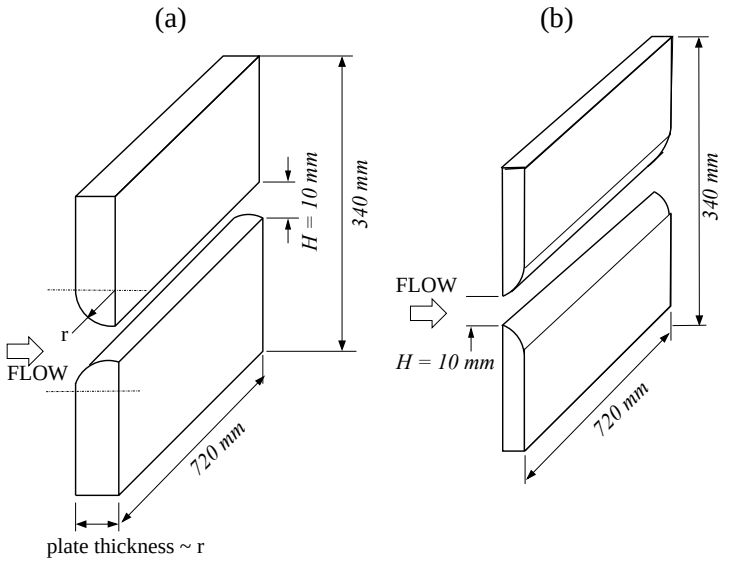

Figure 4.1: Nozzle plates used for inner-wall nozzle profile variation for the cases in (a) $4.5 \leq r^* \leq 36$ mm with radial contraction facing upstream and (b) radial contraction facing downstream i.e. $r^* \simeq 0$.

Note that the configuration for $r^* \simeq 0$ (Fig. 4.1b) was obtained by reversing the plates to provide a sharp-corner. Hence, this configuration is referred to as the sharp-edged orifice nozzle. The wind tunnel fan was set to provide a jet exit Reynolds number based on slot opening width H and the exit centerline mean velocity $U_{o,c}$ of 18,000. Then, the effect of nozzle exit contraction profile on the initial flow was determined by interchanging each configuration and subsequently measuring the initial velocity profiles at $x/H \simeq 0.25$ for $0.45 \leq r^* \leq 3.60$ and at $x/H = 1.25$ for $r^* \simeq 0$. The centerline streamwise velocity from $x/H \simeq 0$ to $x/H = 85$ was measured. The lateral distribution of the streamwise velocity was also measured.

4.3 Results and Discussion

4.3.1 The Initial Velocity Field

Figure 4.2a displays the lateral profiles of the normalized mean velocity measured as near as practical to the nozzle exit. Their locations are at $x/H \simeq 0.25$ for the radially contracting (r^* between 0.45 and 3.60) configurations and at $x/H = 1.25$ for the sharp-edged orifice ($r^* = 0$) nozzle. These measurement locations were chosen to avoid probe damage, since it was difficult to perform measurements at the nozzle exit.

It is noticeable that the initial velocity profiles change with r^*. Thus, the bulk mean velocity $U_{o,b}$ will not be equal to the exit centerline mean velocity $U_{o,c}$. To deduce the bulk mean velocity, the initial velocity profiles, measured at $x \simeq 0.25H$ are used. While it is true that such a method may under-estimate the true value of $U_{o,b}$, it will nevertheless provide a relative magnitude of $U_{o,b}$. Hence, the bulk mean velocity $U_{o,b}$ is computed from the exit velocity profiles as follows

$$U_{o,b} = \frac{1}{H} \int_{y=-H/2}^{y=+H/2} U(x,y)_{x=0}\, dy \tag{4.1}$$

Note that this calculation utilises the principles of mass and momentum conservation. A complete derivation is given in Appendix E.2. Figure 4.3 plots the ratio of $U_{o,c}$ and $U_{o,b}$ for different r^*. It is evident that $U_{o,c}/U_{o,b} \to 1$ as $r^* \to 3.60$. For instance, when $r^* = 3.60$, $U_{o,c}/U_{o,b} \simeq 0.98$, confirming that the exit velocity profile closely approximates to a top hat (Figure 4.2a). Given the difficulty in undertaking measurements at the exit plane for the sharp-edged orifice nozzle, the present $U_{o,c}/U_{o,b}$ are used to interpolate $U_{o,c}/U_{o,b}$ for this configuration. This suggests that $U_{o,c}/U_{o,b} \simeq 0.88$ for the sharp-edged orifice nozzle. Hence, to quantify the downstream flow, the computed values of $U_{o,b}$ rather than $U_{o,c}$ will

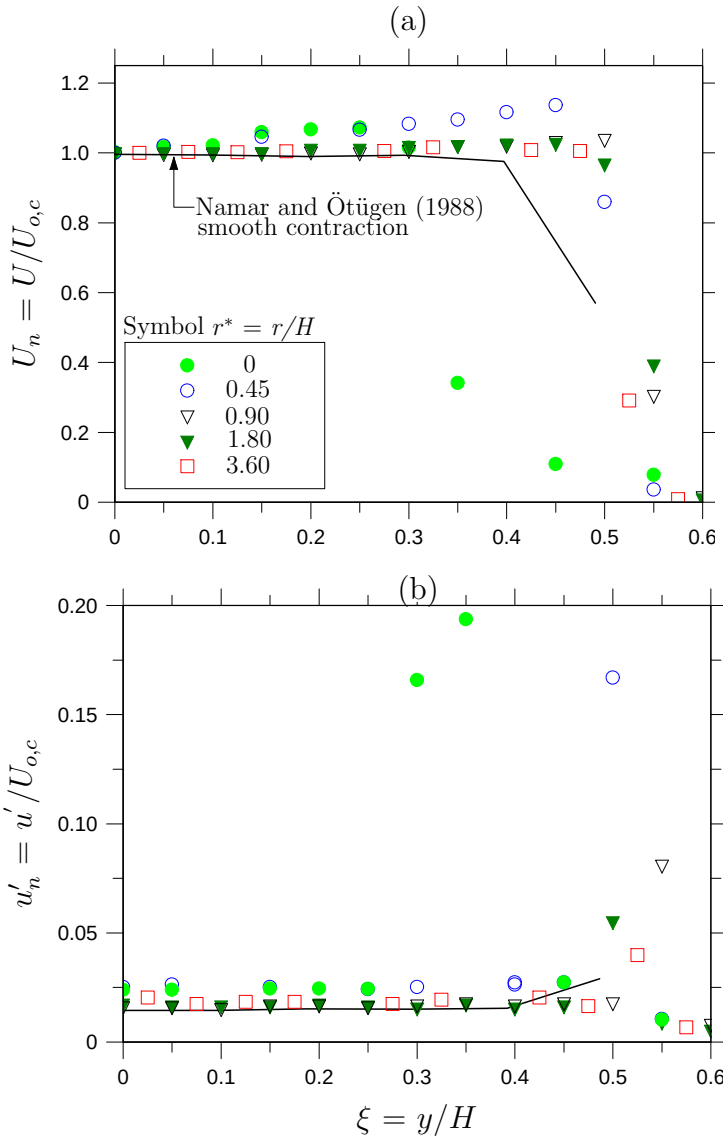

Figure 4.2: Lateral profiles of (a) the normalized mean velocity U_n and (b) the turbulence intensity $u_n^{'}$ at the $x/H \simeq 0.25$ for $0.45 \leq r^* \leq 3.60$ and $x/H = 1.25$ for $r^* \simeq 0$.

be used as the normalization constant.

From Figure 4.2a, distinct initial velocity profiles are evident for all nozzles due to the different inner-wall nozzle contraction profiles. Notably, as r^* is increased from 0 to 3.60, the normalized mean velocity profile changes from being clearly saddle-backed (for $0 \leq r^* \leq 0.90$) to approximately top hat (for $r^* = 1.80$ and 3.60). Saddle-backed profiles are a characteristic of a sharp-edged orifice nozzles - e.g. see Mi, Nathan and Nobes (2001) for saddle-backed initial velocity profiles from a round orifice nozzle or Tsuchiya et al. (1989) for a rectangular orifice nozzle. For the present saddle-backed profiles, the central 'dip' is deepest for the sharp-edged orifice nozzle i.e. for $r^* \simeq 0$. The local minimum in the center of the saddle-back is probably caused by an initial lateral contraction of the emerging fluid

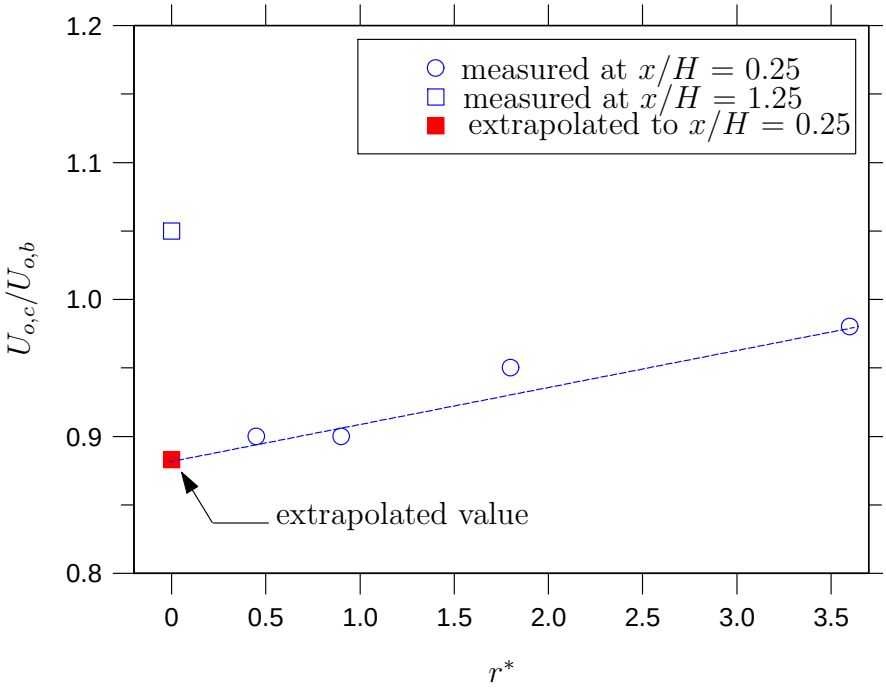

Figure 4.3: Variation of the exit centerline mean velocity $U_{o,c}$ relative to the bulk mean velocity $U_{o,b}$ for different r^*, calculated from initial velocity profiles obtained at $x/H \simeq 0.25$.

termed the 'vena contracta'. It also appears that the initial velocity profiles converge for $r^* \geq 1.80$ to approximate a top hat profile. Slight differences between $r^* = 1.80$ and 3.60 appear to be within the experimental uncertainty. The top hat region is found for $\xi \leq 0.45$. Also, the approximate top hat profile for $r^* \geq 1.80$ is comparable with the top hat profiles from a conventional smoothly contoured nozzle e.g. Namar and Ötügen (1988). Note that subtle differences are, in part, due to a different downstream location chosen by Namar and Ötügen (1988) (at $x/H = 1$), and in part, due to a slight difference in nozzle type e.g. smoothly contoured, no front plate.

The present nozzles exhibit a laminar boundary layer at $x = 0.25H$. Using equations 3.1 and 3.2, the displacement thickness δ^*, the momentum thickness θ and the shape factor $H = \delta^*/\theta$ were determined. These are presented in Table 4.1. From Table 4.1, one concludes that the shape factor, $H \geq 2.40$ for all investigations. This leads to the conclusion that the present configurations exhibit a laminar boundary layer.

From Figure 4.2a, it appears that the thickness of the nozzle boundary layer depends on the nozzle inner-wall nozzle contraction profile. To quantify the effect of inner-wall nozzle contraction profile on the near exit boundary-layer development, the pseudo-boundary

r^*	**Displacement Thickness**, δ^*	**Momentum Thickness**, θ	**Shape Factor**, H
0	0	-	-
0.45	0.707	0.300	2.40
0.90	0.840	0.348	2.36
1.80	1.274	0.518	2.46
3.60	4.881	1.968	2.48

Table 4.1: Summary of the pseudo-boundary-layer characteristics (mm) of the plane jet for different inner-wall nozzle contraction profiles, r^*.

layer[1] (displacement) thickness δ at $x/H \simeq 0.25$ was computed from the integral equation below.

$$\delta = \int_{y=0}^{y=\infty} \left(1 - \frac{U}{U_{o,c}}\right) dy \tag{4.2}$$

Here, the normalized velocity profiles at $x/H \simeq 0.25$ (in Figure 4.2a) were used. Given the coarse measurement grid in Figure 4.2a, a best-fit curve was used to perform an integration of the profile $1 - \frac{U}{U_{o,c}}$ to obtain an estimated value of δ from the present measurements. Figure 4.4 shows that as r^* is increased from 0.45 to 3.60, the pseudo-boundary layer thickness (calculated at a distance of $0.25H$ from the nozzle exit plane) increases. Of course the magnitude of δ for the sharp-edged orifice nozzle ($r^* \simeq 0$) does not truly represent the pseudo-boundary layer thickness and hence was not calculated from the initial velocity profile. A true sharp-edged orifice nozzle is expected to have a very thin initial boundary layer ($\delta \simeq 0$). Hence, it was assumed that $\delta \simeq 0$ at $x/H \simeq 0$ for the sharp-edged orifice nozzle. On this basis, the best-fit curve for the calculated δ values were translated to estimate δ for $0.45 \leq r^* \leq 3.60$. A consistent trend is seen, that is, as the nozzle inner-wall contraction profile changes from a sharp-edged orifice to a radially contoured configuration, the pseudo-boundary layer thickness increases. It is likely that the variation of δ will have an influence on the downstream development of the plane jet.

Figure 4.2b presents the lateral profiles of the normalized turbulence intensity $u_n^{'}$ at $x/H \simeq 0.25$ for the radially contracting and at $x/H = 1.25$ for the sharp-edged orifice nozzle. Very high turbulence intensity is found in the shear layer ($\simeq 20\,\%$) for the sharp-edged orifice nozzle while the lowest shear layer intensity occurs (only $\simeq 4\,\%$) for the radially contoured ($r^* = 3.60$) configuration. The high turbulence intensity in the shear layer is

[1]The term 'pseudo-boundary layer' is used because of the measurement location of 0.25 nozzle widths downstream. Ideally, boundary-layer thickness only refers to measurements at nozzle exit only.

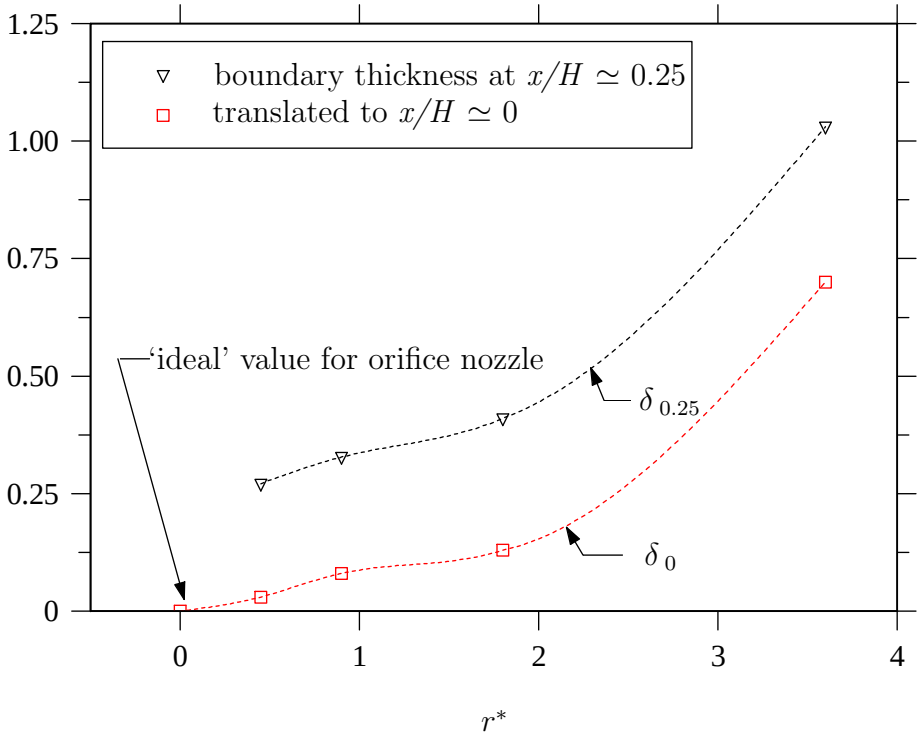

Figure 4.4: The calculated boundary thickness (mm) obtained at $x/H \simeq 0.25$ and translated to $x/H \simeq 0$ to provide a pseudo-exit boundary layer thickness (mm) δ for different inner-wall nozzle contraction profiles r^*.

expected for a sharp-edged orifice nozzle because its initial shear layer is the thinnest, tending to $\delta \simeq 0$, and thus highly unstable. It is also likely that an upstream separation causes the greatest instability in the shear layer. Hence, its instantaneous position in space will oscillate substantially. On the other hand, large radially contoured nozzles e.g. $r^* \geq 1.80$ produce a more initially laminar flow with lower turbulence intensity in the shear layer. For these cases, as r^* is increased from 0.45 to 3.60, a corresponding decrease in the peak of $u_n^{'}$ (from $\simeq 17\,\%$ to $4\,\%$) is evident. The turbulence intensity in the central region varies between $u_n^{'} = 2.8\,\%$ and $u_n^{'} = 1.7\,\%$ as r^* is varied between 0 and 3.60. In particular, the sharp-edged orifice nozzle produces a higher core turbulence intensity. Furthermore, identical values of core turbulence intensity are found for $r^* = 1.80$ and 3.60.

4.3.2 The Mean Velocity Field

The near field mean velocity on the centerline normalized as $U_{n,c} = U_c/U_{o,c}$ is presented in Figure 4.5. Normalization by $U_{o,b}$ showed the same general trend and is presented in Appendix E.5. The present figure demonstrates that the decay of mean centerline velocity is dependent on r^*. It is noticeable that the velocity decay of the sharp-edged orifice

nozzle differs significantly from those of the radially contracting nozzles. In particular, a local maximum in $U_{n,c}$ is evident at $x/H \simeq 3$ for $0 \leq r^* \leq 1.80$ whose magnitude is r^*-dependent. This hump confirms the presence of a vena contracta. A sharp-edged orifice nozzle is known to generate a local maximum of the centerline mean velocity as shown for example by Quinn (1992a). For this reason, we introduce the term $U_{m,c}$ to denote the maximum of the centerline mean velocity.

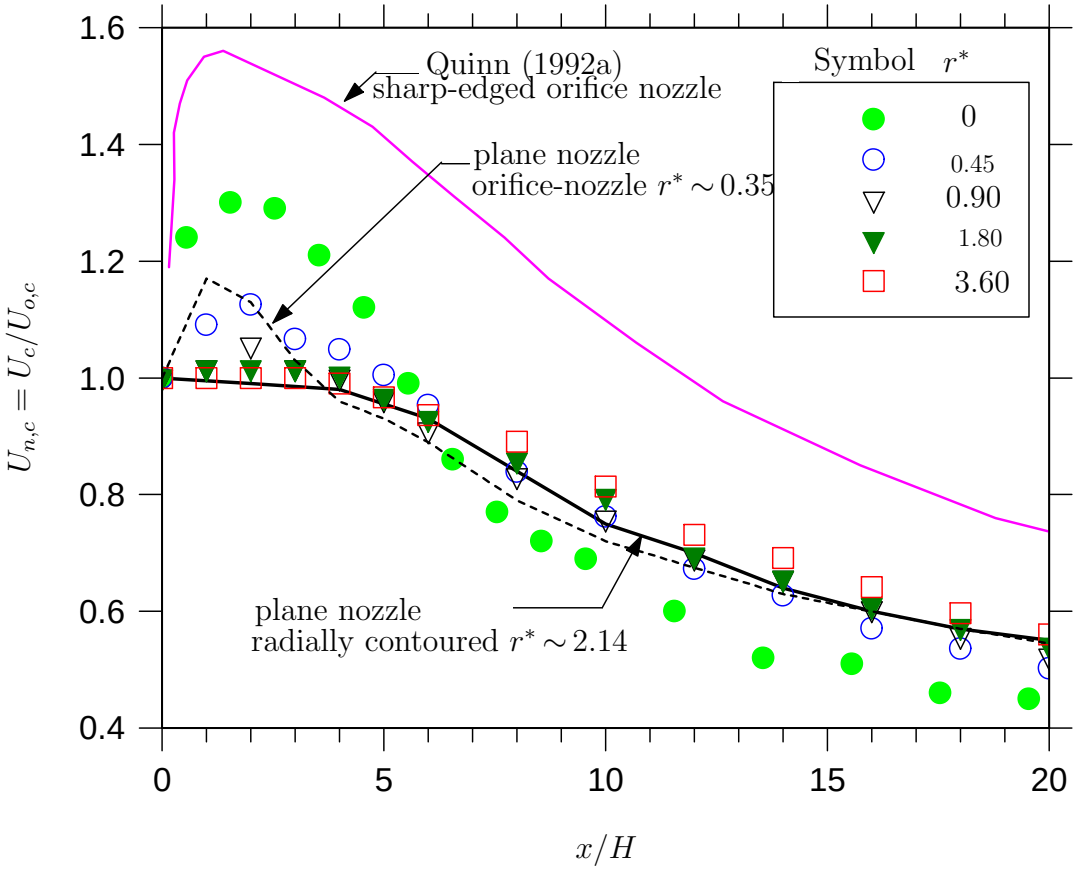

Figure 4.5: Near field evolution of the normalized mean centerline velocity $U_{n,c}$ on the nozzle contraction profile factor r^*.

To assess the relative magnitudes of these local maxima for present nozzle configurations, Figure 4.6 plots $U_{m,c}/U_{o,c}$ obtained at $x/H \simeq 3$. As r^* is increased from 0 to 3.60, $U_{m,c}/U_{o,c}$ decreases from $\simeq 1.3$ to $\simeq 1.0$. Clearly, for the sharp-edged orifice nozzle i.e. $r^* \simeq 0$, a strong vena contracta is present with at least 30% higher centerline velocity than its nominal exit centerline value. Vena contracta have also been noted for rectangular and round jets issuing from sharp-edged orifice nozzles. For his sharp-edged rectangular nozzle, Quinn (1992a) found $U_{m,c}/U_{o,c}$ to be $\simeq 1.55$. His data has been included in Figure 4.6. The difference between his and our $U_{m,c}/U_{o,c}$ can be attributed to a combination of differences e.g. nozzle aspect ratio (his 20 versus ours 72), Reynolds number (his 36,000

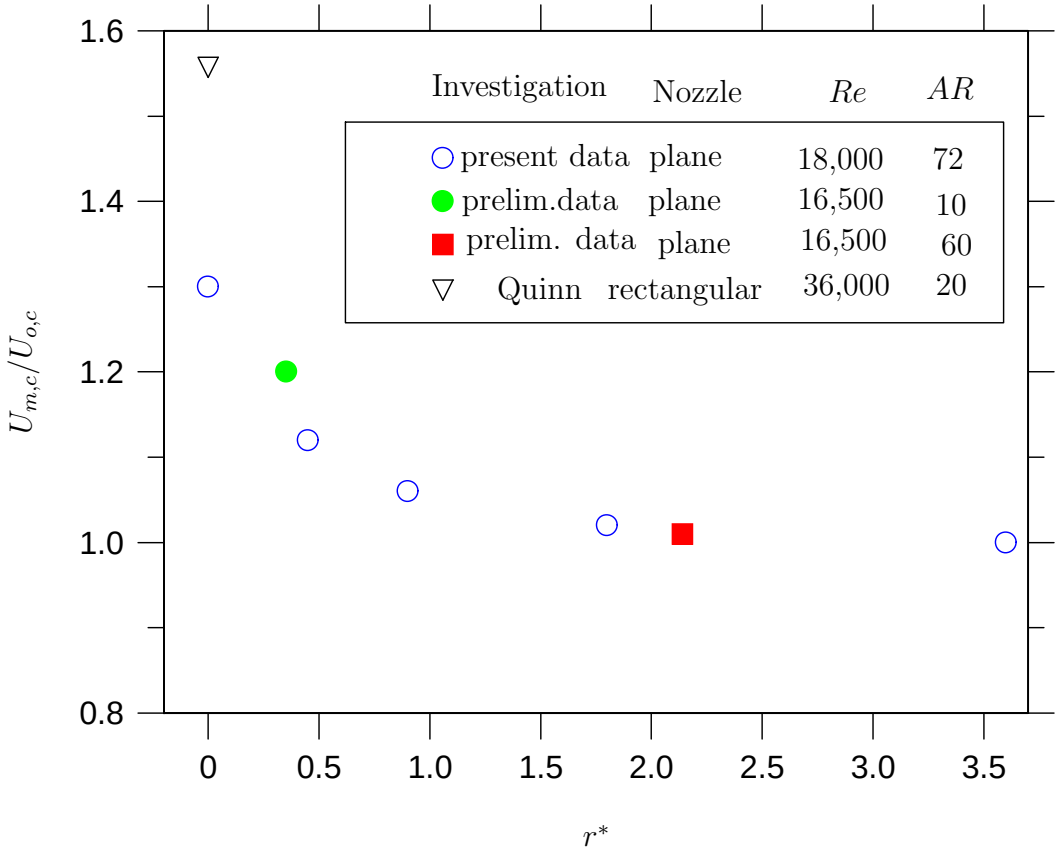

Figure 4.6: The dependence of the ratio of the centerline mean velocity maximum $U_{m,c}$ to the exit centerline mean velocity $U_{o,c}$ (i.e. $U_{m,c}/U_{o,c}$) on the nozzle contraction profile factor r^* at $x/H \simeq 3$.

versus ours 18,000) and/or slight differences in nozzle geometry (refer to his paper). Unfortunately, the plane jet investigation of Heskestad (1965) did not identify this feature because his velocity decay was only presented for $x/H \geq 15$.

Also included in Figure 4.6 is the result from our preliminary study on initial conditions using a plane nozzle of $AR = 60$, $Re = 16{,}500$ and $r^* = 2.14$ and of $AR = 10$, $Re = 16{,}500$ and $r^* \simeq 0.35$. It was found that $U_{m,c}/U_{o,c} \simeq 1.02$ for $AR = 60$, $Re = 16{,}500$ and $r^* = 2.14$ at a similar axial location, which compares quite well with $U_{m,c}/U_{o,c} \simeq 1.01$ at $r^* = 1.80$ for the present study. Furthermore, at $AR = 10$, $Re = 16{,}500$ and $r^* \simeq 0.35$, the study found $U_{m,c}/U_{o,c} \simeq 1.20$. The initial velocity profile for this case was also saddle-backed, indicating the flow from a sharp-edged orifice nozzle. Evidently, from Figure 4.6, $U_{m,c}/U_{o,c}$ asymptotes to 1 when $r^* \geq 1.80$, where the vena contracta does not occur.

Now, we discuss the near field decay of centerline mean velocity. Figure 4.5 suggests

that for $x/H > 6$, the rate of centerline velocity decay is greater for the sharp-edged orifice nozzle. (In fact, normalizing the mean centerline velocity using $U_{o,b}$ provides the same conclusion. For further reference, see Figure E.4.) Increased decay of centerline mean velocity for $x/H > 6$ for this configuration is plausibly a consequence of the rapid 'expansion' of the jet, thus, increased entrainment by the jet as it emerges from the sharp-edged nozzle. Such an expansion would probably be caused by an initial separation of the flow due to a lateral contraction of the emerging fluid. This is somewhat demonstrated by a saddle-backed initial velocity profile in Figure 4.2. The radially contoured nozzles allow a more smooth flow from their exit. The radial contraction probably reduces a flow separation thus producing an approximate top hat velocity profile, a lower decay of centerline mean velocity and no vena contracta when compared with a sharp-edged orifice nozzle. The present observation is well supported by Mi, Nathan and Nobes (2001), who demonstrated that the decay of the centerline mean scalar field was higher for a sharp-edged round nozzle than for a smoothly contoured round nozzle.

Figure 4.7 presents the inverse of the normalized centerline mean velocity decay for the entire measured range. The well-known dependence of the form

$$\left(\frac{U_{o,b}}{U_c}\right)^2 = K_u \left[\frac{x}{H} + \frac{x_{01}}{H}\right] \tag{4.3}$$

is demonstrated, where K_u is the decay rates determined from experimental data over the range $20 \leq x/H \leq 80$ and x_{o1} is the x-location of the virtual origin. Figure E.5 in Appendix E.5 presents the graphs normalized using $U_{o,c}$, but the trends are quite similar to the present figure.

For reference to the present data, the plane jet data of Heskestad (1965) (sharp-edged orifice nozzle) and Jenkins and Goldschmidt (1973) (conventional smooth contraction nozzle) are plotted. As evident from Figure 4.7, the highest decay of centerline mean velocity occurs for the jet issuing through the sharp-edged orifice nozzle. A collapse of $U_{n,c}$ is also noticeable for $r^* = 1.80$ and 3.60. Any differences between them are within the experimental uncertainty.

Figure 4.8 presents the relationship between K_u and r^*. As r^* is increased from 0 to 3.60, K_u decreases from $\simeq 0.301$ to 0.198. Consistent with Figure 4.7, K_u asymptotes to a constant value for $r^* = 1.80$ and 3.60. Indeed, any differences between them are within the experimental uncertainty.

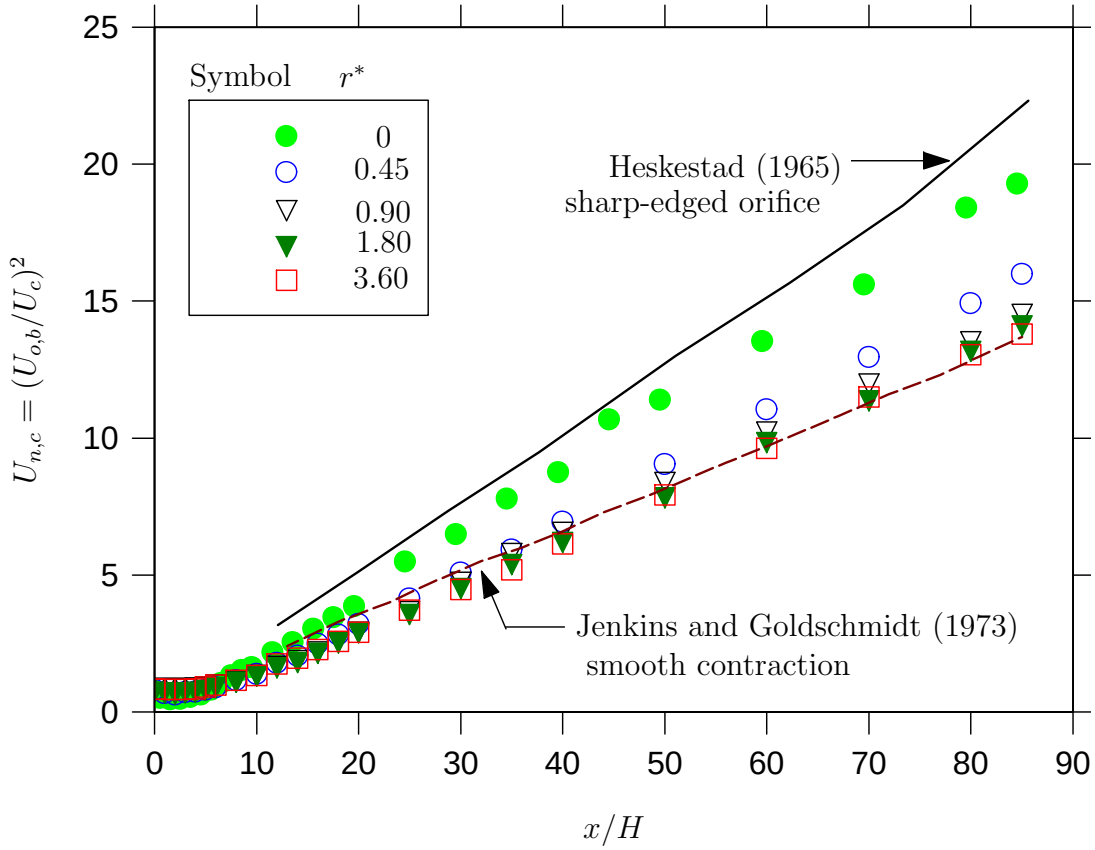

Figure 4.7: The far field centerline mean velocity in the inverse square form, normalized using the bulk mean velocity $U_{o,b}$ for different nozzle profiles r^*.

An analysis of virtual origins of the centerline mean velocity decay x_{01} shows that x_{01} increases monotonically with r^* from $x_{01} = 2.0$ at $r^* \simeq 0$ to $x_{01} = 4.7$ at $r^* = 3.60$. Hence, x_{01} is smallest for the sharp-edged orifice nozzle. This dependence of x_{01} on initial conditions is in agreement with the postulate of Gouldin et al. (1986). They suggested that the large scatter in the measured virtual origins of plane jet is associated with different initial conditions. Indeed, Flora and Goldschmidt (1969) studied the relationship between plane jet virtual origins and its initial and upstream turbulence intensity at the center-plane of the nozzle exit and at two other positions, further upstream from the nozzle exit. They found that the location of the virtual origin x_{01} is changed drastically by changing the turbulence intensity. With an increase in exit turbulence intensity from 1.06 % to 1.28 %, they found that virtual origin moved upstream from $x_{01} = 2.0$ to $x_{01} \simeq 0$. Thus, they concluded that a slight increase in turbulence at the exit and upstream of the nozzle exit, moves the virtual origins considerably upstream. For the present measurements, Flora and Goldschmidt's conclusion appears to be true. That is, as the initial turbulence intensity increases from 1.7 % to 2.8 %, the virtual origin, x_{01}, moves upstream from 4.7 to 2.0. The present reduced magnitude of x_{01} for $r^* \simeq 0$ relative to the x_{01} for $r^* = 3.60$ is,

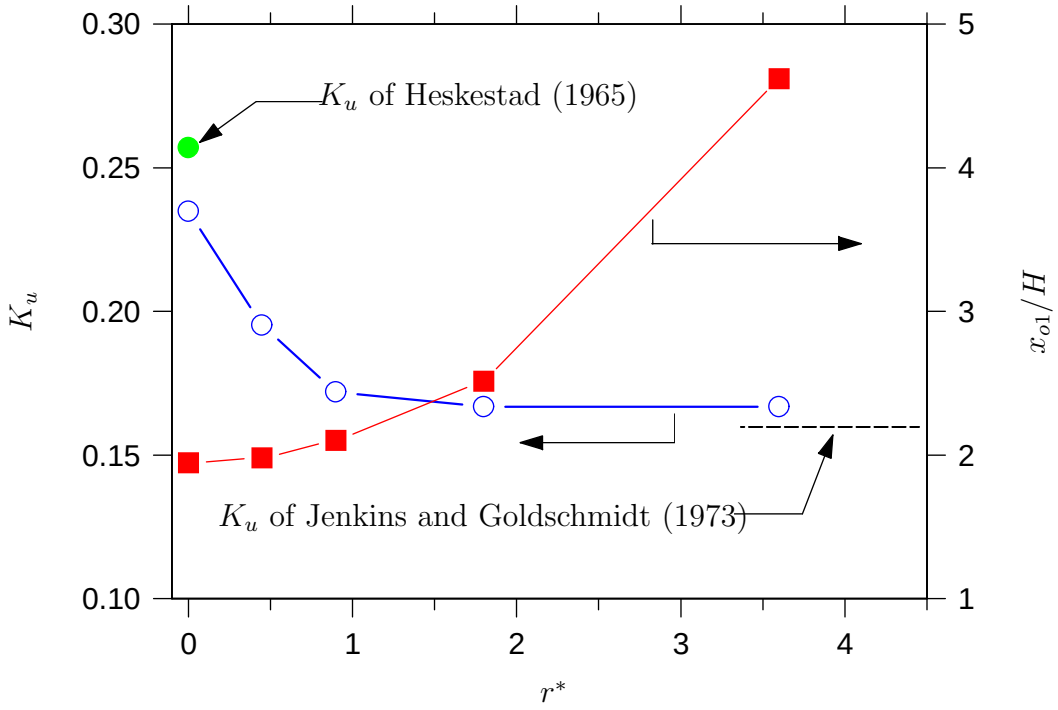

Figure 4.8: Dependence of the centerline decay rate of mean velocity K_u and the virtual origin, x_{01} on the nozzle contraction profile factor r^*.

perhaps, also associated with the presence of a vena contracta for the sharp-edged orifice nozzle, or for other reasons. For $r^* \simeq 0$, an initial lateral inflow could produce a smaller virtual 'width' of the potential core. However, the exact cause of this is unknown.
Lateral profiles of the normalized mean velocity for $r^* \simeq 0$, 0.45 and 3.60 are shown in Figure 4.9. It is demonstrated that the mean profiles become self-similar at $x/H \simeq 20$ for the sharp-edged orifice i.e. for $r^* \simeq 0$ and at $x/H \simeq 5$ for the radially contoured i.e. for r^* = 3.60 configuration. This provides a distinction between the development of the mean velocity profiles for the two configurations. When the profiles have become self-similar, they conform closely to a Gaussian, given by an expression of the form $U_n = e^{-\ln 2(y_n)^2}$. The results indicate that the profiles attain self-similarity at a greater axial distance from the nozzle for the sharp-edged orifice than for the radially contoured nozzle.

Figure 4.10 presents the streamwise variations of the normalized velocity half-widths $y_{0.5}/H$. It is clear that the present data conforms to the following far field relation

$$\frac{y_{0.5}}{H} = K_y \left[\frac{x}{H} + \frac{x_{02}}{H}\right] \tag{4.4}$$

where K_y and x_{02} are spreading rates and virtual origins determined by the experiment.

As r^* is decreased from 3.60 to 0, the jets spread at increased rates. The orifice-jet

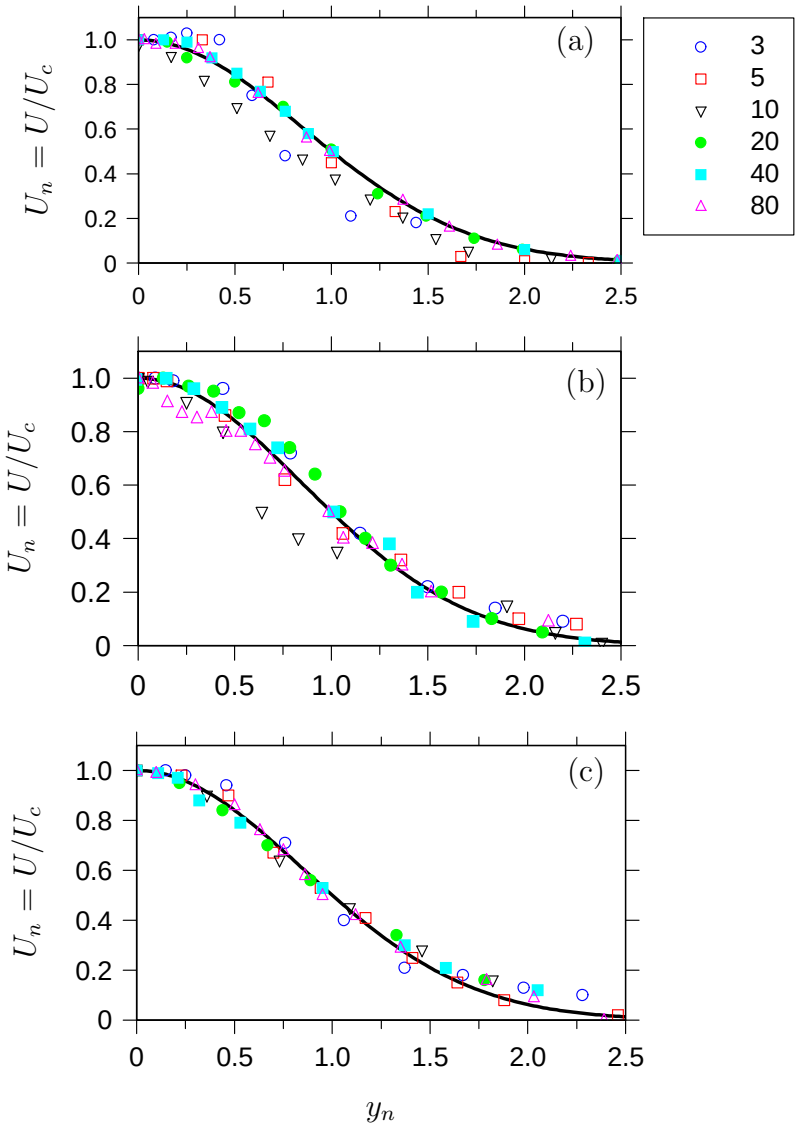

Figure 4.9: Lateral profiles of the normalized mean velocity U_n. (a) $r^* \simeq 0$ (b) $r^* \simeq 0.45$ and (c) $r^* = 3.60$.

has the greatest spreading rate. This trend is consistent with the result that a smaller r^* produces a higher decay of U_c (Figure 4.8). The slope K_y a measure of the spreading rate is presented in Figure 4.11. Increased far field spreading rate indicates a greater entrainment of ambient fluid by the orifice-jet. Mi, Nathan and Nobes (2001) calculated the mixing rates from a sharp-edged orifice and a smoothly contracting round nozzle. Their planar images of the scalar field showed highest mixing, decay and spreading rates for the orifice-jet. Hence, we can infer that our deduction that the orifice-jet has the highest mixing rates is somewhat justified.

As demonstrated by Figure 4.11, the virtual origins x_{02}/H depend on r^* too. As r^*

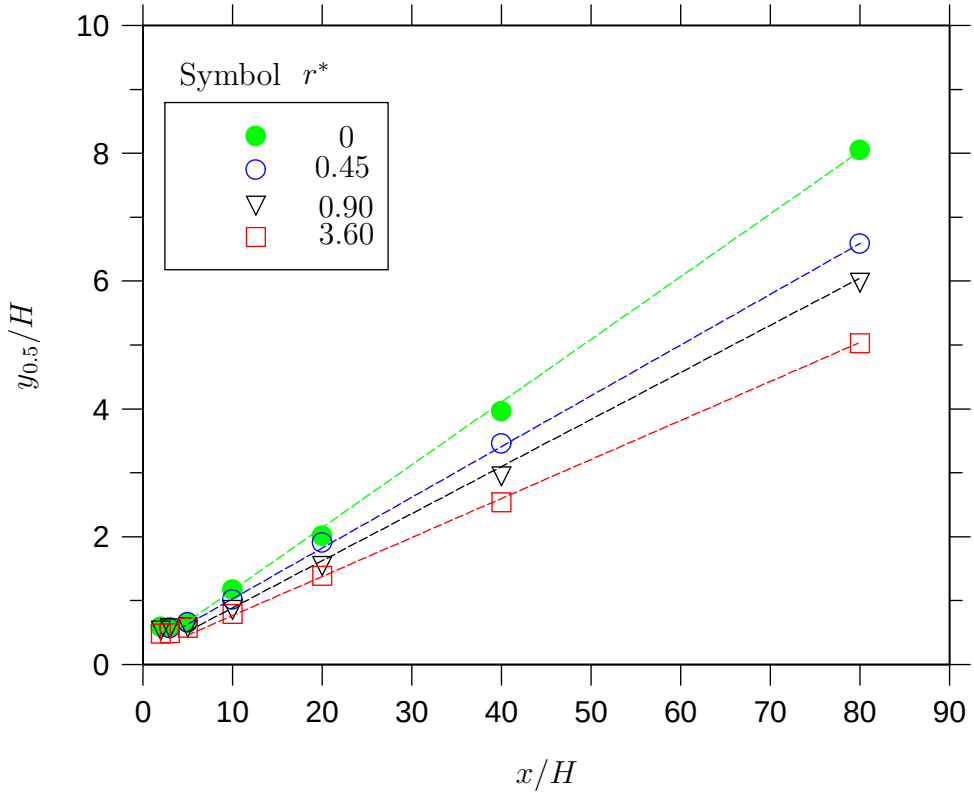

Figure 4.10: The streamwise variation of the velocity half-width $y_{0.5}$ for different nozzle contraction profile factors r^*.

is increased from 0 to 3.60, the magnitude of x_{02}/H increases from $\simeq 0$ to 4. Thus, the sharp-edge orifice nozzle generates a virtual origin closer to the exit than does the radially contoured nozzle.

4.3.3 The Fluctuating Velocity Field

The turbulent velocity fluctuations can be analyzed statistically, by separating the mean U from the instantaneous signal U_i. Hence, the moments of $u = U_i$ - U are presented. Figure 4.12 demonstrates the centerline evolution of the locally normalized turbulence intensity $u'_{n,c}$. For reference, $u'_{n,c}$ of a our preliminary measurements for a sharp-edged orifice nozzle and a radially contoured nozzle at (Re, AR) = (16,500, 10) and (16,500, 60) are included. Also included are the smoothly contracting plane jet data of Gutmark and Wygnanski (1976) and Heskestad (1965), measured at (Re, AR) = (30,000, 39) and (36,900, 120).

Turbulence intensity shows a significant dependence on r^*. Such a dependence is greatest in the near field, although even in the far field, their asymptotic values also differ. In particular, the near field of the orifice jets are distinct from the radiused nozzle jets.

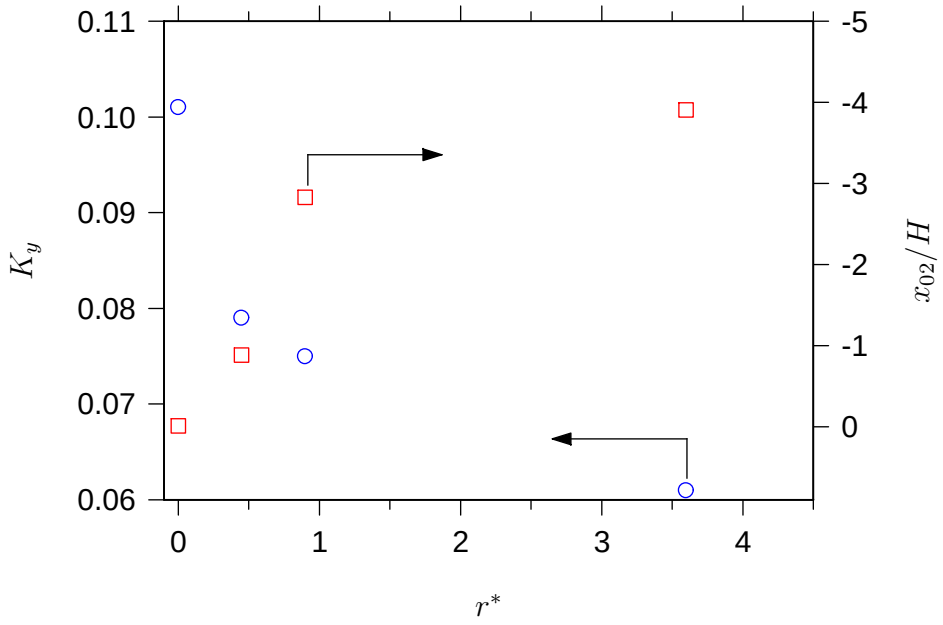

Figure 4.11: Dependence of the jet spreading rates K_y and virtual origin x_{02}/H on the nozzle contraction profile factor r^*.

The initial relative turbulence intensity is higher for the orifice jet with a significant 'hump' around $x/H = 10$. This is also supported by our preliminary measurement (Deo et al. 2004) for a sharp-orifice nozzle whose (r^*, AR) = (0.35, 10). There is a similarity in the shape and the occurrence of a hump around $x/H = 10$. The differences in $u'_{n,c}$ are due to the differences in the aspect ratio (10 for our previous plane jet data compared with 72 for present data). For the present measurements at Re = 18,000, the radially contoured nozzles ($r^* > 0.45$) do not produce a hump. Also, the hump for $r^* \simeq 0.45$ is very small. It is relevant to note that, although, the hump is absent for the present nozzles of $r^* > 0.45$, a hump will be present if the same nozzle is used but measured at a lower Reynolds number. Our preliminary measurements for (r^*, AR) = (2.14, 60) shows excellent agreement with the present data for $r^* = 1.80$. Quinn (1992a), who measured at (Re, AR) = (36,000, 20) also noted a pronounced near field hump in turbulence intensity, produced by their orifice plate rectangular jet. Hill et al. (1976) have attributed the presence of the hump to initial conditions. It is deduced that the occurrence of these humps is due to the highly turbulent large-scale vortices in the interaction region (Browne et al. 1982). At this location, the centerline turbulent kinetic energy was notably higher, as envisaged by Browne et al. (1982) who found a peak in turbulent kinetic energy at $x/H = 8$ for their smoothly contoured plane jet. Therefore, as the growing vortices move downstream from $x/H \simeq 0$ to $x/H \simeq 10$, the collision of vortices (Schultz-Grunow 1981) from both sides of the symmetric mixing layers is inevitable. This could produce a higher turbulence intensity around $x/H \simeq 10$ for the sharp-edged orifice nozzle. Unfortunately,

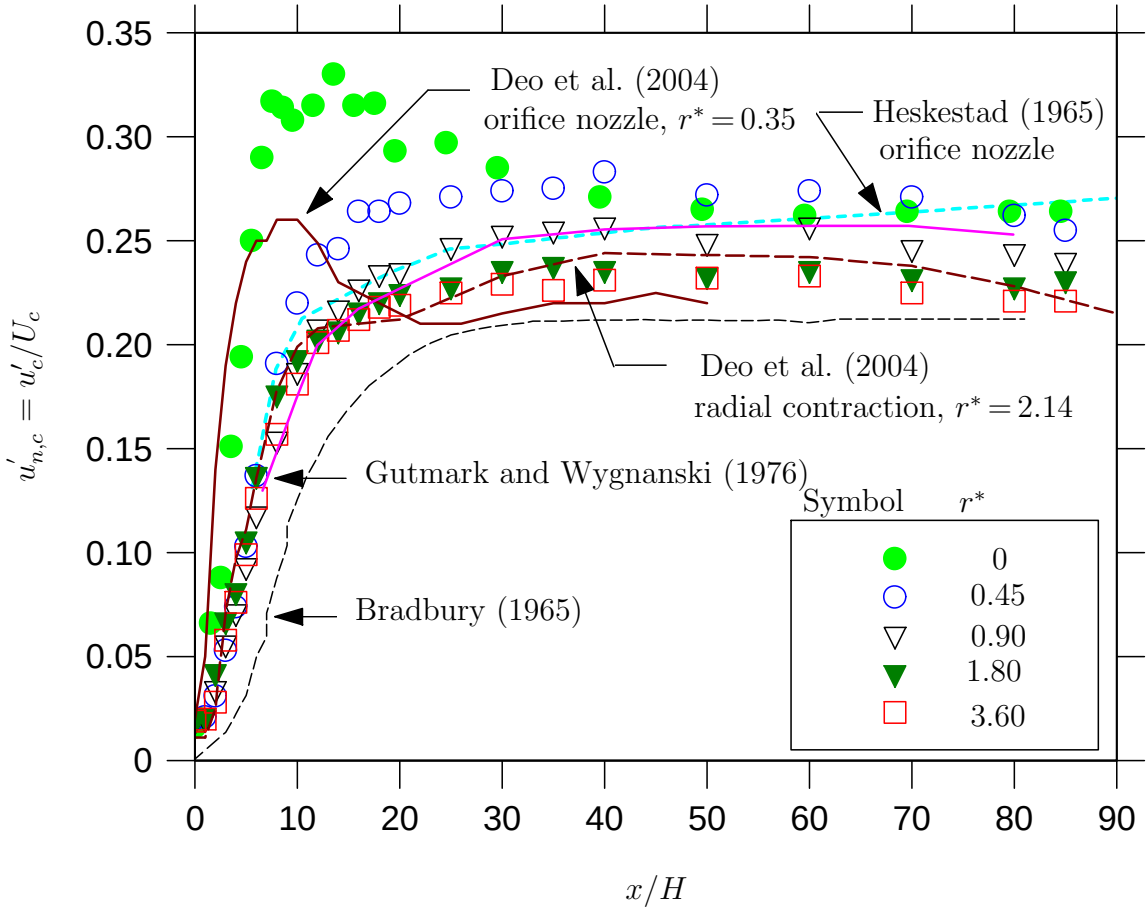

Figure 4.12: Evolutions of the centerline turbulence intensity $u'_{n,c}$ for different nozzle contraction profile factor r^*.

it is not possible to assess whether or not a hump was present in the sharp-edged orifice nozzle studied by Heskestad (1965) at (Re, AR) = (36,900, 120). A careful check of his data shows that his measurements were mostly taken in the far field and very few points in the near field. On the other hand, the present radially contoured nozzles ($r^* > 0.45$) produce a smoother transition of turbulence intensity, with no near field humps. Namar and Ötügen's (1988) smoothly contoured quasi-plane nozzle whose measurements were conducted at (Re, AR) = (7,000, 56) did not show a discernable hump. However, a small hump in their turbulence intensity can be observed at $x/H = 18$, possibly due a low Reynolds number effect. Other investigations of jets issuing from smooth contractions, such as Antonia et al. (1980), Browne et al. (1982), Bradbury (1965) and Gutmark and Wygnanski (1976) conducted at (Re, AR) = (20,000, 44), (7,000, 20), (30,000, 44) and (30,000, 39) respectively, did not observe a hump. The absence of the near field hump for the present radially contoured nozzles (i.e. for $r^* > 0.45$) is, therefore, unambiguously supported by previous investigations.

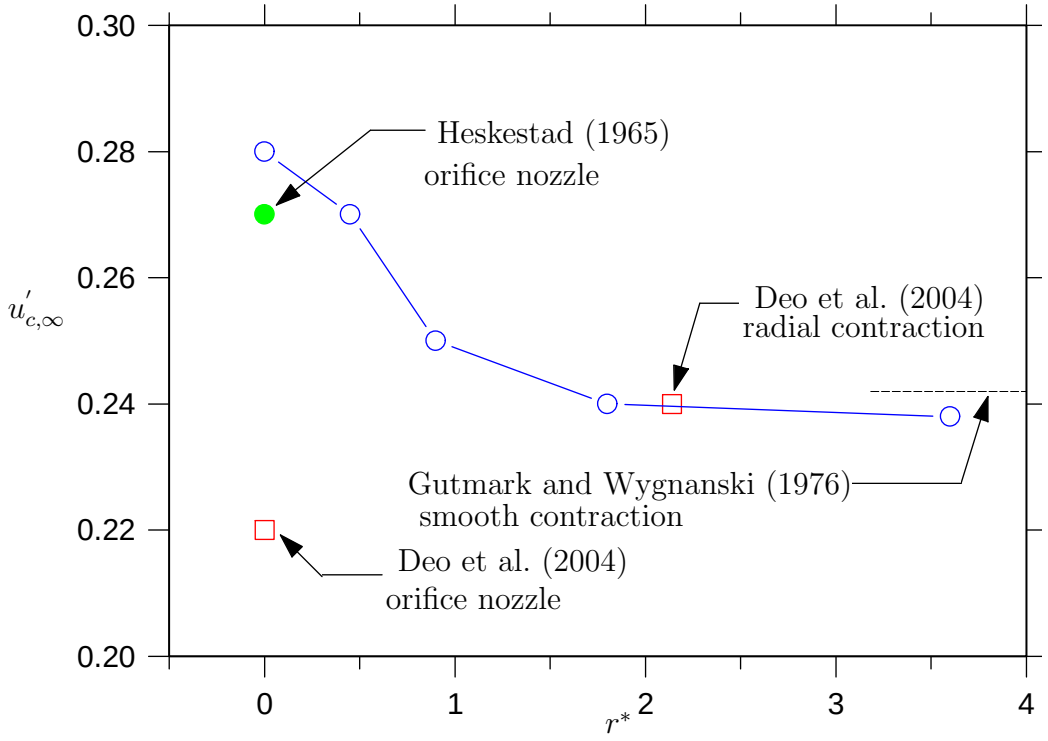

Figure 4.13: Dependence of the far field asymptotic turbulence intensity $u'_{c,\infty}$ on the nozzle contraction profile factor r^*.

The locally normalized turbulence intensity attains self-similarity for $x/H \geq 30$ with each jet reaching its respective asymptotic value of $u'_{c,\infty}$. The magnitude of $u'_{c,\infty}$ is plotted as a function of r^* in Figure 4.13. A consistent trend is evident in the present dependence of $u'_{c,\infty}$ on r^*. As r^* is increased from 0 to 3.60, $u'_{c,\infty}$ decreases from 0.28 to 0.24. This is the opposite trend to the asymptotic value of the centerline scalar intensity ($T'_{c,\infty}$) of a round smooth contraction and a round sharp-edged orifice nozzle (Mi, Nathan and Nobes 2001), where the magnitude of $T'_{c,\infty}$ was smaller for the sharp-edged orifice nozzle than for the smoothly contoured configuration. The most likely reason for this apparent discretion is the geometric difference i.e. planar versus circular, however, this cannot be stated with certainty. Furthermore, the difference in $u'_{c,\infty}$ for $r^* > 1.80$ is quite small.

Also from Figure 4.13, the far field value of $u'_{c,\infty}$ of Gutmark and Wygnanski (1976) conforms 'closely' with $u'_{c,\infty}$ at $r^* = 3.60$. While differences exist between the $u'_{c,\infty}$ of Bradbury (1965) and that of the present ($r^* = 3.60$), these differences are probably due to different experimental conditions. For instance, Bradbury (1965) used a co-flow to jet velocity ratio $\simeq$ 7-16 %. On the other hand, the published asymptotic value of turbulence intensity of a plane jet issuing through a sharp-edged orifice nozzle by Heskestad (1965) compares extremely well with present turbulence intensity from our sharp-edged orifice

nozzle. Slight differences in $u'_{c,\infty}$ are attributable to the differences in initial conditions i.e. differences in Re, AR and nozzle geometry[2]. Further, our previous measurement from a plane jet of aspect ratio 60 at (Re, r^*) = (16,500, 2.14) compares well with present results taken at $r^* = 1.80$. However, present results at $r^* \simeq 0$ differ from our previous measurements at (Re, r^*) = (16,500, 0.35). This is attributable to the differences in nozzle aspect ratio (72 for present versus 10 for our previous measurements). Indeed, the present thesis shows in Chapter 5 that a reduction in nozzle aspect ratio leads to a decrease in $u'_{c,\infty}$. (see Figure 5.20). Thus, the present data is entirely consistent with previous work.

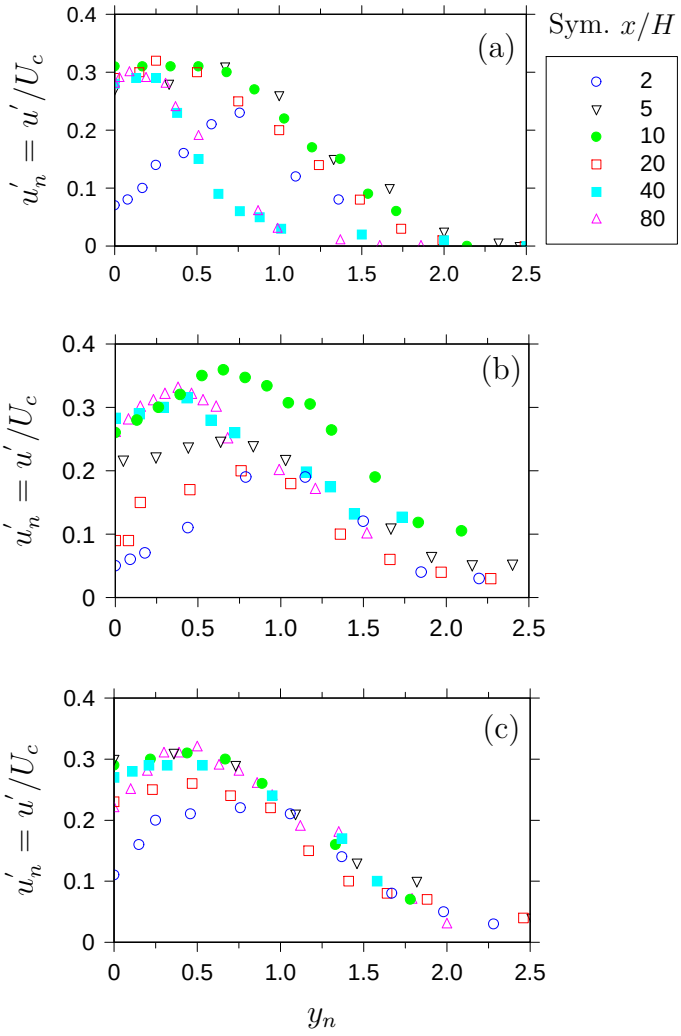

Figure 4.14: Lateral profiles of the turbulence intensity u'_n for (a) $r^* \simeq 0$ (b) $r^* \simeq 0.45$ and (c) $r^* = 3.60$.

Figure 4.14 explores the lateral distributions of the turbulence intensity field for three

[2]Heskestad (1965) used a sharp-edged orifice plane nozzle, but his nozzles' bevelled edge faced upstream rather downstream as in a standard sharp-edged nozzle. Compare Figure 1.10 which shows his plane nozzle and Figure 4.1b for the present sharp-edged plane nozzle.

selected nozzle contraction profiles. The development of the turbulence field for the sharp-edged orifice nozzle is distinctly different from the radially contoured nozzles. It appears that the turbulence intensity profiles become self-similar at $x/H \simeq 40$ and 10 for the sharp-edged orifice ($r^* \simeq 0$) and radially contoured nozzle ($r^* = 3.60$) respectively. Thus, the figures suggest that as r^* is increased, the x-location of the self-similar profiles moves further downstream. It is also clear that for $x/H = 40$ and 80, the turbulence intensity collapses to zero for $y_n \geq 1.50$ for the sharp-edged nozzle but for the radially contoured nozzle, it does not collapse to zero until at least $y_n = 2.50$.

Further insight into the turbulence field can be obtained from the skewness S_u and flatness F_u factors of the fluctuations in u. Figure 4.15 plots the streamwise evolutions of S_u and Figure 4.16 plots the streamwise evolutions of F_u. Both evolve from the nearly Gaussian values (S_u, F_u) = (0,3) at the origin to highly non-Gaussian values at $x/H \simeq 5$ and back to Gaussian again in the self-similar field. The initial departure from Gaussian indicates the transition of the flow from initially laminar to turbulent. Figures 4.15 and 4.16 also show a clear dependence of S_u and F_u on r^*.The insert of the Figures of 4.15 and 4.16 present the maximum values of $\left|S_u^{\min}\right|$, $|F_u^{\max}|$, which occur near to the end of the potential core. While in the near field, $|F_u^{\max}|$ is found to decrease with increasing r^*, $\left|S_u^{\min}\right|$ increases with increased r^*. Further departure from Gaussian values are consistent with increased coherence in the underlying large scale structures. Turbulent flow instabilities can cause velocity distributions to be more skewed, with larger spikes in u. The sharp-edged orifice nozzle causes an upstream flow separation, and has a thinnest shear layer at the nozzle lip. These could be responsible for the higher skewness.

In the far field, S_u and F_u appear to asymptote (see inserts in Figure 4.15 and 4.16), but remain strongly dependent on the nozzle profile. Identical values of S_u^{∞} and F_u^{∞} are evident for $r^* \geq 1.8$. A clear departure of $F_u^{c,\infty}$ from the Gaussian is evident as r^* is increased. This suggests that the flow exhibits more coherent underlying structures and hence that the flow is less random.

4.4 Further Discussion

Statistical analysis of the mean and turbulence properties have revealed that inner-wall nozzle contraction profile factor r^* has a significant influence on the development of the initial and downstream flow. Such a systematic variation of r^* for plane jets has not been performed previously. Indeed, even studies on round jets are less comprehensive.

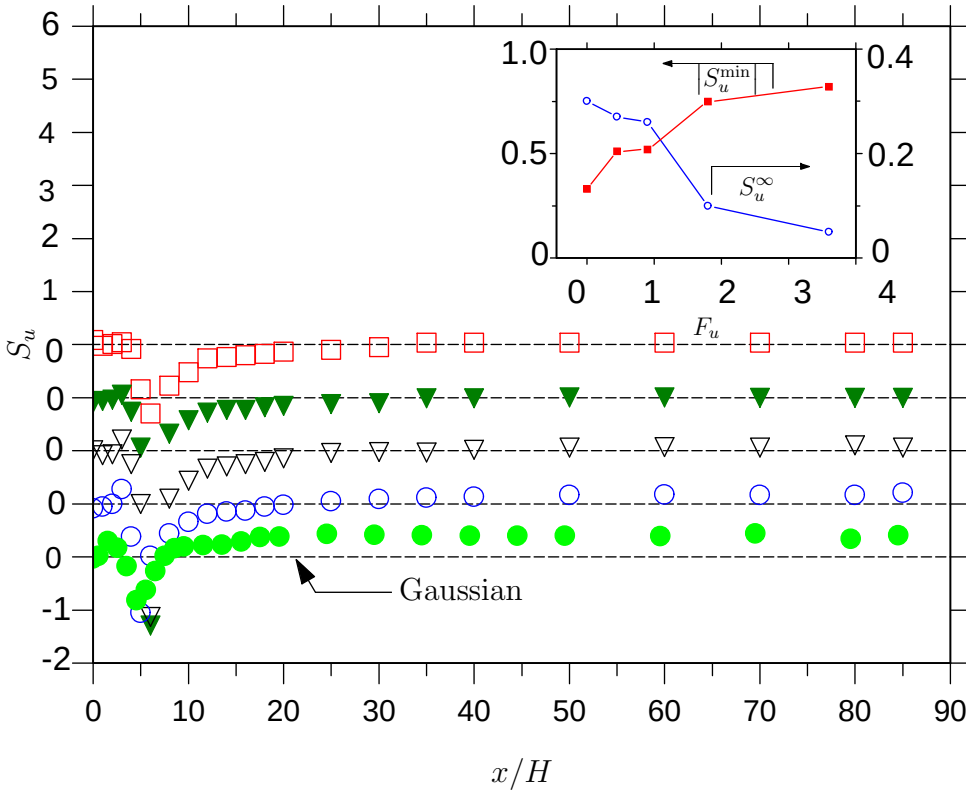

Figure 4.15: The nozzle profile dependence of the centerline skewness S_u factors. Note that profiles have shifted by 1 for clarity. Symbols identical to Figure 4.12.

Importantly, the present measurements have been performed at identical aspect ratio and Reynolds number. Thus, it is truly an independent assessment of the profile factor r^*.

Evidence from the present results has shown that the nozzle profile determines the initial flow (imposed by nozzle boundary conditions), and the influence of this initial flow propagates downstream. The pseudo-boundary layer thickness calculated at $x \simeq 0.25H$ depends upon the nozzle profile too. An increase in the radius of contraction leads to an increase in the thickness of the boundary layer as measured by displacement thickness. The initial turbulence intensity measured at $x/H \simeq 0.25$, decay rates of centerline mean velocity, jet spreading rates and downstream turbulence properties correlate with the boundary layer thickness.

The present findings indicate that the flow through a sharp-edged orifice decays and spreads faster than a radially contoured nozzle. Hence, that the orifice is characterized as having to a higher entrainment rate and probably increased mixing. Such a finding is consistent with the velocity decay, spreading and the subsequent mixing rate of the round sharp-edged orifice and in smoothly contracting nozzle. These are verified by the

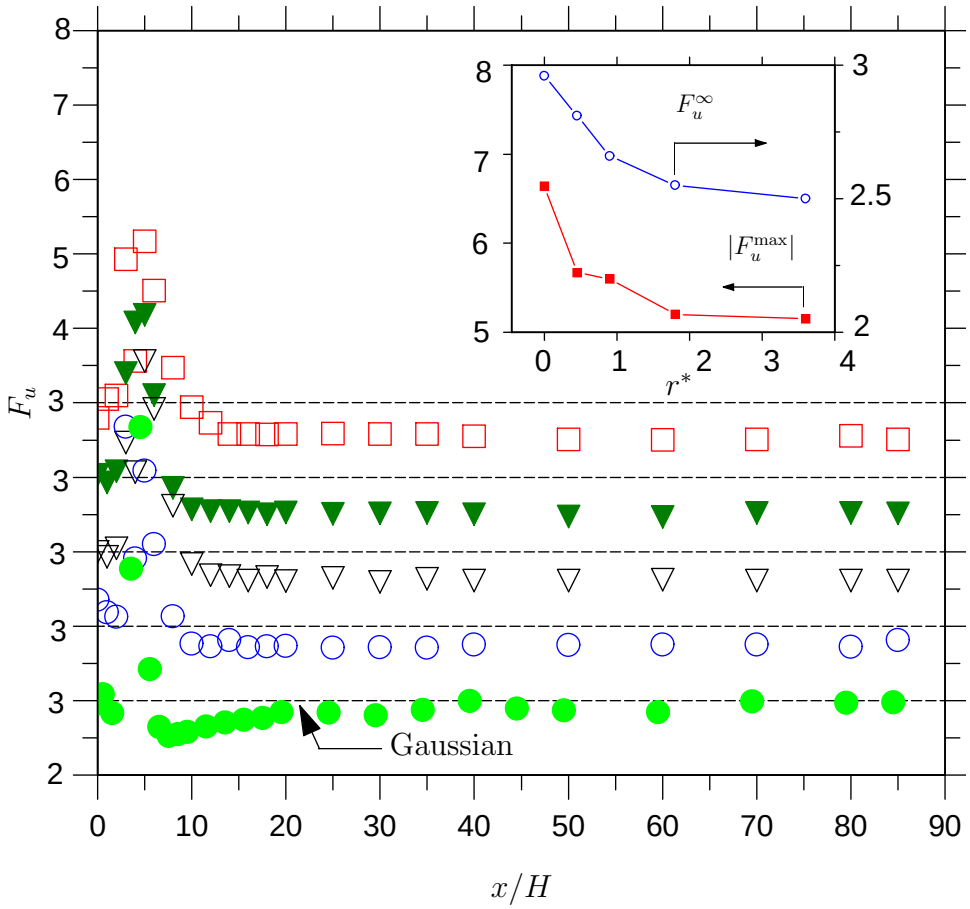

Figure 4.16: The nozzle profile dependence of the centerline flatness, F_u factors. Note that profiles have shifted by 1 for clarity. Symbols identical to Figure 4.12.

planar images of the instantaneous scalar field, Figure 4.17, which is reproduced from Mi, Nathan and Nobes (2001). The figure shows a presence of high concentration unmixed nozzle fluid (white color) up to $x/D = 14$ in the smooth contraction and up to $x/D = 12$ in the sharp-edged orifice nozzle. A larger concentration of the unmixed nozzle fluid at a greater axial distance supports the notion for lower mixing rate for the smooth contraction and a higher mixing rate for the sharp-edged orifice nozzle.

An increased jet spread and the decay of centerline mean velocity measured for the present sharp-edged orifice nozzle is consistent with the presence of an unstable and thinner shear layer at the nozzle exit. That is, a more unstable shear layer is likely to cause increased growth of coherent vortex motions. Further support for this is found in the near field power spectrum of the velocity fluctuations defined by $\int \phi_u(f)df = \overline{u^2}$. Figure 4.19 presents $\phi_u(f)$ measured close to the potential core, at $x/H = 3$. The dimensionless vortex shedding frequency St_H for the dominant peaks in velocity power spectra has been computed.

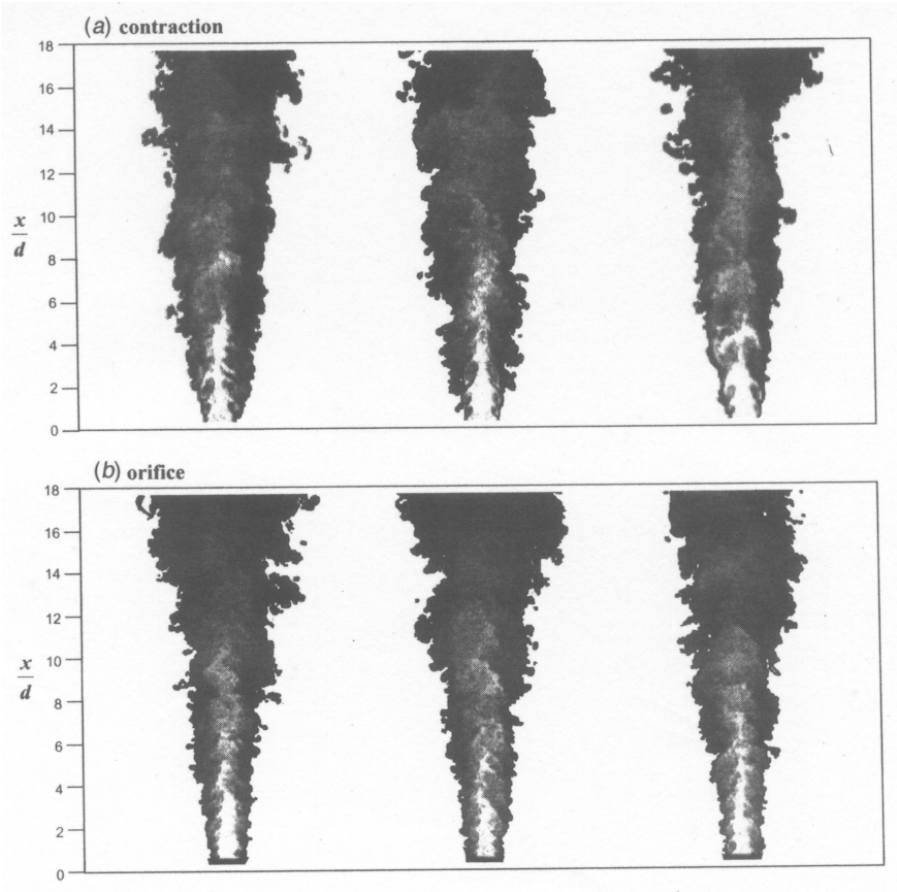

Figure 4.17: Instantaneous planar images of the scalar fields of jets issuing from (a) a (round) smooth contraction and (b) a sharp-edged round nozzle. (Mi, Nobes and Nathan 2001)

Figure 4.20 explores the relationship between the non-dimensional vortex shedding frequency St_H and r^*. Clearly, as r^* is increased, St_H decreases. For example, when $r^* \simeq 0$, $St_H \simeq 0.39$ whereas at $r^* = 3.60$, $St_H \simeq 0.24$. A lower St_H evident for the radially contoured nozzle i.e. $r^* = 3.60$ shows existence of larger structures, relative to those from the sharp-edged orifice nozzle. Hence, it is deduced that the characteristic of the vortex structures are a function of the nozzle contraction profile.

The dominant peak in power spectra characterize the shedding of the emerging large-scale coherent vortices. Such peaks have also been noted for jets from a planar, rectangular and a round nozzle. To make a definitive comparison of vortex shedding between the present and previous investigations, Table 4.2 summarizes the Strouhal numbers obtained from round and planar geometries. The nozzle profile for each configuration, Reynolds numbers and aspect ratios are also listed. Also produced in Figure 4.18 are the schematic

Investigation	**Configuration**	**Profile**	**Re**	**AR**	**St**
Beavers and Wilson (1970)	planar	sharp-edged	500-3,000		0.43
Tsuchiya et al. (1989)	rectangular	sharp-edged	3,500	5	0.40
Sato (1960)[3]	planar	sharp-edged	1,500-8,000	10-67	0.23
Namar and Ötügen (1988)	planar	contoured	1,000-7,000	44	0.27
Beavers and Wilson (1970)	round	sharp-edged	500-3,000	-	0.63
Johansen (1929)	round	sharp-edged	200-1,000	-	0.60
Mi et al. (2001a)	round	sharp-edged	16,000	-	0.70
Ko and Davis (I971)	round	contoured		-	0.20
Crow and Champagne (1971)	round	contoured	10,500-30,900	-	0.30
Mi et al. (2001a)	round	contoured	16,000	-	0.40
present	planar	sharp-edged	18,000	72	0.39
present	planar	contoured	18,000	72	0.24

Table 4.2: The normalized vortex shedding frequency St, for previous round, rectangular and plane jets. Note: Sato (1960)[3]: has a planar nozzle with an upstream channel of length between 300-1100 mm.

views of the sharp-edged orifice nozzles used in the past and the present investigations.

For the present sharp-edged orifice nozzle, a St_H of 0.39 is in excellent agreement with Beavers and Wilson (1970) who measured a St_H of 0.43. Furthermore, Tsuchiya et al. (1989) measured from a sharp-edged rectangular nozzle, a St_H of 0.40. Slight differences between the present St_H and those obtained by Beavers and Wilson (1970) and Tsuchiya et al. (1989) are attributable to the differences in the nozzle aspect ratio, Reynolds number or other experimental conditions which may not be known from their paper. In particular, the present study found that Reynolds number could possibly affect the vortex formation rate, although, its magnitude is not expected to be large (see Figure 3.29). Thus, this may account for some differences between the sharp-edged orifice nozzle of the present and previous investigations. Slight differences between the present St_H and those obtained by Tsuchiya et al. (1989) are perhaps due to near field three-dimensional effects, if any, in their free rectangular jet. The present St_H of 0.24 obtained from a radially contoured nozzle (whose $r^* = 3.60$) compares extremely well with $St_H \simeq 0.27$ obtained by Namar and Ötügen (1988) for their quasi-plane jet. Again, slight differences are subject to differences in experimental conditions. In particular, the absence of sidewalls in Namar's setup could explain such a difference. Overall, the agreement is reasonable, given the differences

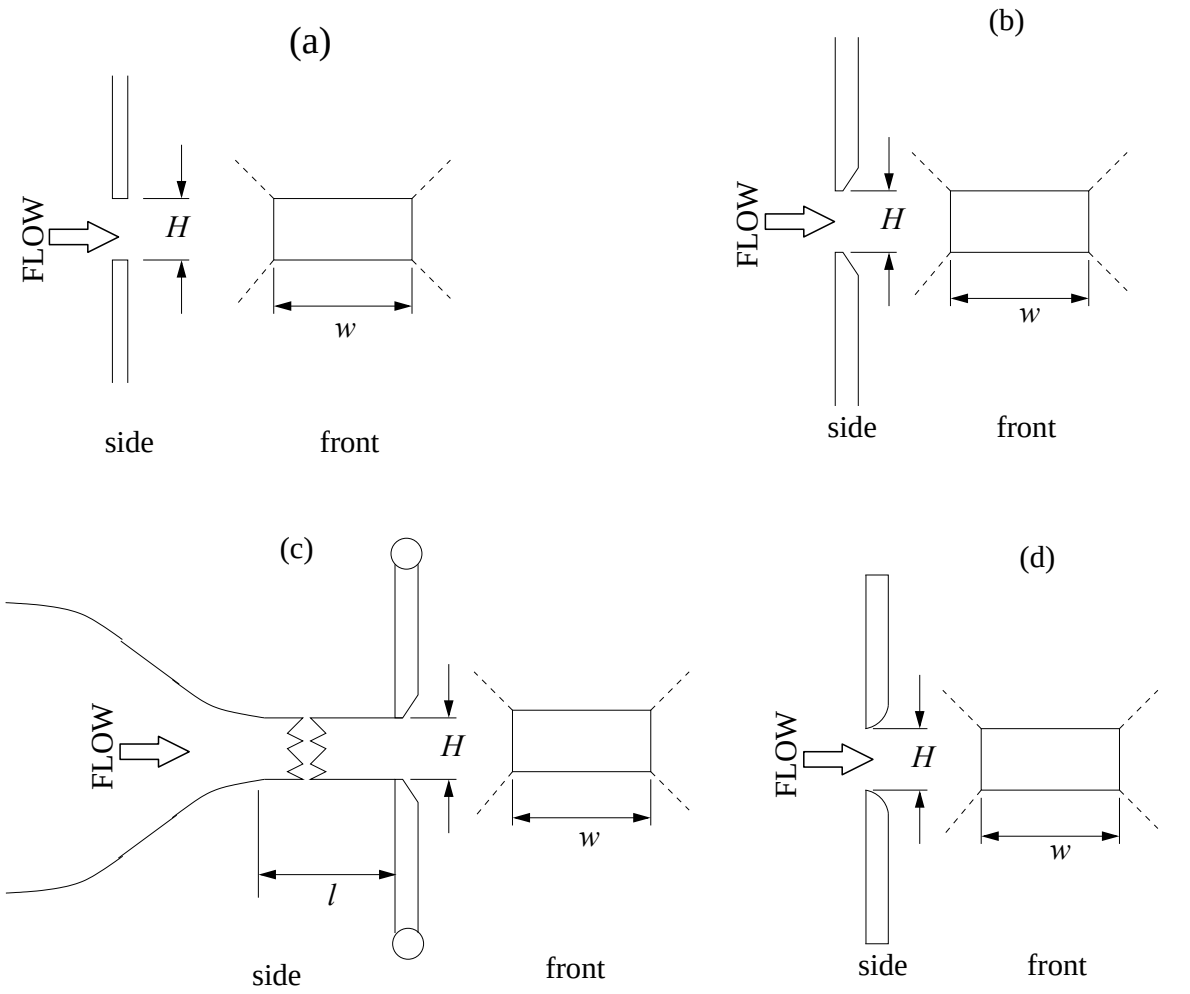

Figure 4.18: Schematic views of the sharp-edged nozzle profiles used by (a) Tsuchiya et al. (1989) for their rectangular nozzle (b) Beavers and Wilson (1970) for their plane nozzle (c) Sato (1960) for their plane nozzle with a channel of length l at the exit (d) present investigation.

in initial conditions.

From Table 4.2, it appears that round nozzles (both a sharp-edged and a smoothly contoured contraction profile) generally display a higher vortex shedding frequency than the plane nozzles. For example, both Mi, Nathan and Nobes (2001), Johansen (1929) and Beavers and Wilson (1970) found St_D of 0.70, 0.60 and 0.63 for their round nozzle with a sharp-edged contraction profile whereas Ko and Davies (1971), Crow and Champagne (1971) and Mi, Nathan and Nobes (2001) achieved a St_D of 0.20, 0.30 and 0.40 for their smoothly contoured round nozzle. Again, the trends in the magnitude of vortex shedding frequencies found for the sharp-edged and the smoothly contoured round nozzles are similar to those found for plane nozzles. That is, higher vortex shedding frequency for the sharp-edged orifice and lower for the smoothly contoured nozzle. In fact, Mi, Nathan

and Nobes (2001), who measured the velocity power spectrum at $x/D = 3$ of a round jet, found that the sharp-edged nozzle produced a broader peak in power spectra than the smoothly contoured nozzle, whose peak was narrow. It is possible that a sharp-edged orifice produces large-scale vortices, which are not as well-defined as those present in the smoothly contoured nozzle. With regard to the differences in vortex shedding between the planar and round configurations (which have identical nozzle profiles), the nozzle geometry e.g. circular or planar may play some role in determining their vortex motions. Nevertheless, both the circular and planar nozzle geometry reveal higher vortex formation frequency for the sharp-edged orifice as opposed to the smaller frequency for the radially contoured nozzles.

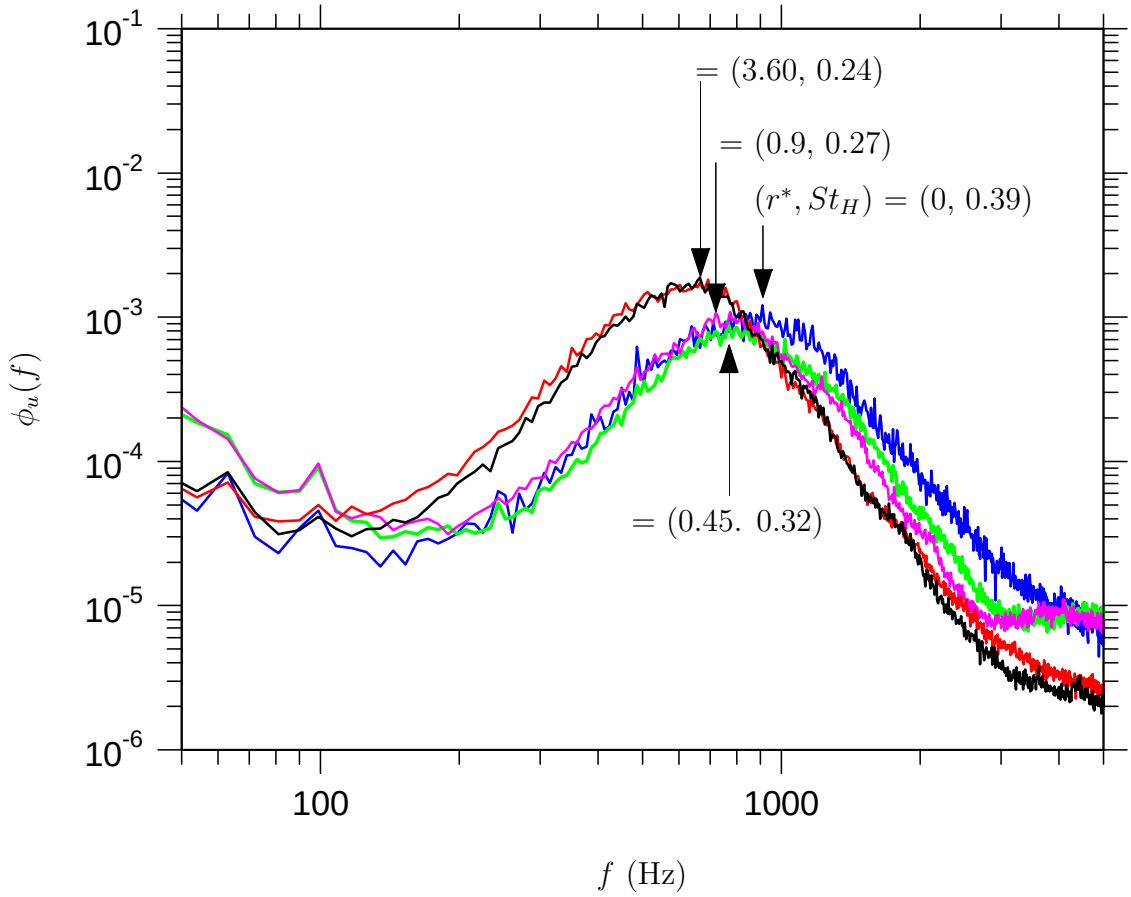

Figure 4.19: Power spectrum ϕ_u of the centerline velocity fluctuations u at $x/H = 3$.

The mechanisms responsible for the vortex formation from the different nozzle profiles in the present plane jet are not clearly understood. As explained for round jets by Mi, Nathan and Nobes (2001), the concentration of vorticity (or circulation) near to the edge of a round jet can lead to a formation of azimuthal vortex rings. Indeed, Beavers and Wilson (1970) contemplated that at sufficiently high Reynolds numbers, the nozzle design,

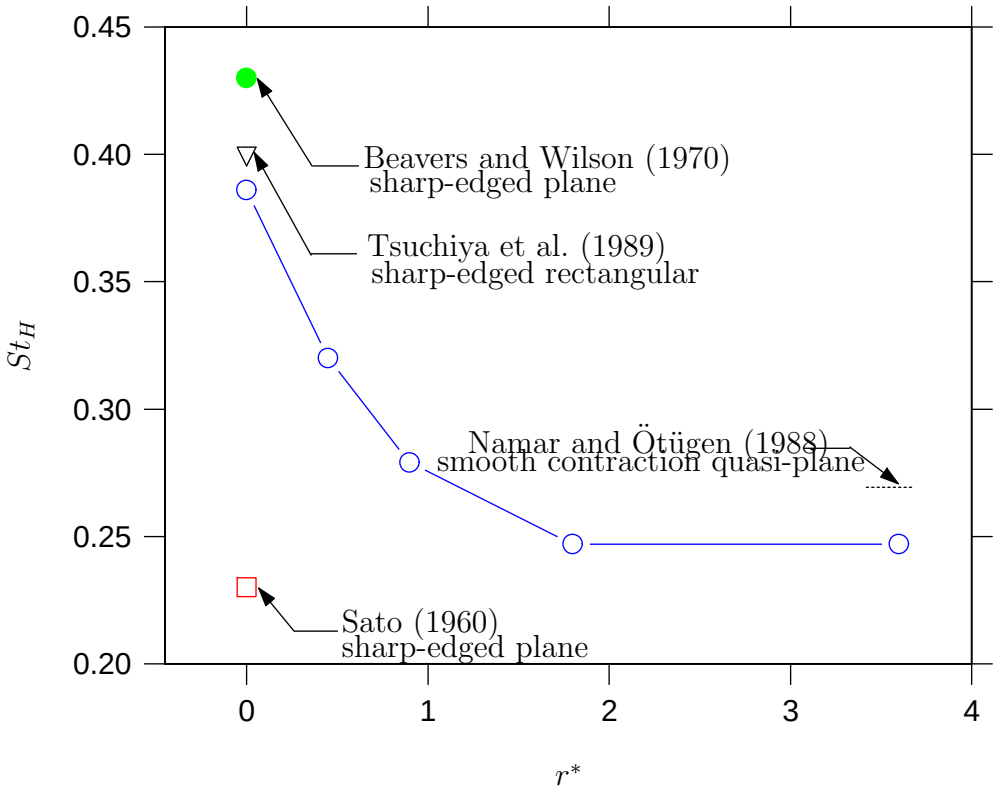

Figure 4.20: The normalized vortex shedding frequency St_H calculated at $x/H = 3$. Included are: the previous data obtained from a profile with a sharp-edged orifice measured by Tsuchiya et al. (1989) for their rectangular nozzle, Beavers and Wilson (1970) for their plane nozzle and Sato (1960) for his plane nozzle with an upstream channel of length l; and Namar and Ötügen (1988) obtained from their smoothly contoured quasi-plane nozzle.

which determines the boundary layer thickness, has a significant influence on the vortex shedding. For the present plane jet, it was found that the initial shear layer thickness depends on the nozzle profile, that is, the sharp-edged orifice nozzle has the thinnest initial shear layer. Just like the round jet, it is possible that a reduced vorticity near to the edges of the plane jet can stimulate the formation of counter-rotating streamwise vortices, typical in a plane jet. Based on this, one concludes that the rate of vortex shedding will be higher in the sharp-edged orifice nozzle (whose initial shear layer is thinner) relative to the radially contoured nozzle (which has a thicker initial shear layer).

It is also well-known that smoothly contoured nozzles are famous for generating coherent vortex structures (Namar and Ötügen 1988). In fact, Grinstein et al. (1995) provided a documentation of the vortex roll-up, merging and pairing mechanisms in smoothly contoured nozzles. Hence, the observed dominant peak in velocity power spectrum (Figure 4.19) for the radially contoured nozzle must be linked to roll-merge-pair process, although the magnitude of the vortex formation frequency largely depends on the nozzle geometry

(i.e. planar, circular etc). Published data of round and plane jets show St over the range from 0.20 to 0.70 (Mi, Nathan and Nobes 2001). Therefore, the present dependence of St_H on the nozzle exit profile is consistent with previous findings, although subtly different, due the different nozzle profiles used in the present study.

Browne et al. (1984) suggested that, although not fully understood, the evolution of $u'_{n,c}$ and the humps in $u'_{n,c}$ depend on the nature of the exit boundary layer. That is, for an initially turbulent boundary layer, a monotonic increase in $u'_{n,c}$ is possible with significant humps. In contrast, for an initially laminar boundary layer, $u'_{n,c}$ may tend to show a distinct hump just before the interaction region (around $x/H < 20$). Verification of their hypothesis is provided using their own, Krothapalli's (1981) and Hill's (1976) plane jet data, all of which showed distinct humps in $u'_{n,c}$ and also had initially laminar boundary layer at their nozzle lip. On the other hand, the $u'_{n,c}$ data of Hill et al. (1976) demonstrated a monotonic increase, without any hump. The latter had an initially turbulent boundary layer at the nozzle lip. However, in contrast to this, it is important to note that the plane jet data of Weir et al. (1981) had an initial laminar boundary layer but they did not produce a hump in $u'_{n,c}$. Antonia, Browne, Chambers and Rajagopalan (1983) demonstrated the existence of symmetric and asymmetric roll-up structures in the shear layers of a plane jet. Thus, $u'_{n,c}$ is expected to depend on the symmetry or asymmetry of such structure. In particular, Antonia, Browne, Chambers and Rajagopalan (1983) explain that, while the exact cause of such different structures are unknown, the occurrences and subsequent interactions of the asymmetric structures on both sides of the jet shear layers will not cause a significant redistribution of turbulence quantities, while they do when the structures are symmetric. Importantly, the flow visualization by Hussian (1983) for a plane jet with an initially laminar boundary layer, but of two different nozzle configurations exhibited both asymmetric and symmetric roll-up structures within its shear layer. Coherent structures from nozzle configurations similar to Hussian (1983) were studied by Chambers et al. (1985). Using schlieren photography and spectral coherence measurements, they showed the existence of organized, coherent and symmetric structures for their smoothly contoured plane nozzle. When they measured the flow from a smoothly contoured plane nozzle but attached to a long duct (of length $\sim 40\,H$), Chambers et al. (1985) found three-dimensional and asymmetric structures. Even the interaction between the structures in the latter nozzle was weak (reflected by a reduced hump in $u'_{n,c}$). Clearly, our results and sufficient evidence from previous investigations indicate that the type of large-scale motions in a plane jet are clearly a function of the nozzle configuration. Hence, whether or not a hump in $u'_{n,c}$ is present in the plane jet

depends largely on the nozzle type, and thus on nozzle boundary conditions.

The pronounced hump in the present $u'_{n,c}$ for the sharp-edged orifice nozzle indicates more organized and coherent and/or of more unsteady vortices. Further, since the sharp-edged orifice nozzle produces a higher vortex shedding frequency than the radially contoured nozzle, it may actively facilitates more effective large-scale engulfment of the ambient fluid. This could result in higher relative streamwise turbulence intensity and more pronounced hump in $u'_{n,c}$.

The observation of a larger magnitude of $u'_{c,\infty}$ for the sharp-edged orifice nozzle and a lower magnitude for the radially contoured nozzle is owed an explanation. This can be provided in part by studying the dissipation (ϵ) of the turbulent kinetic energy (q). A calculation of ϵ at $x/H = 80$ for both the orifice ($r^* \simeq 0$) and radially contoured nozzle ($r^* \simeq 3.60$) yields $\varepsilon H/U^3_{o,c} \simeq 0.85 \times 10^{-3}$ and 1.77×10^{-3} respectively. (The approach used to calculate ϵ is described in Mi et al. (2005a)). As evident from the relative magnitudes of $\varepsilon H/U^3_{o,c}$, the orifice dissipates less turbulent kinetic energy than the contoured nozzle. Consequently, it must sustain a greater amount of the total kinetic energy q. Correspondingly, $q_\infty/U^2_{o,c}$ and hence $u'_{c,\infty}$ is expected to be larger in magnitude for the orifice nozzle. The reason for reduced dissipation of q for the orifice is probably related to the nature of underlying large-scale structures that evolve differently from that of the radially contoured nozzle, as the jet propagates downstream. This study is beyond the scope of the present thesis.

It is also important to elaborate on the distinctions between the entrainment characteristics of the present radially contoured plane nozzle and the smooth contraction plane nozzles used in previous investigations. The front plate of the present radially contoured plane nozzle imposes lateral direction of the inflow of entrained ambient fluid while conventional smooth contraction nozzles do not (see Figure 4.21 redrawn from Papadakis and Staiano (1993)). That is, the present radially contoured nozzles do not permit fluid entrainment from upstream of the nozzle exit. It is well known that introducing a jet through a plate causes a decrease in the spreading angle due to this effect. For instance, Abdel-Rahman et al. (1997) investigated the use of a front plate at the exit plane of an axisymmetric round nozzle. Their LDA measurements showed that a reduction in the velocity spreading rate and reduced kinematic mass flux occurred for the case with front plates (for a schematic view of their nozzle configurations, see Figure 1.16). This was attributed to the plate, causing reduced interaction with the ambient fluid. Likewise,

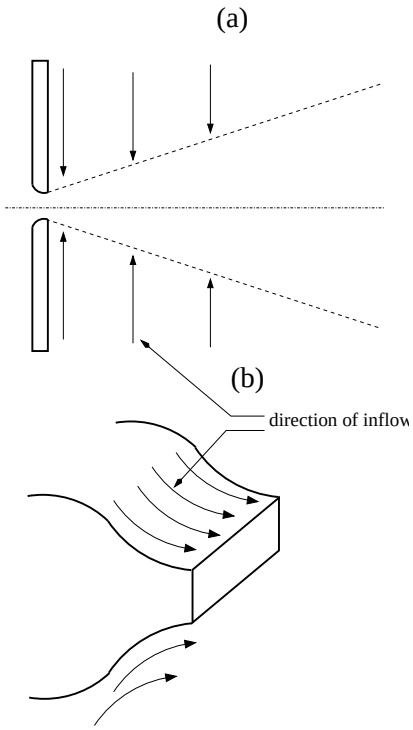

Figure 4.21: Entrainment by (a) a radially contoured nozzle (with front plate) and (b) a smoothly contoured nozzle (without front plate).

Papadakis and Staiano (1993) measured two plane nozzles, one with a front plate at exit plane and the other without front plate. Their nozzles have been reproduced in Figure 4.22. Surprisingly, Papadakis and Staiano (1993) observed that there were insignificant differences between the flow from their two nozzle configurations. In particular, they noted that the centerline decay of mean velocity and jet spreading rates to be almost identical, a finding that conflicts the results of Abdel-Rahman et al. (1997) for their axisymmetric round jet. However, in principle, we do not expect to obtain an identical flow from the two nozzle configurations which are significantly different, in terms of imposing a different direction of the entrained flow. In fact, Kotsovinos (1978) showed that the conservation of momentum for a plane jet out of a wall does not hold true because of the induced flow towards the jet that has a direction lateral to the main flow. Thus, the generation of axial pressure fields in the ambient fluid tends to reduce the momentum flux from the input value. However, as tested and shown in Chapter 3.3.2, at least 97 % of the initial axial momentum is conserved for all present experiment. Thus, momentum loss is not a major concern for the present investigation.

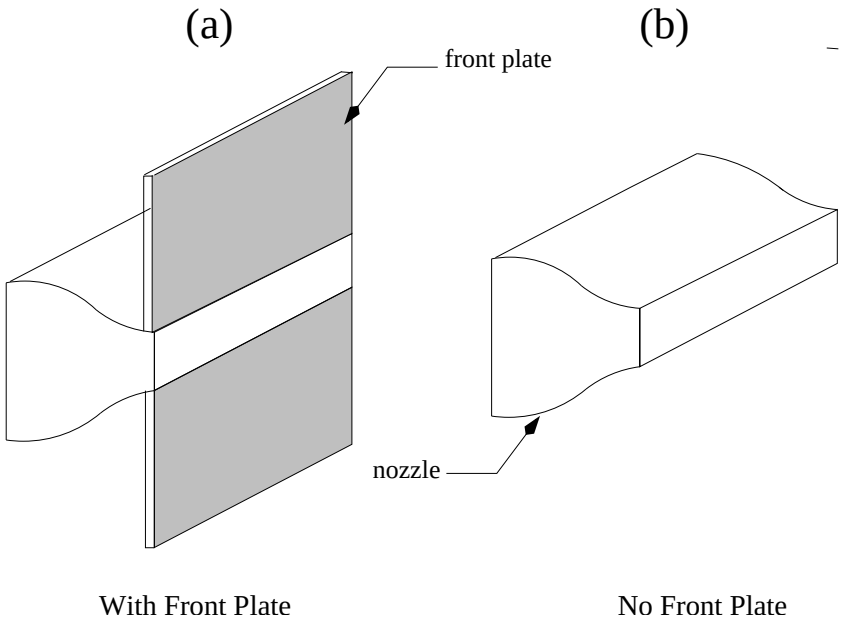

Figure 4.22: A plane nozzle (a) with front plate at the exit plane and (b) without front plate. Re-drawn after Papadakis and Staiano (1993).

4.5 Conclusions

A systematic variation of the inner-wall nozzle contraction profile over the range $0 \leq r^* \leq 3.60$ has provided insight into the statistical variations of plane jets up to 85 nozzle widths downstream. Resulting from this study, significantly new findings have emerged. These are summarized below.

(1) The initial mean velocity profiles measured at $x/H \simeq 0.25$ depend systematically upon r^*. For $r^* \simeq 0$, the mean velocity profile is saddle-backed, agreeing with previous measurements of jet from sharp-edged orifice nozzles. As r^* is increased, the profile converges towards a top hat. For $r^* = 1.80$ and 3.60, the profiles become almost indistinguishable.

(2) For $r^* \geq 1.80$, the initial mean velocity profiles approximate to a top hat.

(3) The boundary layer thickness of the nozzle measured at $x \simeq 0.25H$ increases as r^* is increased.

(4) The initial turbulence intensity is the highest in the shear-layer of the sharp-edged orifice nozzle. That is, $u_n^{'} \simeq 20\,\%$ for the orifice and $4\,\%$ for the radially contoured nozzle, $r^* = 3.60$. Increased turbulence intensity for the sharp-edged orifice nozzles' shear layer is often associated with increased near field growth of the jet although

not necessarily, since a pipe has the highest initial turbulence intensity but lowest growth rate (Mi, Nathan and Nobes 2001).

(5) Vena contracta are found for plane nozzles whose $0 \leq r^* \leq 0.90$ suggesting that they produce significant upstream separation. The centerline values of $U_{m,c}/U_{o,b}$ indicate that the $r^* \simeq 0$ (orifice) jet produces the most pronounced vena contracta with the maximum downstream centerline velocity 30 % higher than its nominal exit value.

(6) In the far field, both the decay rate (K_u) and spreading rate (K_y) of centerline mean velocity for the orifice-jet are higher than the radially contoured nozzle. The normalized mean centerline velocity collapses onto a single curve for $r^* \geq 1.80$.

(7) The locally normalized streamwise turbulence intensity in the near field depends on r^*. Between $0 \leq x/H \leq 10$ higher turbulence intensity are found for the sharp-edged orifice nozzle than the radiused nozzles.

(8) The orifice-jet shows a hump in the near field turbulence intensity in the interaction region (around $x/H \simeq 10$) just after the potential core, possibly caused by the collisions of the counter-rotating streamwise vortex motions (Browne et al. 1982, Schultz-Grunow 1981), typically expected from a planar jet. Such a hump is not present for the radially contoured nozzle.

(9) The far field asymptotic values of turbulence intensity depends on r^* too. Its magnitude for the sharp-edged orifice nozzle ($r^* \simeq 0$) is $u'_{c,\infty} \simeq 0.28$ while for the radially contoured nozzle ($r^* = 3.60$) is $u'_{c,\infty} \simeq 0.24$.

(10) The orifice-jet also has a vortex shedding frequency $St_H \simeq 0.39$. In contrast, the radially contoured nozzle ($r^* = 3.60$) sheds vortices at a frequency of $St_H \simeq 0.24$. This suggests that the vortical structures for an orifice plate are different and probably smaller.

(11) In the near field ($x/H < 20$), the skewness and flatness factors vary dramatically depending on r^*. A maximum in S_u around at $x/H \simeq 3$ is noted for all nozzle configurations. However, its magnitude is larger for the sharp-edged orifice ($r^* \simeq 0$) relative to the radial contraction ($r^* = 3.60$).

(12) The occurrence of a minima in S_u around $x/H \simeq 5$ is also dependent on r^*. The magnitude of the minima is larger for $r^* = 3.60$. This could possibly be associated with a lateral oscillation of its potential core, which was found to be larger.

The mean and turbulence field show a systematic dependence on r^*, providing evidence that the present measurements are reliable. The dramatic change in the entire field are probably due to the development and subsequent downstream propagation of large-scale structures and their interaction with the ambient fluid. Distinct trends in S_u and F_u are evident for the sharp-edged orifice, indicating that its velocity field is more complex than that from a radially contoured nozzle.

Chapter 5

EFFECT OF NOZZLE ASPECT RATIO

5.1 Introduction

Nozzle aspect ratio is a dominant boundary condition of a turbulent plane jet (see Section 1.5.3). The effect of nozzle aspect ratio on rectangular jet nozzles (without sidewalls) has been well documented for instance by Sforza et al. (1966), Trendscoste and Sforza (1967), Sfeir (1979), Marsters and Fotheringham (1980) and Quinn (1992a). These investigations demonstrate a rectangular jet has a limited axial region in which a quasi-planar flow occurs. In particular, a smoothly contoured rectangular nozzle is characterized by a uniform velocity potential core region, a quasi-planar zone and then an axisymmetric three-dimensional zone. Importantly, these experimental work have shown that not only the initial flow, but also the downstream flow, is affected by a change in nozzle aspect ratio. Quite recently, we have characterized the flow-field of high-aspect-ratio rectangular nozzles over the range $15 \leq AR \leq 120$ (Mi et al. 2005b). Even in the quasi-planar zone, our analysis indicated that the mean and turbulence field differs significantly. This provides an indirect indication that the flow field of a two-dimensional (or plane) jet may show some variation in its mean and turbulence properties when the nozzle aspect ratio is varied.

For truly plane jets, the only investigation which is directly relevant to the aspect ratio dependencies are Bashir and Uberoi (1975) and Van Der Hegge Zijnen (1958). These studies are concise, not comprehensive and the data presented are quite limited. Nevertheless, they measured the centerline decay of mean velocity of a slightly heated plane jet issuing from a nozzle of aspect ratios AR = (20, 40 and 144) and (20 and 25) respectively. Even though the former indicated some dependence of the velocity field on the AR, their centerline measurements lack data points in the near field i.e. $x/H < 10$. Hence, no information about the near field flow structure can be determined. The latter measured

AR-dependence over a relatively small range i.e. $AR = 20$ to 25 so provided only limited information on the effect of nozzle aspect ratio.

No previous study has explored the relationship between nozzle aspect ratio and the corresponding 'critical' jet aspect ratio at which a plane jet ceases to be planar[1]. For instance, the critical jet aspect ratio (calculated at an axial distance at which the flow ceases to be planar) of a plane jet will obviously vary with its nozzle aspect ratio. While there can be a number of definitions of the critical jet aspect ratio, we define it here $AR_{jet,crit}$ as

$$AR_{jet,crit} = \frac{y_{0.5,crit}}{w} \tag{5.1}$$

where $AR_{jet,crit}$ is the critical jet aspect ratio at a location $x_{p,\,\max}$ where the flow ceases to be planar, $y_{0.5,crit}$ is the lateral velocity half-width at $x_{p,\,\max}$ and w is the spanwise length of the plane nozzle. Such information will provide data for future designs of plane nozzles which require an optimization of the critical jet aspect ratio for any given plane nozzle.

Thus, in light of the previous published work on AR-dependence of a plane jet, the present investigation is carried out not only to extend the work of Bashir and Uberoi (1975) and Van Der Hegge Zijnen (1958) but also to provide more detailed insight into the influence of nozzle aspect ratio on a plane jet. We have conducted the present research using one of the radially contoured plane nozzles that was used in the experiments for Chapter 4. The next sections state the experimental details, results, discussions and conclusions.

5.2 Experiment Details

To investigate the effect of nozzle aspect ratio, a nozzle contraction was chosen with $r = 36$ mm and $H = 10$ mm. This $r^* = r/H = 3.60$ is sufficiently large to ensure a top hat initial velocity profile, see Chapter 4.3.1. The nozzle plates were fixed to the wind tunnel exit and the spanwise dimension of the rectangular nozzle w was varied systematically between 150 mm and 720 mm by moving the sidewalls. This arrangement produces nozzle aspect ratios of between 15 and 72. Figure 5.1 shows a schematic view for $AR = 15$ and 72. To minimize secondary circulations (or room drafts) in the laboratory, the openings at the ends of the nozzle for $AR < 72$ were blocked so that the plane jet was enclosed within the sidewalls. However, blocking the ends may produce an additional influence, but this influence was found to be small compared to the effect of nozzle aspect ratio

[1] A plane jet with cease to be planar at a certain axial distance downstream, which depends on nozzle aspect ratio

itself.

For each aspect ratio, the initial velocity profile close to the nozzle exit ($x = 0.25H$) was measured to assess the influence of aspect ratio on the initial flow field. The axial (x) distribution of the streamwise centerline velocity was measured from $x/H = 0$ to $x/H = 85$. The lateral (y) distribution of the streamwise velocity was also measured.

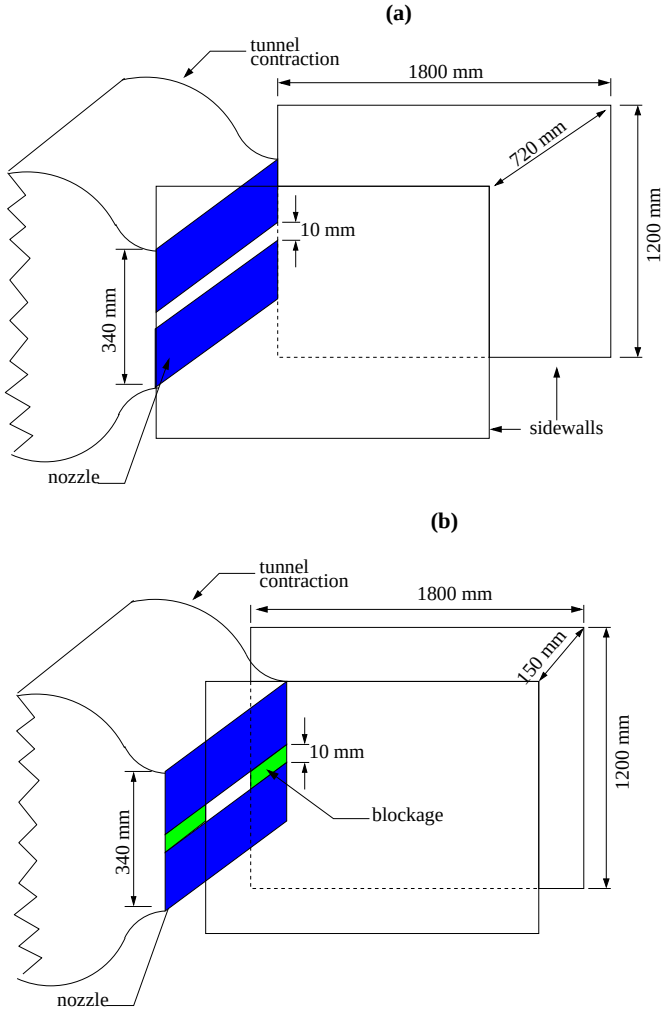

Figure 5.1: A schematic view of the experimental setup for (a) $AR = 72$ and (b) $AR = 15$.

5.3 Results and Discussion

5.3.1 The Initial Velocity Field

Figure 5.2a and b displays the normalized mean velocity and turbulence intensity profiles respectively at $x/H = 0.25$ for the different nozzle aspect ratios. The central sections of the mean velocity profiles are top hat. The extent of the uniform velocity region is, however, dependent on nozzle aspect ratio. For $AR = 15$ and 20, the profile is top hat over

the range $\zeta < 0.40$ while for $AR \geq 30$, this region extends up to $\zeta < 0.45$. Interestingly, the largest nozzle aspect ratios exhibit the steepest top hat and have the lowest shear layer turbulence intensity while the lowest aspect ratios have slightly rounder top hat and higher shear layer turbulence intensities.

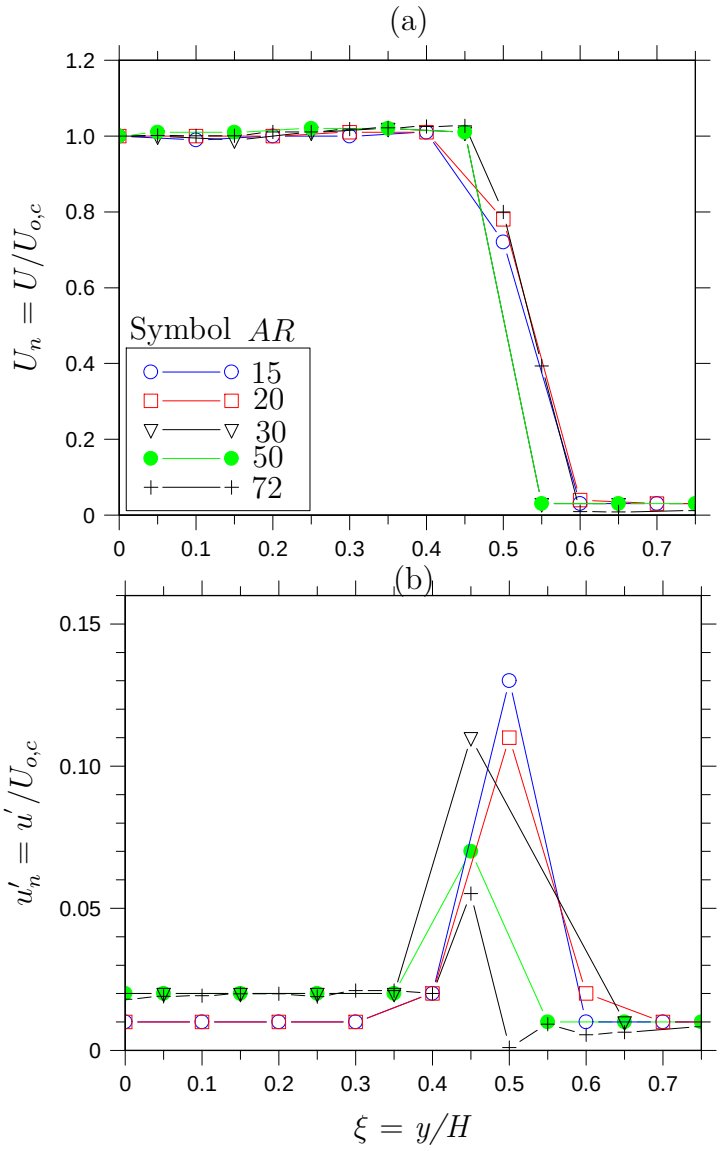

Figure 5.2: Lateral profiles of (a) normalized mean velocity U_n and (b) the turbulence intensity $u_n^{'}$ at $x/H = 0.25$ for different nozzle aspect ratios AR.

Using equations 3.1 and 3.2, the displacement thickness δ^*, the momentum thickness θ and the shape factor $H = \delta^*/\theta$ are calculated to determine the nature of the boundary layer for the different nozzle aspect ratios. Table 5.1 shows that, the shape factor H which determines whether the exit flow is laminar or turbulent, takes an average value of 2.4

AR	**Displacement Thickness**, δ^*	**Momentum Thickness**, θ	**Shape Factor**, H
15	1.89	0.802	2.35
20	1.78	0.725	2.45
30	1.55	0.642	2.42
50	1.49	0.610	2.45
72	1.06	1.431	2.46

Table 5.1: Summary of the pseudo-boundary-layer characteristics (mm) of the plane jet for different nozzle aspect ratios.

for all nozzle aspect ratios. Thus we conclude that the present nozzles have a laminar boundary layer.

In the central section, the turbulence intensity is about 1 % for $AR = 15$ and 20 while for $AR \geq 30$, the central turbulence intensity are about 2 %. Further, as the nozzle aspect ratio is varied between $15 \leq AR \leq 72$, the shear layer turbulence intensity decreases from 13 % for $AR = 15$ to 5 % for $AR = 72$. Almost identical magnitudes of turbulence intensity are notable for $AR = 50$ and 72. Note that the absolute magnitudes of the shear layer turbulence intensity are not reliable because of poor grid resolution. However, their relative magnitudes provide a consistent trend. A reduced turbulence intensity in the shear layer at larger nozzle aspect ratio is suggestive of decreased instability in the nozzle boundary layer. It is evident that by moving the sidewalls to vary the aspect ratio, we produce an influence on the lateral profiles of the initial mean velocity and turbulence intensity. For the present study, there is sufficient evidence that, the sidewalls exert a significant influence on the initial transverse mean velocity and turbulence intensity.

Further evidence of the influence of nozzle aspect ratio on the initial velocity profiles is provided by Figure 5.3. The figure presents the pseudo-boundary layer thickness δ estimated using Equation 4.2. As AR is increased from 15 to 72, δ decreases from $\simeq 1.9$ mm to 1.0 mm. It is worth noting that there are significant uncertainties in the present magnitudes of δ, given the relatively coarse measurement grid. Nevertheless, the consistent trend which emerges gives confidence in the trend, if not the absolute numbers. It is also consistent with the initial mean velocity profiles, (Figure 5.2), although the profiles are not particularly well-resolved. A decrease in the pseudo-boundary layer thickness with an increase in nozzle aspect ratio possibly provides an explanation for the observed difference in the shear layer turbulence intensity and shape of the mean velocity profile.

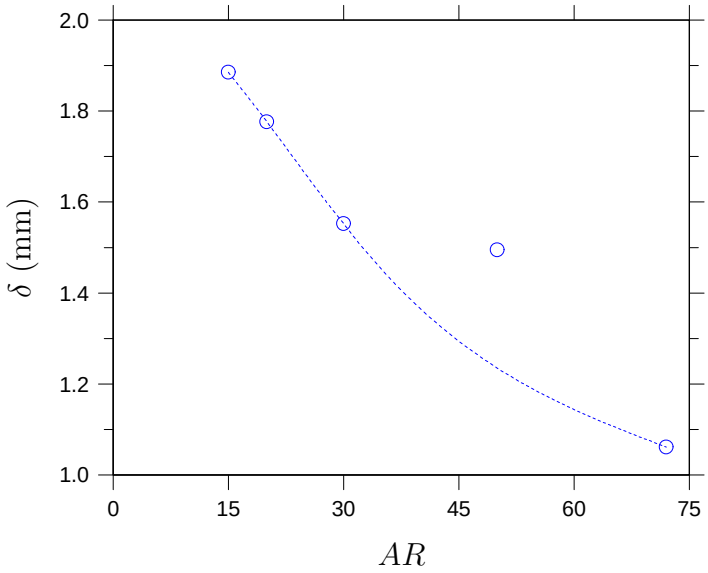

Figure 5.3: Pseudo-boundary layer thickness δ at $x = 0.25H$ computed from the initial velocity profiles. The best fit polynomial curve is also shown.

It is possible that the sidewall exert a drag due to a boundary layer. As the walls get closer, the magnitude of the drag increases relative to the jet momentum. Thus, higher shear layer turbulence intensities become evident. This phenomenon occurs for the low aspect ratio jet, which probably encounters the largest drag. For higher aspect ratios e.g. $AR = 72$, the walls are further apart. Thus, the influence of the drag on the initial mean velocity and turbulence intensity is lower. In summary, a change in nozzle aspect ratio causes a change in the relative influence of the wall boundary layer.

5.3.2 The Mean Velocity Field

Figure 5.4 presents the near field velocity measurements on the jet centerline. The approximate size of the jet potential core x_p, where the mean velocity U_c is constant and equal to $U_{o,c}$, is a function of AR. As AR is increased from 15 to 72, x_p increases from $x_p \simeq 2H$ to $x_p \simeq 5H$. The length of the potential core is one measure of the near field entrainment rate of the jet i.e. a smaller x_p implies a higher near field entrainment rate. Hence, it appears that the initial entrainment rate decreases with an increase in AR. This is confirmed by Figure 5.5 which plots the lateral profiles of normalized mean velocity at $x/H = 3$. This location is a region within the jet potential core. A relatively larger jet spreading rate is evident for $AR = 15$ than for $AR = 72$. Therefore, as aspect ratio is increased, both the near field spreading and the entrainment decreases.

Figure 5.6 shows the normalized mean velocity decay for $x/H \leq 45$. It is notable that

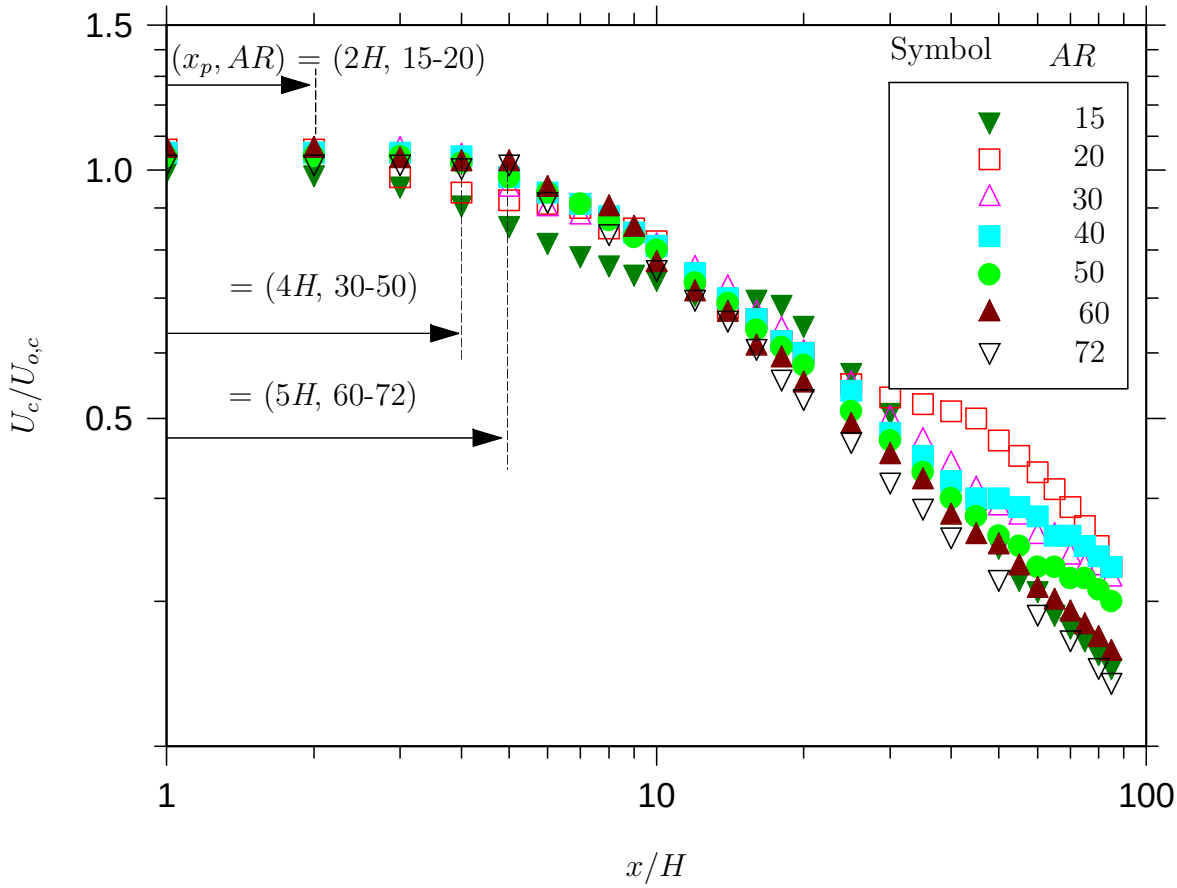

Figure 5.4: The near field centerline velocity variation $U_c/U_{o,c}$, for different nozzle aspect ratios AR and the corresponding potential core lengths, x_p.

the axial decay of centerline mean velocity is a linear relation from $x/H \geq 20$ for most aspect ratios. The linear function is represented by

$$\left(\frac{U_{o,c}}{U_c}\right)^2 = K_u \left[\frac{x}{H} + \frac{x_{01}}{H}\right] \tag{5.2}$$

where K_u is a measure of the decay rate of the centerline mean velocity and x_{01} is the virtual origin.

Figure 5.7 plots K_u against AR. For reference, literature data of various other investigators are included. For the present data, a clear trend is evident. As AR is increased from 15 to 72, K_u increases approximately linearly from 0.113 to 0.180, with a small difference in the K_u values still evident for $AR = 50$ and 72. This suggests that the flow is not independent of aspect ratio even at $AR = 72$. Bashir and Uberoi (1975) and Everitt and Robbins (1973) obtained similar trends in the decay of their mean velocity. (Figure 5.7). The results of other previous investigations also support the present trends in K_u. However, the present magnitudes of K_u are not very close to those obtained in previous

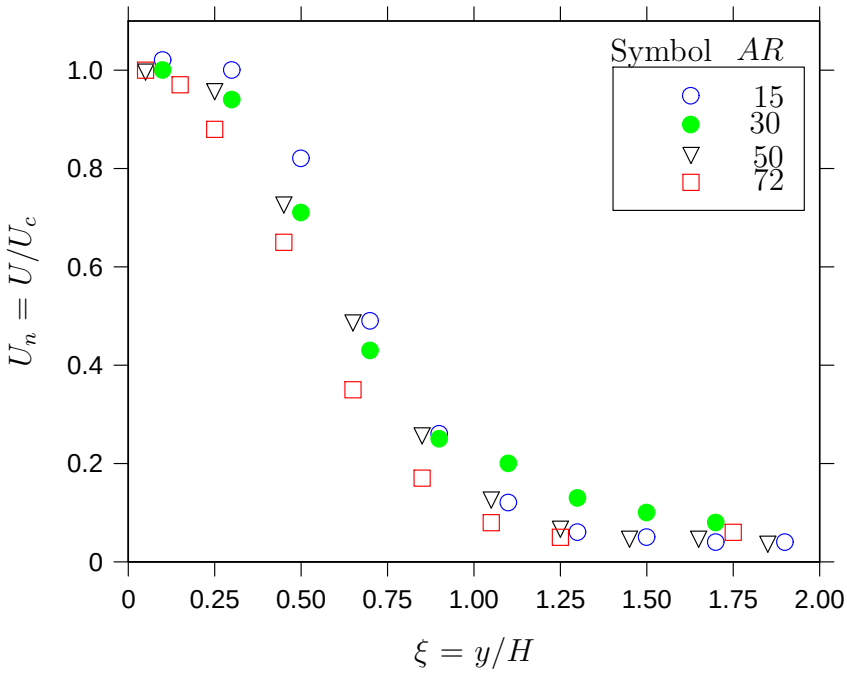

Figure 5.5: Lateral profiles of U/U_c at $x/H = 3$.

investigations. For instance, the K_u of Hitchman et al. (1990) and ours at similar nozzle aspect ratios are different. This is surely due to the combined effect of different Reynolds number (7,000 theirs versus 18,000 ours), different nozzle profile (conventional smooth contraction versus radial contraction ours) and differences in initial conditions not clearly specified. As argued in Chapter 1.5.3, even a slight difference in initial conditions can produce a significantly different flow. Thus, any comparison of the present results needs to be made with caution.

Figure 5.8 shows the decay of mean centerline velocity for the full measured range. The smaller nozzle aspect ratio jets, $AR = 15$ and 20 display entirely different behaviour to the larger aspect ratio jets. That is, the centerline velocity decay for these aspect ratios diverge from the inverse square law more significantly, and at and smaller downstream distance, than the others. A probable reason for this is due to the earlier influence of sidewalls on these low aspect ratio nozzles. It appears that for these low aspect ratios, statistically two-dimensional flow occurs over a very limited axial distance. In fact, for $AR = 15$, the self-similar two-dimensional region (i.e. $U_c \sim x^{-1/2}$) is present only up to $x/H = 10$ (see Figure 5.6). Indeed in our recent measurements presented in Mi et al. (2005b) on rectangular jets over the nozzle aspect ratio range $15 \leq AR \leq 120$, we found that $AR = 15$ jet has a quasi-two-dimensional region between $6 \leq x/H \leq 10$ only (for a pre-print of paper, see Appendix), indicating that such a low aspect ratio is insufficient to

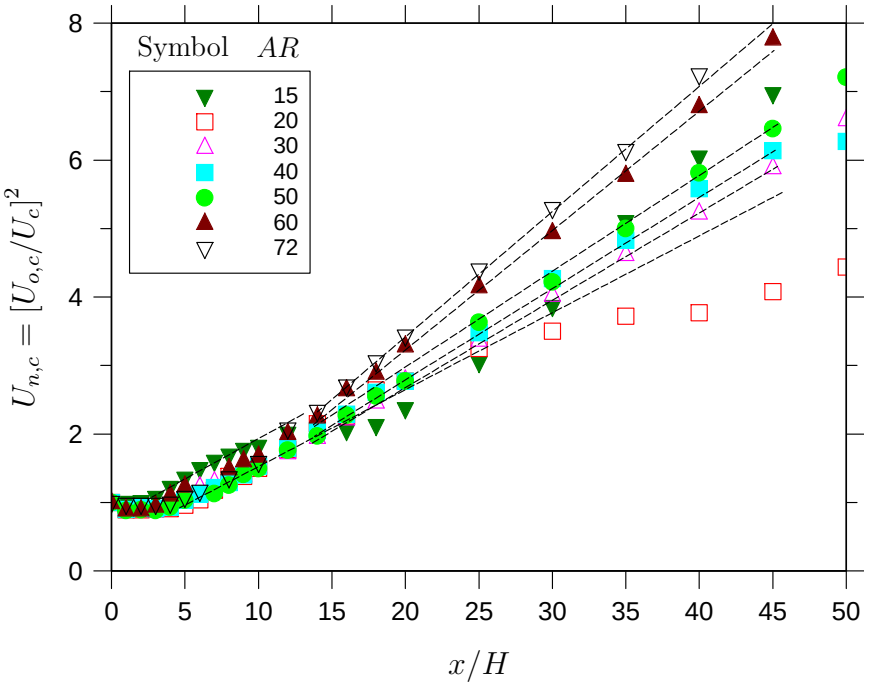

Figure 5.6: Centerline variations of normalized mean velocity $U_{n,c}$ up to $x/H = 45$.

obtain a fully developed two-dimensional flow. The present results also indicate the same thing. An increasingly significant influence of the wall-boundary layer on sidewalls with decreased aspect ratio is a probable cause of these. This finding provides strong supports for the postulate by Gouldin et al. (1986) that a very low aspect ratio plane jet may never attain true self-similarity.

It is of prime interest to explore the relationship between the extent of the planar (two-dimensional) region of the jet and nozzle aspect ratio. This is quite an important feature of a plane jet and its dependence on nozzle aspect ratio is owed an explanation. The maximum axial distance up to where the flow is statistically two-dimensional (i.e. $U_c \sim x^{-1/2}$), $x_{p,\,\max}$, is extracted from Figure 5.8 for each nozzle aspect ratio. This is presented in Figure 5.9. Also presented in the figure are the $x_{p,\,\max}/H$ values for previous investigations, extracted by deductions from previous measurements based on the axial extent of their data provided. These values were not presented directly in their papers.

It is quite clear that $x_{p,\,\max}/H$ scales almost linearly with AR. Using the best-fit 'linear'interpolation, the relationship between $x_{p,\,\max}/H$ and AR can be described by

$$\frac{x_{p,\max}}{H} \simeq m\,[AR + C] \tag{5.3}$$

where m, C are some constants determined by experiments. For the present study, m and C are 1.40 and 2.10 respectively.

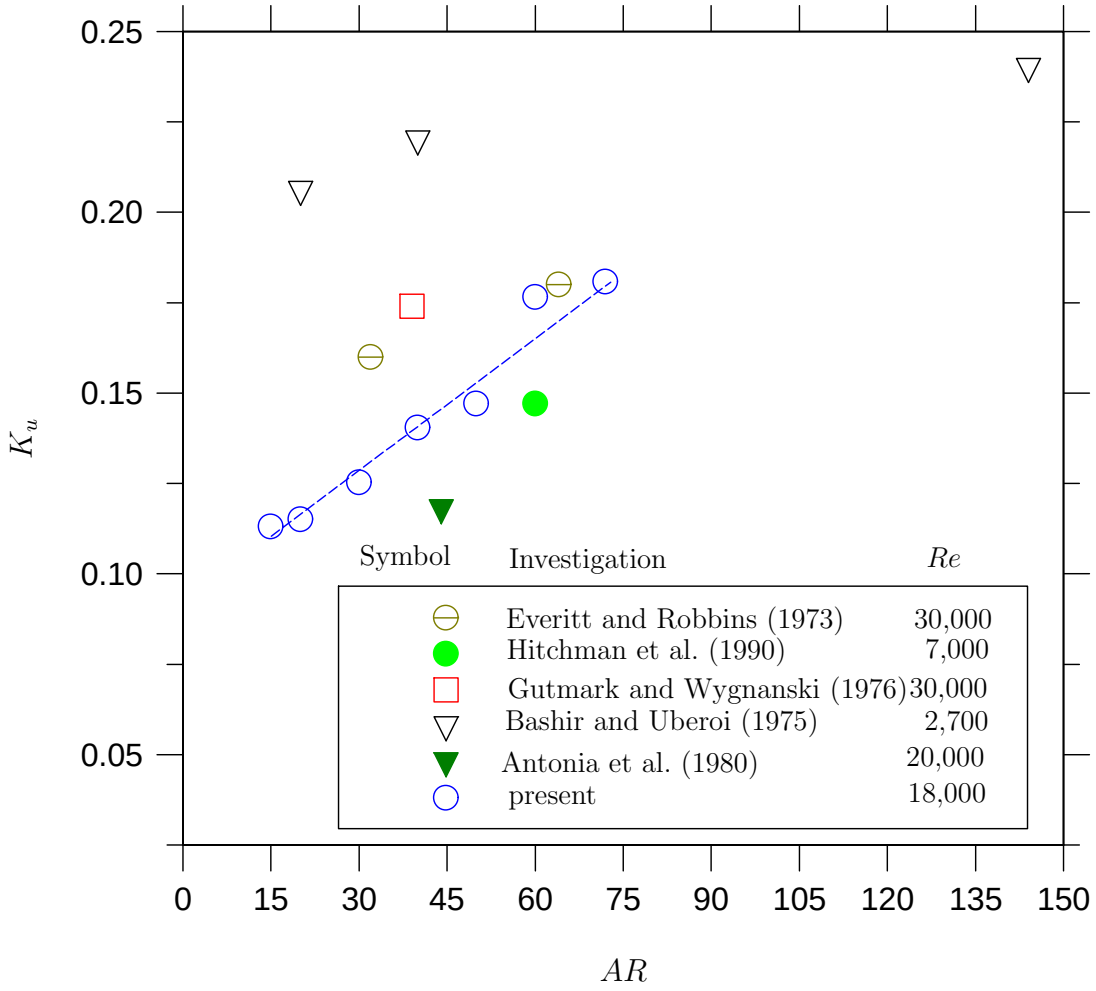

Figure 5.7: Dependence of the centerline decay rate of mean velocity K_u obtained for $x/H > 20$ on the nozzle aspect ratio AR. The Reynolds number is also listed.

The present findings validate the arguments in the Chapter 1.5.3, that the ranges of x/H in published data appeared to be limited by the nozzle aspect ratio for plane jets. Many investigations have recognized that nozzle aspect ratio is a limiting factor to the extent of the planar region $x_{p,\,\max}/H$ but the relationship has not been investigated directly. For example, Browne et al. (1983) measured a plane jet up to $x/H = 20$ with a nozzle aspect ratio of only 20. Also, Heskestad (1965) measured up to $x/H = 160$ with a nozzle aspect ratio of 120. Likewise, the results of other investigators also follow the same trend (see Figure 1.13). However, $x_{p,\,\max}/H$ is unlikely be universal for every experiment but is expected to depend on experimental conditions such as Reynolds number and nozzle geometry. Nevertheless, the linear relation (Equation 5.3.2) may well be upheld with some relative differences in the magnitudes of m and C that depends on experimental conditions. Our results are broadly supported by Krothapalli et al. (1981) whose measurements

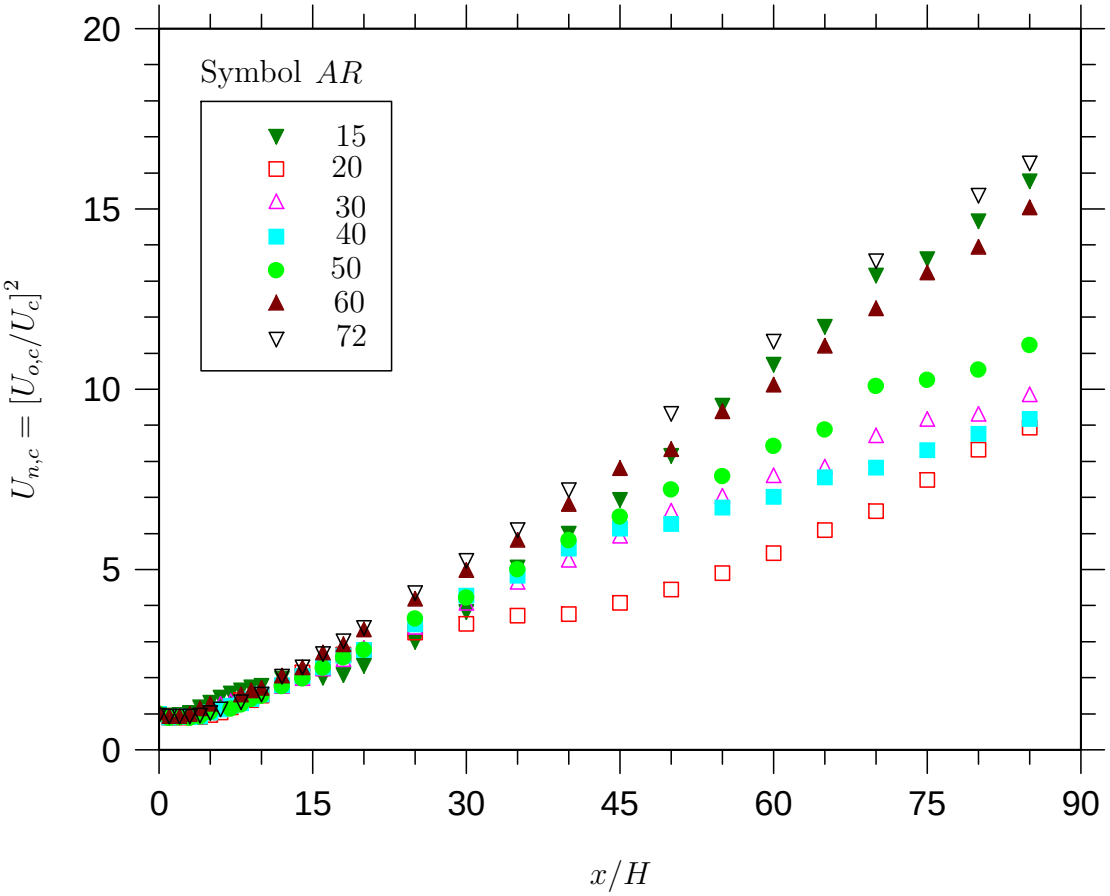

Figure 5.8: The centerline variation of the normalized mean velocity $(U_{o,c}/U_c)^2$ in the inverse square form, for different nozzle aspect ratio AR up to $x/H = 90$.

on rectangular jets indicate that the position at which the centerline velocity first assumes an axisymmetric character moves upstream (towards the nozzle exit) as nozzle aspect ratio decreases. In other words, the extent of the quasi-two-dimensional (planar) region for their rectangular jet was dependent on its nozzle aspect ratio. In fact, Trendscoste and Sforza (1967) and Sfeir (1979) have also shown that the exponent in centerline mean velocity decay is dependent both on nozzle geometry and aspect ratio. Our findings do not support theirs. Although these investigations indirectly imply a dependence of the extent of the planar region on nozzle aspect ratio, no study actually determined how the relation between $x_{p,\,\max}/H$ and AR would vary. Hence, our results have not only added to the previously existing knowledge but also broadened it substantially.

Figures 5.10 to 5.14 present the lateral distributions of the normalized mean velocity for the different nozzle aspect ratios. The mean velocity profiles collapse onto a Gaussian at about $x/H = 20$ for $AR = 15$ and at $x/H = 5$ for $AR = 72$. At these locations, the normalized profiles of the mean velocity are well represented by the Gaussian relation of

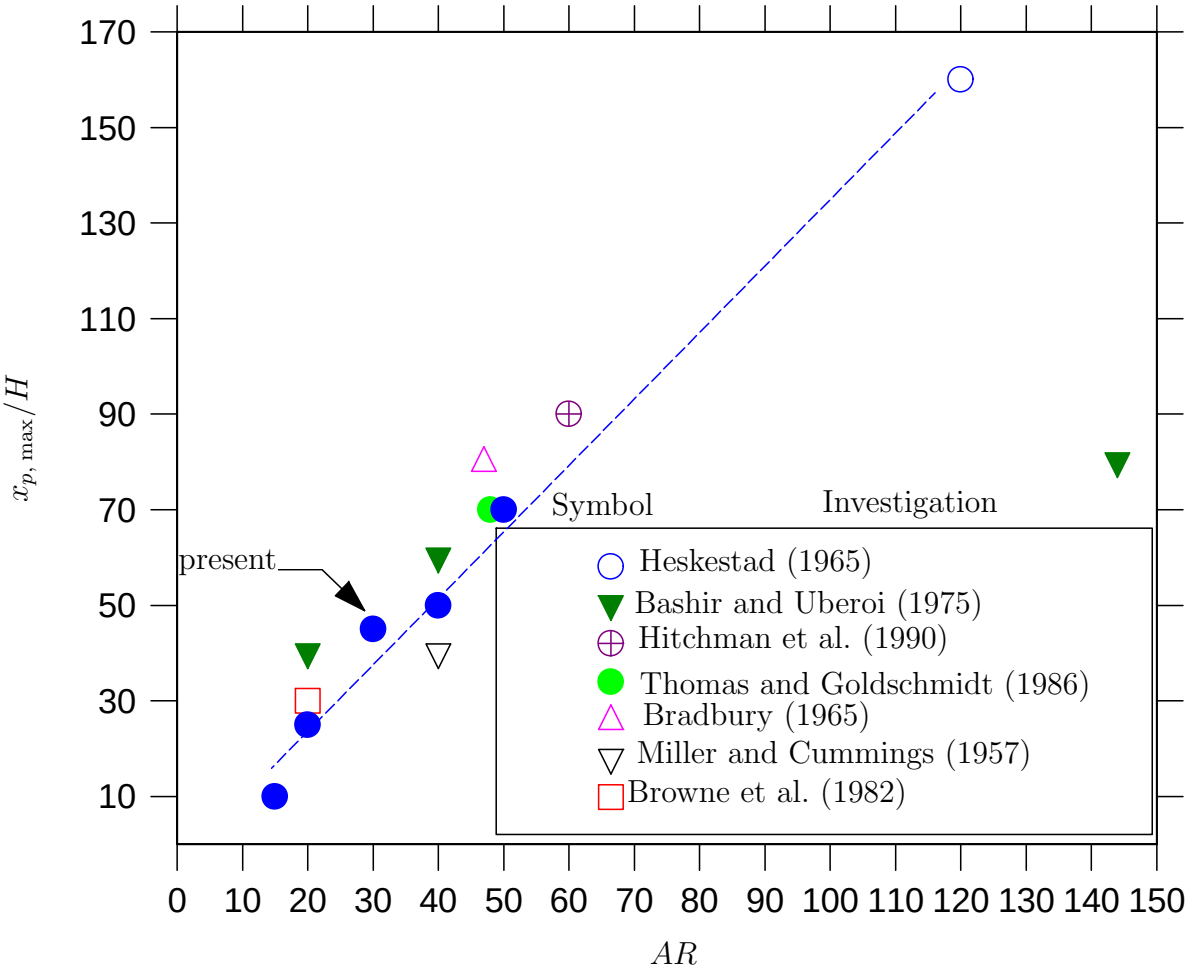

Figure 5.9: The planar region $x_{p,\,\max}/H$ of the jet, at different nozzle aspect ratios AR

the form $U_n = e^{-ln2(y_n)^2}$. Note the departure of the profile at $x/H = 40$ for $AR = 20$ may be due to the sidewall effects. Using these mean velocity profiles, one determines the spreading rates of a plane jet. Thus, the velocity half-widths $y_{0.5}$ was determined and its dependence on nozzle aspect ratio are explored next.

Figure 5.15 displays the streamwise variations of the lateral velocity half-widths $y_{0.5}$. The normalized velocity half-widths $y_{0.5}/H$ spread linearly with x/H for each nozzle aspect ratio. They all agree well with the well-known far field relation

$$\frac{y_{0.5}}{H} = K_y \left[\frac{x}{H} + \frac{x_{02}}{H}\right] \tag{5.4}$$

where K_y and x_{02} are spreading rate and virtual origin determined by the experiment. A clear dependence of spreading rate on AR is evident. Figure 5.16a presents the spreading rates for each nozzle aspect ratio of present and the published values of K_y. There is a good agreement between our K_y and those from previous investigations. It is clear that the spreading rate increases with AR. That is, a larger aspect ratio produces a wider

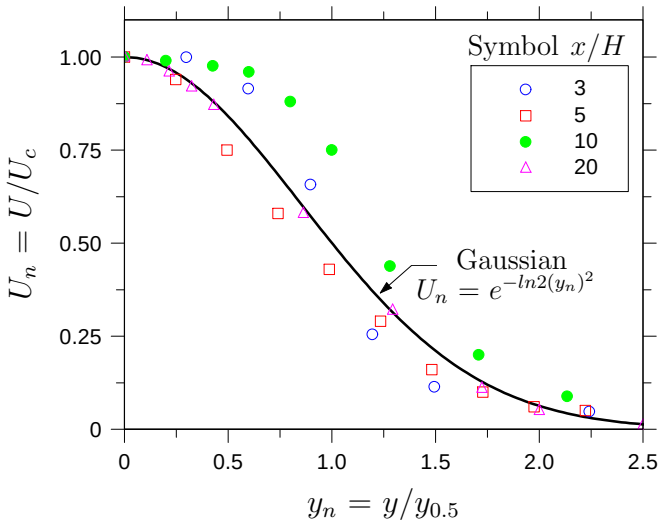

Figure 5.10: Lateral profiles of the normalized mean velocity U_n for $AR = 15$.

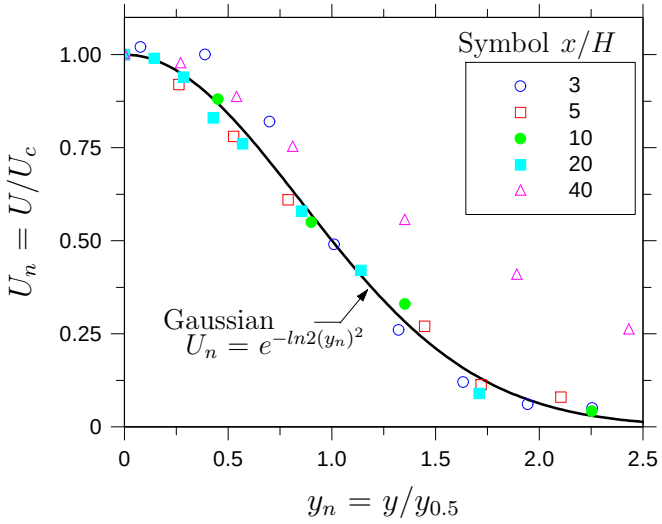

Figure 5.11: Lateral profiles of the normalized mean velocity U_n for $AR = 20$.

jet and increased entrainment. Again, it is noted that the linear relation in Equation 5.4 only applies to a limited axial distance for the low aspect ratios. For example, when $AR = 15$ the linear region is limited to $x/H < 10$. Likewise for $AR = 20$, the half-widths vary linearly up to $x/H = 20$. For larger x/H, the half-width deviates from a linear dependence. This is entirely consistent with the decay of mean centerline velocity in Figure 5.6. It appears that the velocity half-widths are also influenced by the wall boundary layer, which scales with x/H. Hence, when AR is too small i.e. for 15 and 20, the mean field is strongly influenced by the widening boundary layer due to the sidewalls.

The variation of the virtual origin x_{02} with AR is shown in Figure 5.17. As the nozzle aspect ratio is increased from 15 to 72, x_{02} increases monotonically from about -8.0 to

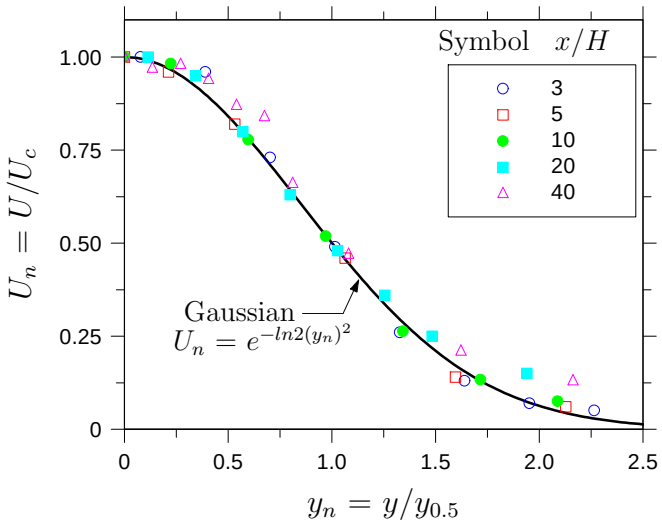

Figure 5.12: Lateral profiles of the normalized mean velocity U_n for $AR = 30$.

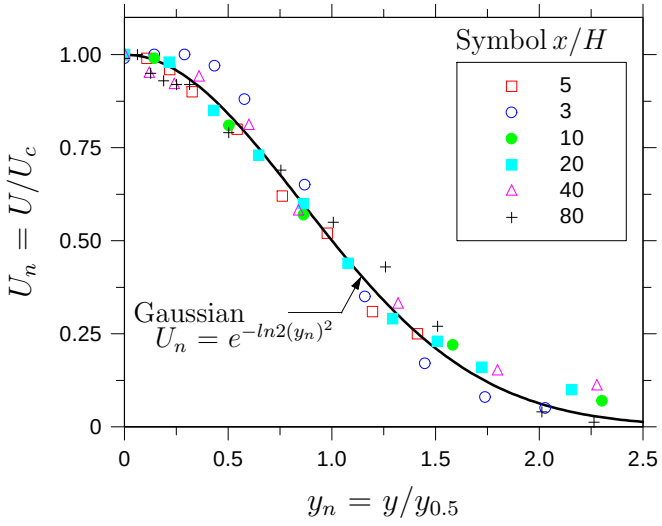

Figure 5.13: Lateral profiles of the normalized mean velocity U_n for $AR = 50$.

-4.5. Published papers have attributed variations in the location of the virtual origin to the experimental conditions. For instance, Gouldin et al. (1986) states that considerable scatter in previously obtained x_{02} in literature are due to experimental conditions. The present experiment has been performed under a fixed set of conditions, hence the only cause for its variation is the nozzle aspect ratio. With a change in nozzle aspect ratio, it is possible that the development of the structures in the initial shear layers of the potential core, undergo a transition (Hussain and Clark 1977). It is well known that a low aspect ratio nozzle encounters more earlier three-dimensional effects (Gouldin et al. 1986). Thus, there is evidence for a direct influence on the transverse (z-direction) structure of a plane jet from a low aspect ratio nozzle. This effect, if genuine, will produce a significant difference in the virtual origins.

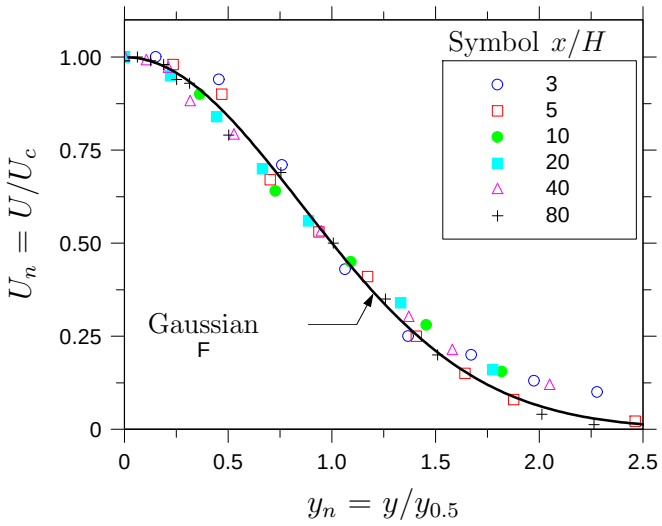

Figure 5.14: Lateral profiles of the normalized mean velocity U_n for $AR = 72$.

Of particular interest to the present study is the role of the **critical jet aspect ratio**[2] $AR_{jet,crit}$ on the axial extent of the planar flow. A definition of $AR_{jet,crit}$ is provided in Section 5.1. Such information is lacking in literature and may assist future nozzle designers to optimize their designs. From previous arguments, it is evident that nozzle aspect ratio limits the extent of the statistically two-dimensional region of the plane jet. Thus, it is plausible that a critical jet aspect ratio may control the downstream location at which three-dimensional effects (due to sidewalls) first emerge. A characteristic measure of the critical jet aspect ratio may be obtained from the velocity half widths of the jet at a location where three-dimensional effects start to become significant. Thus, using Figure 5.9 to determine the $x_{p,\,\max}$ and then using Figure 5.15 to calculate the velocity half-widths at $x_{p,\,\max}$, we determined the critical jet aspect ratio for $15 \leq AR \leq 72$. The critical jet aspect ratio is thus denoted as $AR_{jet,crit}$.

Figure 5.18 presents the relationship between $AR_{jet,crit}$ and AR. A clear evidence of an 'elbow point' emerges. As the nozzle aspect ratio is increased from 15 to 30, the critical jet aspect ratio increases rapidly. However, for $AR \geq 30$, $AR_{jet,crit}$ is approximately constant. The slight variations in $AR_{jet,crit}$ for $AR \geq 30$ are within the experimental uncertainty. The physical meaning of this plot is clear: The aspect ratio of the jet grows with axial distance (as the jet becomes wider) but is always less than the aspect ratio of the nozzle. Eventually, the jet flow will cease to be two-dimensional. Furthermore,

[2]**Critical jet aspect ratio** $AR_{jet,crit}$ is defined by the ratio of the velocity half-widths $y_{0.5}$ at a location where the flow ceases to be planar and the separation between the sidewalls w. See the discussion in Section 5.1.

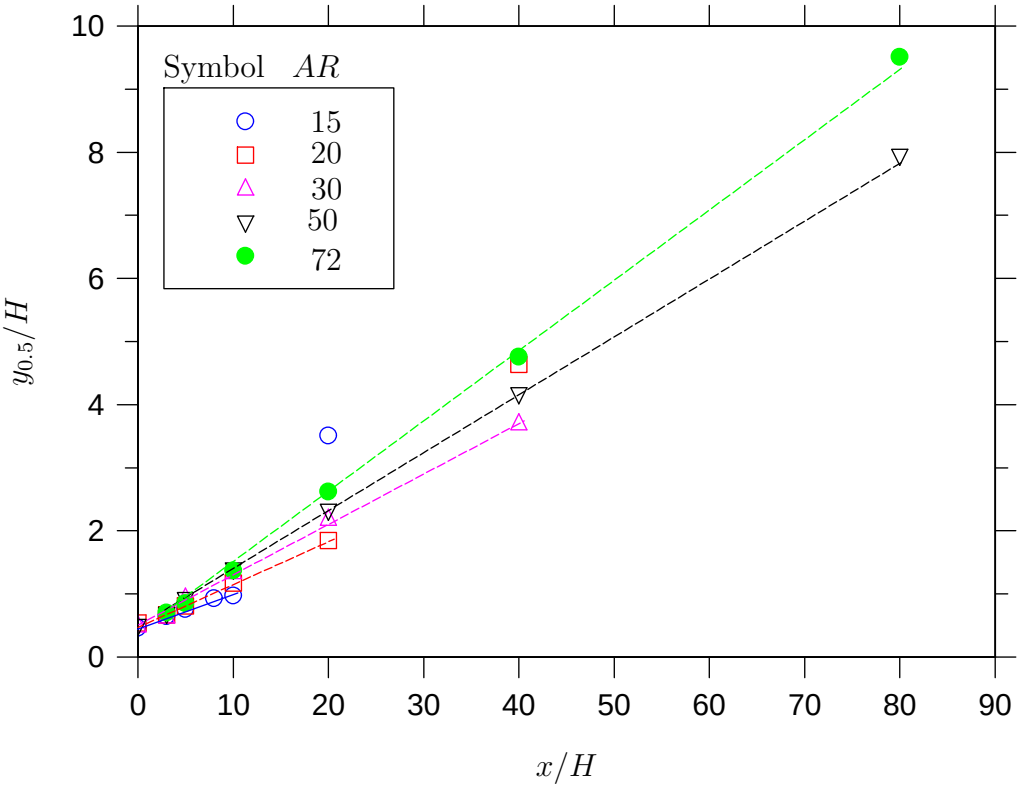

Figure 5.15: The streamwise variation of the velocity half-width $y_{0.5}$ for different nozzle aspect ratios AR.

the magnitude of $AR_{jet,crit}$ is about 0.15. Since the outer width of the jet is about three times the half-width, it is clear that the jet undergoes a transition from planar to three-dimensional flow when the width of the jet approximately equals the spacing between the sidewalls. The present measurements show that the minimum criteria for nozzle designs to achieve a reasonably good jet aspect ratio would be a nozzle whose aspect ratio ≥ 30. Due to limitations in the present data (i.e. maximum aspect ratio studied equals 72), this relation may lie within a limited range.

5.3.3 The Fluctuating Velocity Field

The turbulence field, determined from the fluctuations of the velocity signal about its mean values are also used to characterize behavioural features of a plane jet. Figure 5.19 shows the axial evolution of the streamwise turbulence intensity $u'_{n,c}$ for different nozzle aspect ratios. Here, the normalization is carried out using the local centerline velocity U_c. For reference, the turbulence intensity of Antonia et al. (1980), Bashir and Uberoi (1975) and Browne et al. (1982) at (Re, AR) = (20,000, 44), (2,700, 20-144) and (7,700, 20) have also been included.

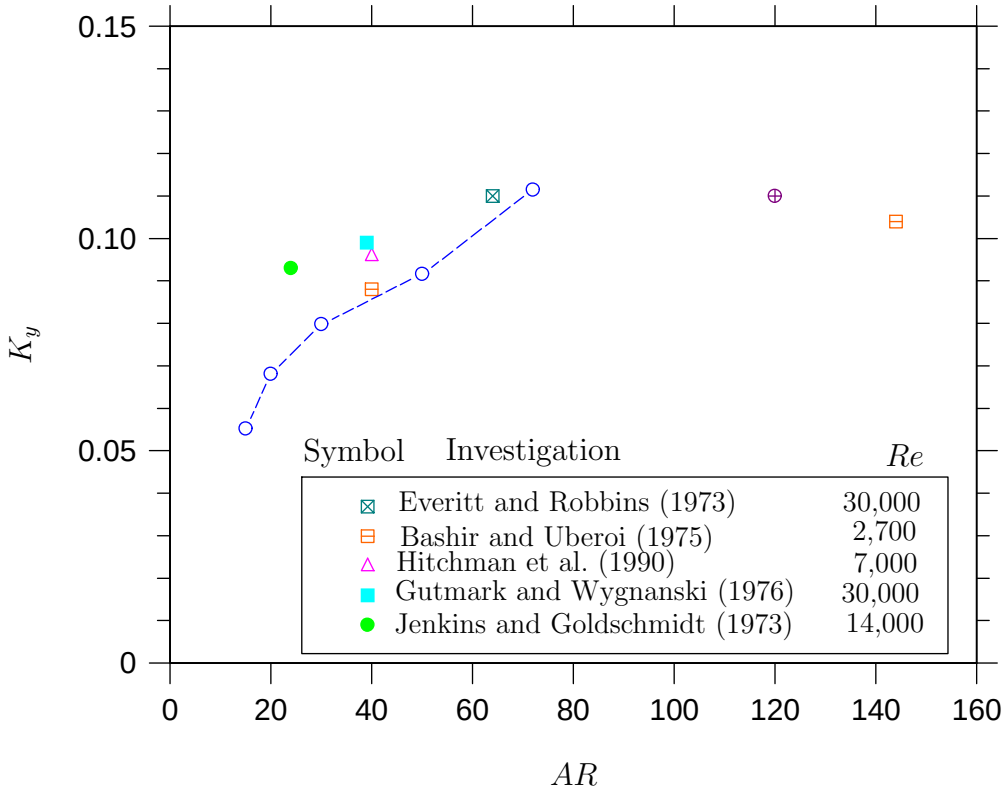

Figure 5.16: Dependence of the jet spreading rate K_y on the nozzle aspect ratio AR.

The development of the turbulence intensity is similar to previous investigations. For instance, our turbulence intensity at $AR = 20$ is similar to Browne et al. (1982). Very slight differences exist, especially in the far field ($x/H > 20$), which are attributable to the differences in Reynolds number (our $Re = 18{,}000$ versus their $Re = 7{,}700$). The magnitude of the local maximum, which occurs at about $x/H = 10$, are almost identical for the present and Browne's data. Similarly, the turbulence intensity of Antonia et al. (1980) measured at (AR, Re) = (44, 20,000) is similar to ours at $AR = 50$. Surprisingly, the far field asymptotic values are almost identical. Similarly, the trends in turbulence intensity measured by Bashir and Uberoi (1975) for aspect ratios 20, 40 and 144, all of which were measured at $Re = 2{,}700$, are in good agreement with ours, considering the differences in Reynolds number, nozzle profiles and other experimental conditions (see their paper). Subtle differences are expected, particularly due to the nozzle profile. The literature measurements were conducted using a standard smoothly contoured nozzle (no front plates) whereas the present measurements were conducted using a radially contoured nozzle. See Figure 1.16 and 4.21 and the respective discussions in those sections. Their far field asymptotic value for $AR = 144$, are comparable with ours for the $AR = 72$ configuration. Thus, bearing in mind the differences, the present measurements are in reasonable agreement with previous investigations.

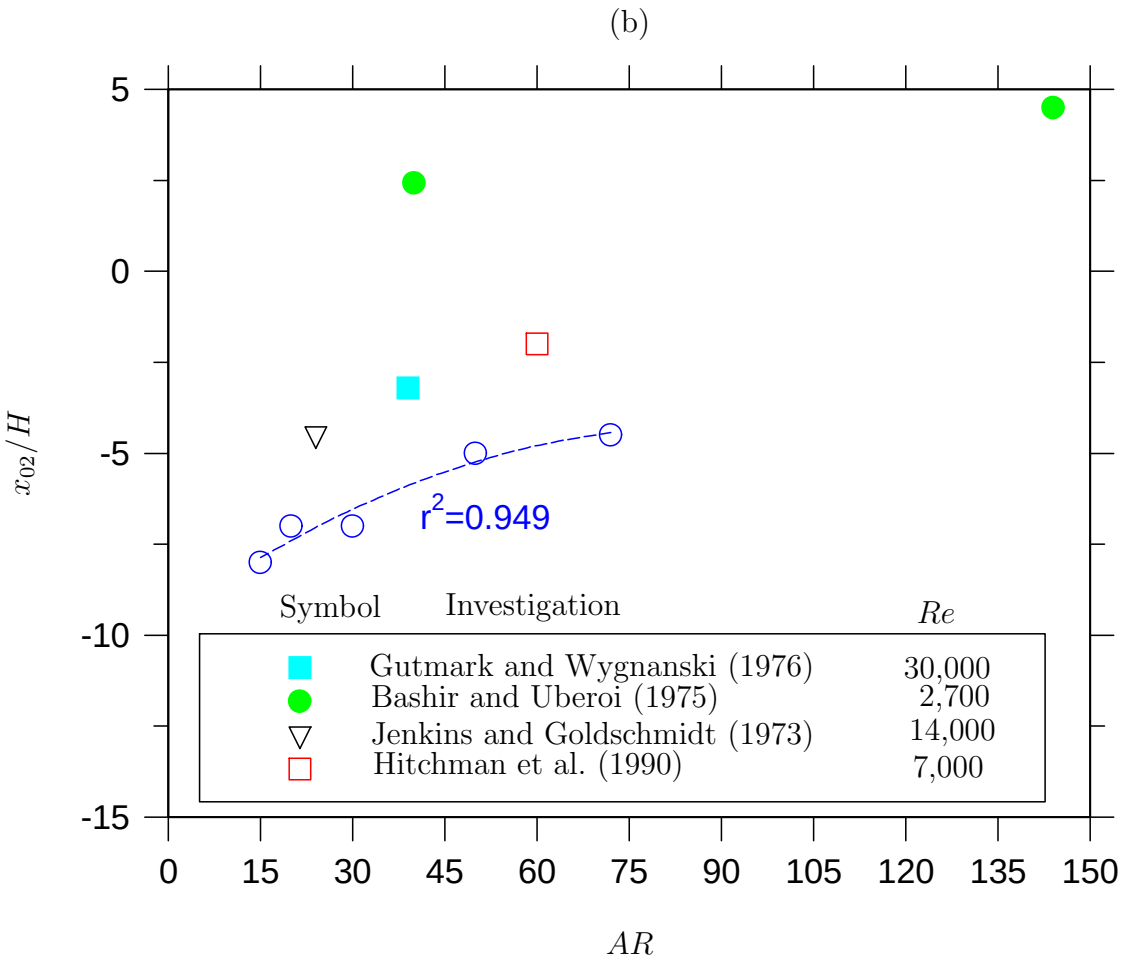

Figure 5.17: Dependence of the virtual origin x_{02}/H on the nozzle aspect ratio AR. A quadratic best-fit with its regression coefficient is shown.

For the present data, the turbulence intensity shows a monotonic increase from $x/H = 0$ to $x/H = 8$ for all nozzle aspect ratios. It is important to mention that, in the near field, only $AR = 15$ and 20 show significantly different turbulence intensity. As the shear layer grows, so do the large-scale structures and their randomness. Hence, the deviation of the instantaneous velocity from its mean value is higher thus increasingly higher $u'_{n,c}$ is evident. Notably, the lowest nozzle aspect ratio ($AR = 15$) nozzle has the highest turbulence intensity between $x/H = 0$ and $x/H = 8$. This possibly indicates enhanced three-dimensionality for $AR = 15$.

Between $x/H = 8$ and 14, distinct hump $u'_{c,\max}$ occur for all nozzle aspect ratios (Figure 5.20) whose magnitude $u'_{c,\max}$ and position x_m changes. The magnitudes of $u'_{c,\max}$ decreases with an increase in nozzle aspect ratio with identical values found for $AR = 60$

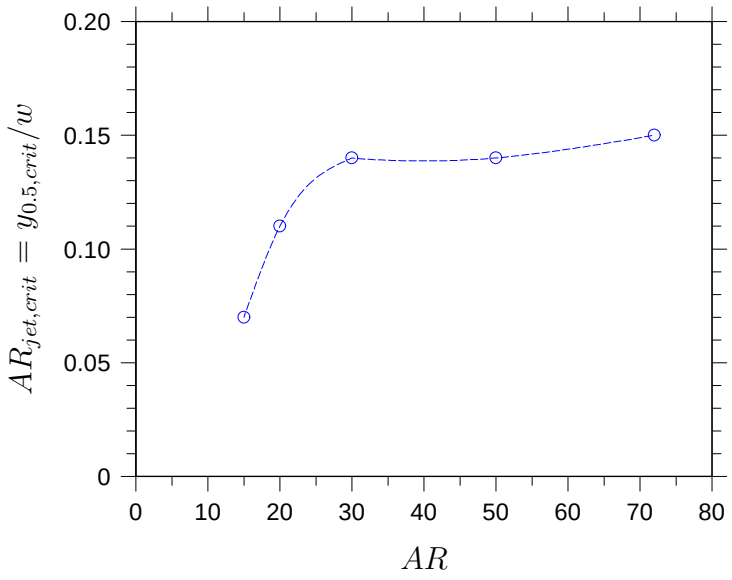

Figure 5.18: Dependence of the critical jet aspect ratio $AR_{jet,crit}$ at which the flow ceases to be planar, on the nozzle aspect ratio AR.

and 72. Published literature shows that the occurrence of pronounced hump in scalar intensity depend upon initial conditions (Mi, Nathan and Nobes 2001). Hence, the present finding is consistent with the well-established concepts of the influence of initial conditions. The occurrence of a pronounced hump is presumably associated with the behaviour of the large-scale coherent vortices. For a lower aspect ratio, higher turbulence intensity implies that the large-scale structures are more coherent, periodic and highly organized. The decrease in the magnitude of the hump for larger aspect ratio nozzles suggest that underlying structures become more three-dimensional, possibly aperiodic and less coherent. It is also evident that the axial location x_m of the hump in turbulence intensity $u'_{c,\max}$ decreases from $x_m = 15$ to $x_m = 8$ as nozzle aspect ratio decreases from $AR = 72$ to $AR = 15$. The downstream movement of $u'_{c,\max}$ also follows a consistent trend, which changes with nozzle aspect ratio.

For $x/H > 15$, $u'_{n,c}$ increases asymptotically to a self-similar value (Figure 5.20) whose magnitude $u'_{c,\infty}$ and position $x_{m,\infty}$ are AR dependent. Comparisons between the $u'_{c,\infty}$ obtained for different AR shows that a higher nozzle aspect ratio leads to a larger magnitude of $u'_{c,\infty}$. However, it appears that $u'_{n,c}$ asymptotes to $u'_{c,\infty} = 0.24$ when $AR \geq 60$. The appearance of $u'_{c,\infty}$ at $AR = 60$ clearly indicates that the turbulence intensity of these jets is truly self-similar beyond this aspect ratio. Further, the x-location of the self-similar region ($x_{m,\infty}$) is not universal, but depends on aspect ratio. However, for $AR = 15$, no self-similar region for the turbulence intensity exists. On the other hand, for $AR = 20$, it appears that the turbulence intensity becomes self-similar at $x_{m,\infty} = 40$. The

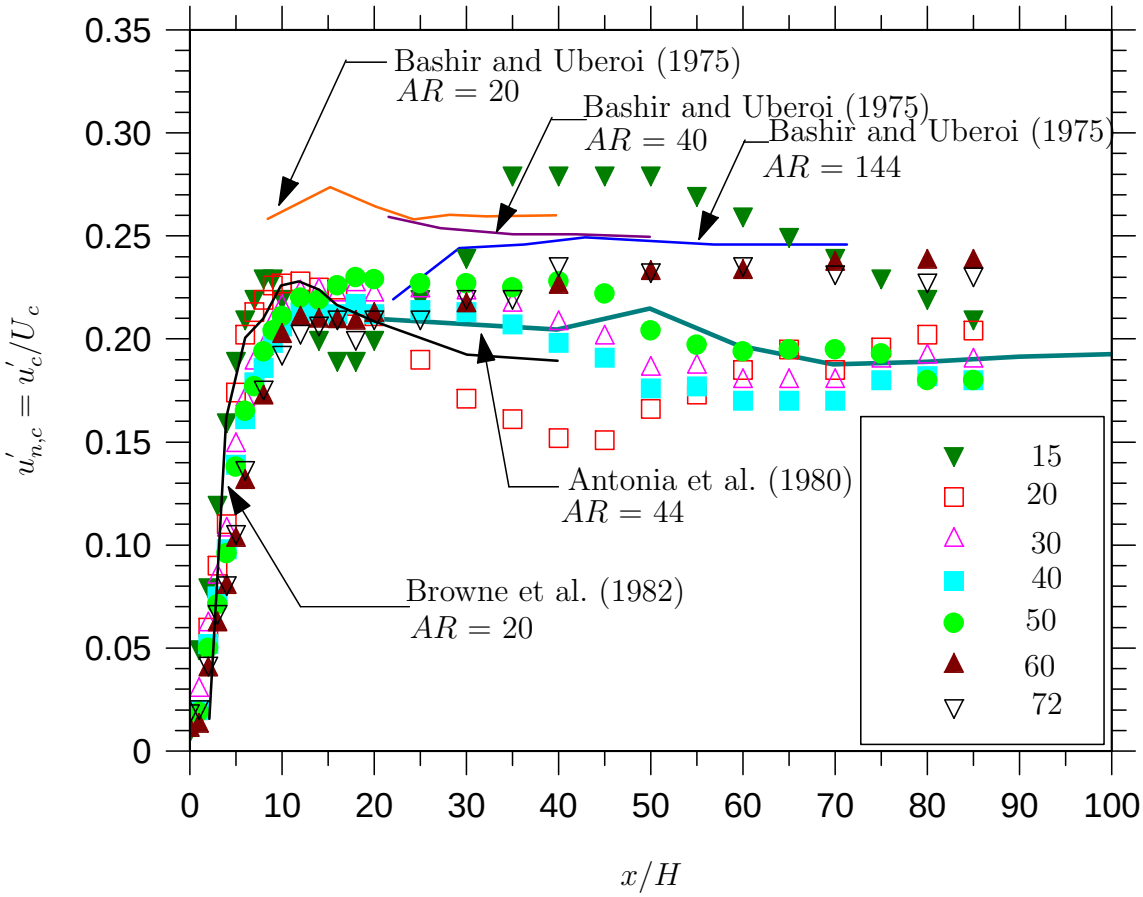

Figure 5.19: Evolutions of the centerline turbulence intensity $u'_{n,c}$ for different aspect ratios AR.

unexpected increase in turbulence intensity after a small region of nearly constant value for $AR = 15$ and 20 is a yet another indication of the effect of the sidewalls on the local centerline mean velocity. For $AR \geq 30$, identical values of $x_{m,\infty}$ are noted. These occur at $x_{m,\infty} = 50$. In light of the present discussion, it is thus evident that nozzle aspect ratio influences the entire turbulence intensity field of the plane jet.

Figures 5.21 to 5.25 present the lateral distributions of the turbulence intensity profiles for different nozzle aspect ratios. The turbulence intensity profiles do not collapse onto a single curve (or become congruent) for $AR = 15$ and 20 even at $x/H = 40$. However, for $AR = 30$, turbulence intensity collapses onto a single curve at $x/H \geq 20$. For $AR = 50$ and 72, the profiles collapse onto single curve for $x/H \geq 10$. The results clearly indicate that, with an increase in nozzle aspect ratio, the x-location of the self-similarity of the turbulence intensity profiles move upstream. These results are entirely consistent with the turbulence intensity profiles measured from a plane nozzle of aspect ratio 60 and $r^* = 2.14$ (see Chapter 4, for the profiles measured at $Re = 16{,}500$, which became congruent

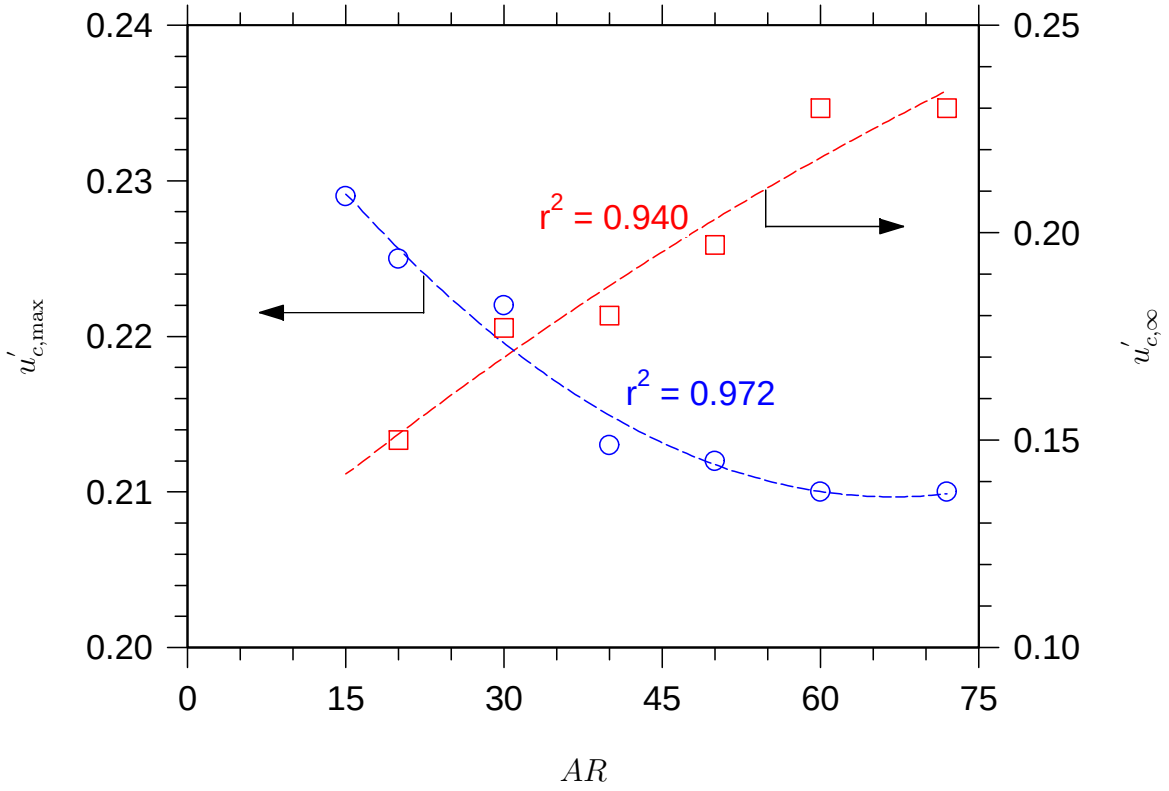

Figure 5.20: Nozzle aspect ratio AR effect on the near field hump in turbulence intensity $u'_{c,max}$ and on the far field asymptotic turbulence intensity $u'_{c,\infty}$. A quadratic best-fit with its regression coefficient is shown.

at $x/H \simeq 10$).

The turbulence field can also be characterized using the skewness and flatness factors. Figures 5.26 and 5.28 investigate the centerline distributions of S_u and F_u. The figures show a clear dependence of S_u and F_u on nozzle aspect ratio. Both evolve from near Gaussian value (S_u, F_u) = (0, 3) at the exit plane, to highly non-Gaussian values further downstream. Further, S_u exhibits a local maximum $|S_u^{\max}|$ and a local minimum $|S_u^{\min}|$ at $x/H = 3$ and 5, (see Figure 5.27 and insert in Figure 5.28) respectively, while F_u produces a maximum at $x/H = 5$. The maximum in skewness at $x/H = 3$ is probably associated with the acceleration of the vortex cores on the plane jet centerline. On the other hand, the minima in both S_u and F_u noted at $x/H = 5$ appears to be associated with the lateral oscillations of the jet potential core. This reasoning is supported by Figure 5.4 which shows that $AR = 72$ has a larger potential core than $AR = 20$. Correspondingly, $|S_u^{\min}|$ for $AR = 72$ has a larger magnitude than for $AR = 20$. It is plausible that a longer potential core will be more unstable and thus undergo larger lateral oscillations with a larger amplitude of oscillation resulting in a larger magnitude of $|S_u^{\min}|$. Moving downstream from $x/H = 5$, both S_u and F_u increase to near Gaussian values (0, 3) for all nozzle

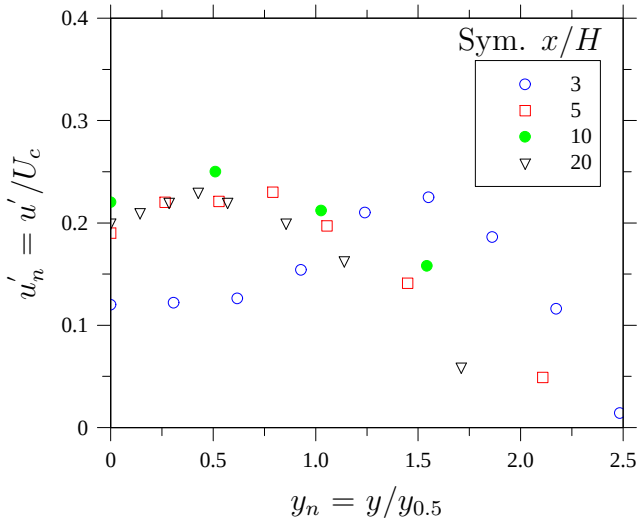

Figure 5.21: Lateral profiles of the turbulence intensity $u_n^{'}$ for $AR = 15$.

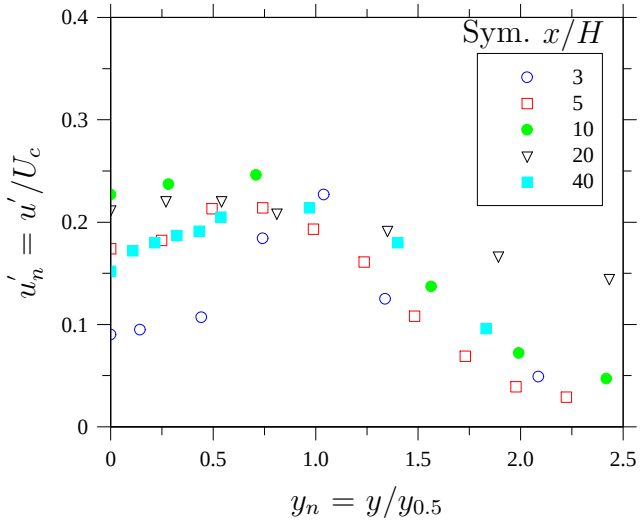

Figure 5.22: Lateral profiles of the turbulence intensity $u_n^{'}$ for $AR = 20$.

aspect ratios. Their asymptotic magnitudes are almost independent of the nozzle aspect ratio. Any differences between the asymptotic values may well be due to experimental uncertainties. The unusual departures of S_u from the Gaussian for $AR = 15$ and 20 are possibly due to the insufficient nozzle aspect ratio.

5.4 Further Discussion

The mean and turbulence properties of a plane jet issuing from a radially contoured plane nozzle ($r^* = 3.60$) measured over the range $15 \leq AR \leq 72$ are reported above. Changes in the nozzle aspect ratio were found to produce differences in the initial velocity profiles. Such differences are more conspicuous near to the edges of the initial jet. The differences

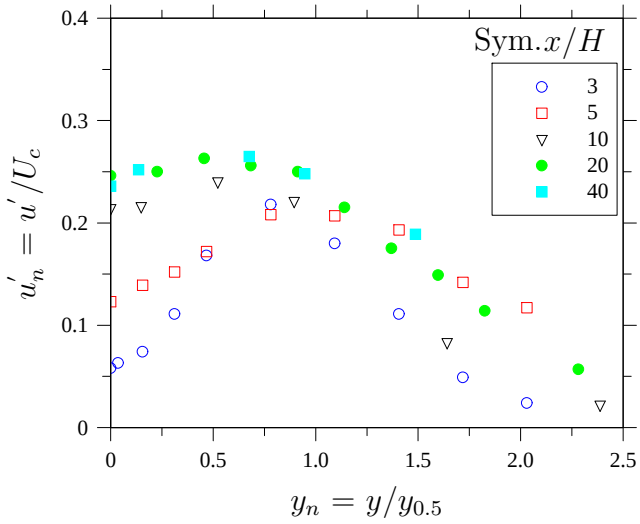

Figure 5.23: Lateral profiles of the turbulence intensity $u_n^{'}$ for $AR = 30$.

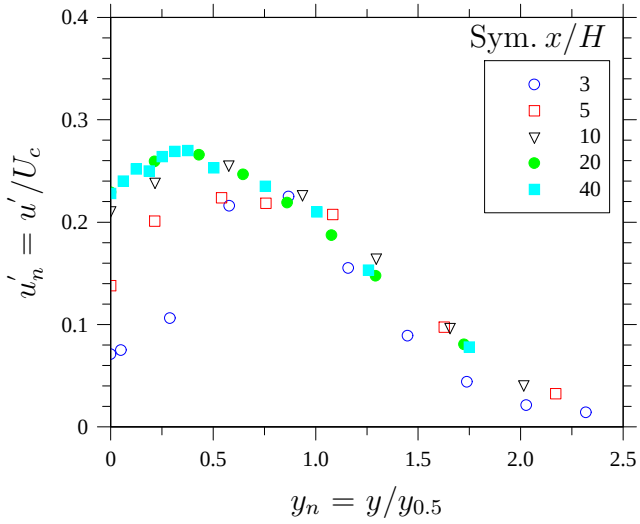

Figure 5.24: Lateral profiles of the turbulence intensity$u_n^{'}$ for $AR = 50$.

are attributable to the sidewalls being moved closer to achieve a low aspect ratio nozzle. In short, the present findings confirm that the exit flow and the influence of the sidewalls are coupled. The lower aspect ratio jet experiences a larger impact of sidewalls. A small contribution to this effect in the present experiment could be induced by the blocking of the ends of the plane nozzle (see Figure 5.1) to achieve nozzle aspect ratios lower than 72. We found that the effect of the sidewalls is far more significant than the effect of the upstream secondary circulation that may be caused due to blocking the sides of lower aspect ratio nozzles.

The average lengths of the jets' potential cores were found to depend on nozzle aspect ratio with increasing length at a higher aspect ratios. Correspondingly, it was also found

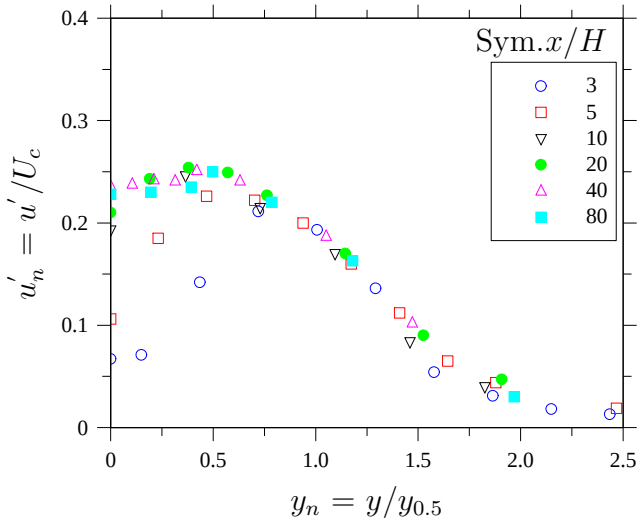

Figure 5.25: Lateral profiles of the turbulence intensity $u_n^{'}$ for $AR = 72$.

that the spreading rate of the jet was higher when aspect ratio was small. This finding contrasts those of Trendscoste and Sforza (1967) for $1 \leq AR \leq 40$, Marsters and Fotheringham (1980) for $3.39 \leq AR \leq 11.88$ and Quinn (1992b) for $2 \leq AR \leq 20$ for their unconfined jets from a rectangular nozzle. They measured increased near field entrainment (and correspondingly shorter potential cores) with an increase in nozzle aspect ratio. For a free rectangular nozzle without sidewalls, the jet can spread in both the lateral (y) and spanwise (z) directions while a plane jet can only spread in the lateral (y) direction. It may for this reason that their rectangular jet showed an increase an increase in the entrainment rate with an increase in nozzle aspect ratio. On the other hand, Quinn (1992b), who measured a free rectangular jet, attributed the increase in entrainment (and decreased length of potential cores) to increased three-dimensional effects. For a plane jet, however, increasing the aspect ratio has the opposite effect, because there are less three-dimensional effects in a plane jet.

The far field decay of centerline mean velocity and spreading rates of plane jet were found to increase with an increase in nozzle aspect ratio. This is consistent with Trendscoste and Sforza (1967) for $1 \leq AR \leq 40$, Marsters and Fotheringham (1980) for $3.39 \leq AR \leq 11.88$ and Quinn (1992b) for $2 \leq AR \leq 20$ for their free rectangular nozzle. We have noticed that in the quasi-plane-jet zone, the free rectangular and plane jet are both similar. Thus, the increase far field in decay and spreading rates with an increase in nozzle aspect ratio for our plane jet is well supported by published literature. Increased decay and spreading rates of the plane jet may be attributable to the changes in the vortical structures, if any, especially in the shear layers. Indeed, Zaman (1999), for

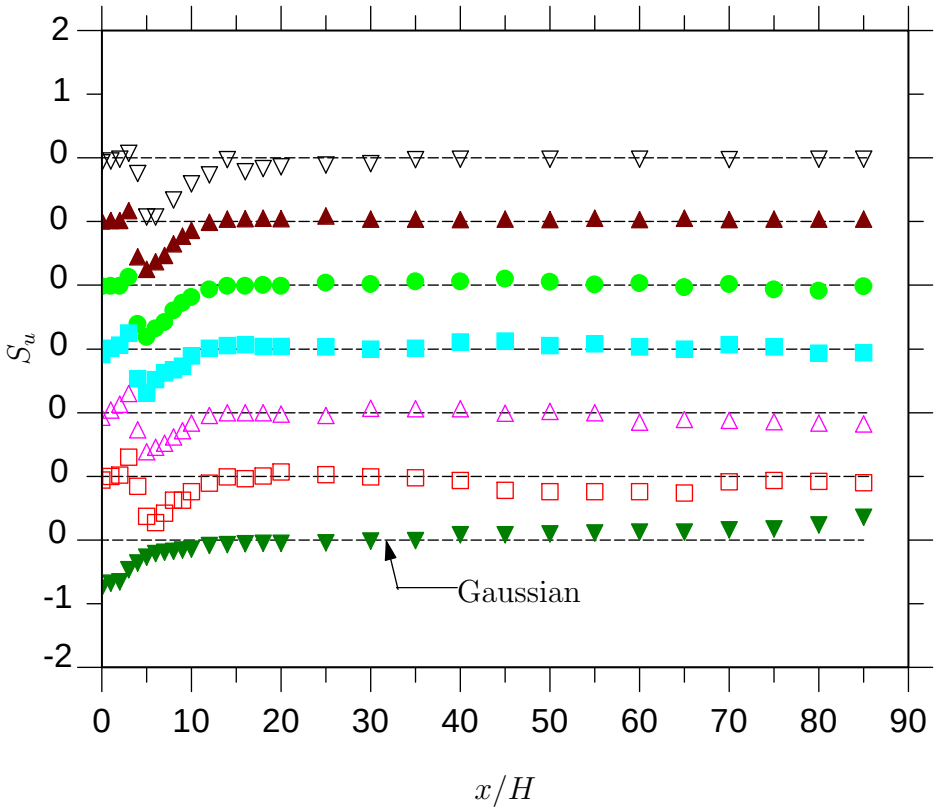

Figure 5.26: Centerline variations of the skewness factors S_u. The profiles have been shifted by 1. Symbols identical to Figure 5.19

their investigation on nozzle aspect ratio effect of free rectangular nozzles with a Mach number 0.95 for AR = 2 - 38, suggested that the entrainment and spreading rate only increases significantly with aspect ratio for $AR \geq 8$. For their free rectangular jets, no increase in the spreading rates were noted for $AR < 8$. Thus, the increase in spreading were not attributable to the 'shear layer perimeter-stretching'[3] for $AR < 8$, for a given cross-sectional area of the free rectangular nozzle. Having said that, they explained that this mechanism was a relatively inefficient mechanism for increasing jet spreading if nozzle aspect ratios were small. On the other hand, their data suggested that the effect of shear layer perimeter-stretching on the spreading of a free rectangular jet becomes significant only, when the aspect ratio is large (typically 10 or more). For the present experiment, the aspect ratios were very large ($\geq$ 15). However, for a plane jet, we do not expect an increase in the shear-layer perimeter-stretching. Nevertheless, any increase in the spreading of the free rectangular jet by Zaman (1999), was directly linked to the presence of streamwise vortices and their inter-scale interactions. Therefore, it is possible that the present increase in spreading and decay rates of plane jet at a higher nozzle aspect ratio

[3]'Shear-layer perimeter stretching' refers to stretching the perimeter of the shear layer which is exposed to the ambient fluid, so that more entrainment takes place.

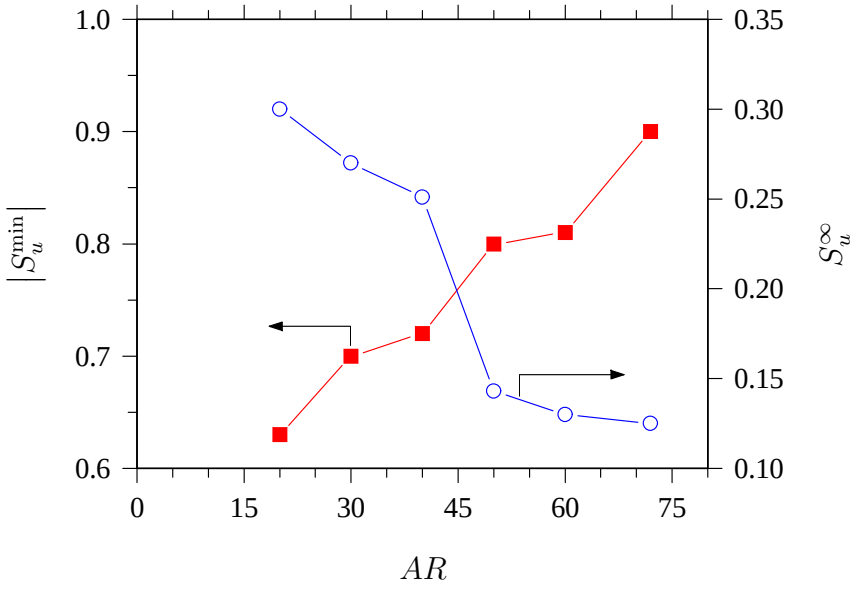

Figure 5.27: The minima $\left|S_u^{\min}\right|$ and far field asymptotic value S_u^{∞} of the centerline skewness factors.

is probably due to the underlying differences in large-scale primary vortices.

The apparent near field humps in centerline turbulence intensity are attributable to the underlying large-scale structures as well. Such humps were also found by Quinn (1992b) for their rectangular jet. The pronounced humps in turbulence intensity were attributed to the presence of a laminar initial boundary layer at nozzle lip (Hill et al. 1976). Based on the initial velocity profiles in the present study, the initial boundary layers are laminar. Thus, it is probable that the movement of the downstream large scale structures is responsible for producing the distinct humps in turbulence intensity, which occurs between 8 and 15 nozzle widths downstream for nozzle aspect ratios between 15 and 72 respectively. It may be that the vortical structures are more coherent and highly organized for a lower aspect ratio e.g. $AR = 15$.

The present data extends the previous plane jet measurements of Bashir and Uberoi (1975) and Van Der Hegge Zijnen (1958) and provides a more complete assessment of nozzle aspect ratio issues. Such data were not available in from published literature. The point of transition from two to three-dimensionality due to the changing aspect ratio has also been explored in the present study.

An influence of aspect ratio in cylindrical wake flows has already been demonstrated. To generate a two-dimensional wake, a cylinder with end plates can be used. The downstream flow of the wake was found to depend on aspect ratio of the cylinder. For example,

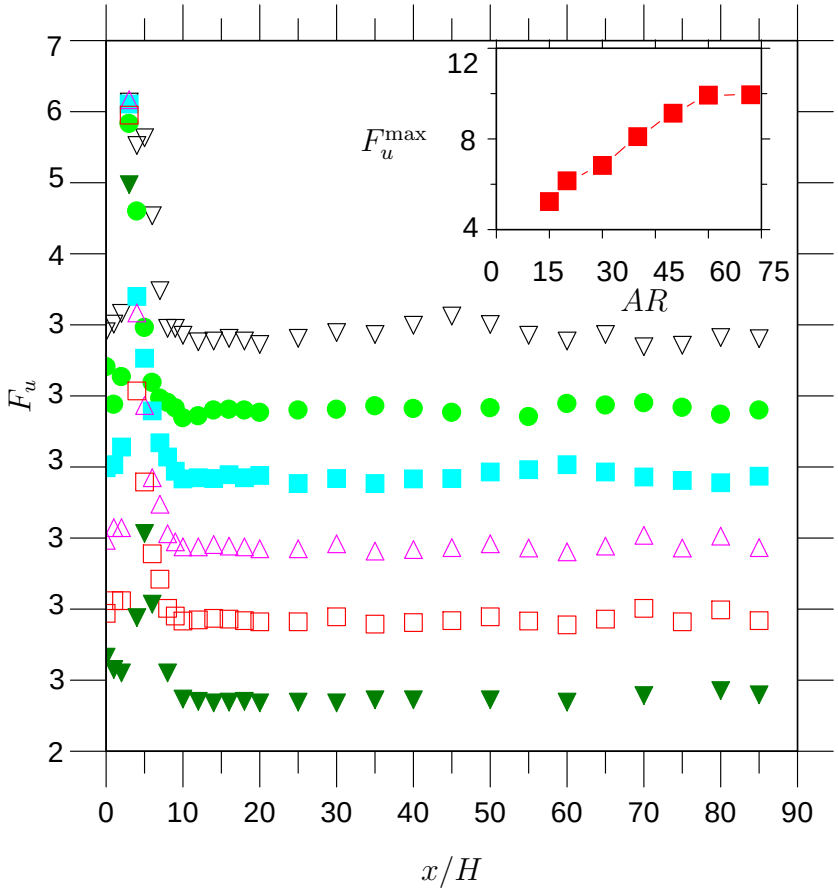

Figure 5.28: The nozzle aspect ratio effect on the centerline flatness F_u factors. The profiles have been shifted by 1. The insert shows the near field maximum values of F_u. Symbols identical to Figure 5.19.

Szepessy and Bearman (1992) stated that the end plates in a cylinder limits its aspect ratio, L/D, where L is the cylinder span length and D is the cylinder diameter. Hence, the use of end plates minimize three-dimensional effects in the wake flow. The flow behind the cylinder is also affected i.e. the wake flow, through a limitation of the crossflow along the cylinder axis near the end plate. Hence, an instability of vortex filaments lead to a shedding of 'cell-like' vortices, either in organized or a random fashion. Nishioka and Sato (1974) studied a circular wake flow at low Reynolds numbers and showed that the onset of vortex shedding does not occur at a universal Reynolds number but is strongly dependent on aspect ratio of the cylinder. In most wake flow experiments, end effects are noticeable beyond 30 body diameters downstream. Such effects contribute to the shedding of vortices which are not two-dimensional but exhibit spanwise variations in strength and location. When aspect ratio is too small, the effects of sidewalls on the jet flow becomes obvious. The flow visualization (pp. 497) of Williamson (1996) shows the dynamics of the two-dimensional vortex shedding induced by different end boundary conditions. An interference of three-dimensional effects in the two-dimensional wake is evident at increased

downstream distance. A similar analogy can be applied to plane jets. For very low aspect ratio, the effect of the boundary layer induced by sidewalls become significant. Hence, increased three-dimensionality due to the merging of the sidewall boundary layer into the jet flow produces an effect on the underlying vortex structures, leading to a change in the mean and turbulence properties of the jet flow.

5.5 Conclusions

In conclusion, the systematic variation in the nozzle aspect ratio over the range $15 \leq AR \leq 72$ has revealed significant variations in flow properties that are directly attributable to nozzle aspect ratio. Specifically, the findings from the present investigation are

(1) The normalized mean exit velocity profiles are all generally top hat for the entire range of nozzle aspect ratios. However, the pseudo-boundary layer thickness of the emerging jet decreases with an increase in nozzle aspect ratio. A significant change in its thickness is noted for $AR = 15$ and 20.

(2) A coupled dependence between the initial velocity profiles and nozzle aspect ratio was found. In particular, for $AR = 15$ and 20, the top hat region spans over $|\xi| \leq 0.40$ while for $AR \geq 30$, it spans over $|\xi| \leq 0.45$. The initial turbulence intensity shows a dependence on AR. For $AR = 15$ and 20, the central region turbulence intensity is approximately 1 % while for $AR \geq 30$ it is approximately 2 %. Such a difference is also evident for the shear layer turbulence intensity (i.e. for $AR = 15$ and 20, the shear layer turbulence intensity is $\simeq 13$ %, while for $AR \geq 30$, it is reduced at 5 %).

(3) The potential core of the jet changes with nozzle aspect ratio. As AR is increased from 15 to 72, the length of the jet potential core increases from $2H$ to $5H$.

(4) The decay rates of the centerline mean velocity and jet spreading rates are dependent on nozzle aspect ratio. The velocity decay rate, K_u, calculated over the axial range $20 \leq x/H \leq 45$, increases from 0.125 to 0.181 as AR is increased from 30 to 72 and the spreading rate, K_y increases from 0.055 to 0.112 as AR is increased from 15 to 72. Also, the effect of nozzle aspect ratio on the mean flow seems to persist, even at $AR = 72$.

(5) The axial extent of a plane jet over which a planar flow exists, is found to depend strongly on the nozzle aspect ratio. The $AR = 15$ jet does not have a significant

planar region. This indicates that for $AR \leq 15$, the jet becomes statistically three-dimensional due to the end wall effects even in the near field. For $AR \geq 20$, the jet is statistically two-dimensional but only between $5 \leq x/H \leq 20$. The maximum planar axial distance to which the jet is planar varies almost linearly with aspect ratio.

(6) An increase in the critical jet aspect ratio $AR_{jet,crit}$ with an increase nozzle aspect ratio AR immediately prior to the point of three-dimensionality was noted for $AR < 30$. For $AR \geq 30$, $AR_{jet,crit}$ attains a constant value of around 0.15. Furthermore, it is evident that the critical half-width of the jet $y_{0.5,crit}$ and spacing between the sidewalls (w) determine where the transition from 2-D to 3-D flow occurs.

(7) Lower aspect ratio leads to an enhanced hump in the locally normalized centerline turbulence intensity. The hump disappears as the aspect ratio is increased. For instance, $AR = 15$, $u'_{c,\max} \simeq 0.23$ while for $AR = 72$ $u'_{c,\max} \simeq 0.21$. There is an insignificant difference in $u'_{c,\max}$ between AR 50 and 72 but the trend with further increase in AR cannot be stated with certainty, given our limited range of aspect ratios. However, a lower Reynolds number or a different nozzle profile with a smaller r^* will produce a hump even at a very high nozzle aspect ratio.

(8) The position x_m of the near field hump in turbulence intensity $u'_{c,\max}$ changes its axial location as nozzle aspect ratio is varied. Hence, as AR is increased from 15 to 72, x_m changes from 8 to 15.

(9) The location and the magnitude of the far field asymptotic values of the turbulence intensity depends on nozzle aspect ratio. For $AR = 20$, the turbulence intensity asymptotes for $x/H \geq 45$ with a magnitude of $u'_{c,\infty} \simeq 0.15$. On the other hand, $AR = 30$ shows $u'_{c,\infty} \simeq 0.18$ occurring at $x/H = 50$. Likewise, for $AR \geq 50$, the turbulence intensities asymptote to different values but at a location of $x/H \geq 60$. The magnitudes of asymptotic values are consistent with the results of Bashir and Uberoi (1975), who also noted that lower aspect ratios produce smaller asymptotic values.

(10) It is deduced that a growth of boundary layer on sidewalls affects the turbulence intensity. This effect appears to be greater for the low aspect ratio plane jet . For example, the locally normalized turbulence intensity of the $AR = 15$ jet does not asymptote at all, while for the $AR = 20$ jet, turbulence intensity asymptote at $x/H = 45$, but then vary slightly at a larger axial distance. For the present range of

aspect ratios, the turbulence field is not influenced by the sidewalls for $AR \geq 50$ up to $x/H = 85$.

The boundary layer induced by the sidewalls, and its subsequent increase in thickness with axial distance is quite complex. With changes in nozzle aspect ratio, the influence of the wall boundary layer, on the jet flow, changes. Thus, this effect is difficult to counter with non-parallel sidewalls.

Chapter 6

EFFECT OF SIDEWALLS

6.1 Introduction

Sidewalls are a practical requirement for obtaining a plane jet (Pope 2002). They force a jet to entrain and/or mix the ambient fluid only in the direction normal to the long-sides of the rectangular nozzle. No entrainment and/or mixing can take place in the direction normal to the short-sides. As stipulated in Chapter 1.5.4, a large body of literature has examined both a free rectangular jet, without sidewalls and a plane jet, with sidewalls. A free rectangular jet is a jet that issues through a large aspect ratio rectangular nozzle (no sidewalls). This has a two dimensional region for a limited axial extent. A plane jet has a longer two-dimensional region than a free rectangular jet if both have the same nozzle aspect ratios.

To our best knowledge, Hitchman's (1990) investigation of a free rectangular and a plane jet is the only published data available to compare the differences in flows from these two configurations using identical facilities. Hitchman's work showed a decrease in the centerline velocity decay and an increase in the growth (spreading) rate of their free rectangular jet relative to their plane jet. It is surprising to note these significant inconsistencies between the centerline velocity decay and jet spreading rate of the two configurations. Unfortunately, their data are very limited and present only the mean velocity field. No measurement of the fluctuating velocity field was made. Thus, a more comprehensive study of a free rectangular and a plane jet is required to provide more insight into the differences in the flow field between these two configurations.

Sidewalls are believed to affect the relative entrainment of ambient fluid, both in the near and far field (Figure 1.17). The absence of sidewalls are known to produce three-dimensional effects both in the near and far field. It was already shown e.g. Mi et al.

(2005b) that a rectangular jet (no sidewalls) maybe characterized by three distinct zones: (1) an initial quasi-planar-zone (2) a transition zone and (3) a final axisymmetric-jet-zone. Thus, the present study is undertaken not only to extend the study by Hitchman et al. (1990) but also to investigate and compare the extent of the three zones that are believed to exist in a free rectangular jet using the same experimental facility.

6.2 Experiment Details

To investigate the influence of the sidewalls on the flow from a rectangular nozzle, jets were tested using the experimental arrangement in Figure 3.1. The two jets were produced from the same nozzle but configured with and without sidewalls. These are referred to as the free rectangular and the plane nozzle, respectively. The nozzle has an inner-wall nozzle contraction profile of $r^* \simeq 2.14$ and a nozzle aspect ratio AR of 60. The wind tunnel fan was set to a jet exit Reynolds number based on the nozzle opening width H, exit centerline velocity $U_{o,c}$ and the kinematic viscosity of air ν of $Re_H = 7{,}000$. Firstly, the initial velocity profiles in the centerplane ($z = 0$) at an axial location of $x = 0.5H$ were measured for both jets. It was found that both jets have an approximate top hat exit velocity profile. The boundary layers at the nozzle exit are laminar, with a shape factor H of 2.04. The centerline streamwise velocity was also measured from $x/H = 0$ to $x/H = 160$. Then, the lateral distribution of the streamwise velocity was measured at selected downstream locations.

6.3 Results and Discussion

6.3.1 The Mean Velocity Field

Figure 6.1 presents the centerline profiles of the normalized mean velocity for the free rectangular and the plane jet, displayed on a logarithmic scale. The present data are obtained for (Re, AR) = (7,000, 60) both for the free rectangular and plane jet and (Re, AR) = (30, 10,000) only for the free rectangular jet. Note that for the free rectangular jet, the data for $AR = 30$ is later used to assess an aspect ratio effect on the two-dimensional region, if any.

The nozzle opening width H rather than the equivalent diameter D_e is used to normalize the abscissa. The choice of H over D_e is important and must be acknowledged. The present study compares data from a free rectangular and a plane jet. In the initial quasi-plane-jet zone, the behaviour of both jets will be similar and statistically two-dimensional. Using H as the scaling parameter will allow one to compare the jet properties e.g. decay,

spreading etc more appropriately. The use of D_e is relevant only for a free rectangular jet when it has transformed into a round jet in the far field. If D_e is used for a free rectangular jet, the scaling will only be appropriate strictly in the far field where an axisymmetric-jet behaviour is displayed (as shown later). Also importantly, the equivalent diameter D_e is more appropriate to act as a length scale to characterize the rectangular (three-dimensional) jets only e.g. Quinn (1992b), Mi et al. (2005b) etc.

For reference, we have included the data of Quinn (1992b) for his free rectangular jet. The shape of Quinn's and the present plot for a free rectangular jet is similar. The present free rectangular jet (of nozzle aspect ratio 30 and 60) exhibits a potential core region where U_c is constant and equal to $U_{o,c}$, a quasi-two dimensional zone where $U_c \sim x^{-0.5}$ and a final axisymmetric-jet-zone where $U_c \sim x^{-1}$. In contrast, the plane jet demonstrates a potential core region and a two-dimensional region.

It is essential to elaborate on the differences between the present free rectangular and plane jet. In particular, the length of the potential core x_p is about $x_p \simeq 4H$ for the free rectangular and about $6H$ for the plane jet using the same nozzle. Thus, it is shown that in the near field, the mean velocity decays more rapidly for the free rectangular jet. This also suggests an increase in entrainment of ambient fluid for the free rectangular jet. After the potential core region, the mean centerline mean velocity profile becomes self-similar with the following dependence $U_c \sim x^{-0.5}$, where the exponent of 0.5 is a characteristic of a statistically two-dimensional jet. The two-dimensional region extends up to $x/H = 160$ for the plane jet. Conversely, for the free rectangular jet, this region extends only up to $x/H = 40$ for the same nozzle. Thus, without sidewalls, the free jet behaves like a quasi-planar jet up to 40 nozzle widths downstream and three-dimensional effects begin to dominate beyond this location. While the data of Quinn (1992a) support our deduction, he did not present his data on a logarithmic scale. Hence, he was unable to determine the extent of his quasi-planar zone or his point of transition to three-dimensionality.

For two free rectangular jets of nozzle aspect ratio 30 and 60, the axial positions of their transition from a two-dimensional to a three-dimensional jet occur at $x/H \simeq 30$ and 40 respectively. Thus, an effect of nozzle aspect ratio on two-dimensionality is demonstrated. That is, a larger nozzle aspect ratio leads to a longer two-dimensional region. On the spreading rates of a rectangular jet, Tsuchiya et al. (1985) showed that a smaller nozzle aspect ratio exhibits increased three dimensionality at a shorter axial distance. In our recent measurements for a rectangular jet presented by Mi et al. (2005b), we also noted

that, as nozzle aspect ratio is increased from 15 to 120, the extent of the quasi-planar zone increased. The transition zone occurs between $30 \leq x/H \leq 80$ and $40 \leq x/H \leq 150$ for our free rectangular jets measured at $AR = 30$ and 60 respectively. This proves, unambiguously, that the transition point appears earlier i.e. at $x/H \simeq 30$ for a low nozzle aspect ratio jet. Thus, the present investigation proves that as nozzle aspect ratio decreases, the transition point where three-dimensional effect first emerge moves upstream.

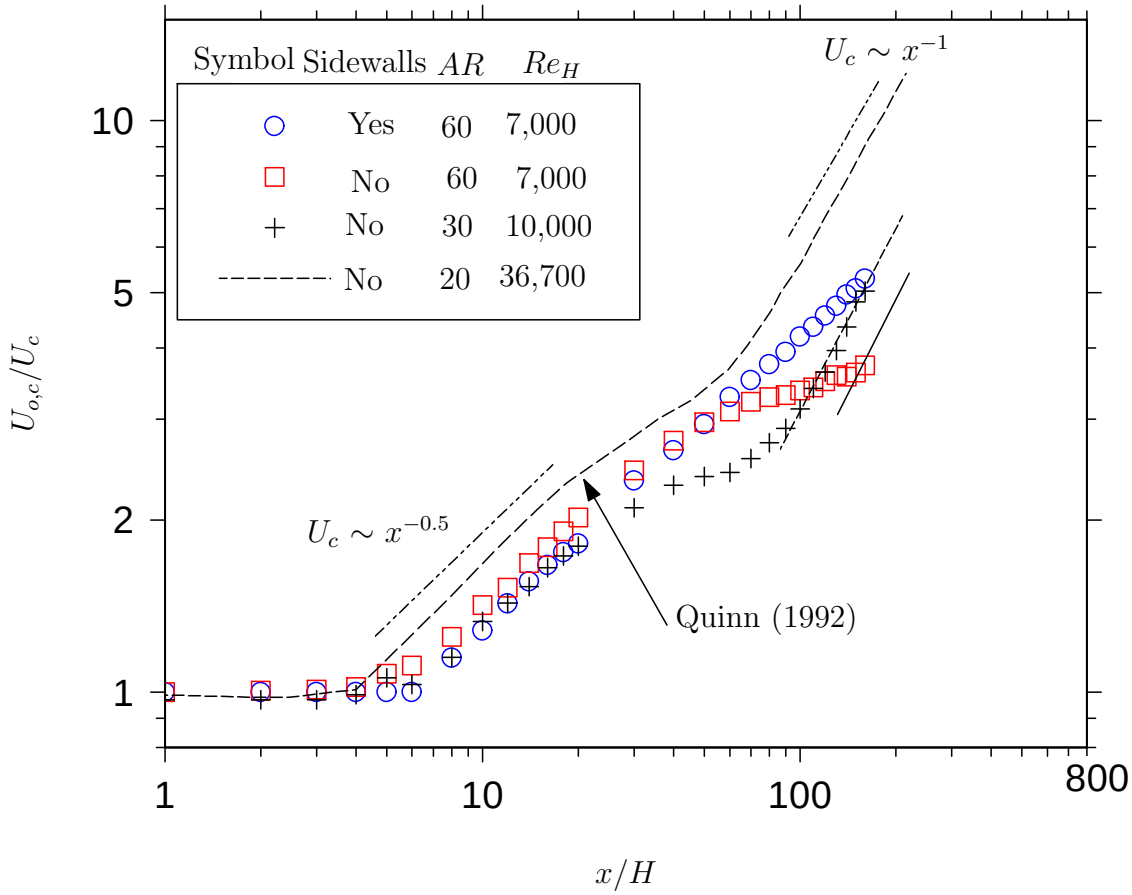

Figure 6.1: The centerline mean velocity variation $U_{o,c}/U_c$ for a free rectangular jet (without sidewalls) and a plane jet (with sidewalls) on a logarithmic scale. The data of Quinn (1992a) for his free rectangular jet is shown.

After the transition region, the centerline mean velocity for our free rectangular jet decays in a manner similar to that of a round jet. That is, $U_c \sim x^{-1}$ downstream from the transition region, i.e. from $x/H > 80$ for $AR = 30$ and for $x/H > 150$ for $AR = 60$ respectively. This linear dependence resembles that of a round jet. However, this does not necessarily imply that the free rectangular jet has transformed completely into a round jet. Nevertheless, based on the present data, we conclude that the free rectangular jet behaves statistically like a round jet beyond the transition zone. In fact, Sfeir (1976)

measured the velocity and temperature field of a free rectangular jet and found that at large axial distances, its centerline velocity decay behaves similar to that of a circular jet. Thus, our measured far field relationship of $U_c \sim x^{-1}$ is well supported by published literature.

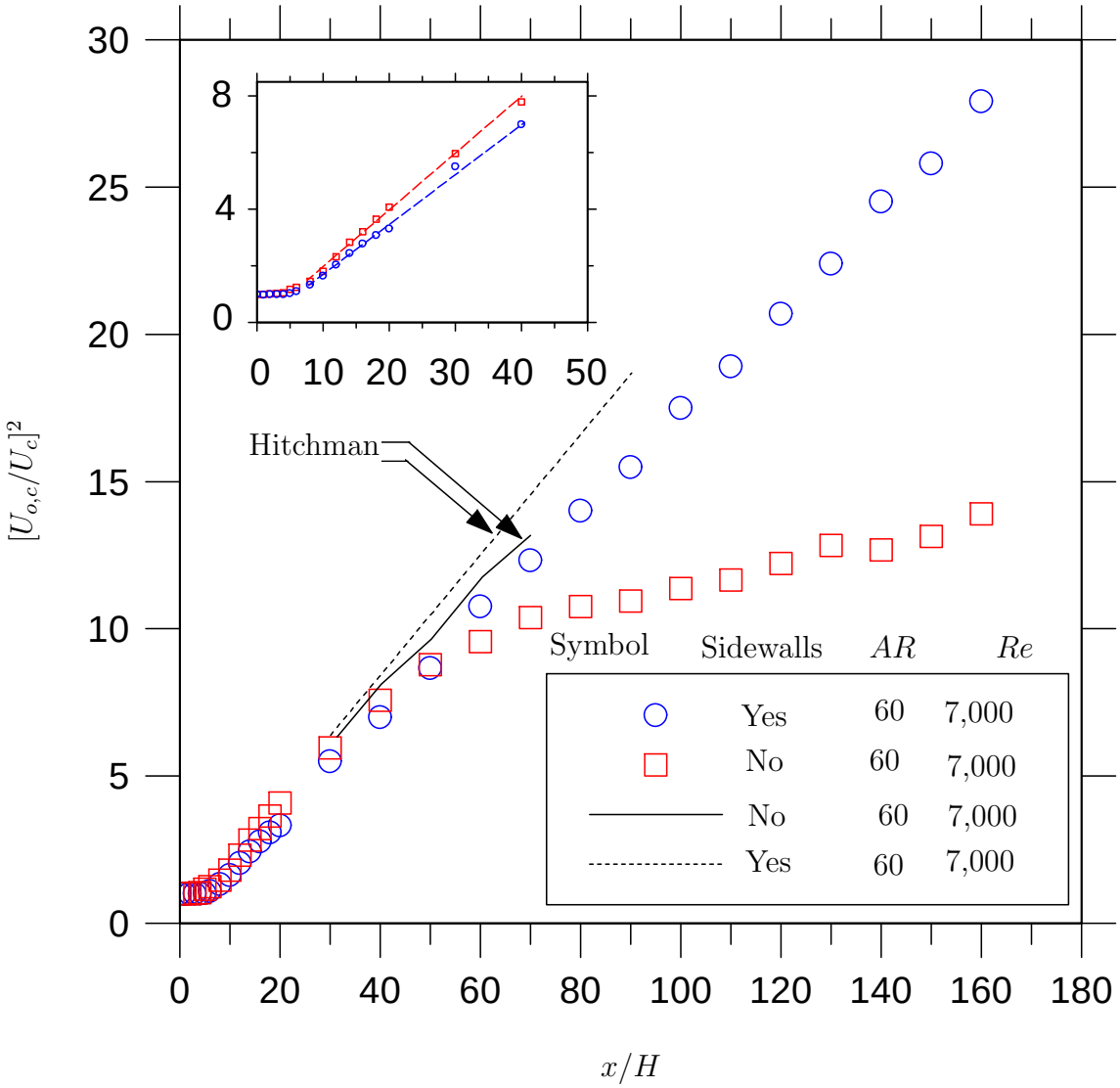

Figure 6.2: The centerline variation of the normalized mean velocity $(U_{o,c}/U_c)^2$ in the inverse square form for the free rectangular and plane jet.

More attention is now given to the two-dimensional region of the free rectangular and plane jet. To quantify the decay rates of centerline mean velocity for the present free rectangular and plane jets within their planar zones, the normalized centerline mean velocity is presented in the inverse square form in Figure 6.2. For clarity, the near field data ranging from $x/H = 0$ to $x/H = 40$ is inserted. In fact, the presentation of the normalized centerline mean velocity in the inverse square form is often taken as a test for

two-dimensionality (Pope 2002). That is, if $U_c \sim x^{-0.5}$ in a particular region, then the jet is considered to be statistically two-dimensional (Pope 2002). Thus, Figure 6.2 plots $(U_{o,c}/U_c)^2$ versus x/H for the free rectangular and plane jet. As evident from this figure, the free rectangular jet is characterized by $U_c \sim x^{-0.5}$ in the range $8 \leq x/H \leq 40$ and the plane jet is characterized by $U_c \sim x^{-0.5}$ in the range $8 \leq x/H \leq 160$. Note the divergence of $(U_{o,c}/U_c)^2$ from the linear relation for $x/H > 40$ for the free rectangular jet is deduced to be due to three-dimensional effects.

The relative magnitudes of decay rate of the centerline mean velocity K_u are now compared. The difference between the decay rates of the two jets is approximately 15 %. That is, within the two-dimensional region, $K_u \simeq 0.20$ for the free rectangular jet while for the plane jet, $K_u \simeq 0.17$. Thus it is evident that, although, both jets demonstrate a two-dimensional region, there are statistical differences between their decay rates of the centerline mean velocity. In other words, the behaviour of both jets are similar but not identical within the two-dimensional region. This finding is, again, consistent with Mi et al. (2005b). The virtual origin x_{01} is also different for the two cases. For the free rectangular jet, $x_{01} \simeq$ -0.19, whereas for the plane jet, x_{01} is -4.57. Thus, it is likely that a plane jet has a longer potential core and poorer near field entrainment of the ambient fluid relative to a free rectangular jet.

The trends in K_u for the present investigation differ from those found by Hitchman et al. (1990). Our K_u of 0.20 for free rectangular jet differs by 10 % from the K_u of 0.18 obtained by Hitchman et al. (1990) for their free rectangular jet. Likewise for the present plane jet, we found a K_u of 0.17 while Hitchman et al. (1990) found a K_u of 0.20 for their plane jet. More significantly, the trends in the magnitude of K_u of Hitchman et al. (1990) also conflict those found in the present investigation. That is, Hitchman found a lower decay of centerline mean velocity for the free rectangular jet than for the plane jet, while we found the opposite trend. In general, a free rectangular jet does not have sidewalls so that its centerline velocity decay is expected to be higher than the plane jet which has sidewalls, as found by the present results. The cause of the opposite trend of Hitchman et al. (1990) is not known.

Figure 6.3 displays the streamwise variation of the normalized mean velocity half-width $y_{0.5}$ for the free rectangular and plane jet. The nominal spreading rates of the two jets are compared using the relative magnitudes of the slope (i.e. using the values of K_y). Evidently, the free rectangular jet spreads at a rate of about 24 % higher (with $K_y \simeq 0.14$)

than the plane jet (with $K_y \simeq 0.11$). Taken together, Figures 6.2 and 6.3 are internally consistent since they find that the free rectangular jet decays and spreads at a greater rate than the plane jet. Surprisingly, Hitchman et al. (1990) found that the decay rate of their free rectangular jet was lower than that of their plane jet ($K_u = 0.170$ for free rectangular versus 0.200 for plane). In contrast to the trend for the decay rate of centerline mean velocity, they found that the spreading rate of their free rectangular jet was higher than the plane jet ($K_y = 0.110$ for free rectangular versus 0.108 for plane). This inconsistency questions the validity of their data.

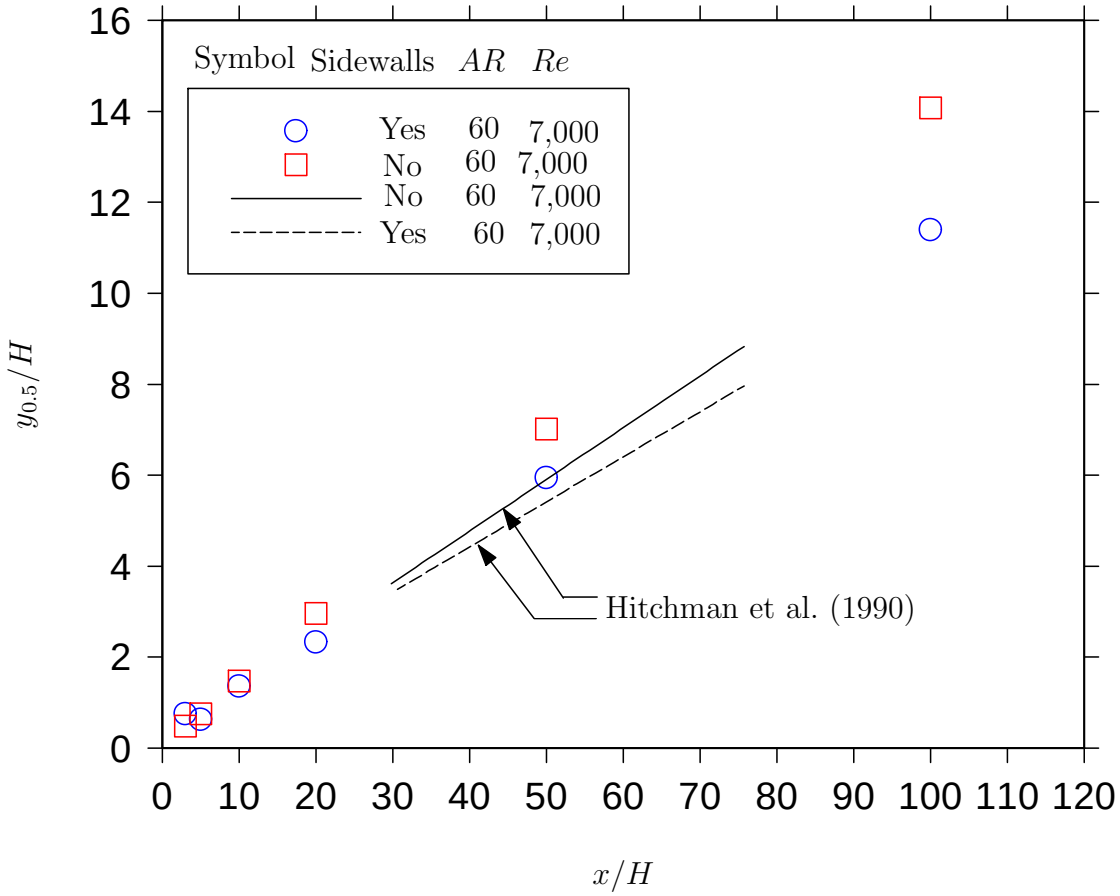

Figure 6.3: The streamwise variation of the velocity half-width $y_{0.5}$ for the free rectangular and plane jet.

The virtual origins x_{02}/H of the velocity half-widths are found to be -0.83 for the free rectangular and -1.71 for the plane jets respectively.

6.3.2 The Fluctuating Velocity Field

The streamwise variation of the centerline turbulence intensity $u'_{n,c}$ are presented in Figure 6.4 for $AR = 60$ and for previous investigations. Between the region $0 \leq x/H \leq 12$, a

monotonic increase in $u'_{n,c}$ with x/H is found for all jets. This initial monotonic increase is typical of a plane jet. The relative magnitudes of $u'_{n,c}$ for the present plane jet is slightly higher than the present free rectangular jet at every axial distance. This indicates that the sidewalls have an effect, even on the near field centerline turbulence intensity. The present evolutions of $u'_{n,c}$ for the plane jet are similar to those of Browne et al. (1982) and Antonia et al. (1980) and of the free rectangular jet of Quinn (1992a). The shape of our trend in near field turbulence intensity for the plane jet is also similar to that of Browne et al. (1982). The far field turbulence intensity compares well with Antonia et al. (1980). In particular, a near field hump in present $u'_{n,c}$ is present for both Browne et al. (1982) and the present investigation. Subtle differences in the magnitude of the hump are attributable to the differences in experimental conditions, e.g. Reynolds number, nozzle aspect ratio and nozzle geometry. For the free rectangular jet, the present data shows a similar trend to the data of Quinn (1992b) for his free rectangular jet from a nozzle. Note the similarity in the shape of the centerline turbulence intensity profile for both cases with particular attention to the 'dip' in the graph around $x/H = 60$ which occurs for both investigations.

A distinct hump $u'_{c,\max}$ in present turbulence intensity for the present flows is found near to $x/H = 12$. As mentioned above, Browne et al. (1982) and Quinn (1992a) also encountered a hump in $u'_{n,c}$ at the same location. Browne et al. (1982) classified this region as the beginning of the interaction zone. The counter-rotating streamwise vortices from both sides of the shear layers interact, merge and pair up in this zone (see Figure 3.30). The instabilities associated with the merging and/or pairing of vortices produce significant velocity fluctuations. The occurrence of a larger $u'_{c,\max}$ for the plane jet ($u'_{c,\max} \simeq 0.24$) than for the free rectangular jet ($u'_{c,\max} \simeq 0.22$) implies more coherent, organized and/or periodic motions for the former case. As deduced from Figure 3.30 and other sources, vortices grow as they move downstream from the nozzle exit towards the interaction region. Hence, they must merge or collide within this zone. The near field peak in turbulence intensity $u'_{c,\max}$ is likely to be generated by such collisions of large scale vortices from both sides of the jet. (Rockwell and Nicholas 1973).

For $x/H > 12$, the centerline turbulence intensity reduces dramatically for the free rectangular jet while it remains approximately constant for the plane jet. Specifically, for the plane jet, $u'_{n,c}$ asymptotes to around $u'_{c,\infty} \simeq 0.22$ for $x/H \geq 30$. Browne et al. (1982) measured a plane jet at (Re, AR) = (7,000, 20) and found an asymptotic value of $u'_{c,\infty} \simeq 0.19$. Antonia et al. (1980) found their u'_n to asymptote at 0.20 for a plane jet. In the

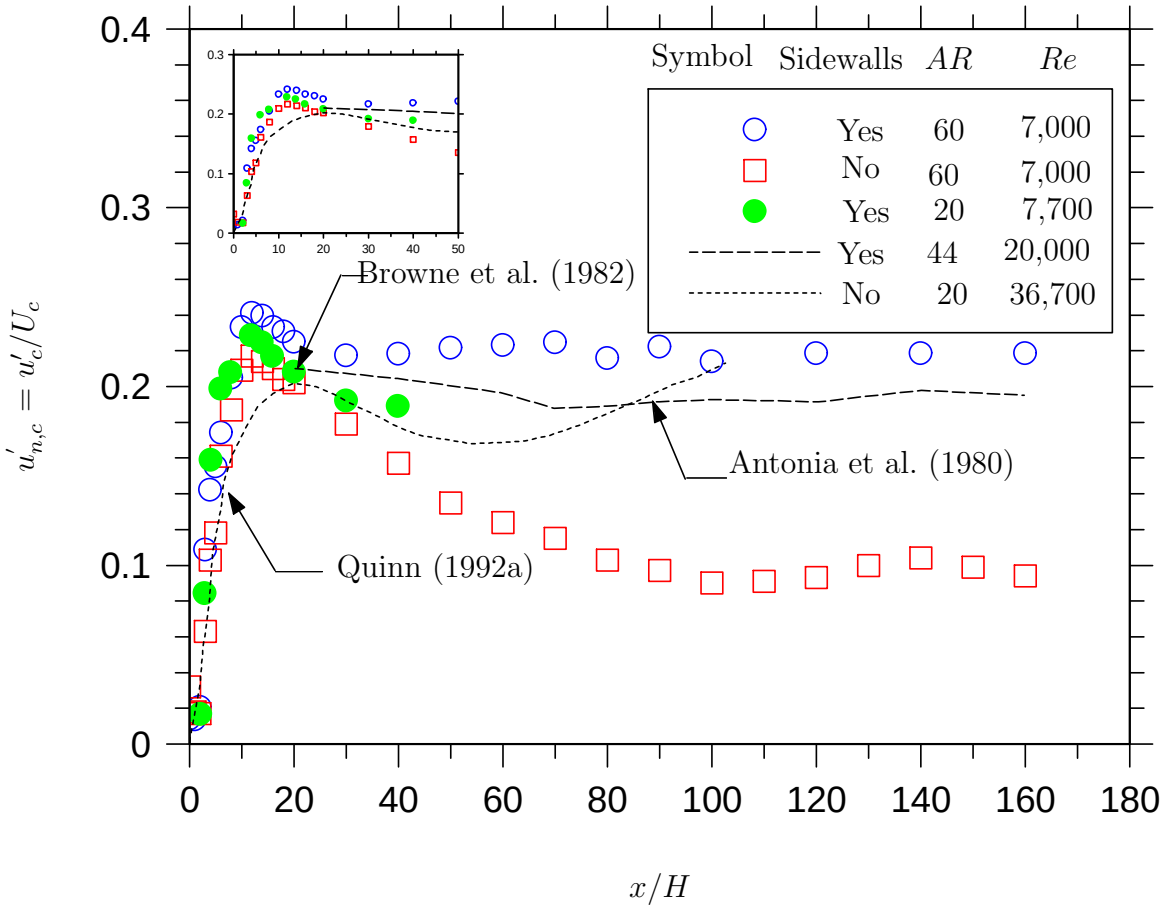

Figure 6.4: Evolutions of the centerline turbulence intensity $u'_{n,c}$ for free rectangular and plane jet. The inserted figure shows the close-up view for the near field.

latter, (Re, AR) = (20,000, 44). The differences in the present and previous asymptotic $u'_{c,\infty}$ are attributable to the differences in aspect ratios and Reynolds numbers. Chapter 3 finds that a higher Reynolds number leads to a lower asymptotic value of the centerline turbulence intensity. Also noted in Chapter 5, was a reduction in the centerline asymptotic turbulence intensity with reduced aspect ratio nozzle. Conversely, for the present free rectangular jet measured at (Re, AR) = (7,000, 60), $u'_{n,c}$ decreases for $x/H > 12$ to a local minimum $u'_{n,c} \simeq 0.10$ which occurs around $x/H \simeq 100$. It is clear from Figure 6.4 that the asymptotic values of centerline turbulence intensity for the free rectangular jet are approximately half that of the plane jet. Furthermore, the trends in $u'_{c,\infty}$ noted by Quinn (1992a) for his free rectangular jet measured at (Re, AR) = (36,700, 20) are similar to our free rectangular jet. In particular, his local minimum in the magnitude $u'_{n,c}$ ~ 0.17 occurred around $x/H \simeq 50$. Again, the deviation of the present local minimum in $u'_{n,c}$ from that of Quinn (1992a) is likely to be caused by the differences in experimental conditions i.e. Reynolds number and nozzle aspect ratio.

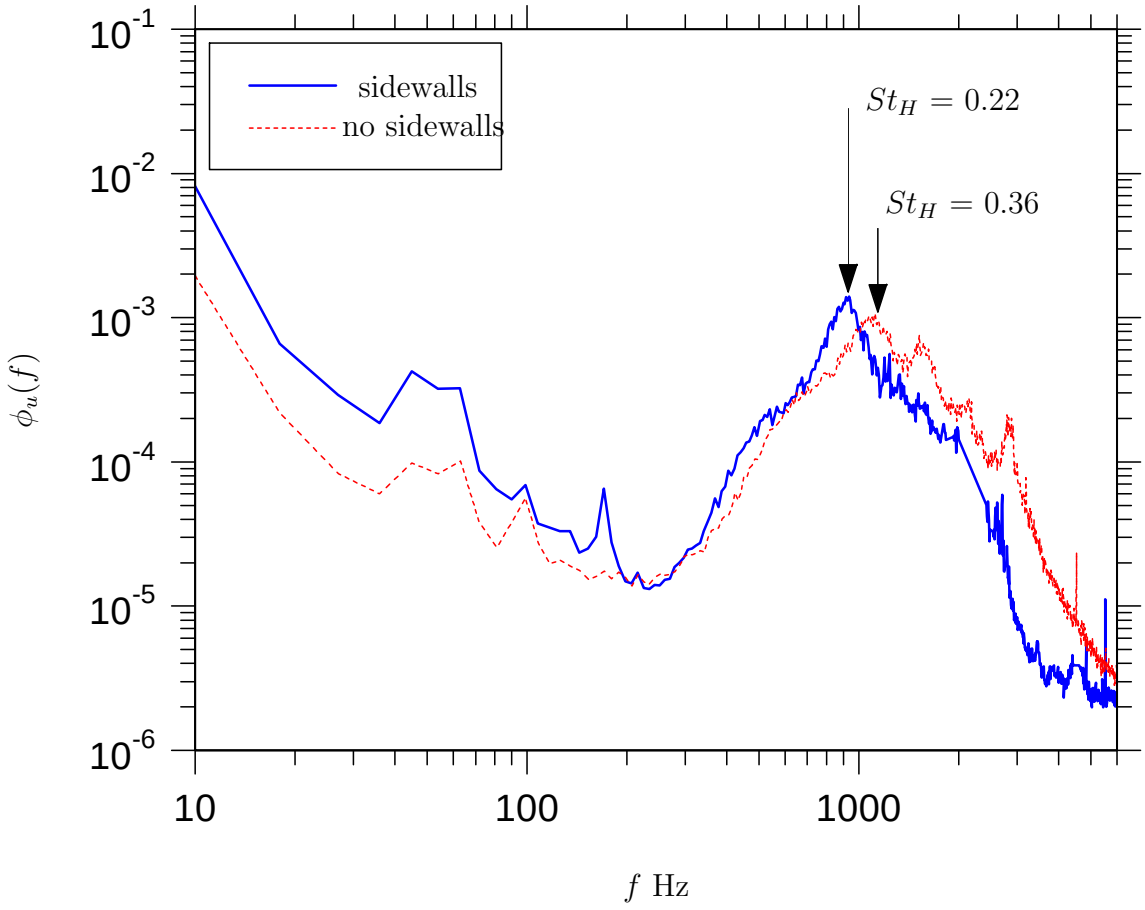

Figure 6.5: Power spectra ϕ_u of the centerline velocity fluctuations u at $x/H \simeq 3$ showing the normalized vortex shedding frequency.

Figure 6.5 represents the power spectra of velocity fluctuations at $x/H = 3$ for both jets. These clearly demonstrate that the peak frequency differs for the free rectangular and plane jets. The peak dominant frequency characterizes the motions of the large-scale vortices. A higher frequency peak is evident for the free rectangular jet with a normalized vortex shedding frequency St_H of 0.36 in contrast to a St_H of 0.22 for the plane jet. A larger St_H for the free rectangular jet indicates a higher rate of vortex formation. It is also evident that the spectrum of the free rectangular jet exhibits a multi-modal behaviour with four distinct peak frequencies. While the exact cause of such multi-modal behaviour is not known, these modes are usually classified to be harmonics which are typical of the convective instability of the jet.

Figure 6.6 examines the centerline evolutions of the skewness and flatness factors of the free rectangular and plane jets. Over the range $0 \leq x/H \leq 20$, almost identical magnitudes of S_u and F_u are noticeable, with S_u displaying a local maximum at $x/H = 4$ and a local

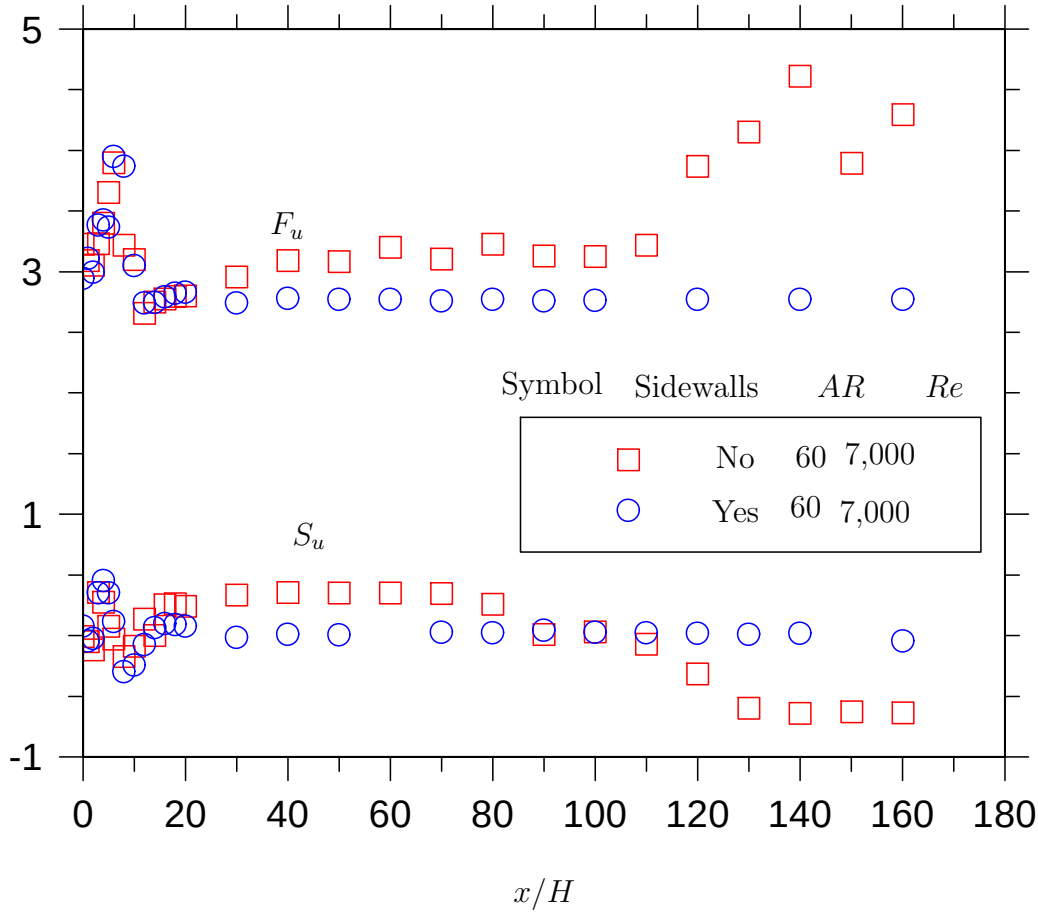

Figure 6.6: The sidewall effect on the centerline skewness S_u and the centerline flatness F_u factors.

minimum at $x/H = 8$. The minimum in S_u at $x/H = 8$ corresponds to the maximum in F_u at the same location. Such evolutions of S_u and F_u are typical of a plane jet, and are noted in previous chapters of the thesis. For $x/H > 80$, S_u and F_u vary dramatically for the free rectangular jet, while for the plane jet, S_u and F_u appear to be a constant. In particular for the free rectangular jet, (S_u, F_u) 'appears to asymptote'[1] to values close to ($S_u^{c,\infty}$, $F_u^{c,\infty}$) = (0.30, 3). This occurs over the range $30 \leq x/H \leq 80$. Within this region, slightly different asymptotic values of ($S_u^{c,\infty}$, $F_u^{c,\infty}$) = (0.03, 2.70) are found for the plane jet. The difference in $S_u^{c,\infty}$ and $F_u^{c,\infty}$ arise due to the differing nature of the free rectangular and plane jets.

While the S_u and F_u of the plane jet continue to asymptote for $x/H > 80$, this does not happen for the free rectangular jet. That is, both factors diverge to entirely non-Gaussian values for $x/H > 100$ for the free rectangular jet. Such significant divergence of

[1]'appears to asymptote' is used because the skewness and flatness of the free rectangular jet may diverge with increased three-dimensionality when the jet assumes a round-jet character.

both factors clearly indicate that the free rectangular jet transforms into totally different flow. More specifically, it transforms into a round jet as discussed earlier e.g. Figure 6.1.

6.4 Further Discussion

Previous studies on rectangular jets found that if the nozzle aspect ratio is sufficiently large, then the mean flow remains statistically two-dimensional up to a reasonable axial distance (Gouldin et al. 1986). Such a notion is also supported by the present measurements of a free rectangular jet. The present free rectangular jet measurements of AR = 30 and 60 have shown the nozzle aspect ratio determines the extent of the statistically two-dimensional region. A smaller two-dimensional region exists for a lower nozzle aspect ratio. It is deduced that beyond the statistically two-dimensional region, three-dimensional effects dominate.

Previous free rectangular jet investigations of nozzle aspect ratio 56 and 44 by Namar and Ötügen (1988) and Hussain and Clark (1977) respectively, showed an existence of a two-dimensional region up to 120 nozzle widths for Namar and Ötügen (1988) and 40 nozzle widths for Hussain and Clark (1977). However, our studies have shown that the entire flow statistics are affected by the presence or absence of sidewalls even in the near field where the statistically two-dimensional flow exists. Namar and Ötügen (1988) provided velocity measurements at $x/H = 1$ and 25 along the spanwise direction (z) to justify the existence of a two-dimensional region. They noted that the jet discharge velocity was uniform over the middle two-third sections of the nozzle. Indeed, our measurements of the centerline velocity is no different to theirs in providing evidence for the existence of a two-dimensional region. Further downstream, three-dimensional effects emerge. However, although they did not check the two-dimensionality till $x/H = 100$, it is surprising to note that their centerline mean velocity varies as $U_c \sim x^{-0.5}$ up to 100 nozzle widths downstream. On the other hand, the present data showed that the decay of centerline mean velocity is not identical for free rectangular and plane jets. Thus, Namar's data cannot be directly compared with a plane jet. The present work has also extended the findings of Hitchman et al. (1990) who studied the effect of sidewalls. However, theirs was a less comprehensive study which provided only the mean velocity data. Hence, the present work has added new data for a free rectangular and a plane jet.

In the present study, increased decay of centerline mean velocity and jet spreading rates, both in the near and the far field were noted for a free rectangular jet relative to a plane

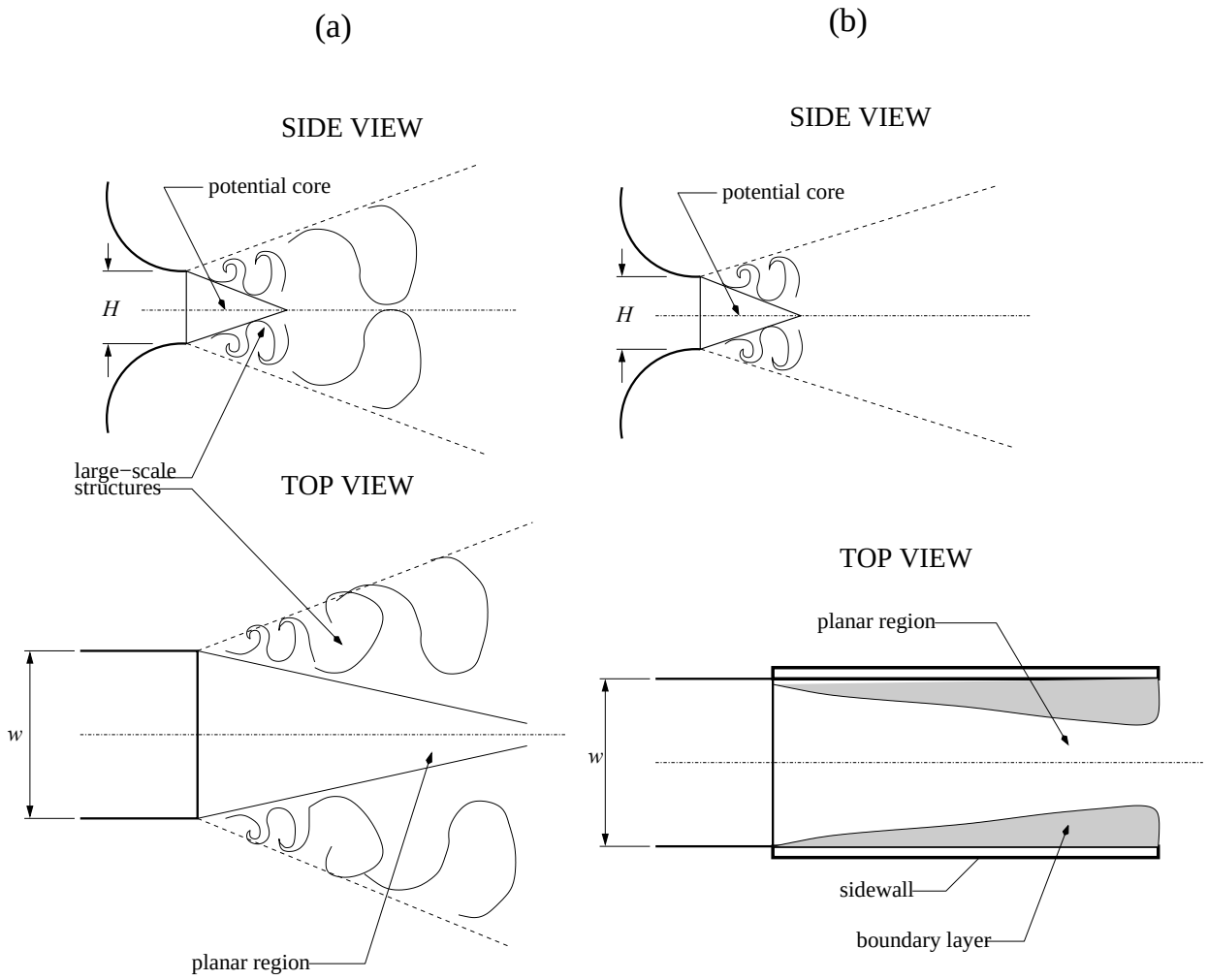

Figure 6.7: Side and top views of the typical flow field of (a) a free rectangular jet and (b) a plane jet.

jet. The significant point is that, although both configurations demonstrate a statistically two-dimensional flow, the near field decay and spreading rates of both configurations are different. This, itself, shows the strong dependence of the jet flow on sidewalls. In particular, the higher decay rate of centerline mean velocity and increased spreading rates can be explained using Figure 6.7. This shows schematic views of the typical flow field obtained from a free rectangular and a plane jet. It is deduced that a free rectangular jet encounters more three-dimensional effects induced by the merging of the large-scale vortical structures emanating from both sides of the shear layers via the spanwise directions, (Figure 6.7a: top view). In contrast, a plane jet (Figure 6.7b: top view) shows that the growth of vortices via the spanwise directions are prohibited by the sidewalls. Thus, the large-scale 'folding motions' which originate along the spanwise directions of the nozzle, entrain the ambient fluid more effectively for a free rectangular jet relative to a plane jet which does not encompass such large-scale 'folding motions'. The restricted flow of

ambient fluid will reduce the decay rate of mean velocity and spreading rate of the plane jet.

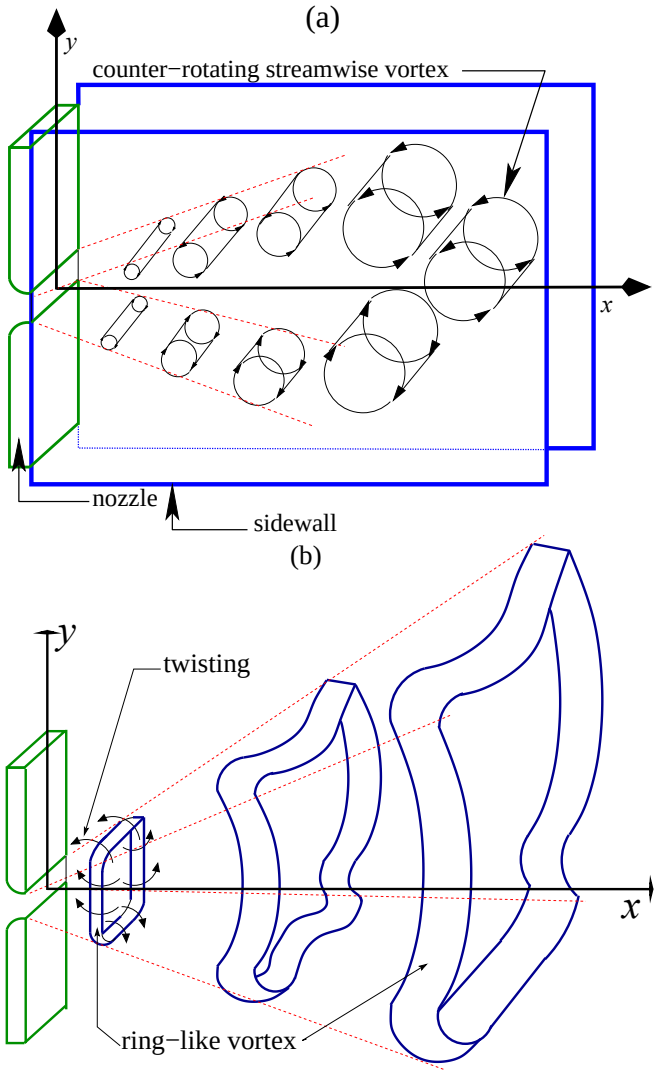

Figure 6.8: A schematic view of (a) counter-rotating streamwise vortices in a plane jet (b) primary ring-like vortices in a free rectangular jet.

The turbulence field for free rectangular and a plane jet differs significantly. In particular, the magnitude of the near field hump in turbulence intensity differ, possibly owing to the underlying differences in the vortex structures for the two configurations. It is well known that a plane jet contains counter-rotating streamwise vortices, emanating from both sides of the shear layers of the jet (Browne et al. 1984, Schultz-Grunow 1981). These streamwise vortices roll-over, merge and pair up as they enter the interaction zone (approx. $x/H > 12$). By contrast, the free rectangular jet comprise of primary ring-like vortices that undergo substantial twisting and turning as they propagate downstream (Sfeir 1976). To

compare the differences, Figure 6.8 demonstrates a schematic view of the two types of possible vortex structures in a free rectangular and plane jet. Particular emphasis should be given to the primary-ring like vortices present in a free rectangular jet. These are initially inter-connected along the spanwise (z) and transverse (y) directions of the rectangular nozzle. In the immediate near field (say $x/H \leq 10$), the ring-like vortices undergo substantial twisting and turning, due to an initial increase in spreading rate along the short sides of the nozzle. Hence, the ring-like vortex structures for the free rectangular jet are more three-dimensional than the two-dimensional symmetric roller vortex structures present in a plane jet. As the ring-like vortices move downstream, they change their shape, get distorted and destroyed. In their high speed photographic experiments, Trendscoste and Sforza (1967) described the characteristic decay of a three-dimensional primary vortex ring in their rectangular jet. They found that; "different stages of the decay of the vortex rings were noted, in particular, that the vortex ring issued as an ellipse with its major axis aligned with the major axis of the nozzle. Then, it proceeded upwards, became circular and further downstream became elliptical again, but with its major axis rotated 90^o to the major axis of the nozzle opening". This appears to be due to multiple axis switching. This characteristic of these primary ring-like vortices, present in the free rectangular (rectangular) jet are, thus, far more complex than the counter-rotating roller vortices in a plane jet. Importantly, Trendscoste and Sforza (1967) acknowledged that the decay of these three-dimensional vortex rings showed similarity with the behaviour of a three-dimensional, presumably a round jet.

In their flow visualizations of rectangular jets, Grinstein (2005) also noted the existence of such ring-like primary vortex structures. A reproduction of their flow visualization is shown in Figure 6.9. In fact, they also found a few secondary (hairpin or braid) vortices, extending from the sides of the the primary ring-like vortices. Using direct numerical simulations (DNS), the dynamics and flow topology of rectangular jets were described in detail. Their jet development was characterized by the large-scale vortex rings and

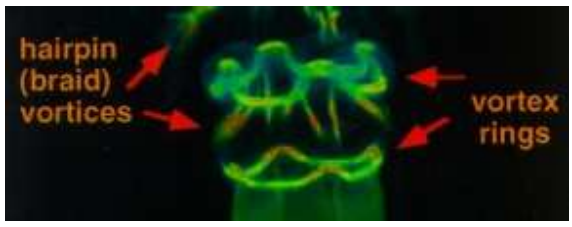

Figure 6.9: Visualizations of ring-like vortices in a free rectangular jet. The direction of the flow is towards the bottom. From Grinstein (2005).

braid vortices, their strong interactions that produced a more disorganized and hence three-dimensional flow. They also noted vortex self-deformation and reconnection mechanisms. Within the development zone of the rectangular jet (or within the so called 'non-linear Kelvin Helmholtz instability regime'), large-scale vortex rings rolled up and become highly three-dimensional. In fact, due to the three-dimensionality of the ring vortices and the increased streamwise vorticity (or circulation) along the axial direction, an efficient entrainment mechanism of the surrounding fluid was found. Further downstream, self-induction, vortex stretching and re-connection occurs. The ring-like vortices in a rectangular jet e.g. those found by Trendscoste and Sforza (1967) and Grinstein (2005), have large structural differences to the counter-rotating streamwise vortices found in the present plane jet. In particular, higher entrainment of the ambient fluid (as evidenced by the increased decay of the centerline mean velocity and a higher jet spreading rate) caused by the ring-like vortices are due to their three-dimensional nature (and higher axial vorticity).

The larger hump in the centerline turbulence intensity around $x/H \simeq 12$ for the plane jet relative to the free rectangular jet presumably indicates that the large-scale counter-rotating streamwise vortices are more coherent and organized for the former, than the primary ring-like vortex structures, for the latter. For $x/H > 12$, the turbulence intensity of the plane jet attains an asymptotic state while the free rectangular jet shows a monotonic decrease. Thus, it maybe conceived that the plane jet attains a fully developed state for $x/H > 12$ while the free rectangular jet does not. It is possible that within this region, the change of the primary ring-like vortices from elliptical to circular and then to elliptical (Krothapalli et al. 1981) may account for the varying centerline turbulence intensity for the free rectangular jet. Beyond $x/H = 100$, the free rectangular jet attains a asymptotic turbulence intensity whose magnitude is almost half the magnitude of that of the plane jet. The reduction in the asymptotic value of centerline turbulence intensity ($u'_{c,\infty}$), implies that the free rectangular jet exhibits a lower centerline turbulent kinetic energy ($q_{c,\infty}$), and thus has a higher dissipation rate ($\varepsilon H/U^3_{o,c}$). Our calculations of $\varepsilon H/U^3_{o,c}$ at $x/D_e = 16$ yields 2.78×10^{-6} and 3.80×10^{-6} $\mathrm{m^3 s^{-1}}$ for the free rectangular jet and plane jet respectively. Therefore, the lower value of asymptotic turbulence intensity is supported by these calculations.

6.5 Conclusions

The present study has quantified statistically, the effect of sidewalls on a free rectangular and a plane jet. The effect of the use of sidewalls, on the mean and turbulence field is significant and verifies that the differences are of sufficient magnitude that cannot be neglected. Specifically,

(1) The length of the jet potential core x_p is different for the free rectangular and the plane jet. The plane jet displays a longer potential core, $x_p \simeq 4\,H$, while the free rectangular jet has $x_p \simeq 2\,H$. This implies increased near field entrainment of the free rectangular jet than for the plane jet.

(2) The decay of centerline mean velocity becomes self-similar at $x/H \simeq 8$ for both the jets, indicating statistically, that the mean flow beyond this location is two-dimensional. The region of two-dimensionality extends over an axial distance of $160\,H$ for the present plane and up to $70\,H$ for the present free rectangular jet. This axial distance can be expected to depend on nozzle aspect ratio. The set of measurements for a free rectangular with $AR = 30$ supports this deduction. For this lower aspect ratio free jet, the region of two-dimensionality extended only to $x/H = 30$.

(3) For $AR = 60$, the free rectangular jet undergoes a transition from a two-dimensional to three-dimensional jet from $x/H > 70$. At greater axial distances, the free rectangular jet is evolves like a round jet. For this case, $U_c \sim x^{-1}$.

(4) In the far field and within the two-dimensional region, the centerline mean velocity decays at a rate of $K_u \simeq 0.20$ for the free rectangular jet while for the plane jet, it decays at a rate of $K_u \simeq 0.17$. Consistent with this, the spreading rate $K_y \simeq 0.14$ for the free rectangular jet and 0.114 for the plane jet. Increased decay and spreading rates of the free rectangular jet indicates that it is more effective in entraining the ambient fluid than for the plane jet.

(5) The locally normalized turbulence intensity field $u'_{n,c}$ is influenced by the presence or absence of sidewalls. Between $0 \leq x/H \leq 12$, the streamwise centerline turbulence intensity is relatively higher for the plane jet.

(6) Around $x/H \simeq 12$, a distinct hump in $u'_{n,c}$ is evident for both jets. The relative magnitudes of $u'_{c,\max}$ are 0.24 and 0.22 for the plane and free rectangular jets respectively.

(7) At axial distances greater than $12H$, the free rectangular jet $u^{'}_{n,c}$ decreases monotonically to an asymptotic value of $u^{'}_{c,\infty} \simeq 0.10$ at $x/H = 100$. On the other hand, turbulence intensity for the plane jet asymptotes to $u^{'}_{c,\infty} \simeq 0.22$ at $x/H = 30$. The significant difference in $u^{'}_{c,\infty}$ for both jets implies that their turbulence field is highly sensitive to whether sidewalls are used or not.

(8) The moments of higher order fluctuations in u are indistinguishable for the free rectangular and plane between over the range $0 \leq x/H \leq 20$.

(9) For $30 \leq x/H \leq 80$, (S_u, F_u) asymptotes to ($S_u^{c,\infty}$, $F_u^{c,\infty}$) = (0.30. 3.0) and (0.03, 2.7) for the free rectangular and plane jets respectively. For the free rectangular jet, the flatness factors asymptote to $x/H = 110$ while the skewness factor decreases to 0.03. Skewness and flatness factors for plane jet remains asymptotic to $x/H = 160$.

(10) Skewness and flatness continue to vary for the free rectangular jet. For $x/H \geq 110$, a monotonic increase in F_u is noted while S_u appears to again reach an asymptotic value of -0.37.

Chapter 7

CONCLUSIONS

A systematic study has been performed of the influence of jet exit Reynolds number, nozzle aspect ratio, the inner-wall nozzle exit contraction profile and effect of sidewalls on the axial and lateral velocity field of a turbulent plane jet using an extensive review of published literature and measurements with hot wire anemometry. For each condition, the statistical properties of the plane jet, arising from the changes in the inlet and boundary conditions were quantified. Such comprehensive data sets on inlet and boundary conditions of plane jets were not previously available.

The present study on the influence of jet exit Reynolds number, over an axial distance of 160 nozzle width verifies *Re* affects the entire mixing field. A small effect of Reynolds number on the initial velocity profiles was also found. Nevertheless, this effect appears to become negligible above Re = 10,000, although this range may differ when measured with a different inner-wall nozzle contraction profile or nozzle aspect ratio. Notably, a significant dependence on *Re* of the mean velocity field was found to persist up to Re = 16,500, while the *Re*-effect on the turbulent properties becomes very small above Re = 10,000. The present investigation also found that an increase in *Re* leads to higher rates of spread and decay in the near field but lower rates in the far field. This suggests a consequent increase in the mixing between the jet and ambient fluid. However, the mixing rates were not investigated explicitly, since no measurement of a scalar fields were performed. In the self-similar field, decreased rates of the centerline mean velocity decay and jet spreading with an increase in Reynolds number is consistent with trends in our calculations of the turbulent kinetic energy dissipation ($\epsilon H/U_{o,c}^3$) of the small-scale eddies.

A decrease in $\epsilon H/U_{o,c}^3$ occurred when *Re* was increased. Namar and Ötügen (1988) argued, but did not verify experimentally, that, with increased *Re*, the turbulent kinetic energy was distributed through a broader range of eddy scales. From our analysis, a decrease

in $\varepsilon H/U_{o,c}^3$ with increased Re indicates that the transfer of energy from larger to smaller scales causes a reduction in the relative strength of larger eddy structures. Consequently, the effectiveness of turbulent mixing due to large-scale eddies is expected to decrease. The present work supported the well established concept that Reynolds number had an insignificant effect on Strouhal number. Interestingly, this notion is supported well by Namar and Ötügen (1988), who found a broadening in the power spectra as Re was increased. Their results clearly support the present finding. That is, decreased dissipation $\varepsilon H/U_{o,c}^3$ and hence increased turbulent kinetic energy $q = 0.5\,(u^2 + v^2 + w^2)$ occurs at increased Re. Conclusively, the evidence from published and the present data indicates that the portion of the relative turbulent kinetic energy is in large-scale structures decreases with increased Re. Because the role of large-scale eddies is to initiate the engulfment of the ambient into the jet fluid, the relative significance of large-scale engulfment is reduced as Re is increased. This explains why the decay of mean centerline velocity and the spreading rates of the jet is lower when Re is higher.

The turbulence intensity, skewness and flatness factors are also influenced by Reynolds number. In particular, when Re is increased, the axial distance at which turbulence intensity asymptotes is found to decrease. For instance, at $Re = 1{,}500$, $u_{n,c}^{'}$ asymptotes at $x/H = 100$ while for $Re = 10{,}000$ and $16{,}500$, we noted that $u_{n,c}^{'}$ asymptotes at $x/H = 30$. The axial location at which asymptotic values in $u_{n,c}^{'}$ occurred for other Re falls within this range. This experimental finding verifies the analytical results of George (2005), who showed (for a plane jet) using equilibrium similarity analysis that the higher the source Reynolds number, the closer to the exit plane the similarity of the moments will be realized.

A statistical dependence of the plane jet flow on the inner-wall nozzle contraction profile has been clearly demonstrated in the present study. As the nozzle profile was varied from a sharp-edged orifice ($r^* = 0$) to a contoured nozzle with $r^* = 3.60$, the initial velocity profiles changed asymptotically from a saddle-backed to an approximately top hat profile. An increased thickness of the pseudo-boundary layer was found as r^* was increased. The highest initial shear layer turbulence intensity ($u_n^{'} \simeq 20\,\%$) was noted for the orifice case in contrast to the lower value ($u_n^{'} \simeq 4\,\%$) for the contoured nozzle whose $r^* = 3.60$. Vena contracta were found for the nozzle profiles whose r^* were between 0 to 0.90. Importantly, these nozzles also produced a saddle-backed initial velocity profile, indicating an initial upstream flow separation and a rapid increase in spread and decay of the jet. A stronger vena contracta was found for the sharp-edged orifice nozzle, as evidenced by a

30 % higher mean centerline velocity than its nominal exit mean centerline value. Vena contracta is known to cause an increase in spread of the jet in its initial near field region (Quinn 1992b). The far field decay of the centerline mean velocity and jet spreading rates were found to depend on the inner-wall nozzle contraction profile. In particular, the far field centerline mean velocity decay and jet spreading rates from the sharp-edged orifice nozzle were larger than from a contoured nozzle of $r^* = 3.60$. Increased decay and spreading rate of the circular orifice-jets relative to smooth contractions have been noted by previous investigations of round jets for instance, Mi, Nathan and Nobes (2001). The centerline distributions of the turbulence intensity, skewness and flatness factors are also dependent on the inner-wall nozzle contraction profile. The orifice-jet was characterized by a distinct hump in centerline turbulence intensity around $x/H = 10$. This is probably caused by the occurrence of coherent and organized large-scale structures, within the shear layers of the plane jet. In the far field, the centerline turbulence intensity attains a higher asymptotic value for the orifice-case than the radially contoured nozzle.

It was also found that the inner-wall nozzle contraction ratio impacts on the vortex shedding frequency for the plane jet. A higher rate of vortex shedding in the near field was found for the orifice-jet ($r^* = 0$). This implies that the rate of vortex formation is a function of the nozzle contraction profile. That is, the structure of the large-scale vortices depend on the boundary conditions of the plane nozzle. The higher vortex formation frequency, $St_H = 0.39$, observed in the near field for the sharp-edged orifice suggests greater natural shear-layer instability. This instability is likely to be due to highly unstable and thin boundary layer at the nozzle lip. In addition, the initial structure of the orifice jet can be expected to be three-dimensional due to the presence of the upstream separation region. By contrast, the radially contoured nozzle with $r^* = 3.60$ does not produce any upstream separation, thus, its flow is expected to be more two-dimensional (Mi, Nobes and Nathan 2001). The differences in the formation and the motions of near field large-scale vortices on the nozzle profile are clearly demonstrated by the differences in the magnitudes of the present St_H.

Nozzle aspect ratio was found to affect the mean and rms velocity profiles of the turbulence field at the nozzle exit. Although the entire range of nozzle aspect ratios produced an approximately top hat velocity profile, subtle differences in the velocity profile near to the edges of the jet were found. For example, the uniform velocity region extended to $\zeta = 0.40$ for $AR \leq 20$, while for $AR \geq 30$, this region extends to $\zeta = 0.45$. This difference in the initial profile was not expected from the present study. Every effort was taken to

ensure that the initial velocity profiles would remain identical e.g. using the same nozzle profiles, Reynolds number etc. The change in initial conditions is likely account for some of the downstream variations in flow properties.

The axial extent over which a statistically 'two-dimensional' flow is achieved was found to depend upon nozzle aspect ratio. This is deduced to be due to the influence of the evolving boundary layers imposed by the sidewalls. The extent of the two-dimensional region can thus be expected not to be universal, but rather be subject to variation from one experiment to another. However, the present work demonstrates that the nozzle aspect ratio is indeed a significant parameter in governing the two-dimensionality of the planar jet. It was also found that the region of statistically two dimensional region is very small, if present at all, for $AR < 15$. The dependence of the axial extent of this region of 'two-dimensional flow' on AR was determined. At greater distances three dimensional effects, presumably induced by sidewall effects were found to dominate. An assessment of the relationship between the critical jet aspect ratio $AR_{jet,crit}$ and the nozzle aspect ratio AR was made. It was found that the critical jet aspect ratio $AR_{jet,crit}$ increases with nozzle aspect ratio AR, immediately prior to the point of three-dimensionality, for $AR < 30$. For $AR \geq 30$, $AR_{jet,crit}$ attains a constant value of around 0.15. Thus, it is found that the critical half-width of the jet $y_{0.5,crit}$ and spacing between the sidewalls (w) determine where the transition from 2-D to 3-D flow occurs. In particular, the axial distance at which the flow ceases to be statistically 2-D coincides with the width of the jet being approximately equal to its span.

In the self-similar 2-D region, the rates of centerline velocity decay, jet spreading and entrainment increased with an increase in nozzle aspect ratio. It was noted that a distinct peak, at an axial distance of about 10 nozzle widths downstream characterized the centerline turbulence intensity, for all nozzle aspect ratios. Its magnitude was smaller with larger nozzle aspect ratios and found to asymptote at $AR = 50$. The skewness and flatness factors were found to vary significantly with nozzle aspect ratio through the entire data field. Significantly, the turbulence statistics in the near field are dependent upon aspect ratio even at $AR = 72$. This indicates that aspect ratio affects the turbulence field more strongly in the near field than in the far field.

The effect of sidewalls on the velocity field of a turbulent plane air jet from a nozzle of aspect ratio 60 and of Reynolds number 7,000 was also investigated using hot wire

anemometry over an axial distance of 160 nozzle-widths. In this study, the nozzle profile was identical to the study conducted for Reynolds number experiments. Results display the dependence of the mean properties, e.g., centerline decay of mean velocity, jet-spreading rates and the turbulence properties, e.g., centerline turbulence intensity, skewness and flatness factors on the sidewalls. The transition of a free rectangular jet (without sidewalls) from a two-dimensional to three-dimensional flow was clearly evident. The axial location of this transition is also dependent on the nozzle aspect ratio. Well beyond the transition region, it develops, statistically, into a round jet. Sidewalls were also found to affect the frequency of the near-field vortex shedding, resulting in a Strouhal number of 0.36 without sidewalls, in contrast to 0.22 with sidewalls. This indicates that the structure, rate of formation of large-scale vortices for a free rectangular jet is significantly different from those emanating from a plane jet. The difference is deduced to be caused by the primary vortex structure being generally 'ring-like' for the free rectangular jet and is cylindrical for the plane jet. This strongly suggests that previous investigations of high-aspect ratio plane jets without sidewalls are not comparable to that with sidewalls. That is, sidewalls are a necessary requirement to achieve a true plane jet.

The classical theory for jets that the influence of initial conditions decay with downstream distance and eventually becomes unimportant appears to be questionable for a plane jet. Indeed, Richards and Pitts (1993) emphasized that the round jet flow should subsequently converge to a universal far field single decay and spreading rate. According to their classical notion, an effect of the initial condition is only to shift the virtual origins of the jet, e.g. x_{01} and x_{02} for the present study (Townsend 1976). In other words, to eliminate the effect of any difference in initial conditions requires only a shift in the location of the 'point' source from which the far field jet originates (Chen and Rodi 1980). The present study on plane jets has identified significant differences both in near field and the self-similar far field for all variations in inflow boundary conditions. Our study, therefore, does not support the classical hypothesis that the asymptotic state of a jet flow is independent of its source (initial) conditions. Our findings are consistent with a growing body of literature. Bevilaqua and Lykoudis (1978), who compared of a spherical wake flow and a disk-generated wake flow, revealed significantly larger turbulence intensity within the self similar region for the former than the latter case. Similarly, Wygnanski et al. (1986) found that, within the self-similar field, the lateral profiles of the normalized streamwise turbulence intensity and Reynolds stresses are different when produced using different wake generators. Many other studies have documented the relevance of initial conditions to the statistical development of plane wake flows (Bonnet et al. 1986, Louchez

et al. 1987, Zhou and Antonia 1995). Similarly, round jet flows have also been shown to exhibit a significant dependence on initial conditions (Mi, Nathan and Nobes 2001). Thus, the finding in our study is no exception to previously established concepts on the dependence of jet flow properties on source (initial) conditions. The extensive review of published data and the present experiments on plane jet flows, fully support the analytical notion by George (1989), that jet flows are governed by initial conditions. In other words, even in the fully developed state, a plane jet does not 'forget' its origin. In simple terms, any downstream development is entirely governed by the nozzle initial (inlet) and nozzle boundary conditions plus the laws of fluid motion. Thus, the classical hypothesis, which argues that at sufficiently large distances from the source, the perception that all jets should become asymptotically independent of the source conditions and will depend only on the rate at which momentum is added and the distance from its source, does not hold true for a plane jet.

The present findings are not only limited for those interested in plane jet flows, but also for the CFD community, since they imply that there exist no set of parameters for a single Reynolds Averaged Navier Stokes (RANS) model which can describe more than one nozzle configuration. This view is consistent with George (2004), which shows that the only hope for predicting these flows is with structure-based turbulence models or two-point models (like Large-Eddy Simulations, LES).

Appendix A

THESIS ASSESSMENT DETAILS

A.1 Examination Documents

Please see the end of the Appendix.

A.2 Examiners Reports

Please see the end of the Appendix.

Appendix B

PUBLICATIONS FROM THIS WORK

(1) **Deo R C.**, Mi J and Nathan G J.: 2004, An Investigation on the Influence of Nozzle Aspect Ratio on the Velocity Field of a Turbulent Plane Jet, In Proc. *15^{th} Australasian Fluid Mechanics Conference*, (Ed. Behnia, M, Lin W and McBain G D,), In Proc. [CD-ROM], Paper No: **AFMC00062**, The University of Sydney, 13-17 December.

(2) Mi., J, **Deo R C** and Nathan G J.: 2005, A Fast Convergent Scheme for Filtering Velocity Signals and Finding Kolmogorov Scales, *Phys. Rev. E* June Issue, **71**(6)

(3) Mi, J, **Deo R C** and Nathan G J.: 2005, Characterization of a Large Aspect Ratio Rectangular Jet, *Phys. Fluids*, June Issue, **17**(6).

(4) **Deo R C.**, Mi J and Nathan G J.: 2005, Experimental Investigation of the Effects of Reynolds Number on a Turbulent Plane Jet From a Radially Contoured Nozzle, *Phys. Fluids*, **To Be Submitted**.

(5) **Deo R C.**, Mi J and Nathan G J.: 2005, Dependence of a Plane Turbulent Jet on Its Nozzle Contraction Profile , Int. Conf. Jets, Wakes and Separated Flows, 5-8 October 2005, In Proc. [CD-ROM], Toba-shi Mie Japan.

(6) **Deo R C.**, Mi J and Nathan G J.: 2005, Effect of Nozzle Exit Profile on Development of a Plane Turbulent Jet, *Exp. Fluids*, **Under Review**.

(7) **Deo R C.**, Mi J and Nathan G J.: 2005, Characterization of a plane and a free rectangular jet, *Phys. Fluids*, **To Be Submitted**.

(8) Mi, J, **Deo R C** and Nathan G J.: 2005, Characterization of Turbulent Jets from High-Aspect-Ratio Plane Nozzles, *Exp. Fluids*, **To Be Submitted**.

(9) **Deo R C.**, Mi J and Nathan G J.: 2005, Effect of Reynolds Number on Small-Scale Statistics of a Plane Jet, *Exp. Thermal Fluid Sc.*, In Preparation.

(10) Mi, J, **Deo R C** and Nathan G J.: 2005, The Two-Dimensional Region of a Turbulent Plane Jet, *Phys. Fluids*, **In Preparation**.

(11) **Deo R C**, Mi J, and Nathan G J.: 2005, Dependence of a Plane Jet on Its Nozzle Exit Size, *Exp. Fluids*, **In Preparation**.

Appendix C

PREPRINT OF PUBLICATIONS

These publications are included on pp. 194-232 in the print copy of the thesis in the University of Adelaide Library.

Paper 1.

Deo, R.C., Mi, J. and Nathan, G.J. 2004
'An investigation of the influence of nozzle aspect ratio on the velocity field of turbulent plane jet'.
In *Proc. 15th Australasian Fluid Mechanics Conference, (Ed. Behnia, M, Lin W and McBain G. D.), In Proc. [CD-ROM], Paper No: AFMC00062, The University of Sydney,13-17 December.*

Paper 2.

Deo, R.C., Mi, J. and Nathan, G.J. 2005
'Dependence of a plane turbulent jet on its nozzle contraction profile.
International Conference on Jets, Wakes and Separates Flows, ICJWSF-2005, Oct. 5-8 2005, Toba-shi, Mie, Japan'

Paper 3.

Mi, J., Deo, R.C. and Nathan, G.J. 2005
'Characterization of turbulent jets from high-aspect-ratio rectangular nozzles',
Physics of Fluids 17, 068102
This publication is available online to authorized users:
http://dx.doi.org/10.1063/1.1928667

Paper 4.

Mi, J., Deo, R.C. and Nathan, G.J. 2005
'Fast-convergent iterative scheme for filtering velocity signals and finding Kolmogorov scales',
Physical Review E 71, 1
This publication is available online:
http://www.geocities.com/physrcd/proof_copy_phys_rev_e.pdf

Paper 5.

Deo, R.C., Mi, J. and Nathan, G.J. 2005
'Effect of nozzle exit profile on development of a plane turbulent jet,
Experiments in fluids
Manuscript to be submitted.

Appendix D

MATLAB PROGRAMS

This section of the appendix outlines the MATLAB programs used to analyze the instantaneous velocity signal from the hot-wire sensor.

D.1 General Data Reading and Writing

```
% This routine loads the instantaneous voltage signal and then
% performs the following tasks :

% 1. Writes separate voltages into a single file of voltages.
% 2. Converts the single file of voltages to velocity (using calibration).
% 3. Writes REAL INSTANTANEOUS VELOCITY into a single separate file.
% 4. Calculates the MEAN AND RMS of the velocity.
% 5. Writes MEAN AND RMS values into a single separate file.

% Now loading the voltages.

load F:\RE_Effect_Data\Data\Ar_60\21_Oct\Axial\Re_1500\AXIAL0.TXT;
load F:\RE_Effect_Data\Data\Ar_60\21_Oct\Axial\Re_1500\AXIAL1.TXT;
load F:\RE_Effect_Data\Data\Ar_60\21_Oct\Axial\Re_1500\AXIAL2.TXT;
load F:\RE_Effect_Data\Data\Ar_60\21_Oct\Axial\Re_1500\AXIAL3.TXT;
load F:\RE_Effect_Data\Data\Ar_60\21_Oct\Axial\Re_1500\AXIAL4.TXT;
load F:\RE_Effect_Data\Data\Ar_60\21_Oct\Axial\Re_1500\AXIAL5.TXT;
load F:\RE_Effect_Data\Data\Ar_60\21_Oct\Axial\Re_1500\AXIAL6.TXT;
load F:\RE_Effect_Data\Data\Ar_60\21_Oct\Axial\Re_1500\AXIAL8.TXT;
load F:\RE_Effect_Data\Data\Ar_60\21_Oct\Axial\Re_1500\AXIAL10.TXT;
load F:\RE_Effect_Data\Data\Ar_60\21_Oct\Axial\Re_1500\AXIAL12.TXT;
```

```
load F:\RE_Effect_Data\Data\Ar_60\21_Oct\Axial\Re_1500\AXIAL14.TXT;
load F:\RE_Effect_Data\Data\Ar_60\21_Oct\Axial\Re_1500\AXIAL16.TXT;
load F:\RE_Effect_Data\Data\Ar_60\21_Oct\Axial\Re_1500\AXIAL18.TXT;
load F:\RE_Effect_Data\Data\Ar_60\21_Oct\Axial\Re_1500\AXIAL20.TXT;
load F:\RE_Effect_Data\Data\Ar_60\21_Oct\Axial\Re_1500\AXIAL30.TXT;
load F:\RE_Effect_Data\Data\Ar_60\21_Oct\Axial\Re_1500\AXIAL40.TXT;
load F:\RE_Effect_Data\Data\Ar_60\21_Oct\Axial\Re_1500\AXIAL50.TXT;
load F:\RE_Effect_Data\Data\Ar_60\21_Oct\Axial\Re_1500\AXIAL60.TXT;
load F:\RE_Effect_Data\Data\Ar_60\21_Oct\Axial\Re_1500\AXIAL70.TXT;
load F:\RE_Effect_Data\Data\Ar_60\21_Oct\Axial\Re_1500\AXIAL80.TXT;
load F:\RE_Effect_Data\Data\Ar_60\21_Oct\Axial\Re_1500\AXIAL90.TXT;
load F:\RE_Effect_Data\Data\Ar_60\21_Oct\Axial\Re_1500\AXIAL100.TXT;
load F:\RE_Effect_Data\Data\Ar_60\21_Oct\Axial\Re_1500\AXIAL110.TXT;
load F:\RE_Effect_Data\Data\Ar_60\21_Oct\Axial\Re_1500\AXIAL120.TXT;
load F:\RE_Effect_Data\Data\Ar_60\21_Oct\Axial\Re_1500\AXIAL130.TXT;
load F:\RE_Effect_Data\Data\Ar_60\21_Oct\Axial\Re_1500\AXIAL140.TXT;
load F:\RE_Effect_Data\Data\Ar_60\21_Oct\Axial\Re_1500\AXIAL150.TXT;
load F:\RE_Effect_Data\Data\Ar_60\21_Oct\Axial\Re_1500\AXIAL160.TXT;

% Loading the DIMENSION (x/H-locations).
load DIMENSIONS.TXT; DIMENSIONS = DIMENSIONS';
AXIAL(:,1) = AXIAL0(:,1);
AXIAL(:,2) = AXIAL1(:,1);
AXIAL(:,3) = AXIAL2(:,1);
AXIAL(:,4) = AXIAL3(:,1);
AXIAL(:,5) = AXIAL4(:,1);
AXIAL(:,6) = AXIAL5(:,1);
AXIAL(:,7) = AXIAL6(:,1);
AXIAL(:,8) = AXIAL8(:,1);
AXIAL(:,9) = AXIAL10(:,1);
AXIAL(:,10) = AXIAL12(:,1);
AXIAL(:,11) = AXIAL14(:,1);
AXIAL(:,12) = AXIAL16(:,1);
AXIAL(:,13) = AXIAL18(:,1);
AXIAL(:,14) = AXIAL20(:,1);
AXIAL(:,15) = AXIAL30(:,1);
```

```
AXIAL(:,16) = AXIAL40(:,1);
AXIAL(:,17) = AXIAL50(:,1);
AXIAL(:,18) = AXIAL60(:,1);
AXIAL(:,19) = AXIAL70(:,1);
AXIAL(:,20) = AXIAL80(:,1);
AXIAL(:,21) = AXIAL90(:,1);
AXIAL(:,22) = AXIAL100(:,1);
AXIAL(:,23) = AXIAL110(:,1);
AXIAL(:,24) = AXIAL120(:,1);
AXIAL(:,25) = AXIAL130(:,1);
AXIAL(:,26) = AXIAL140(:,1);
AXIAL(:,27) = AXIAL150(:,1);
AXIAL(:,28) = AXIAL160(:,1);

% These are the calibration constant of the polyfit:
% U(m/s) = AV^4 + BV^3 + CV^2 + DV + E
% 0.0329    0.4855    2.4907    4.2701  1.2545

Q = [AXIAL]; Q = Q';
save REAL_VOLTAGE_RE1500.TXT /ascii Q

REAL_VELOCITY = 0.0329*AXIAL.^4 + 0.4855*AXIAL.^3 + 2.4907*AXIAL^2
+ 4.270*1AXIAL + 1.2545;

MEAN_VEL = mean(REAL_VELOCITY); RMS_VEL  = STD(REAL_VELOCITY);

Q = [DIMENSIONS; MEAN_VEL; RMS_VEL]; Q = Q';
save ANALYSIS_RE1500.TXT /ascii Q

Q = [REAL_VELOCITY]; Q = Q';
save REAL_VELOCITY_RE1500.TXT /ascii Q
% end end end end end end end end end end end end end end
```

D.2 Skewness and Flatness Factors

```
% SKEWNESS & FLATNESS
```

```
% SKEWNESS FACTOR CALCULATION
% THIS PROGRAM CODE WILL CALCULATE THE SKEWNESS FACTOR FOR A FLUCTUATING SIGNAL.
% THE SIGNAL SHOULD BE RAW REAL TIME SIGNAL.
% VARIABLES - N: THE NUMBER OF SAMPLES
% IT WILL CALCULATE SKEWNESS POINT - BY POINT.

SKEW1     = AXIAL(:,1);
V_BAR1     = mean(SKEW1);
V_SIGMA1   = STD(SKEW1);
N = 400000

S1     = SKEW1 - V_BAR1;
S2     = S1.^3;
S3     = S2 / (N*V_SIGMA1.^3);
A1     = sum(S3(:,1));

% PLACING SKEWNESS VALUES IN MATRIC FORM.
SKEW(:,1) = A1;

%=========================================================================
% FLATNESS FACTOR CALCULATION
% THIS PROGRAM CODE WILL CALCULATE THE FLATNESS FACTOR FOR A FLUCTUATING SIGNAL.
% THE SIGNAL SHOULD BE RAW REAL TIME SIGNAL.
% VARIABLES - N: THE NUMBER OF SAMPLES
% IT WILL CALCULATE FLATNESS POINT - BY POINT.

FLAT1     = AXIAL(:,1);
V_BAR1     = mean(FLAT1);
V_SIGMA1   = STD(FLAT1);
N = 400000

S1     = FLAT1 - V_BAR1;
S2     = S1.^4;
S3     = S2 / (N*V_SIGMA1.^4);
A1     = sum(S3(:,1));
%=======================================
```

```
% PLACING ALL FLATNESS VALUES IN MATRIC FORM.
FLAT(:,1) = A1;

%=====================================================================
% PHASE 4 - SAVING MEAN AND TURBULENT STATISTICS TO A FILE

load DIMENSIONS.TXT;
DIMENSIONS = DIMENSIONS';

STATS = [DIMENSIONS; MEAN_VEL; RMS_VEL; SKEW; FLAT]; STATS =
STATS'; save STATISTICS.TXT /ascii STATS
```

D.3 PDF and Power Spectrums

```
% PROBABILITY DENSITY FUNCTIONS CALCULATIONS

load REAL_VELOCITY_RE1500.TXT;
REAL_VELOCITY_RE1500 = REAL_VELOCITY_RE1500';

VAR = REAL_VELOCITY_RE1500(:,1);
e=VAR;
ebar=mean(e);
erms=std(e);
e=(e-ebar)/erms;
emin=min(e);
emax=max(e);
sum=length(e);
dx=(emax-emin)/200;
[p]=hist(e,201);
for k=1:200
pd(k)=(p(k)+p(k+1))/2/sum/dx;
x(k)=emin+(k-0.5)*dx;
end

% H = SUBPLOT(2,3,1)
plot(x,pd)
```

```
hold on
title 'Probability Density Function (PDF)';
xlabel('u')
ylabel('p(u)');
v=[x; pd]; w=v';
save PDF_XH0.TXT w /ascii
============================================================
% THIS PROGRAM CALCULATES THE POWER SPECTRUMS OF ANY SIGNAL.

load REAL_VELOCITY_RE1500.TXT;
REAL_VELOCITY_RE1500 = REAL_VELOCITY_RE1500';

% SPECTRUM OF THE ORIGINAL FLUCTUATION SIGNALS.
variable = REAL_VELOCITY_RE1500(:,1);
rate=18400

e=variable;
ebar=mean(e);
e=e-ebar;
N=length(e)/2048;
Py=zeros(1,1024);
for k=1:N
    j=(k-1)*2048+1;
    Y=fft(e(j:(j+2047)),2048);
    P=Y.*conj(Y)/2048;
    for l=1:1024
        Py(l)=Py(l)+P(l)/N;
    end
end
f=rate/2048*(0:1023);
s=sum(Py); s=f(2)*(s-0.5*(Py(1)+Py(1024)));
Py=Py/s;
loglog(f,Py);
title 'X/H = 100';
xlabel('Frequency (Hz)')
ylabel('Spectrum');
```

```
v=[f; Py]; w=v';
save SPEC_LARGE_XH0.dat w /ascii
```

D.4 Filtering Routines for Real-time Instantaneous Velocity Signals

```
% THE FOLLOWING PROGRAM IS USED TO FILTER REAL-TIME VELOCITY DATA.
% AFTER FILTRATION IS PERFORMED, IT CALCULATES THE FINITE DIFFERENCE
% OF THE FILTERED INSTANTANEOUS DATA.
% THIS FINITE DIFFERENCE IS USED TO CALCULATE THE SMALL-SCALE STATS.
% NOTE THAT ONLY A SAMPLE IS SHOWN.
%===============================================================
load REAL_VELOCITY_RE1500.TXT;
REAL_VELOCITY_RE1500 = REAL_VELOCITY_RE1500';
%===============================================================
variable = REAL_VELOCITY_RE1500(:,1);
rate = 18433;

% REMOVE THE NOISE - FILTER DATA WITH LOW PASS AT Fc = SOME VALUE.

[b,a] = butter(5, [1599/9200]);   % Defined the Filter Type - Butterworth is
                                  % MOST Common.
                                  % BUTTER(5,[1599/9200]) MEANS Filter Designed
                                  % for 5th Order,, 1599 Hz is NEW CUT-OFF FREQ.
                                  % Original Cut Off was 9200 Hz.
freqz(b,a)                        % Plots the Filter Response to See if Good
                                  % Enough Yfiltered = filter(b,a, variable);
                                  % Apply the filter. Yfiltered is the Filtered
                                  % Original Data.

A = mean(Yfiltered);
B = diff(Yfiltered);
B = std(B);
XH0 = B;
```

Appendix E

DERIVATIONS, CONCEPTS AND SUPPLEMENTARY RESULTS

E.1 Derivation of Axial Loss in Momentum for Plane Jet

A jet which is confined in a room may encounter momentum loss due to room entrainment effect (Hussain et al. 1994). The presence of a wall at finite distance from the jet, causes momentum back-flow outside the jet. Consider the initial jet momentum to be $M_o = U_o^2\, H\, w$, where U_o, H and w are the exit bulk-mean velocity, and nozzle exit dimensions, respectively. The total momentum, M_o can be divided into two parts: the jet momentum (going downstream), $M_{jet}(x)$ and reverse flow momentum, $M_{back-flow}$ (which must feed the jet entrainment). In this regard, we have $M_{jet}(x) + M_{back-flow} = M_o$.

To deduce M_{jet}, it is reasonable to integrate the lateral profile of the mean velocity, leading to:

$$M_{jet}(x) = \int_{bottom}^{top} U^2 dy = II\; U_c^2\, \delta \tag{E.1}$$

where $II = \int_{bottom}^{top} {U/U_c}^2\, d\,(y/\delta)\,.$

To estimate the momentum back-flow, $M_{back-flow}$ we need to ignore the small amount of mass entering at the source (compared with the entrained flow downstream). Therefore, the mass flow by the jet going downstream is approximately equal to the new back-flow mass into the room. Here, the mass going downstream is given by:

$$\int_{jet} U\, dy = U_c\, \delta\, I \tag{E.2}$$

where $I = \int U/U_c \, d(y/\delta)$. This must balance the estimate of the jet back-flow momentum. For simplicity, we assume that the momentum due to back-flow is uniform, and ignore the little part of the room occupied by the plane jet. Thus, the momentum due to back-flow will be given by 'back-flow' velocity, $U_{back-flow} \times$ room area, A_R. From similarity, we know that $U_{back-flow} = (-\delta/H)\, U_c\, I$. Note that using equilibrium similarity analysis, $U_c^2/U_o^2 = B\,(H/x)$ and $(\delta/H) = A\,(x/H)$. Here, A and B are only the constants of proportionality, related to the momentum integral equation by $A\,B\,I^2 = 1$.

We now can easily compute the momentum back-flow using $M_{back-flow} = U_{back-flow}^2\, A_R$:

$$M_{back-flow} = (\delta/H)^2 U_c^2 I^2\, A_R \tag{E.3}$$

Now, using the original expression, $M_{jet}(x) = M_o$ - $M_{back-flow}$, we get:

$$M_{jet}(x) = M_o - (\delta/H)^2 U_c^2 I^2\, A_R \tag{E.4}$$

Further simplification of equation E.4 leads us to:

$$\frac{M_{jet}(x/H)}{M_o} = 1 - A^2 I^2 B \left(\frac{A_R}{A_n}\right)\left(\frac{x}{H}\right) \tag{E.5}$$

This equation is used to estimate the axial losses in the plane jet momentum. The required parameters are, the room and nozzle area, A_R and A_n (in the same plane) respectively, and the lateral velocity profiles at that location. Equation E.4 assumes that the exit velocity profiles are top hat. For the case of a non-top hat exit velocity profile, the equation becomes:

$$\frac{M_{jet}(x/H)}{M_o} = 1 - A^2 I^2 B \left[\frac{U_o^2 A_n}{M_o}\right]\left(\frac{A_R}{A_n}\right)\left(\frac{x}{H}\right) \tag{E.6}$$

where the term, $\frac{U_o^2 A_n}{M_o} \simeq 1$, at least for the top-hat exit condition.

The assistance provided by Professor W K George, in deriving this equation, is humbly acknowledged.

E.2 Derivation of Bulk Mean Velocity from Initial Velocity Profiles

The initial mass flow rate, m_0 at a plane nozzles' exit plane is given by $m_0 = \rho\, V_0$, where ρ and V_0 are the fluid density and exit volume. The exit volume, V_0 can be calculated

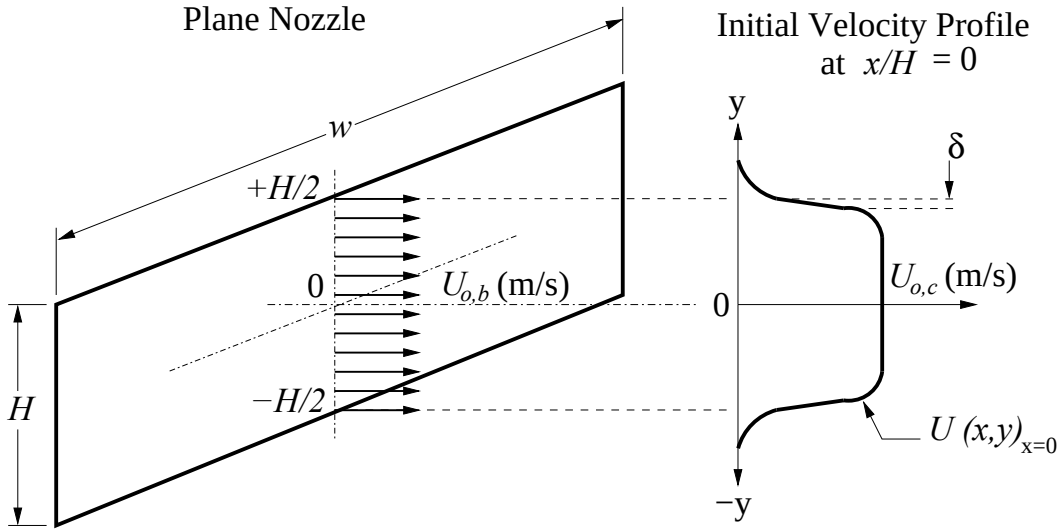

Figure E.1: The plane nozzle exit geometry, with dimensions and the initial velocity profile at $x/H = 0$.

using the expression, $V_0 = U_{o,b} \times$ nozzle area, where $U_{o,b}$ is bulk mean velocity and nozzle area is given as $w \times H$. Therefore, the mass flow rate (m^3/s) at the nozzle exit will be given by

$$m_0 = \rho\,(U_{o,b}\,w\,H) \tag{E.7}$$

Consider an initial velocity profile, measured at the centerplane of the plane nozzle (Fig. E.1). We can state that the exit mass flow rate (m^3/s) will be given by

$$m_0 = \left[\int_{y=-H/2}^{y=+H/2} U(x,y)_{x=0}\,dy\right]\,\rho\,w \tag{E.8}$$

Using the principle of mass conservation, equations E.7 and E.8 must be equal. This leads to

$$\rho\,U_{o,b}\,H\,w = \left[\int_{y=-H/2}^{y=+H/2} U(x,y)_{x=0}\,dy\right]\,\rho\,w \tag{E.9}$$

Further simplification of equation E.9 allows us to calculate the bulk mean velocity, $U_{o,b}$ using the exit velocity profile, via;

$$U_{o,b} = \frac{1}{H}\int_{y=-H/2}^{y=+H/2} U(x,y)_{x=0}\,dy \tag{E.10}$$

Note that $U(x,y)_{x=0}$ represents the exit velocity profile at $x/H = 0$.

E.3 General Formulation of Reynolds Number

Reynolds (1883) demonstrated that turbulent flows transport and mix fluids more effectively than a comparable laminar flow. Thus, an inlet condition was established, which characterized the flow by a single non-dimensional parameter. This non-dimensional parameter was termed as the *Reynolds number* and abbreviated as *Re*. Reynolds (1883) proposed the Reynolds number to be defined by the characteristic velocity U, characteristic length scale L and the kinematic viscosity ν of the fluid, to be related by

$$\mathrm{Re} = \frac{UL}{\nu} \tag{E.11}$$

This general formulation of Reynolds number is applied to many turbulent flows, that include jets, wakes and others. The formula is modified accordingly to incorporate a different characteristic length scale and velocity (Pope 2002).

Re-Dependence of Flow Regimes

Reynolds (1883) pipe flow experiments demonstrated that when the inlet Reynolds number was below 2,300, the laminar flow did not achieve a change in fluid velocity with time and the injected dye did not increase its diameter along the jet centerline. In other words, the mixing rate of the dye with water was poor. Interestingly, when *Re* was increased to around 4,000 (i.e. turbulent regime), the dye disappeared significantly with downstream distance. Such a demonstration proved that pipe flow turbulence was, indeed governed by the non-dimensional Reynolds number. Based on the description of Reynolds (1883), the general formulation of Reynolds number for a variety of flows were thus established.

Frank (1999) outlined a number of flow regimes, that classify the Reynolds number dependencies into various turbulent flow regimes. These flows could be jets, wakes or other shear flow. These flow regimes comprise of; (1) a highly viscous laminar 'creeping' motion where $0 \leq Re \leq 1$ (2) laminar regime with strong *Re*-dependence over the range $1 \leq Re \leq 10^2$ (3) laminar, in which boundary layer theory applies over the range $10^2 \leq Re \leq 10^3$ (4) transition region to turbulence over the range $10^3 \leq Re \leq 10^4$ (5) turbulent, moderate *Re*-dependence over the range $10^4 \leq Re \leq 10^6$ and finally (6) turbulent and slight (or even no) *Re*-dependence for $Re > 10^6$. However, for turbulence research, the range of various Reynolds number dependent somewhat on flow geometry and experimental conditions. Nevertheless, a 'baseline' to define the transition from a laminar to turbulent flow is usually used to classify its flow properties.

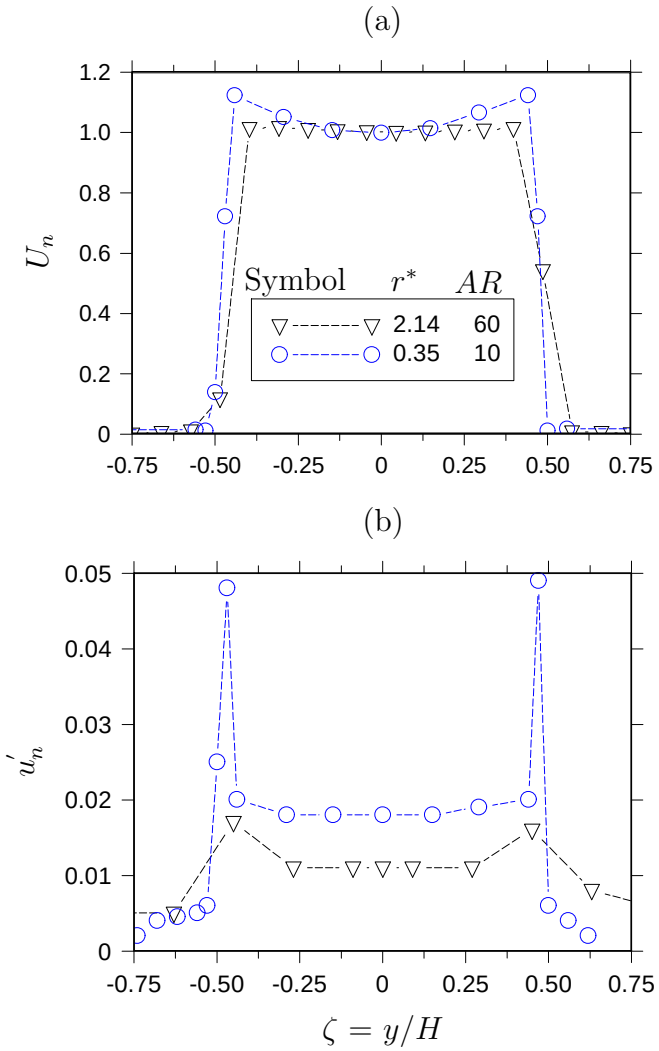

Figure E.2: Lateral profiles of (a) the normalized mean velocity, U_n (b) the turbulence intensity, $u_n^{'}$ at $x = 0.5H$ for a sharp-edged orifice and a radially contoured nozzle, measured at $AR = 10$ and 60 respectively.

E.4 Re-Effect on Axial Distribution of Strouhal Numbers

The centerline velocity power spectra (not shown here) demonstrates a peak frequency, caused by the regular (periodic) passage of coherent flow structures. Figure E.3 plots the relationship between the Strouhal numbers of oscillation and axial distance for different Re-jets. The figure shows that, in general, the Strouhal numbers are approximately independent of Re over the axial distance of 3 to 5 nozzle widths. This region represents the passage of the K-H vortices in the mixing layers of the plane jet. Further downstream, it is noted that St_H decreases for $Re \geq 3{,}000$ but stays the same for $Re = 1{,}500$. The clear near-field changes in St_H $(x/H > 5)$ presumably indicates vortex pairing, evidenced by a drop, with downstream distance, of the dominant peak frequency. The figure shows that,

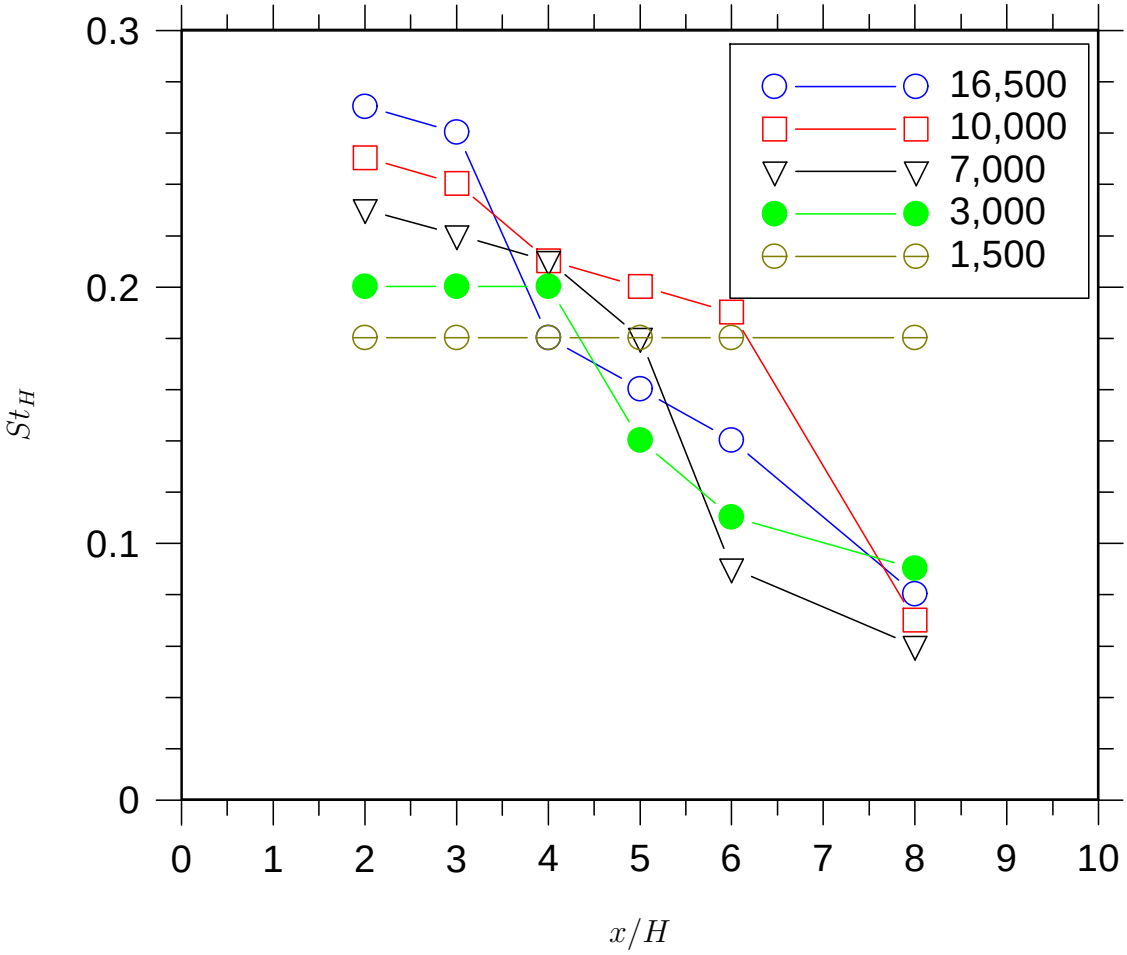

Figure E.3: Dependence of St_H and x/H for different Reynolds numbers.

the merging of the large-scale structures cause a reduction in St_H, for $Re \geq 3{,}000$. For $Re = 1{,}500$, a constant St_H may indicate least pairing of large-scale vortex structures. Further downstream, the coherent structures appear less frequently, thus more intermittently as the jet propagates from $x/H = 0$ to $x/H = 8$.

E.5 Preliminary Assessment of Nozzle Exit Contraction Profile

Our previous study on plane jets (Deo et al. 2004), varied r^* from 0.35 to 2.14. The lateral profiles of the mean velocity for the pseudo-sharp-edged orifice ($r^* = 0.35$) and the radially contoured nozzle ($r^* = 2.14$) at $x = 0.5H$ is reproduced in Figure E.2. The figure indicates that the pseudo-orifice produced a saddle-backed velocity profile, and almost a 5 % shear-turbulence intensity when compared with an approximate top-hat profile and a 2 % shear-turbulence intensity for the radial contraction. Note that these measurements

were conducted at $Re = 16{,}500$. Although we acknowledge the large difference in the nozzle aspect ratio (10 for the pseudo-orifice vs. 60 for the radial contraction), the differences evident in the near initial flow are not expected to be affected to such a magnitude by the aspect ratio differences. (see Figure 4.1 in Chapter 5 which presents the effect of aspect ratio on the velocity profiles and turbulence intensity at $x = 0.25H$). Thus, the figure indicates a downstream flow-dependence on r^*. Given that the aspect ratio was varied from 10 to 60, it was not possible to isolate the effect of nozzle contraction profile alone. Therefore, an independent investigation was carried out, whose results are presented in Chapter 4.

E.6 Different Normalizations of Centerline Mean Velocity

Figures E.4 and E.5 show the normalized mean velocity profiles normalized using the bulk mean and exit centerline mean velocity respectively.

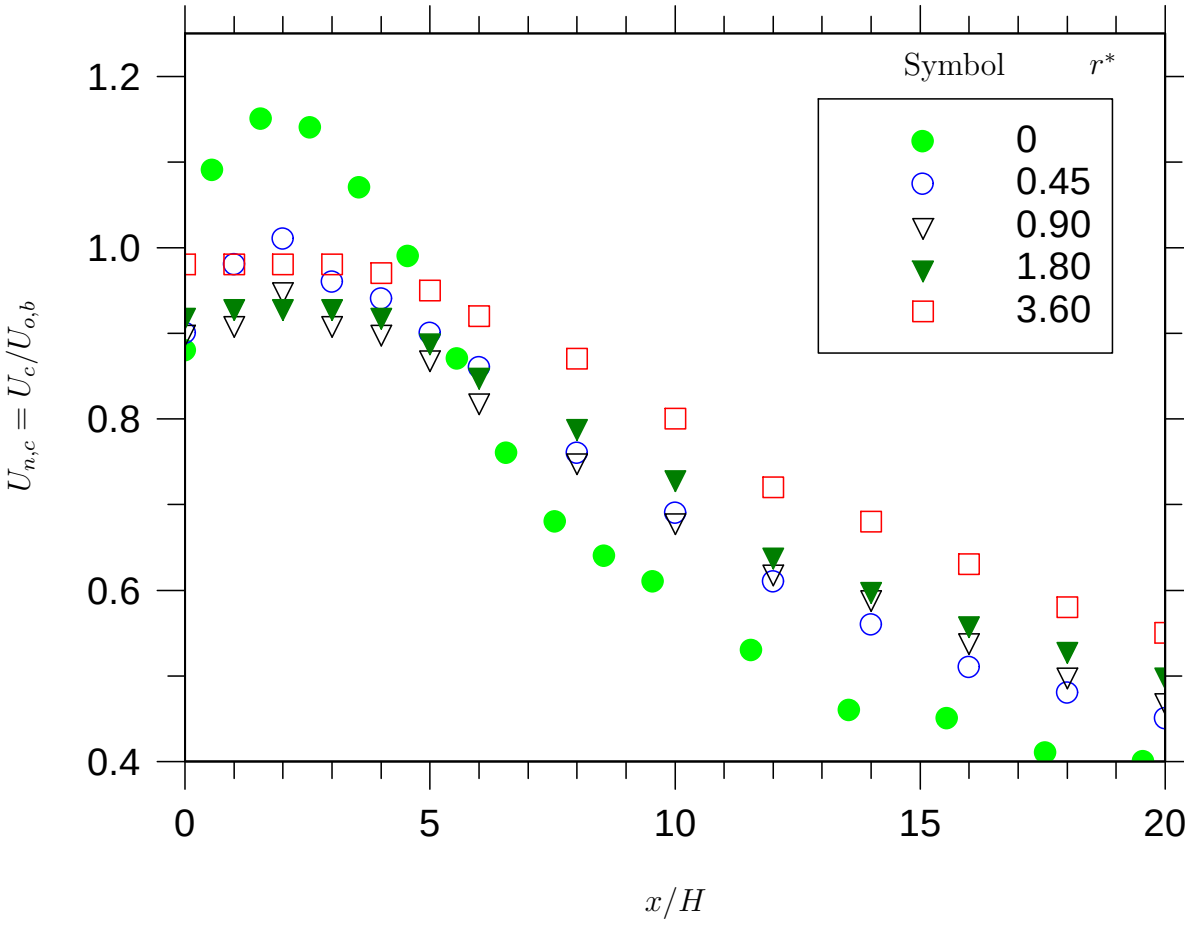

Figure E.4: Near field evolution of the normalized mean centerline velocity, $U_{n,c}$ (normalized using the bulk-mean velocity $U_{o,b}$) on the nozzle contraction profile factor, r^*.

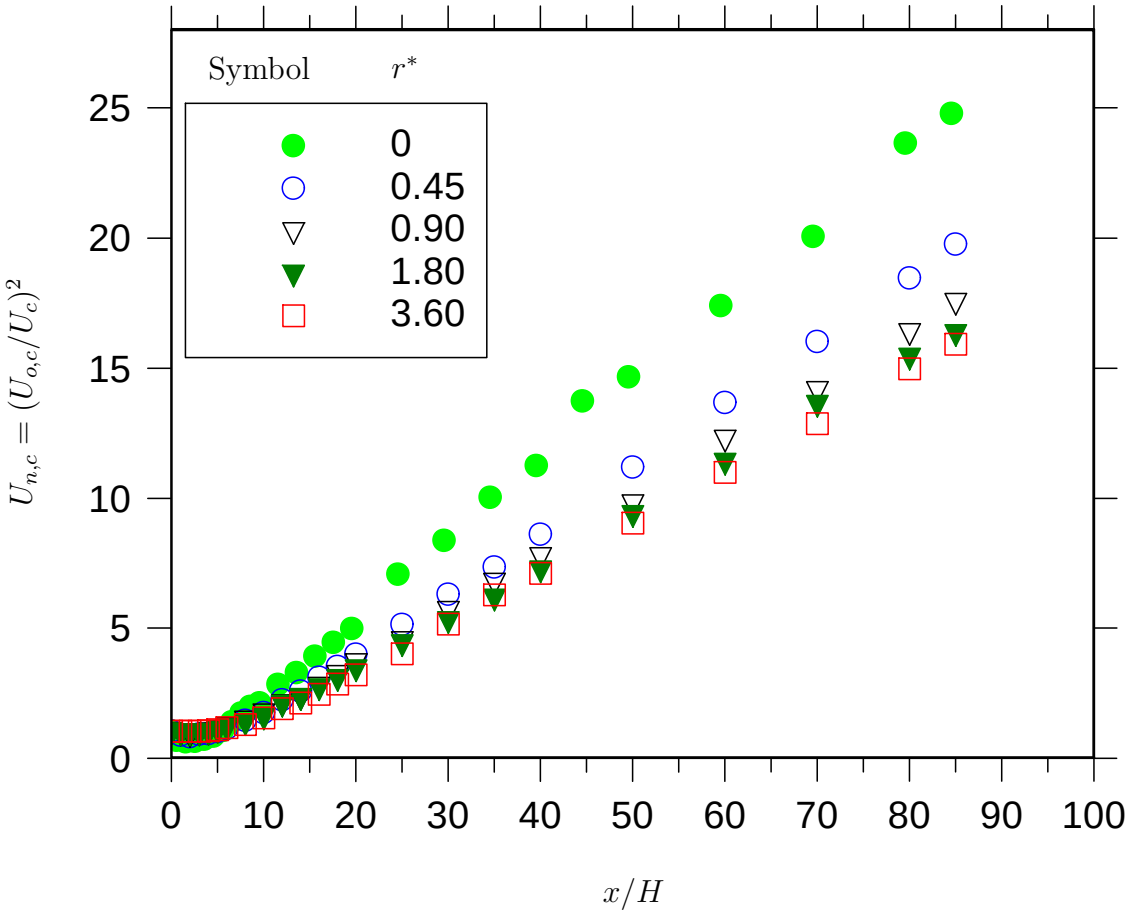

Figure E.5: The far field centreline mean velocity in the inverse square form, normalized using the exit centerline mean velocity $U_{o,c}$ for different nozzle profiles.

E.7 More Discussion on Initial Conditions

George (1989) deduced analytically that the flow field of a turbulent round jet is dependent on initial (inlet) conditions. It has also been well recorganized that the attainment to self-similarity[1] (and thus the convergence of the jet flow to their respective asymptotic states) of round jets are governed by the inlet conditions of the nozzle. Such governance not only dominates the near field but also in the far field (Nathan et al. 2004). Thus, inlet conditions play a vital role in the control of the round jet dynamics, ranging from the near to the far field.

The decay of centerline mean velocity of any jet (whether it be round or planar) is primarily due to the entrainment of the ambient fluids by the jet. Figure E.6 illustrates the variation of normalized mass flow with downstream distance. Here, m and m_o are the

[1] 'Self-similarity occurs when the velocity profiles (or any other quantity) is brought into congruence by simple scale factors which depend only on one of the variables': from George (1989)

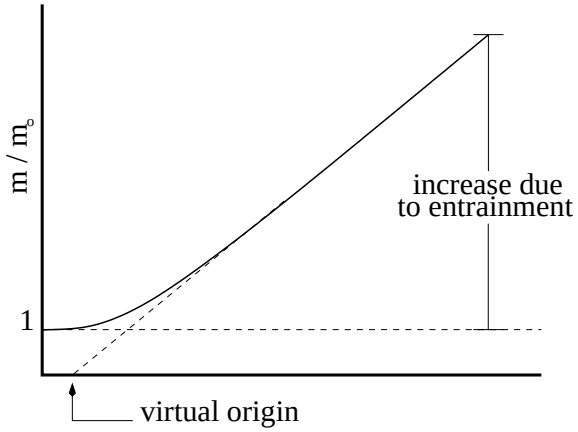

Figure E.6: Variation of jet mass flow with downstream distance, showing the effect of jet entrainment. After George (1989).

mass flux at any axial distance and the mass flux at the nozzle exit respectively. Note the increase in the normalized mass flow (m/m_o) with the axial distance. Thus, the mass flow arising from the entrainment overwhelms the mass flow at the nozzle exit. This notion proposes that the source conditions may become 'unimportant' due to the asymptotic nature of the jet development (George 1989). Nevertheless, there is considerable evidence that the growth rates of round jets (usually derived from the lateral velocity profiles where $U = \frac{1}{2}U_c$) depend on source conditions. Indeed, Gutmark and Ho (1983) stated that although flow measurements were conducted using the same experimental facility by single investigators, the flow field showed significant differences when variable source conditions were used. Therefore, the classical notion that at sufficiently large axial distances, jet shows should become asymptotically independent of initial conditions does not hold true. Thus, all jet flows (round, plane, etc), irrespective of their asymptotic states are likely to depend on initial conditions (George 1989).

Appendix F

Heat Transfer Principles Relevant to Hot Wire Anemometry

Introduced in the first half of the 20^{th} century, hot-wire anemometer has been gaining practical application in fluid mechanics since then. In the 1950s, there was a major breakthrough, when it became available commercially in the presently used CTA operational mode. Since then, hot wire anemometry has been constantly used for studies in turbulence.

Hot wire measures the instantaneous flow velocity based upon the heat transfer between the sensing element, for instance a thin electrically heated wire and the surrounding fluid medium. Principally, the rate of heat loss depends on the excess temperature of the sensing element, its physical properties and geometrical configuration and the properties of the fluid in motion. Hot-wire anemometer is extremely reliable in providing useful spatial and temporal information on the fluctuating components in fluid motions.

To understand the relationship between fluid velocity and heat loss of the cylindrical wire, the assumption that the fluid is incompressible and that the flow around the wire is potential, is often used. When electrical current is passed through wire, heat is generated. To attain an equilibrium, the heat generated is balanced by the convective heat loss to the surroundings. If the fluid velocity changes, then the convective heat transfer coefficient will also change, resulting in a change in wire temperature. This will eventually reach a new equilibrium with the surroundings.

The experimentally obtained static calibration curve is typically plotted as hot-wire voltage versus flow velocity. It is also described by a power law relationship, given in terms of the non-dimensional parameters Reynolds number Re, Nusselt number Nu, and the

Prandtl number Pr. Empirically this type of dependency is valid for $0.01 < \mathrm{Re} < 104$. It is essential to note that the heat loss is influenced by a number of other factors like; natural convection at very low velocities, compressibility effects at high velocities, density effects at low pressures.

Bibliography

Abdel-Rahman, A. A., ChkrounAl, W. and Al-Fahed, S. F.: 1997, LDA measurements in the turbulent round jet, *Mech. Res. Comm.* **24**(3), 277–288.

Alkislar, B. and Lourenco, L.: 2004, Jet flow field, Over Internet: http://www.eng.fsu.edu/ shih/succeed/jet/jet.htm. Last Accessed: 10 Jan 2005.

Antonia, R. A., Anselmet, F. and Chambers, A. J.: 1986, Assessment of local isotropy using measurements in a turbulent plane jet, *F. Fluid Mech.* **163**, 365–391.

Antonia, R. A., Browne, L. W. B., Chambers, A. J. and Rajagopalan, S.: 1983, Budget of temperature varianace in a turbulent plane jet, *Int. J. Heat Mass Transfer* **26**, 41–48.

Antonia, R. A., Browne, W. B., Rajagopalan, S. and Chambers, A. J.: 1983, On organised motion of a turbulent planar jet, *J. Fluids Mech.* **134**, 49–66.

Antonia, R. A., Satyaprakash, B. R. and Hussain, A. K. M. F.: 1980, Measurement of dissipation rate and some other characteristics of turbulent plane and circular jets, *Phys. Fluids* **23**(4), 695–700.

Antonia, R. A. and Zhao, Q.: 2001, Effects of initial conditions on a circular jet, *Exp. Fluids* **31**(319-323).

Ashforth-Frost, S. and Jambunathan, J.: 1997, Effect of nozzle geometry and semi-confinement on the potential core of a turbulent axisymmetric free jet, *Int. J. Heat Mass Transfer* **23**(2), 155–162.

Bashir, J. and Uberoi, S. M.: 1975, Experiments on turbulent structure and heat transfer in a two-dimensional jet, *Phys. Fluids.* **18**(4), 405–410.

Batchelor, G. K. and Proudman, I.: 1954, The effect of rapid distortion of a fluid in turbulent motion, *Quart. J. Mech. Appl. Mech.* **7**, 83–103.

Beavers, G. S. and Wilson, T. A.: 1970, Vortex growth in jets, *J. Fluid Mech.* **44**(1), 97–112.

Bevilaqua, P. M. and Lykoudis, P. S.: 1978, Turbulence memory in self-preserving wake, *J. Fluid Mech.* **80**, 589–606.

Bickley, W.: 1937, The plane jet, *Philosophical Magazine* **23**(Series 7), 727–731.

Boersma, B. J., Brethouwer, G. and Nieuwstadt, F. T. M.: 1998, A numerical investigation on the effect of the inflow conditions on the self-similar region of a round jet, *Phys. Fluids* **10**(4), 899–909.

Bonnafous, S.: 2001, *Experimental Study on Passive and Active Control of Coaxial Turbulent Jet*, Master thesis, Louisiana State University, Mechanical Engineering Department, USA.

Bonnet, J. P., Delville, J. and Garem, H.: 1986, Space and space-time correlations in the turbulent far wake of a flat plate in incompressible flow, *Exp. Fluids* **7**, 475–480.

Boussinesq, J.: 1905, An equation for the phenomena of heat convection and an estimate of the cooling power of fluids, *Journal de Mathematiques* **1**, 285–332.

Bradbury, L. J. S.: 1965, The structure of self-preserving turbulent planar jet, *J.Fluid Mech.* **23**, 31–64.

Bradshaw, P.: 1971, *An Introduction to Turbulence and Its Measurements*, Pergamon.

Browand, F. K. and Laufer, J.: 1975, The role of large scale structures in the initial development of circular jets, *Turbulence in Liquids* **Princeton, N J**, 33.

Browne, L. W. B., Antonia, R. A. and Chambers, A. J.: 1984, The interaction region of a turbulent planar jet, *J. Fluid Mech* **149**, 355–373.

Browne, L. W. B., Antonia, R. A. and Rajagopalan, S.: 1983, The spatial derivative of temperature in a turbulent flow and taylor's hypotheis, *Phys. Fluids* **26**(5), 1222–1227.

Browne, L. W. B., Antonia, R. A., Rajagopalan, S. and Chambers, A. J.: 1982, Structure of complex turbulent shear flows, *IUTAM Symposium*, Marcseille, pp. 411–419.

Brunn, H. H.: 1995, *Hot Wire Anemometry: Principles and Signal Analysis*, Oxford Press.

Capp, S. P.: 1983, *Experimental Investigation of the Turbulent Axisymmetric Jet*, Ph.D. Thesis, University of Buffalo, SUNY.

Carlson, J. I., Johnston, J. P. and Sagi, C. J.: 1967, Effects of wall shape on flow regimes and performance in straight, two-dimensional diffusers, *J. Basic Eng.* .

Chambers, A. J., Antonia, R. A. and Browne, L. W. B.: 1985, Effect of symmetry and asymmetry of turbulent structures on the interaction region of a plane jet, *Exp. Fluids* **3**, 343–348.

Champagne, F. H.: 1978, The fine-scale structure of the turbulent velocity field, *J. Fluid Mech.* **86**(1), 67–108.

Chen, C. J. and Rodi, W.: 1980, *Vertical Turbulent Bouyant Jets - A Review of Experimental Data*, Pergamon.

Christman, P. J. and Podzimek, J.: 1981, Hot-wire anemometer behaviour in low velocity air flow, *J. Phys.* **14**(1), 46–51.

Comte-Bellot, G.: 1977, *Measurement of Unsteady Fluid Dynamic Phenomena*, Hemisphere Publishing Co., chapter Hot-Wire and Hot-Film Anemometers, pp. pp. 123–162.

Corrsin, S.: 1943, Investigation of flow in an axially symmetric heated jet of air, *Technical Report W-94*, NACA.

Corrsin, S.: 1962, Turbulent dissipation fluctuations, *Phys. Fluids* **5**(10), 1301–1302.

Corrsin, S. and Kistler, A. L.: 1955, The free-stream boundaries of turbulent flows, *NACA TN3133, 1954, NACA Report 1244, 1955* .

Corrsin, S. and Uberoi, M. S.: 1950, Further experiments on the flow and heat transfer in a heated turbulent air jet, *NACA TN1865, 1949, NACA Report 998* .

Corrsin, S. and Uerio, M. S.: 1951, Spectra and diffusion in a round turbulent jet, *NACA Report 1040* .

Crow, S. C. and Champagne, F. H.: 1971, Orderly structure in jet turbulence, *J. Fluid. Mech.* **48**(3), 547–591.

Dahm, W. J. A. and Southerland, K. B.: 1997, Experimental assessment of taylors hypothesis and its applicability to dissipation estimates in turbulent flows, *Phys. Fluids* **9**(7), 2101–2107.

Demin, V. S.: 1973, Interpretation of hot-wire anemometer readings in a flow with velocity, pressure and temperature fluctuations, *Fluid Mechanics- Soviet Research* **2**(3).

Deo, R. C., Mi, J. and Nathan, G. J.: 2004, An investigation on the influence of nozzle aspect ratio on the velocity field of a turbulent plane jet, *In Proc. 15th Australasian Fluid Mech. Conference*, The University of Sydney, Sydney Australia.

Deo, R. C., Mi, J. and Nathan, G. J.: 2005, Effect of reynolds number on the small-scale statistics of a turbulent plane jet, *Journal of Turbulence - To be submitted* .

Dimotakis, P. E.: 2000, The mixing transition in turbulent flows, *J.Fluid Mech* **409**, 69–98.

Dimotakis, P. E., Miake-Lye, R. C. and Panpantoniou, D. A.: 1983, Structure and dynamics of round turbulent jets, *Phys. Fluids* **26**, 3185–3192.

Dryden, H. L. and Kuethe, A. M.: 1929, The measurement of fluctuations of air speed by the hot-wire anemometer, *NACA-TR-320* .

Everitt, K. W. and Robbins, A. G.: 1973, The development and structure of turbulent plane jets, *J. Fluid. Mech.* **88**, 563–583.

Feil, O. G.: 1964, Vane systems for very-wide-angle subsonic diffusers, *J. Basic Eng.* pp. 759 – 764.

Ferdman, E., Ötügen, M. V. and Kim, S.: 2000, Effect of initial velocity profiles on round jets, *J. Propul. Power* **16**(4), 676–686.

Flora, J. J. and Goldschmidt, V. W.: 1969, Virtual origins of a free plane turbulent jet, *AIAA J.* **7**(12), 2344–2446.

Forthman, E.: 1934, Uber turbulente strahalusbreitung, *In-genuer-Archiv* **5**, 42–54.

Frank, M. W.: 1999, *Fluid Mechanics*, McGraw-Hill International Editions, Mech. Eng. Series, 4^{th} edn, McGraw-Hill, Printed in Singapore.

George, W. K.: 1989, *Recent Advances in Turbulence*, Hermisphere, New York, chapter The Self-Preservation of Turbulent Flows and Its Relation to initial conditions, pp. 39–73.

George, W. K.: 1995, *Turbulence, Heat and Mass Transfer I*, Lisbon, chapter Some New Ideas for Similarity of Turbulent Shear Flows, pp. 13–24.

George, W. K.: 2004, Role of initial (or upstream conditions) in establishing flow conditions, *AIAA J* **42**(3), 438–446.

George, W. K.: 2005, *Lectures for Turbulence for the 21st Century*, Department of Thermo and Fluid Engineering, Chalmers University of Technology, Gothernberg, Sweden.

George, W. K. and Taulbee, D. B.: 1992, Designing experiments to test closure hypothesis, *J. Exp. Ther. Sci.* **5**(3), 249–260.

Gilbrech, R. J.: 1991, *An Experimental Investigation of Chemically Reacting Gas-Phase Turbulent Jets*, Ph.d. thesis, California Institute of Technology, California.

Goldschmidt, V. W. and Bradshaw, P.: 1981, Effect of nozzle exit turbulence on the spreading (or widening) rate of plane free jets, *Joint Engineering, Fluid Engineering and Applied Mechanics Conference*, ASME, ASME, Boulder, Colarado, pp. 1–7.

Gouldin, F. C., Schefer, R. W., Johnson, S. C. and Kollmann, W.: 1986, Non-reacting turbulent mixing flows, *Prog. Energy Combust. Sc* **12**, 257–303.

Grinstein, F. F.: 2005, Dynamics of turbulent free jets, Over the Internet: http://www.uottawa.ca/publications/interscientia/inter.2/jet.html. Last Accessed: 10 Feb 2005.

Grinstein, F. F., Glauser, M. N. and George, W. K.: 1995, *Vorticy in Jets, S.I.Green Ed.*, Kluwer Academic Publisher, Netherland, chapter Chapter III, Fluid Vorticity, pp. 65–94.

Gutmark, E. and Ho, C. M.: 1983, Preferred modes and spreading rates of jets, *Phys. Fluids* **26**, 2932–2938.

Gutmark, E. and Schadow, K. C.: 1987, Flow characteristics of orifice and tapered jets, *Phys. Fluids* **30**(11), 3448–3454.

Gutmark, E. and Wygnanski, I.: 1976, The planar turbulent jet, *J. Fluid Mech.* **73**(3), 465–495.

Hebber, K. S.: 1980, Wall proximity corrections for hot-wire readings in turbulent flows, *DISA Information* **25**.

Heskestad, G.: 1965, Hot-wire measurements in a plane turbulent jet, *Trans. ASME, J. Appl. Mech.* **32**(721-734).

Hill, W. G., Jenkins, R. C. and Gilbert, B. L.: 1976, Effects of the initial boundary layer state on turbulent jet mixing, *AIAA J.* **14**, 1513–1514.

Hitchman, G. J., Strong, A. B., Slawson, P. R. and Ray, G.: 1990, Turbulent planar jet with and without confining walls, *AIAA J.* **28**(10).

Hsiao, F. B. and Sheu, S. S.: 1996, Experimental studies on flow transition of a plane wall jet, *Aeronaut. J.* **Paper No. 2014**, 373–380.

Husain, H. S. and Hussain, A. K. M. F.: 1983, Controlled excitation of elliptic jets, *Phys. Fluids* **26**, 2763 –.

Hussain, A. K. M. F. and Clark, A. R.: 1977, Upstream influence on the near field of a planar turbulent jet, *Phys. Fluids* **20**(9).

Hussain, A. K. M. F. and Zedan, M. F.: 1978, Effect of the initial conditions of the axisymmetric free shear layer: effect of initial momentum thickness, *Phys. Fluids* **21**, 1100–1112.

Hussain, H. J., Capp, S. P. and George, W. K.: 1994, Velocity measurements in a high reynolds number momentum conserving axisymmetric turbulent jet, *J. Fluid Mech.* **258**, 31–75.

Hussian, A. K. M. F.: 1983, Coherent structures - reality and myth, *Phys. Fluids* **26**, 2816–2850.

Jenkins, P. E. and Goldschmidt, V. W.: 1973, Mean temperature and velocity measurements in a plane turbulent jet, *Trans. ASME J.* **95**, 581–584.

Johansen, F. C.: 1929, Flow through pipe orifices at low Reynolds numbers, *Proc. Roy. Soc.* **126**, 231–245.

Johansson, P. B. V., George, W. K. and Gourlay, M. J.: 2003, Equilibrium similarity, effects of initial conditions and local reynolds number on the axisymmetric wake, *Phys. Fluids* **15**(3), 603–617.

Jorgensen, F. E.: 2002, *Hot-Wire Anemometry - a practical guide*, DANTEC Dynamics, p. 54.

Kelso, R. M., Lim, T. T. and Perry, A. E.: 1994, A novel flying hot-wire system, *Exp. Fluids* **16**, 181–186.

Khoo, B. C., Chew, Y. T. and Teo, C. J.: 2000, On near-wall hot-wire measurements, *Exp. Fluids* **448-469**(29), 448–460.

King, L.: 1914, On the convection of heat from small cylinders in a stream of fluid, *Phil. Trans. of Roy. Soc.* **Ser. A. Vol. 214**(14), 373–432.

Klein, A. and Ramjee, V.: 1972, Effect of contraction geometry on non-isotropic free-stream turbulence, *Aero. Quart.* **23**, 34–38.

Klein, M., Sadiki, A. and Janicka, J.: 2003, Investigation of the influence of the reynolds number on a plane jet using direct numerical simulation, *Int. J. Heat and Fluid Flow* **24**, 785–794.

Kline, S. J., Abbott, D. E. and Fox, R. W.: 1959, Optimum design of straight walled diffusers, *Trans. ASME J. Basic Eng.* pp. 321 – 329.

Ko, N. W. M. and Davies, P. O. A. L.: 1971, The near field within the potential core of subsonic cold jets, *J. Fluid. Mech.* **50**, 49–78.

Konrad, J. H.: 1976, *An Experimental Investigation of Mixing in Two-dimensional Turbulent Shear Flows with Applications to Diffusion-limited Chemical Reactions*, Ph.D. Thesis, California Institute of Technology, California.

Koochesfahani, M. M. and Dimotakis, P. E.: 1986, Mixing and chemical reactions in a turbulent liquid mixing layer, *J. Fluid Mech.* **170**, 83–112.

Kotsovinos, N.: 1978, A note on the conservation of axial momentum of a turbulent jet, *J. Fluid Mech.* **87**(Part 1), 55–63.

Kovasznay, L. S. G.: 1950, The hot-wire anemometer in supersonic flows, *Journal of the Aeronautical Sciences* **17**(9), 565–584.

Krothapalli, A., Baganoff, D. and Karamcheti, K.: 1981, On the mixing of rectangular jet, *J. Fluid Mech.* **107**, 201–220.

Kulman, J. M.: 1985, Survey of near field reynolds number effects and initial condition effects on bouyant and non-bouyant jets, *ASME Paper*, International Symposium on Modelling Environmental Flows, Albuquerque, NM.

Lemieux, G. P. and Oosthuizen, P. H.: 1985, Experimental study of behaviour of planar turbulent jets at low reynolds numbers, *AIAA J.* pp. 1845–1846.

Lemieux, G. P. and Oosthuizenm, P. H.: 1984, Experimental study of the behaviour of plane turbulent air jets at low reynolds numbers, *17th Fluid Dynamics, Plasma Dynamics and Lasers Conference*, Vol. Paper AIAA-84-1661, Snow Mass/Co, USA, pp. 1–6.

Lo, S. H.: 1994, *Eddy structures in a simulated plane jet educed by pattern recognition analysis, Direct and Large-Eddy Simulation I*, Kluwer Academic, Dordrecht.

Löfdahl, L., H, A., B, J. and T, H.: 1997, On the reynolds number dependence of a plane two-dimensional wall-jet, *Doktorsavhandlingar vid Chalmers Tekniska Hogskol* **1292**, 8pp.

Louchez, P. R., Kawall, J. G. and Keffer, J. F.: 1987, Detailed spread on characteristics of plane wakes, *In Turbulent Shear Flows 5 (ed. F. Durst, B. E. Lounder, J. L. Lumley, F. W. Schmidt and J. H. Whitelaw* pp. 98–109.

Malmstrom, T. G., Kirkpatrick, A. T., Christenesen, B. and Knappmiller, K. D.: 1997, Centreline velocity decay measurements in low-velocity axisymmetric jets, *J. Fluid Mech.* **246**, 363–377.

Marsters, G. F. and Fotheringham, J.: 1980, The influence of aspect ratio on incompressible turbulent flows from rectangular slots, *Aeronaut. Quart* **XXXI**(4), 285–305.

Mehta, R. D. and Bradshaw, P.: 1979, Design rules for small low speed wind tunnels, *Aero. J.* pp. 443 – 449.

Mi, J., Deo, R. C. and Nathan: 2005a, Fast-convergent iterative scheme for filtering velocity signals and finding kolmogorov scales, *Phys. Rev. E.* **71**(6).

Mi, J., Deo, R. C. and Nathan, G. J.: 2005b, Characterization of turbulent jets from high-aspect-ratio rectangular nozzles, *Phys. Fluids* **17**(6).

Mi, J. and Nathan, G. J.: 2004, Mean velocity decay of axisymmetric turbulent jets with different initial velocity profiles, *4th International Conference on Fluid Mechanics*, Dalian, China.

Mi, J., Nathan, G. J. and Luxton, R. E.: 2000, Centerline mixing characteristics of jets from nine differently shaped nozzles, *Exp. Fluids* **28**, 93–94.

Mi, J., Nathan, G. J. and Nobes, D. S.: 2001, Mixing characteristics of axisymmetric free jets from a contoured nozzle, an orifice plate and a pipe, *J. Fluid. Eng.* **123**, 878–883.

Mi, J., Nobes, D. S. and Nathan, G. J.: 2001, Influence of jet exit conditions on the passive scalar field of an axisymmetric free jet, *J. Fluid Mech.* **432**, 91–125.

Mi, J., Zhou, Y. and Nathan, G. J.: 2004, The effect of reynolds number on the passive scalar field in the turbulent wake of a circular cylinder, *Flow. Turb. Comb.* **72**, 311–331.

Miller, D. R. and Comings, E. W.: 1957, Static pressure distribution in a free turbulent jet, *J. Fluid Mech.* **3**, 1–16.

Miller, P. L. and Dimotakis, P. E.: 1991, Reynolds number dependence of scalar fluctuations in a high schmidth number turbulent jet, *Phys. Fluids* **A 3**, 1156–1163.

Moshfegh, B., Sandberg, M. and Amiri, S.: 2004, Spreading of turbulent warm/cold plane air jet in a well insulated room, Over the Internet: http://www.hig.se/t-inst/forskning/em/spreading-of-turbulent.htm, Supported by: University of Gavle and KK-Foundation.

Mumford, J. C.: 1982, The structures of large eddies in fully developed shear flows. part 1. the plane jet., *J. Fluid Mech.* **118**, 241–268.

Mungal, G. and Hollingsworth, D. K.: 1989, Organized motion in a high reynolds number jet, *Phys. Fluids* **1**(10), 1615–1623.

Namar, I. and Ötügen, M. V.: 1988, Velocity measurements in a planar turbulent air jet at moderate reynolds numbers, *Exp. Fluids* **6**, 387–399.

Namar, M. V.: 1986, *An Investigation of the Structure of Moderate Reynolds Number Plane Air Jets*, Ph.d. thesis, Drexel University.

Nathan, G. J., Mi, J., Newbold, G. J. R., Nobes, D. S. and Alwahabi, Z. T.: 2004, Effects of subtle and dramatic changes to initial conditions to a jet's turbulent structure, mixing and combustion, *In Proc. 15th Australasian Fluid Mech. Conference*, The University of Sydney, Sydney Australia.

Nishioka, M. and Sato, H.: 1974, Measurements of velocity distribution in the wake of a circular cylinder at low reynolds numbers, *J. Fluid Mech.* **65**, 97–112.

Norman, B.: 1967, Hot-wire anemometer calibration at high subsonic speeds, *DISA Information* **5**.

Nottage, H. B.: 1951, Report on ventilation jets in room air distribution, *Technical report*, Case Inst. of Technology, Cleveland, Ohio.

Oosthuizen, P. H.: 1983, An experimental study of low reynolds number turbulent circular jet flow, Vol. 83-FE-36 of *ASME Applied Mechanics, Bioengineering, and Fluids Engineering Conference*, Houston/TX USA.

Panchapakesan, N. R. and Lumley, J. L.: 1993, Turbulence measurements in axisymmetric jets of air and helium, part 1, air jet, *J. Fluid Mech.* **246**, 197–223.

Papadakis, M. and Staiano, M. W.: 1993, Experimental and computational investigation of free and impinging planar jets, *AIAA Paper* **93-0654**, 1–11.

Perry, A. E.: 1982, *Hot-Wire Anemometry*, Cladrndon Press Oxford.

Piffaut, V.: 2003, *Axis-switching in square coaxial jets*, Master's thesis, Mechanical Engineering, Louisiana State University, USA.

Pope, S. B.: 2002, *Turbulent Flows*, Cambrige University Press, UK.

Quinn, W.: 1994, Development of a large-aspect ratio rectangular turbulent free jet, *AIAA J.* **32**(3), pp –.

Quinn, W. R.: 1992a, Stream wise evolution of a square jet cross-section, *AIAA J.* **30**(12), pp –.

Quinn, W. R.: 1992b, Turbulent free jet flows issueing from sharp-edged rectangular slots: The influence of slot aspect ratio, *Experimental Thermal and Fluid Science* **5**, 203–215.

Ramjee, V. and Hussain, A. K. M. F.: 1976, Influence of the axisymmetric contraction ratio on free-stream turbulence, *J. Fluids. Eng* **507**, 506–515.

Reynolds, O.: 1883, An experimental investigation of the circumstances which determine whether the motion of water shall be direct or sinous, and the law of resistance in parallel channels, *Philos. Trans. R. Soc. London Ser.* **A**(186), 123–161.

Richards, C. D. and Pitts, W. M.: 1993, Global density effects on the self-preservation behaviour of turbulent free jets, *J. Fluid Mech.* **245**, 417–435.

Ricou, F. Q. and Spalding, D. B.: 1961, Measurements of entrainment by axisymetric jets, *J. Fluid Mech.* **11**, 21–32.

Rockwell, D. O. and Nicholas, W. O.: 1973, Natural breakdown of planar jets, *J. Basic. Eng* **94**, 720–730.

Ruck, B.: 1991, Distortion of LDA fringe pattern by tracer particles, *Exp. Fluids* **10**, 349–354.

Sato, H.: 1960, The stability and transition of a two-dimensional jet, *J. Fluid Mech.* **7**, 53–80.

Schlichting, H.: 1933, Laminare strhlausbreitung, *ZAMM* **xiii**, 260–263.

Schlichting, H.: 1979, *Boundary Layer Theory*, seventh edition edn, Mc Graw-Hill, New York, New York, USA.

Schultz-Grunow, F.: 1981, Generation of spatial turbulent spots, *In Proc.7th Biennial Symp. On turbulence, University of Missouri-Rolla* **52-1 to 52-4**.

Sfeir, A.: 1979, Investigation of three dimensional turbulent rectangular jets, *AIAA J.* **17**(10), 1055–1060.

Sfeir, A. A.: 1976, The velocity and temperature field of rectangular jets, *Int. J. Mass Heat Transfer* **19**, 1289–1297.

Sforza, P. M., Steiger, M. H. and Trentacoste, N.: 1966, Studies on three-dimensional viscous jet, *AIAA J.* **4**(5), 800–806.

Smits, A. J., Hayakawa, K. and Muck, K. C.: 1983, Constant temperature hot-wire anemometer practice in supersonic flows, part 1: The normal wire, *Exp. Fluids* **1**(2), 83–92.

Sreenivasan, K. R.: 1995, The energy dissipation in turbulent shear flows, *in* S. S. M. Deshpande, A Prabhu and P. R. Vishwanth (eds), *In Symposium on Developments in Fluid Dynamics and Aerospace Engineering*, Interline Publishers, Banglore, pp. 159–190.

Stanley, S. A., Sarkar, S. and Mellado, J. P.: 2002, A study of the flow-field evolution and mixing in a planar turbulent jet using direct numerical simulations, *J. Fluid Mech.* **450**, 377–407.

Stephane, M., Camille, S. and Michel, P.: 2000, Parametric analysis of the impinging plane air jet on a variable scaled-down model, *ASME FEDSM'00 2000 ASME/JSME Fluids Engineering Division Summer Meeting*, Vol. F-227, Boston, Massachusetts.

Szepessy, S. and Bearman, P. W.: 1992, Aspect ratio and end plate effect on vortex shedding from a circular cylinder, *J. Fluid Mech.* **234**, 191–217.

Tan-Atichat, J., George, W. K. and Woodward, S.: 1996, *Use of Data Acqusition and Processing: Handbook of Fluids and Fluids Engineering*, Vol. 3, Wiley.

Thomas, F. O. and Goldschmidt, V. W.: 1986, Structural characteristics of a developing turbulent planar jet, *J. Fluid Mech.* **163**, 227–256.

Thompson, B. E.: 1987, Appraisal of a flying hot-wire anemometer, *Dantex Information* **4**.

Tong, C. and Warhaft, Z.: 1995, Passive scalar dispersion and mixing in a turbulent jet, *J. Fluid Mech.* **292**, 1–38.

Townsend, A. A.: 1976, *The Structure of Turbulent Shear Flow*, Vol. 2nd Ed., Cambridge University Press.

Trendscoste, N. and Sforza, P.: 1967, Further experimental results for three-dimensional free jets, *AIAA J.* **5**(5), 885–890.

Tsuchiya, Y., Horikoshi, C. and Sato, T.: 1985, On the spread of rectangular jets, *Exp. Fluids* **4**, 197–204.

Tsuchiya, Y., Horikoshi, C., Sato, T. and Takahashi, M.: 1989, A study of the spread of rectangular jets: (The mixing layer near the jet exit and visualization by the dye methods), *JSME Int. J.* **32, SeriesII**(1), 11–17.

Uberoi, M. S.: 1956, Effect of wind tunnel contraction on free-stream turbulence, *J. Aero. Sci.* **23**, 754–764.

Van Der Hegge Zijnen, B. G.: 1958, Measurements of the distribution of heat and matter in a plane turbulent jet of air, *Appl. Sci. Res.* **A7**, 277–292.

Weir, A. D., Wood, D. H. and Bradshaw, P.: 1981, Interacting turbulent shear layers in a plane jet, *J. Fluid. Mech.* **107**, 237–260.

Williamson, C. H. K.: 1996, Vortex dynamics in the cylindrical wake, *Annu. Rev. Fluid Mech.* **28**, 477–539.

Wygnanski, I., Champagne, F. and Marasli, B.: 1986, On the large-scale structures in two-dimensional small-deficit, turbulent wakes, *J. Fluid Mech.* **168**, 31–71.

Wygnaski, I. and Fiedler, H. E.: 1969, Some measurements in a self-preserving jet, *J. Fluid Mech.* **38**(3), 577–6102.

Zaman, K. B. M. Q.: 1999, Spreading characteristics of compressible jets from nozzles of various geometries, *J. Fluid Mech.* **383**, 197–228.

Zhou, Y. and Antonia, R. A.: 1995, Memory effects in a turbulent plane wake, *Exp. Fluids* pp. 112–120.

Zhou, Y., Antonia, R. A. and Tsang, W. K.: 1998, The effect of reynolds number on a turbulent far-wake, *Exp. Fluids.* **25**, 118–125.

Zhou, Y., Antonia, R. A. and Tsang, W. K.: 1999, The effect of the reynolds number on the reynolds stresses and vorticity in a turbulent far-wake, *Exp. Therm. Fluid Sc.* **18**, 291–298.

THE UNIVERSITY OF ADELAIDE
AUSTRALIA

CERTIFICATION OF THESIS FOR EXAMINATION

(* Delete where appropriate.)

To be completed by Principal Supervisor (Please tick the appropriate box)

Student Name: RAVINESH C DEO

Name of Principal Supervisor: GRAHAM (GUS) NATHAN

School/Discipline: MECHANICAL ENGINEERING Program: PhD

I have seen and read the final draft of the above candidate's thesis and, in accordance with the requirement of Section 2.4.15 of Part I of *The Code of Practice*, certify that:

☑ I am satisfied with the technical presentation of the thesis, and it is, *prima facie*, worthy of examination.

☐ I am not satisfied with the technical presentation of the thesis and it should not be accepted for examination in its current form. I attach a statement outlining my reasons.

The format of the thesis to be submitted is:

☑ Traditional	☐ Music Composition	☐ PhD (Creative Writing)
☐ Publication	☐ Music Performance	☐ Doctor of Education

☐ YES ☐ NO An electronic copy of the thesis (identical in all respects to the hard copies) is included

☐ YES ☐ NO An electronic supplement to the thesis is included

It is acceptable for students to engage other people (paid or otherwise) in the candidate's research or in the editing of the thesis, as long as this assistance is appropriately acknowledged in the thesis. I am satisfied that the above candidate has abided by the University's policies [Code of Practice Part II, Section 2.3.4 (f)] and has included the appropriate acknowledgement(s) in the thesis.

☑ I am satisfied that the above candidate has abided by the University's policies with regard to assistance and editing [Code of Practice Part II, Section 2.3.4 (f)] and has included the appropriate acknowledgement(s) in the thesis.

☐ I am not satisfied that the above candidate has abided by the University's policies with regard to assistance and editing [Code of Practice Part II, Section 2.3.4 (f)] and has included the appropriate acknowledgement(s) in the thesis.

GUS NATHAN — Principal Supervisor (Please print name legibly)

Principal Supervisor's signature

27 May 05 — Date

To be completed by *Head of School or Discipline/Postgraduate Coordinator

☑ I endorse the Principal Supervisor's recommendation.

☐ I do not endorse the Principal Supervisor's recommendation and I attach a statement outlining my reasons.

~~*Head of~~ Discipline/Postgraduate Coordinator

27/5/05 — Date

THE UNIVERSITY
OF ADELAIDE
AUSTRALIA

ADELAIDE GRADUATE CENTRE

ADELAIDE UNIVERSITY SA 5005
AUSTRALIA

TELEPHONE +61 8 8303 5882
FACSIMILE +61 8 8303 5725
graduate.centre@adelaide.edu.au

SUBMISSION OF THESIS

Dear Ravinesh Deo

THIS IS TO CERTIFY that on the 7th day of June, 2005, you submitted three copies of your thesis entitled **'EXPERIMENTAL INVESTIGATIONS OF THE INFLUENCE OF REYNOLDS NUMBER AND BOUNDARY CONDITIONS ON A PLANE AIR JET'** for the degree of Doctor of Philosophy. We wish you a successful outcome for the examination.

You must now apply to graduate. Please see overleaf.

ANNE WITT
Manager, Graduate Administration and Scholarships

THE UNIVERSITY OF ADELAIDE
AUSTRALIA

ADELAIDE GRADUATE CENTRE
LEVEL 13 – 10 PULTENEY STREET
THE UNIVERSITY OF ADELAIDE
SA 5005
AUSTRALIA

TELEPHONE +61 8 8303 5882
FACSIMILE +61 8 8303 5725
graduate.centre@adelaide.edu.au
CRICOS Provider Number 00123M

Ref: kc

22 August 2005

Mr Ravinesh Deo
Department of Physics
School of Pure and Applied Sciences
University of the South Pacific
Suva
Fiji

Dear Mr Deo

Outcome of Thesis Examination

I am writing to advise you of the outcome of your thesis examination. I am pleased to inform that, subject to the following conditions, you will be eligible, academically, to be admitted to the degree of Doctor of Philosophy:

- complete minor amendments to the thesis to the satisfaction of your supervisors and Head of School/Discipline;
- deliver three hard-bound copies of the suitably amended thesis to the Adelaide Graduate Centre, together with the enclosed, completed proforma confirming that the required amendments have been made;
- discharge any outstanding obligations to the University.

Please note that this is not an academic qualification letter; once you have fulfilled the conditions stipulated above, an official academic qualification letter will be forwarded to you.

For your information, I enclose copies of the examiners'; to expedite your qualification, please discuss the required thesis amendments with your supervisors and Head of School/Discipline as soon as possible. One hard bound copies of your thesis entitled "EXPERIMENTAL INVESTIGATIONS OF THE INFLUENCE OF REYNOLDS NUMBER AND BOUNDARY CONDITIONS ON A PLANE AIR JET" is available for collection from the Adelaide Graduate Centre. I shall advise you when the other copies are available for collection. On collection, please ensure that you provide photographic identification in the form of, for example, a University card, driver's licence or passport. Should you choose to authorise someone else to collect the copies on your behalf, that person will need to provide evidence of your authorisation (eg a signed letter from you) together with an acceptable form of photographic identification.

You will be aware that students are obliged to submit three hard-bound copies of their theses at the end of the examination process. In order that you may be eligible, academically, to graduate you must supply three hard-bound copies to the Graduate Centre by the relevant closing date (16 February for the March graduation ceremonies; 13 July for the August ceremonies; or 30 November for the December ceremonies).

The University's annual graduation ceremonies are held in March, August and December. The March ceremonies are held offshore and the August and December ceremonies are held in Adelaide. You should have applied to graduate by now. If you have not, please apply via "Access Adelaide" immediately. The web address is http://www.adelaide.edu.au/access/

The following web address sets out the steps you need to take in order to graduate.
http://www.adelaide.edu.au/student/graduations/?b=nocss

You must regularly view "Access Adelaide" to check your current graduation details.

Congratulations on your achievements to date. Do not hesitate to contact the Graduate Centre on 8303 5882 should you require any further information or assistance.

Yours sincerely

ANNE WITT
Manager, Graduate Administration and Scholarships

Encs: Examiners' reports
'Confirmation of Amendments to Thesis' proforma

cc: Postgraduate Co-ordinator via Head, School of Mechanical Engineering
Supervisor(s): (examiners reports enclosed) Dr Gus Nathan, Dr Jianchun Mi
Convenor, Faculty of Engineering, Computer and Mathematical Sciences HDC
International Student Liaison Officer

THE UNIVERSITY OF ADELAIDE
AUSTRALIA

ADELAIDE GRADUATE CENTRE

LEVEL 13 – 10 PULTENEY STREET
THE UNIVERSITY OF ADELAIDE
SA 5005
AUSTRALIA

TELEPHONE +61 8 8303 5882
FACSIMILE +61 8 8303 5725
graduate.centre@adelaide.edu.au
CRICOS Provider Number 00123M

Ref: kc

7 October 2005

Mr Ravinesh Deo
Department Of Physics
School Of Pure And Applied Sciences
University Of The South Pacific
Suva Fiji

Dear Mr Deo

OUTCOME OF THESIS EXAMINATION

I am delighted to inform you that you qualified, academically, for the award of the degree of Doctor of Philosophy for your thesis entitled, **"Experimental Investigations of the Influence of Reynolds Number and Boundary Conditions on a Plane Air Jet"** on 7 October 2005.

The annual graduation ceremonies are held in April, August and December. The April ceremonies are held off-shore and the August and December ceremonies are held in Adelaide. You should have applied to graduate by now. If you have not, please apply via "Access Adelaide" immediately. The web address is: http://www.adelaide.edu.au/access/

The following web address sets out the steps you need to take in order to graduate:
http://www.adelaide.edu.au/student/graduations/?b=nocss

You must regularly view "Access Adelaide" to check your current graduation details.

Please contact the Graduate Centre on 8303 5882 should you require any further information or assistance.

Please accept my congratulations and best wishes for your future endeavours.

Yours sincerely

RICHARD A RUSSELL AM
Dean of Graduate Studies

CERTIFY TRUE COPY
SASHI KANT DHANJI
JUSTICE OF PEACE FIJI

Report on Doctoral Dissertation of Ravinesh C. Deo
"Experimental Investigations of the Influence of Reynolds Number and Boundary Conditions on a Plane Jet"

By
William K. George
Professor of Turbulence
Chalmers University of Technology
Gothenburg, Sweden

Overall evaluation: This dissertation easily meets any reasonable criteria for a Ph.D. dissertation (at least in Sweden or the USA). The work reported was well thought out and well performed. With only the small changes listed below, my recommendation is that it be accepted. I do not need to see the revised manuscript.

Comments for consideration and suggestions for future work

These are by far the most comprehensive work ever carried out on the effects of upstream and external conditions on the plane jet (or for that matter any free shear flow). The two most important points are

(i) All plane jets, no matter how initiated, indeed appear to reach an asymptotic equilibrium similarity state (theoretical details below)
(ii) The final state reached is uniquely dependent on the initial conditions.
(iii) It is possible to mess this all up with sidewalls, etc.

Aside from its obvious value to those interested in plane jet flows, the results are of especial importance to the CFD community, since they imply that there exists no set of parameters for single point RANS models which can describe more than one configuration. This is consistent with the recent AIAA paper (George, W.K. and Davidson, L. (2004) Role of Initial (or Upstream Conditions) in Establishing Asymptotic Flow Conditions, **AIAA Journal**, **42**, 3, 438 – 446.), and shows that the only hope for calculating these flows is with structure-based turbulence models or two-point models (like LES).

Chapter 3 alone is probably a JFM paper, and chapters 4-6 could easily be considered major contributions to engineering journals, e.g., ASME J. Fluids Engineering. Thus the comments below are intended to help guide the authors as what at least this potential reviewer would need to see to make that possible. The primary lack of the dissertation is that it has very little reference to theory (or even the basic equations), all of that is consistent with the findings and lend considerable understanding and support to them. In part this is because the only reference to the plane jet which discusses modern equilibrium theory was not found (most likely since it was rather obscure and probably did not show up in any plane jet search). Moreover a very recent paper (on axisymmetric wakes) which might have given a clue as to how to proceed was not recognized to be of relevance, nor was it obviously so.

EXPERIMENTAL INVESTIGATIONS OF THE INFLUENCE OF REYNOLDS NUMBER AND BOUNDARY CONDITIONS ON A PLANE JET
RAVINESH C. DEO

Examiner: S. Rajagopalan

General:

This thesis presents the results of detailed single hot wire measurements in a plane jet, which develops under the influence of different initial conditions and Reynolds numbers. Plane and circular jets have several industrial applications although seldom is a jet issuing out of a smooth, contoured nozzle is encountered in real life. Apart from this, the Reynolds numbers between industrial and laboratory environment are different. In view of these, it is important to establish the effects of nozzle exit characteristics on the jet development as well as that influence of the Reynolds number. This work, in my judgment, has established a useful database to characterize the influence of various parameters on a plane jet. Although only a single hot wire probe has been used in all the investigations, great care has been taken in making the measurements arid the results are presented in a user-friendly manner and the quality of diagrams is high. The thesis reads well as the main aims are emphasized in each chapter so that the reader does not lose sight of these.

Without detracting from the strength of the work I found it striking that all the important chapters (3 6) have a similar presentation in content, discussion and figures. At times this made reading the thesis somewhat monotonous aid made me feel like looking at several presentations that had the same template but different font'. By including an extra element in different chapters, presentation could have been made more attractive. For example, selective x-*wire* measurements and a few mixing layer results would have enhanced the content and the style of presentation. Nevertheless, what is presented is the result of solid and meticulous effort and the student deserves kudos

In summary, this thesis contains useful and important data that will benefit laboratory-based researchers as well as provides valuable help in the selection of appropriate nozzles for industrial applications. The work does not have new and original concepts that are associated with fundamental research and is more like a set of detailed experiments aimed at collecting large amounts of useful information that will eventually enhance our knowledge of jet development under different initial and boundary conditions. The student has done a commendable job in carrying out difficult measurements in a careful and diligent manner. Several publications have resulted from this work so far and more will follow.

I have no hesitation in recommending the award of Ph.D. degree.